The identification of potential diagnostic biomarkers and disease mechanisms in lysosomal storage disorders

Victoria Manwaring

A thesis submitted for the degree of Doctor of Philosophy (PhD) at University College London

Biochemistry Research Group,

Clinical and Molecular Genetics Unit

Institute of Child Health

University College London

2014

‘I, Victoria Manwaring confirm that the work presented in this thesis is my own. Where information has been derived from other sources, I confirm that this has been indicated in the thesis.’

I dedicate this thesis to my family for their unconditional love and support.

'Success is not final, failure is not fatal: it is the courage to continue that counts'

Winston Churchill (1874-1965)

Acknowledgements

First and foremost, I would like to express my sincere gratitude to my supervisors Dr Kevin Mills, Prof Simon Heales and Dr Wendy Heywood. Your knowledge, guidance and support throughout my PhD has been unwavering. Kev, as well as my supervisor you have been my 'London Dad'. Your help, encouragement, insistence of work/life balance and repeated funding for world travel has truly made my PhD experience! Simon, your passion and commitment to science is infective and a source of great motivation. Wendy, I couldn't have wished for a more dedicated secondary supervisor. My constant questions and repeated interruptions have always been met with help, advice, and solutions; I only hope that as your first PhD student I haven't put you off!

As well as my 'official' supervisors I need to acknowledge and extend my heartfelt thanks to Christiane Auray-Blais who during my time in Quebec was not only an inspirational teacher but also a constant source of support and encouragement. My thanks also go to Michel Boutin for his help and support.

There are also many people who have given up their time, expertise and resources in order to help me and without who this thesis would be incomplete. My thanks go to Dr Iain Hargreaves and Dr Simon Eaton for their help with all things mitochondrial. I would also like to thank Prof David Warnock, your exceptional knowledge of the kidney has helped me to make sense of my results! Thanks also go to Prof John Wood and his group for completing the von Frey assays.

I would like to thank every member of the biological mass spectrometry unit, past and present that I have had the pleasure to work with, your help and more importantly your friendship has been a constant source of support. I particularly need to extend my thanks to Ernestas Sirka whose help has been invaluable.

Last but by no means least I would like to say a special thank-you to my parents who taught me that with hard work and determination anything is possible. However, without the support, love and encouragement of all of my family, particularly my partner Mark, I wouldn't have been able to complete this work.

Abstract

Fabry disease is an X-linked lysosomal storage disorder caused by a deficiency of the enzyme alpha-galactosidase A. The resultant progressive intracellular accumulation of the glycosphingolipids globotriaosylceramide (Gb_3) and globotriaosylsphingosine (lyso-Gb_3) are the source of a variety of clinical consequences. Biomarkers capable of detecting Fabry disease at an early stage of disease progression and that enable monitoring of response to treatment are required urgently.

Using a label-free quantitative proteomic methodology two potential biomarkers, proactivator polypeptide and ganglioside GM_2 activator protein, were identified in the urine of paediatric Fabry disease patients. An ultra-performance liquid chromatography-tandem mass spectrometry (UPLC-MS/MS) assay was then developed for verification and validation purposes. Subsequently a second, larger multiplexed assay was developed to identify biomarkers capable of detecting and monitoring pre-symptomatic kidney disease in those patients most at risk.

A complementary metabolomic approach was also used to identify and evaluate new Gb_3-related biomarkers in the plasma of Fabry disease patients. This aspect of the study revealed five novel Gb_3-related biomarkers as well as existing Gb_3-related analogues and isoforms providing a metabolic profile in these patients.

Potential disease mechanisms involved in Fabry disease were investigated by studying the interactions between proteins and those molecules involved in the glycosphingolipid pathway, with particular interest to Gb_3. A number of mitochondrial proteins were found to interact with Gb_3 resulting in the investigation of the effect of glycosphingolipids and their deacylated counterparts on ATP synthase activity. Increasing concentrations of Gb_3 and lyso-Gb_3 were shown to increase ATP synthase activity. Subsequently the activities of the enzymes preceding ATP synthase, the mitochondrial respiratory chain enzymes, were investigated in a Fabry mouse model. In this aspect of the study complex II/III activity was found to be significantly decreased in kidney tissues. Finally, the assessment of pain thresholds in mice has demonstrated a significant increase in sensitivity to applied mechanical stimuli following exposure to Gb_3 and lyso-Gb_3.

Table of Contents

Chapter 5 - Investigation of globotriaosylceramide and globotriaosylsphingosine toxicity in the Fabry mouse model 250

List of Figures

Chapter 1

Chapter 2

Chapter 3

Chapter 4

Chapter 5

Chapter 6

List of Tables

Chapter 2

Chapter 3

Chapter 4

Chapter 5

Chapter 6

Abbreviations

ACN	Acetonitrile
α-GAL	α-galactosidase A
ATP	Adenosine triphosphate
ADP	Adenosine diphosphate
AUC	Area under the ROC curve
BSA	Bovine serum albumin
Ca2+	Calcium ions
CID	Collision induced dissociation
CKD	Chronic kidney disease
CMA	Chaperone-mediated autophagy
CNS	Central nervous system
CoA	Coenzyme A
CS	Citrate synthase
CSF	Cerebrospinal fluid
Da	Dalton
DB	Disease burden
DNA	Deoxyribonucleic acid
DTE	Dithioerythritol
DTNB	5,5’-dithiobis-(2-nitrobenzoic acid)
EDTA	Ethylenediaminetetraacetic acid
EGTA	Ethylene glycol tetraacetic acid
eGFR	Estimated glomerular filtration rate
ER	Endoplasmic reticulum
ERT	Enzyme replacement therapy
ESI	Electrospray ionisation
eV	Electron volt
FA	Formic acid
FAD	Flavin adenine dinucleotide
FT-MS	Fourier transform ion cyclotron resonance mass spectrometry
FWHM	Full width at half maximum
Gb_3	Globotriaosylceramide
GM_2AP	Ganglioside GM_2 activator protein
GO	Gene ontology

GPM	Global proteome machine
GSG	1-β-D-glucosylsphingosine
h	Hour(s)
H_2O_2	Hydrogen peroxide
H_3PO_4	Phosphoric acid
HbA1c	Glycosylated haemoglobin
HCl	Hydrochloride
HEPES	Hydroxyethylpiperazine-N'-2-ethanesulfonic acid
HPLC	High performance liquid chromatography
ID	Internal diameter
K+	Potassium ion
KCN	Potassium cyanide
kDa	Kilodaltons
KOH	Potassium hydroxide
kV	Kilovolts
LC	Liquid chromatography
LV	Left ventricular
LVH	Left ventricular hypertrophy
LSD(s)	Lysosomal storage disorder(s)
Lyso-Gb_3	Globotriaosylsphingosine
MeOH	Methanol
min	Minute(s)
MRI	Magnetic resonance imaging
MRM	Multiple reaction monitoring
mRNA	Messenger ribonucleic acid
MS	Mass spectrometry
MS1	First mass analyser
MS2	Second mass analyser
MS/MS	Tandem mass spectrometry
mtDNA	Mitochondrial DNA
MWCO	Molecular weight cut-off
m/z	Mass-to-charge
Na+	Sodium ion
NAD	Nicotinamide adenine dinucleotide
NB-DNJ	N-butyldeoxynojirimycin

NBS	Newborn screening
O_2^-	Superoxide
OD	Optical density
·OH	Hydroxyl free radical
OPLS-DA	Orthogonal partial least square-discriminant analysis
OXPHOS	Oxidative phosphorylation
PAF	Platelet activating factor
PBS	Phosphate buffered saline
PSAP	Proactivator polypeptide
QToF	Quadrupole time-of-flight
ROS	Reactive oxygen species
RPC	Reverse phase chromatography
RMSEV	Root mean square error of validation
s	Second(s)
SAP(s)	Sphingolipid activator protein(s)
SD	Standard deviation
SPE	Solid phase extraction
SRT	Substrate reduction therapy
TFA	Trifluroacitic acid
ToF	Time-of-flight
Tris	Tris (hydroxymethyl) aminomethane
Tris-HCl	Tris (hydroxymethyl) aminomethane hydrochloride
UPLC™	Ultra performance liquid chromatography
UPS	Ubiquitin-proteasome system
V	Voltage
VDAC	Voltage dependant anion selective channel

Chapter 1

Introduction

Chapter 1 – Introduction 34

1.0 Introduction

1.1 The lysosome and lysosomal network

Following the first description of the lysosome in 1949 by Christian De Duve and colleagues as ‘a saclike structure containing a variety of acid hydrolases, surrounded by a membrane’ our understanding of the lysosome has evolved significantly. Far from been the ‘suicide bags’ of the cell as first thought lysosomes are now recognised as dynamic organelles characterised by the presence of a limiting external membrane, a low internal pH (4.5-5.0) maintained by proton-pumping vacuolar ATPases and vesicles containing many acid hydrolases (e.g. proteases, glycosidase, nuclease, lipases and phosphatases) responsible for receiving and degrading macromolecules from the phagocytic, autophagic and endocytic pathways (Saftig 2005; Walkley 2009). As a greater understanding of the lysosomes role in cellular biology develops it is becoming clear that lysosomes have a more complex role than simply as organelles dedicated to catabolism (Jeyakumar *et al.*, 2005).

1.1.1 The lysosomal system

The lysosomal system (Figure 1.1) is a major metabolic regulatory network requiring not only the transport of newly synthesised proteins to the lysosome but also the effective operation of the endosomal, autophagic and salvage pathways which are necessary to maintain this highly efficient and co-ordinated network. In addition, the ubiquitin-proteasome system operates in coordination with the lysosomal system ensuring efficient protein turnover. Ultimately at the centre of this intracellular network is the lysosome itself, demonstrating that

lysosomal function is essential, in order to maintain the operation and function of this complex system (Mehta and Winchester 2013; Walkley 2009).

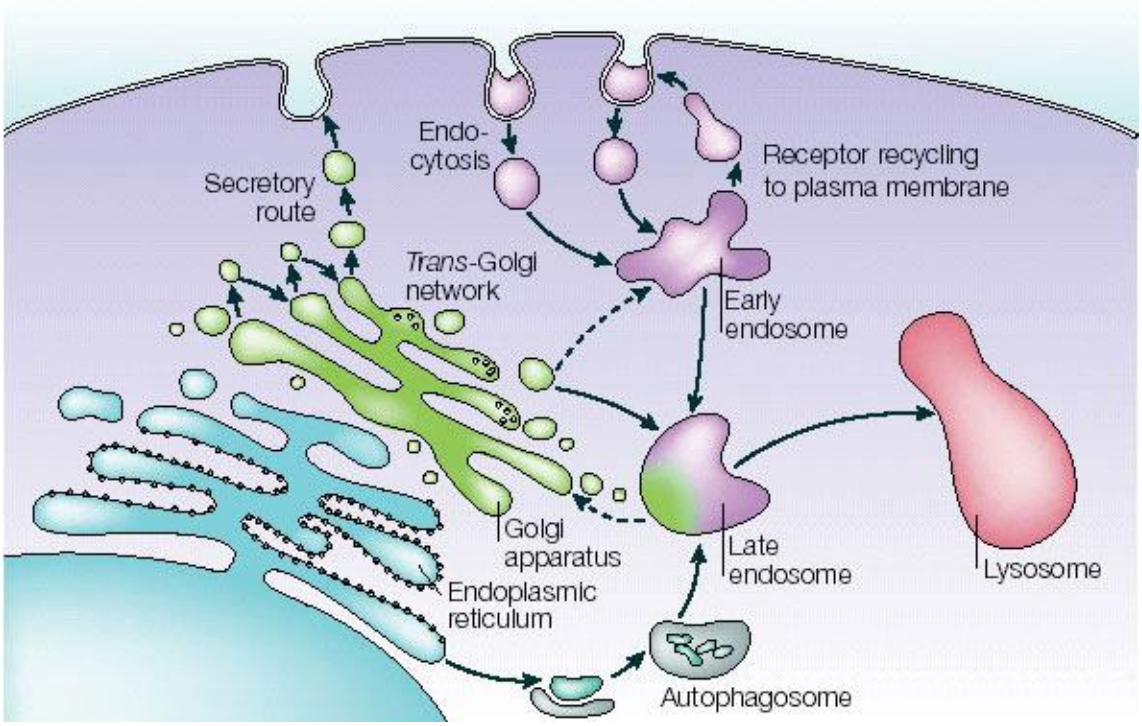

Figure 1.1 The lysosomal system and associated endocytic and autophagic pathways. Reproduced from Jeyakumar *et al.*, 2005.

1.1.2 Endocytosis and lysosome formation

A major function of the lysosome is the degradation of both extracellular and cell surface material delivered by endocytosis, a process which also plays a vital role in the formation of the lysosome (Figure 1.1) (Walkley 2009). The diverse nature of molecules at the cell surface requires a variety of endocytic pathways in order to mediate their internalisation. In addition to the classical clathrin-mediated endocytosis, clathrin-independent endocytic pathways such as macropinocytosis and phagocytosis have recently been described (Mayor and Pagano 2007). Following internalisation and delivery of material by

endocytic vesicles these compartments fuse with early endosomes, which go on to mature into late endosomes. An increasingly acidic gradient during endosome maturation is required to ensure that on fusion of late endosomes with transport vesicles from the Golgi apparatus the acid hydrolases which they are carrying are delivered effectively. Late endosomes mature into lysosomes as they acquire this full complement of lysosomal enzymes. Endosomes can also diverge from this pathway enabling this complex system to recycle and reorganise within the cell (Walkley 2009; Mayor and Pagano 2007; Saftig and Klumperman 2009).

1.1.3 The autophagic pathway for the degradation of intracellular materials

The autophagic pathway targets intracellular materials for degradation though sequestration of cellular materials in double-layered membrane structures termed phagophores (Hung *et al.*, 2013). Depending on how substrates are delivered to the lysosome autophagy can be divided into three subtypes - microautophagy, macroautophagy and chaperone-mediated autophagy (CMA). In microautophagy cytosolic components are sequestered to the lysosome by direct invagination of the lysosomal membrane and subsequent budding of vesicles into the lysosomal lumen (Marzella, Ahlberg and Glaumann 1981; Kunz, Schwarz and Mayer 2004). In macroautophagy, double membrane vesicles, known as autophagosomes, engulf cytosolic material and deliver it to the lysosome for degradation. Although once considered as a vesicle mediated bulk degradation mechanism, macroautophagy has recently been shown to be constitutively active and selective (Lemasters *et al.*, 2002 Klionsky and Schulman 2014). CMA is characterised by its selectivity for soluble monomeric

proteins with a specific peptide signalling motif recognised by heat shock cognate 70 protein which together with its co-chaperones promote protein unfolding and translocation across the lysosomal membrane via the lysosome-associated membrane protein type 2A (LAMP2A) (Kaushik and Cuervo 2012). Impairment of the autophagic pathway has been demonstrated in several lysosomal storage disorders however, the extent to which this impacts on downstream consequences for disease progression remains unclear (Settembre *et al.*, 2008; Fukuda *et al.*, 2006).

1.1.4 The salvage pathway for reutilisation of simple molecular products within a cell

Following degradation of molecules in the lysosome into simple molecular products they must be trafficked out of the lysosome in order to be transported to other organelles throughout the cell for reutilisation. This salvage process involves numerous lysosomal membrane proteins which act as transporters, defects in any such transporter can result in downstream shortages of enzymes essential for multiple metabolic processes within the cell (Ruivo *et al.*, 2009). Compromises in the salvage pathway can also lead to inadequate reutilisation of degradation products in synthetic pathways in the Golgi and in other organelles within the cell (Xie *et al.*, 1999). The cost of this to the cell in terms of energy consumption and altered regulatory processing is currently been investigated. However, needless to say reutilisation of simple molecular components would be favourable energetically over full de novo synthesis (Mehta and Winchester 2013).

1.1.5 The ubiquitin-proteasome system and degradation of protein within a cell

The ubiquitin-proteasome system (UPS) works in association with the autosomal/lysosomal system to maintain proteolytic quality control. In the first instance, it is the pathway responsible for the degradation of short-lived proteins within the cell and plays a vital role in cellular regulatory processes (Cook, Stetler, and Petrucelli 2012). In addition, the UPS is capable of coordinating proteolysis with the autosomal/lysosomal system under certain conditions, for example, if the UPS is inhibited, macroautophagy is upregulated in an attempt to maintain efficient protein degradation through the lysosome. The UPS and autophagic/lysosomal systems also rely on several vital molecules, most notably ubiquitin, to selectively target substrates for degradation. However, differences in the degradative capacity of these pathways mean that this complementation is limited. In circumstances where the lysosome is compromised and therefore unable to perform its role in cellular degradation, for example in a lysosomal storage disorder, it has been suggested that the UPS may be engaged to take care of some of the proteolytic load. It is as yet unknown if there is a limit where the burden on the UPS becomes so great that complete proteolytic failure results (Mehta and Winchester 2013).

1.2 Lysosomal storage disorders

The lysosomal storage disorders (LSDs) are a group of over 50 distinct metabolic diseases caused by defects in proteins essential for lysosomal function (Fuller, Meikle, and Hopwood 2006). These include lysosomal enzymes, lysosomal integral membrane proteins and proteins involved in the post-translational modification and trafficking of lysosomal proteins (Saftig and Klumperman 2009). The resultant consequence of a defect in any of these proteins is primarily a disruption in the catabolism and/or transport of by-products of cellular turnover. A secondary consequence is the accumulation of the undegraded substrate within the lysosome and other cell types (Parkinson-Lawrence *et al.*, 2010).

1.2.1 Clinical aspects and diagnosis of lysosomal storage disorders

The lysosomal storage disorders show extensive clinical heterogeneity (Beck 2001). Age at onset, organ involvement, disease severity and disease course differ significantly between each LSD (Beck 2001; Bekri 2006). There are some acute and severe LSD subtypes with clinical features such as hepatosplenomegaly, coarse facial features and skeletal dysplasia, that may be strongly suggestive of a LSD resulting in a rapid diagnosis (Pastores 2009). For many however, disease progression occurs over weeks, months and even years and the variable and non-specific nature of the presenting clinical symptoms can make diagnosis challenging (Wang *et al.*, 2011; Bekri 2006; Pastores 2009).

1.2.2 Laboratory diagnosis of lysosomal storage disorders

A universal diagnostic test for all LSDs is not currently available. Measurement of the structure and content of the accumulated substrate is often used in screening techniques performed as part of the primary assessment. However, the definitive diagnosis is based both upon clinical suspicion and the appropriate biochemical and/or genetic laboratory based test(s).

1.2.3 Genetic basis of lysosomal storage disorders

All LSDs are monogenic and whilst most are inherited in an autosomal recessive manner (Fuller, Meikle, and Hopwood 2006), there are three exceptions, these are; Fabry disease which follows X-linked inheritance (Germain 2006; Germain *et al.*, 2007), mucopolysaccharidosis type II (Hunter syndrome) which is inherited in an X-linked recessive manner and Danon disease which shows X-linked dominant inheritance (Fuller, Meikle, and Hopwood 2006).

1.2.4 Incidence and prevalence of lysosomal storage disorders

Although individually rare, when combined the LSDs occur with a high incidence. A number of countries have completed retrospective studies to establish the incidence of the LSDs calculated from the total number of patients identified divided by the total number of births during the same time period. In studies from Australia, The Netherlands and the Czech Republic similar incidences of 1 in 7,700 births (Meikle *et al.*, 1999), 1 in 7,100 births (Poorthuis *et al.*, 1999) and 1 in 8,000 births (Poupetová *et al.*, 2010), respectively were

reported. The highest incidence was reported in Northern Portugal where the occurrence of a LSD was 1 in 2,500 births (Pinto *et al.*, 2004).

More recently, newborn screening (NBS) studies performed in dried blood spots to assess the incidence of LSDs have been completed. This has been made possible largely due to advances in the capacity of mass spectrometers to rapidly, sensitively and selectively detect a large number of disorders in a single assay. One study, performed in an Austrian cohort consisting of samples from 34,736 newborn babies was designed to detect four LSDs, Gaucher, Fabry, Pompe and Niemann-Pick A/B. The study found a higher than expected combined incidence of these four LSDs occurring 1 in 2,315 births. The most prevalent was Fabry disease with an incidence of 1 in 3,589 births (Mechtler *et al.*, 2012). Another study performed on 40,024 samples from the Hungarian NBS program identified three cases of Gaucher disease, three cases of Fabry disease, and two cases of Niemann-Pick A/B (Wittmann *et al.*, 2012). An inherent flaw when using studies such as these to determine the incidence of a LSD is that information is provided on a finite number of diseases from this large group of disorders. However, the increased incidence detected from data on the few disorders studied suggests that data from retrospective studies show that LSDs are substantially under-diagnosed in the general population. Studies such as this are not without problems and raise numerous ethical issues not least the fact that a large proportion of patients detected in these studies will not require treatment due to the mild nature of their disease and some patients may never develop clinical manifestations of a LSD.

1.2.5 Classification of lysosomal storage disorders

The lysosomal storage disorders have historically been classified according to the nature of the substrate that accumulates and can broadly be grouped as lipidoses, mucopolysaccharidoses, glycoproteinoses, mucolipidoses and glycogen storage diseases. By classification in this way diseases are grouped according to disturbances in common catabolic pathways for a particular group of metabolites. This provides informative classifications for those diseases that result from a block in a single enzymatic step in a common catabolic pathway such as defects in the catabolism of the glycosphingolipids including those due to a defect in a sphingolipid activator protein (Figure 1.2) (Mehta and Winchester 2013).

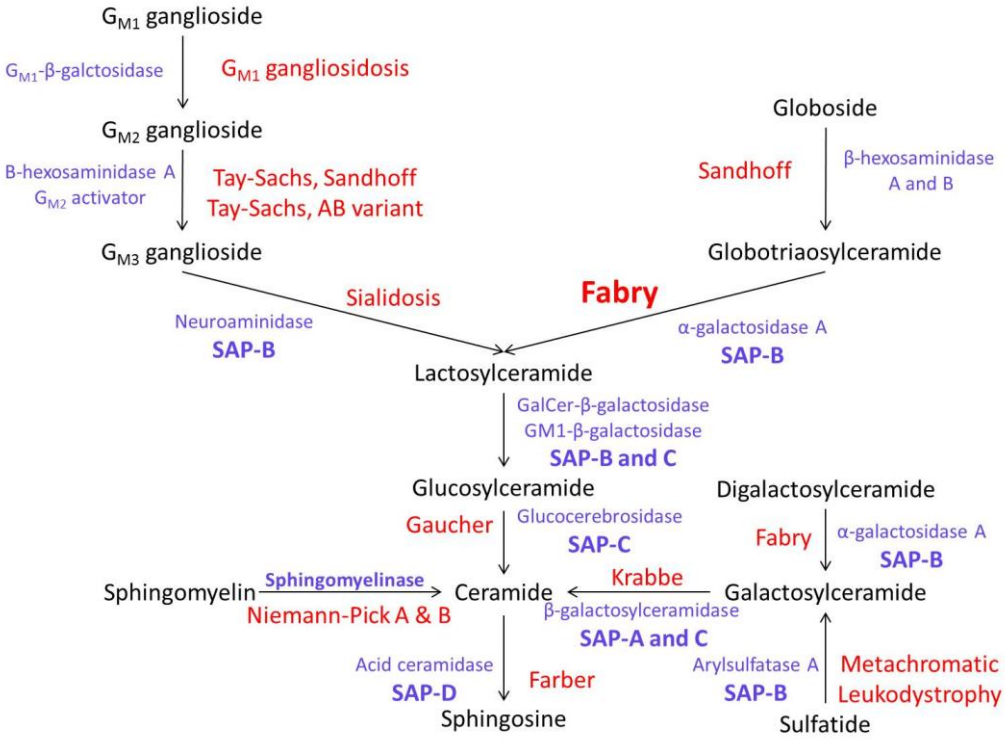

Figure 1.2 The glycosphingolipid biosynthetic pathway. Enzymes and sphingolipid activator proteins are shown in blue and the disease(s) associated with defects in the indicated enzyme are shown in red. Adapted from Platt and Walkley (2004).

1.3 Anderson-Fabry disease

Anderson-Fabry disease, now known simply as Fabry disease, was first described in 1898. Independently, William Anderson and Johannes Fabry described patients with ‘angiokeratoma corporis diffusum’ which is now recognised as one of the first visible signs of the disease. Other clinical symptoms were subsequently described before the lysosome was identified as the organelle responsible for this disease (Anderson 1898; Fabry 1898; Fabry 1916; Fabry 1930).

1.3.1 Genetics of Fabry disease

1.3.1.1 The *GLA* gene encodes α-galactosidase A

Fabry disease results from a deficiency of the enzyme α-galactosidase A caused by mutations in the *GLA* gene. The locus of the *GLA* gene is situated on the long arm of chromosome X, in position Xq22. The *GLA* gene is comprised of seven exons distributed over 12,436 base pairs (Kornreich, Desnick, and Bishop 1989).

1.3.1.2 *GLA* mutations in Fabry disease

To date over six-hundred mutations that result in Fabry disease have been described. The majority of mutations (~75 %) are point mutations, including an assortment of polymorphisms, missense, nonsense and splice site mutations. To a lesser extent short length rearrangements, mainly deletions and duplications are seen with large rearrangements involving one or more exons occurring infrequently (Blaydon, Hill, and Winchester 2001; Davies *et al.*, 1996;

Shabbeer *et al.*, 2006; Eng *et al.*, 1997; Germain *et al.*, 2002b; Ashley *et al.*, 2001; Ashton-Prolla *et al.*, 2000; Altarescu *et al.*, 2001; Sakuraba *et al.*, 1990; Topaloglu *et al.*, 1999). The majority of these mutations result in the production of non-functioning enzyme. Most families have unique ('private') *GLA* mutations which provides some explanation as to the vast phenotypic presentation of the disease. However, a high degree of variability is also observed both between members of the same family and unrelated patients carrying the same mutation (Germain 2010; Altarescu 2010).

1.3.1.3 Inheritance of Fabry disease

Inheritance of Fabry disease is X-linked (Germain 2006). Although disease symptoms present earlier and are generally more clinically severe in affected males, a large proportion of heterozygous females are also affected (MacDermot, Holmes, and Miners 2001; Whybra *et al.*, 2001; Wilcox *et al.*, 2008). The reason for this is attributed to random X-chromosome inactivation (Lyon 1961). In a process called lyonization, one of the two X chromosomes is randomly inactivated during the early stages of embryonic development. As the cells multiply each keeps the same pattern of inactivation. This results in a heterozygote for an X-linked disorder having 2 cell populations, one which will express the normal chromosome and the other which will express the abnormal chromosome. Variability in X-chromosome inactivation is thought to be responsible for the range of clinical and biochemical phenotypes experienced by females with the disease (Happle 1985; Germain 2006).

1.3.2 The structure of human α-galactosidase A

In 1967, Brady and colleagues showed that the defective protein responsible for Fabry disease was α-galactosidase A (α-gal A, also known as GLA and α-GAL) (E.C. 3.2.1.22). α-GAL is required for the removal of the terminal α-galactose groups from substrates such as glycoproteins and glycolipids. In Fabry disease a deficiency of functional α-GAL results in the progressive accumulation of neutral glycosphingolipids, primarily globotriaosylceramide (Gb_3) and globotriaosylsphingosine (lyso-Gb_3; Figure 1.3), in organs, tissues and biological fluids (Eng, Ioannou, and Desnick 2001).

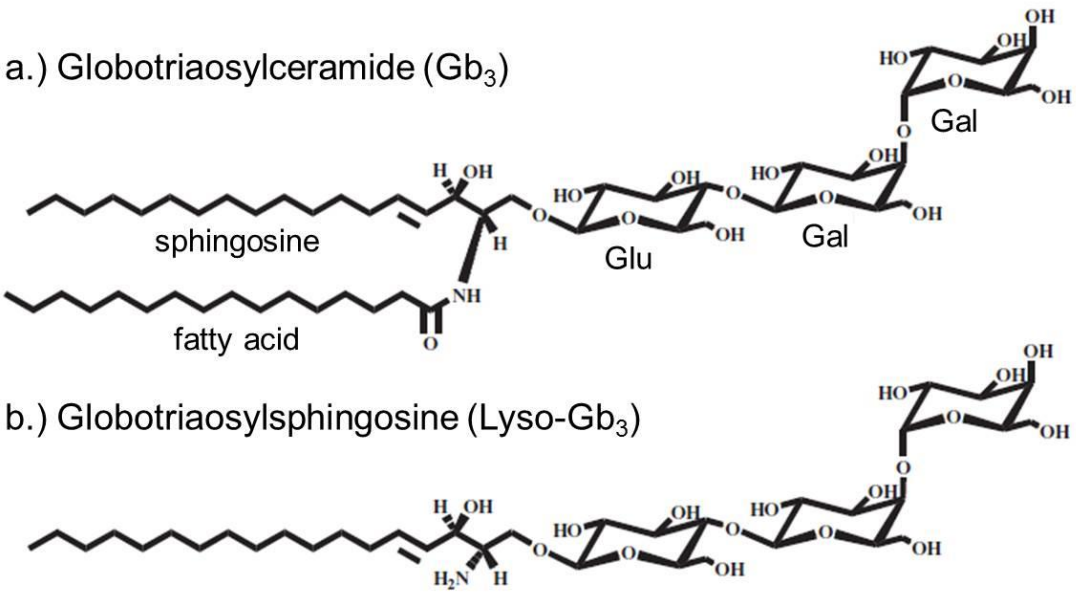

Figure 1.3 Molecular structures of a.) globotriaosylceramide (Gb_3) with palmitic acid (C_{16}) as fatty acid and b.) globotriaosylsphingosine (lyso-Gb_3). Glu: glucose, Gal: galactose.

The structure of human α-GAL was determined by X-ray crystallography in 2004. It was shown to be a homodimeric glycoprotein with each monomer

composed of two domains, a $(\beta/\alpha)_8$ domain containing the active site, and a C-terminal domain containing 8 antiparallel β-strands on two sheets in a β-sandwich (Figure 1.4) (Garman and Garboczi 2004). Three N-linked carbohydrates are located on the surface of the molecule, away from the location of the active sites and the dimer interface. These N-linked carbohydrates are essential for the correct folding and trafficking of this molecule to the lysosome via the mannose-6-phosphate receptor pathway. The dimer has a pronounced negative charge, consistent with a molecule that is most stable in the low pH of the lysosome (Ioannou *et al.*, 2001; Garman and Garboczi 2004).

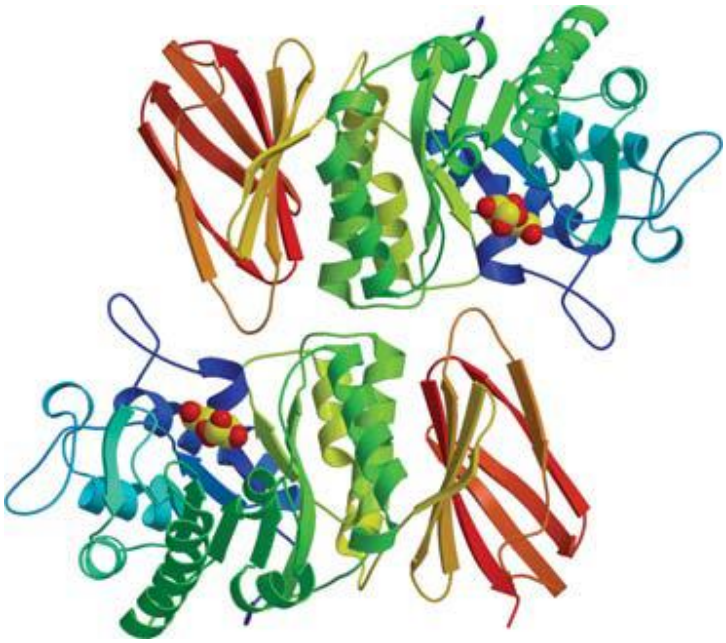

Figure 1.4 The structure of human α-galactosidase A in ribbon presentation. Reproduced from Garman 2007. The ribbon is coloured from blue to red as the polypeptide goes from *N*- to *C*-terminus. The active site is identified by the catalytic product galactose, shown in sphere Corey-Pauling-Koltun (CPK) format. Each monomer in the homodimer contains two-domains, a (β/α)8 barrel containing the active site (blue to yellow) plus a *C*-terminal antiparallel β-domain (yellow to red).

Garman and Garboczi (2004) also elucidated the structure of α-GAL in complex with its catalytic product, the α-galactose monosaccharide, in order to determine how the enzyme cleaves galactose from glycoproteins and glycolipids. As a result, the location of two aspartic acid residues at D170 and D231, which act as a nucleophile and an acid/base respectively, have shown that the enzyme uses a double displacement reaction mechanism in order to cleave terminal α-galactose residues off the substrate and therefore are responsible for the catalytic mechanism of this enzyme (Garman and Garboczi 2004; Garman 2007).

Determination of the structure of α-GAL provides a step toward answering vital questions regarding the structure and function of this enzyme and its relationship to disease processes. Mapping the mutations that result in Fabry disease onto the structure of α-GAL has revealed three groups of mutations: those that compromise the active site leading to loss of enzyme activity, those that perturb the hydrophobic core resulting in folding defects in the protein and those that result in other alterations to the structure such as broken disulphide bonds. The class of mutations that most lead to Fabry disease have been shown to result from perturbation of the hydrophobic core of the protein and as such Fabry disease is primarily caused as a result of protein misfolding. The structure of α-GAL can therefore, to some extent, enable treatment to be tailored to the nature of the mutation. For example, patients with a defect in the hydrophobic core may benefit more from pharmacological chaperone therapy (section 1.3.9.2) which can assist in the correct folding of the enzyme from the endoplasmic reticulum. Whereas for patients with a defect in the active site where the folded protein does not have catalytic capacity, the use of a pharmacological chaperone that assists in the correct folding of the protein is

not likely to show efficacy and enzyme replacement therapy (section 1.3.9.1) may be a more appropriate treatment option (Garman and Garboczi 2004; Garman 2007).

1.3.3 Incidence of Fabry disease

The classic Fabry disease phenotype has an estimated incidence of ~1 in 40,000 – 60 000 males (Desnick, Ioannou, and Eng 2001; Meikle *et al.*, 1999). Recently, the recognition of later-onset variants in males with renal (Choi *et al.*, 2012; Nakao *et al.*, 2003; Ichinose *et al.*, 2005), cardiac (Nakao *et al.*, 1995; von Scheidt *et al.*, 1991; Beer *et al.*, 2002) and cerebrovascular (Brouns *et al.*, 2010; Baptista *et al.*, 2010; Rolfs *et al.*, 2005) disease has suggested that the occurrence of this lysosomal storage disorder is more frequent than historically documented. As a result a number of newborn screening studies, assaying α-GAL activity in dried blood spots have been performed to determine the disease incidence. The frequency of later-onset variants was found to be ~1 in 3100 males in an Italian cohort (Spada *et al.*, 2006), ~1 in 1250 males in a Taiwanese cohort (Hwu *et al.*, 2009) and ~1 in 3859 in an Austrian cohort (Mechtler *et al.*, 2012). Identification of these patients would be beneficial in enabling early therapeutic intervention, genetic counselling and familial screening. However, it raises significant ethical issues for consideration as to the appropriate timing of screening and therefore treatment (i.e. in the neonatal period or at early maturity) for these late onset variants (Müller *et al.*, 2012).

1.3.4 Clinical manifestations of Fabry disease

Fabry disease begins primarily in infancy, or even as early as the fetal stage of development (Bouwman *et al.*, 2010; Popli *et al.*, 1990; Vedder *et al.*, 2006).

However, most patients remain asymptomatic during the first years of life. The average age of onset of the first clinical symptoms is reported to be between 3 and 10 years in boys and a few years later in girls (Hopkin *et al.*, 2008; Wilcox *et al.*, 2008). Lysosomal storage of glycosphingolipids resulting in cellular dysfunction is believed, in part, to be responsible for the multisystemic nature of this disease which progresses with advancing age.

1.3.5 Early signs of Fabry disease

There are a number physical signs associated with Fabry disease that are often apparent during childhood and adolescence. These include neuropathic pain, angiokeratomas, dyshidrosis, gastrointestinal disturbances, ophthalmological, auditory and vestibular abnormalities. Identification of these symptoms is vital in obtaining an early diagnosis and for monitoring of disease progression to ensure the appropriate timing for therapeutic intervention.

1.3.5.1 Neuropathic pain

The neuropathic pain in Fabry disease may be chronic or experienced as episodic Fabry ‘crises’ or acroparaesthesiae. The pain is described as a numbness, tingling or burning sensation in one of more of the extremities. Acroparathesia is believed to result from ischemia of the peripheral nerves or lysosomal accumulation of glycosphingolipids in neurons, dorsal root ganglia and the spinal cord (Lidove, Jaussaud, and Aractingi 2006; Zarate and Hopkin 2008). It occurs most often in males (MacDermot, Holmes, and Miners 2001; Mehta *et al.*, 2004) but also affects a significant number of females with Fabry disease (Whybra *et al.*, 2001; Deegan *et al.*, 2006; Larralde *et al.*, 2004). Painful crises lasting from a few minutes to several days may develop, these can occur

suddenly or be exacerbated by heat, illness, stress or exercise (Lidove, Jaussaud and Aractingi 2006).

1.3.5.2 Angiokeratoma

Angiokeratomas are benign vascular skin lesions characterised by proliferation of dilated blood vessels in the upper dermis and are considered a hallmark of Fabry disease (Figure 1.5) (Lidove, Jaussaud and Aractingi 2006). They are reported to be present in 83 % of male and 80 % of female patients with Fabry disease (Larralde *et al.*, 2004). They may often be the first physical sign of disease presenting during childhood on the knees, elbows and flanks, and increase in both size and number with age becoming visible on the lips, hands and feet (Zampetti *et al.*, 2012; Lidove, Jaussaud and Aractingi 2006).

Figure 1.5 Typical angiokeratomas observed in Fabry disease. Reproduced from (Pastores 2009).

1.3.5.3 Dyshidrosis

Disrupted sweating is a common clinical manifestation of Fabry disease attributed to both a direct effect on the sweat glands as well as to autonomic neuropathy (Zarate and Hopkin 2008). Hypohidrosis (inability to correctly perspire) is reported to have a higher prevalence in males (> 50 %) than females (> 25 %) often manifesting during childhood (Ries *et al.*, 2003). Hypohidrosis results in decreased tolerance to heat and exercise and can have a significant impact on quality of life (Lidove, Jaussaud and Aractingi 2006). Hyperhidrosis (increased sweating) is less common in Fabry disease however, it is reported to be more prevalent in females (14.5 %) than males (4.1 %) (Ramaswami *et al.*, 2006; Lidove *et al.*, 2006).

1.3.5.4 Gastrointestinal disturbances

Gastrointestinal involvement is a frequent and early manifestation in Fabry disease (Hopkin *et al.*, 2008; Ramaswami *et al.*, 2006; Hoffmann *et al.*, 2007a). The most common gastrointestinal symptoms reported are abdominal pain (often after eating) and diarrhoea but constipation, nausea and vomiting have also been reported (Hoffmann *et al.*, 2007a; Hoffmann *et al.*, 2007b). It has been suggested that these symptoms could be as a result of the deposition of Gb_3 in the autonomic ganglia of the bowel and mesenteric blood vessels (Eng *et al.*, 2006).

1.3.5.5 Ophthalmological abnormalities

Whorled corneal opacities (cornea verticillata) that do not affect vision are the most common ocular abnormality in Fabry disease (Figure 1.6), often reported

in childhood (Ramaswami *et al.*, 2006) and frequently observed in adults with disease (Orssaud, Dufier and Germain 2003; Nguyen *et al.*, 2005; Sodi *et al.*, 2007). Vessel tortuosity, cataracts and enlargement of the blind spot have also been noted in Fabry disease but in fewer cases (Orssaud, Dufier and Germain 2003; Cox-Brinkman *et al.*, 2007).

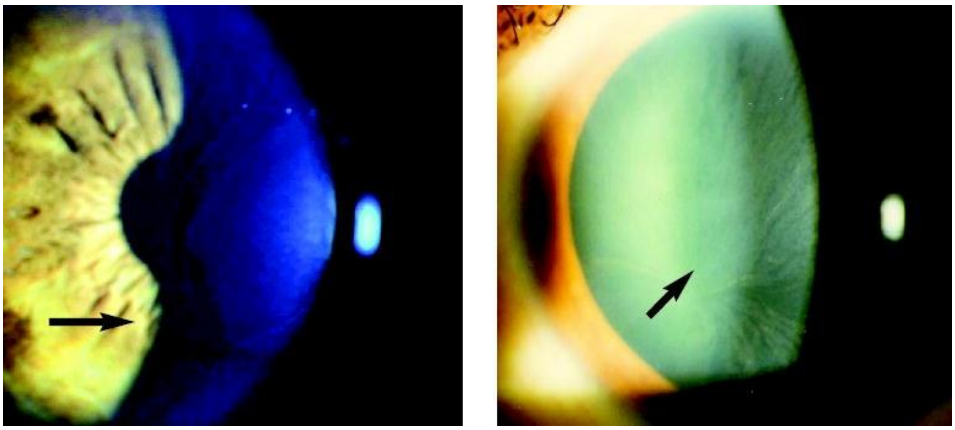

Figure 1.6 Cornea verticillata characteristic of Fabry disease (indicated by arrows). Reproduced from Sodi, Ioannidis and Pitz 2006.

1.3.5.6 Auditory and vestibular abnormalities

A number of auditory and vestibular deficits have been reported in Fabry disease including high frequency sensorineural hearing loss (Sergi *et al.*, 2010; Germain *et al.*, 2002a; Sakurai *et al.*, 2009), tinnitus and vertigo (Conti and Sergi 2003; Germain *et al.*, 2002a). Progressive hearing loss (Palla *et al.*, 2007; Germain *et al.*, 2002a) and sudden deafness (Germain *et al.*, 2002a) has also been reported in a number of cases.

1.3.6 Major organ involvement in Fabry disease

With advancing age the myriad of symptoms experienced by Fabry disease patients develop. This includes worsening of the clinical manifestations that develop in childhood as well as the progression to major organ dysfunction with cardiac, renal and cerebrovascular disease developing in many patients.

1.3.6.1 The heart and cardiovascular dysfunction in Fabry disease

Cardiac involvement is the major cause of morbidity in Fabry disease and cardiac symptoms are reported in approximately 40-60% of both male and female patients with the disease (Kampmann *et al.*, 2002; Senechal and Germain 2003; Schiffmann *et al.*, 2009; Linhart *et al.*, 2000; Shah *et al.*, 2005). These include dyspnoea, angina, chest pain, palpitations and syncope which occur as a result of the development of progressive cardiac hypertrophy, conduction abnormalities and arrhythmias (Linhart 2006). Accumulation of Gb_3 has been shown in cardiomyocytes, conduction system cells, valvular fibroblasts, endothelial cells within all types of vessels and vascular smooth muscle cells (Hůlková *et al.*, 1999). However, it is believed that the amount of stored Gb_3 alone is insufficient to explain the observed level of cardiac involvement in this disease (Linhart 2006).

Left ventricular structural changes are the predominant finding in patients with Fabry disease (Weidemann *et al.*, 2005; Linhart *et al.*, 2000; Kampmann *et al.*, 2002; Senechal and Germain 2003). The hypertrophy, as with other aspects of the disease, is progressive and occurs earlier in males than females. However, despite concentric remodelling and other less common structural changes, systolic function appears to be largely preserved when assessed using conventional techniques such as ejection fraction or fractional shortening

(Weidemann *et al.*, 2005; Linhart *et al.*, 2007; Kampmann *et al.*, 2002; Senechal and Germain 2003; Linhart *et al.*, 2000; Linhart and Elliott 2007). Tissue Doppler imaging has shown that the cardiomyopathy in Fabry disease is characterised by a substantial decrease in myocardial contractile performance and relaxation tissue Doppler velocities. This technique can also be used to provide a pre-clinical diagnosis of Fabry cardiomyopathy (Weidemann *et al.*, 2005; Pieroni *et al.*, 2003; Pieroni *et al.*, 2004). Recently, advances in non-contrast T1 mapping by cardiovascular magnetic resonance imaging (MRI) have been shown to provide a useful measure of left ventricular hypertrophy (LVH) in Fabry disease. This technique has the potential to detect not only early cardiac involvement but also the ability to distinguish LVH due to Fabry disease with LVH attributable to other causes (Sado *et al.*, 2013).

Right ventricular hypertrophy has also been reported in Fabry disease. In two thirds of patients this occurred in addition to LVH and has been shown to have a similar prevalence in both males and females with the disease (Palecek *et al.*, 2008). In addition, a recent study has shown that the degree of right ventricular involvement was directly related to the left ventricular cardiomyopathy stage (Niemann *et al.*, 2010). Ultimately, right ventricular involvement progresses to severe diastolic right ventricular dysfunction (Germain 2010).

A number of other cardiac manifestations have been described in patients with Fabry disease. These include abnormal coronary microvascular function (Elliott *et al.*, 2006), bradycardia resulting in the requirement of a pacemaker (O'Mahony *et al.*, 2011), reduced exercise capacity (Bierer *et al.*, 2005; Lobo *et al.*, 2008), autonomic dysfunction (Hilz *et al.*, 2010), aortic root dilation (Germain 2010) and sudden cardiac death (Linhart *et al.*, 2007).

1.3.6.2 The development of kidney disease and renal involvement in Fabry disease

Renal impairment is reported in approximately 50 % of patients with Fabry disease and often begins with proteinuria in the second to third decade of life (Schiffmann *et al.*, 2009; Branton *et al.*, 2002; Mehta *et al.*, 2004). Proteinuria has also been reported in a number of children and adolescents with Fabry disease (Ramaswami *et al.*, 2006; Hopkin *et al.*, 2008). However, biopsy studies have demonstrated that changes in glomerular and vascular architecture are evident before detectable proteinuria and suggest that at present biopsy may be required for the early detection of renal disease (Tøndel *et al.*, 2008).

As in diabetic nephropathy, the degree of proteinuria is thought to directly contribute to the progression of renal involvement in Fabry disease and worsens with advancing age (Fervenza, Torra, and Lager 2008; Schiffmann *et al.*, 2009). Resultant decline in renal function by the fourth to fifth decade of life is evident by the presence of fibrosis, sclerosis and tubular atrophy which indicates development to end stage renal disease (Ortiz *et al.*, 2008; Schiffmann *et al.*, 2009; Branton *et al.*, 2002). The cause of death of a large proportion of both treated (Mehta, *et al.*, 2009b; Waldek *et al.*, 2009) and untreated (Schiffmann *et al.*, 2009) Fabry patients is attributable to renal disease. However, data from the Fabry Outcome Survey and the Fabry Registry indicates that this is improving, most likely as a result of the improved management of renal disease in these patients (Waldek *et al.*, 2009; Mehta *et al.*, 2009b).

1.3.6.3 Cerebrovascular involvement in Fabry disease

Fabry patients may experience a variety of cerebrovascular manifestations ranging from mild to severe which can include headache, vertigo/dizziness, transient ischaemic attacks (TIAs) and strokes (Sims *et al.*, 2009; Mitsias and Levine 1996; Clavelou *et al.*, 2006; Mehta *et al.*, 2004; Buechner *et al.*, 2008). As with other symptoms associated with Fabry disease these neurological features generally occur earlier in males than females, typically during the third and fourth decade of life respectively (Sims *et al.*, 2009; Mehta *et al.*, 2004). Renal and cardiac disease may already be present at the onset of neurological involvement (Mehta *et al.*, 2005; Sims *et al.*, 2009). However, data from the Fabry Registry shows that in over 70 % of both males and females with the disease, stroke occurred in the absence of other major organ participation (Sims *et al.*, 2009).

A number of imaging techniques can be used to assess cerebrovascular involvement in Fabry disease including MRI (Fellgiebel *et al.*, 2009), trans-cranial Doppler (TCD) (Hilz *et al.*, 2004) and positron emission tomography (PET) (Fellgiebel *et al.*, 2007). These neuroimaging techniques can depict white matter lesions, dolichoectasia, territorial or lacunar strokes and increased tortuosity of the basilar artery (Viana-Baptista 2012; Germain 2010). A highly specific finding, visible by T1 weighted MRI, which is distinctly characteristic of Fabry disease, is the so called “pulvinar sign”, and has been described in both males (Moore *et al.*, 2003; Viana-Baptista 2012; Burlina *et al.*, 2008) and more recently females (Burlina *et al.*, 2012) with the disease. In addition, the presence of the pulvinar sign is more frequently observed in males with cardiomyopathy and severe kidney disease suggesting that there may be a

correlation with the presence of this neurological finding and disease severity (Germain 2010; Burlina *et al.*, 2008).

1.3.7 Other symptoms associated with Fabry disease

1.3.7.1 Depression and quality of life

Depression is a frequent but under-recognised finding in Fabry disease (Germain 2010). In the limited number of studies that have been completed a high proportion of both male and female Fabry patients suffer from acute and often lifelong depression (Cole *et al.*, 2007; Sadek *et al.*, 2004; Crosbie, Packman and Packman 2009; Müller *et al.*, 2006). This can have a serious impact on quality of life in patients with Fabry disease which has been demonstrated using a variety of different assessment criteria (Miners *et al.*, 2002; Street *et al.*, 2006; Gold *et al.*, 2002).

1.3.7.2 Dysmorphology

Dysmorphism, whilst not as prominent in Fabry disease as some of the other lysosomal storage disorders has been reported (Cox-Brinkman *et al.*, 2007; Ries *et al.*, 2006b). Fabry patients share common morphological characteristics of the face, trunk and extremities (Ries *et al.*, 2006b). However, although these differences have been shown to be significant discrimination between affected patients and healthy controls is very small (Cox-Brinkman *et al.*, 2007).

1.3.7.3 Skeletal involvement

In a study of 23 males affected with classic Fabry disease, bone mineral density of the lumbar spine and femoral neck was assessed, osteopenia or osteoporosis was detected at one or both sites in 88% of cases (Germain *et al.*, 2005a; Germain *et al.*, 2005b). Further studies have subsequently been performed confirming the presence of skeletal involvement in Fabry disease (Mersebach *et al.*, 2007; Sacre *et al.*, 2010).

1.3.7.4 Respiratory involvement

Airway obstruction, most likely as a result of glycosphingolipid accumulation, has been reported in 26 % of females and 61 % of males with Fabry disease (Magage *et al.*, 2005; Magage *et al.*, 2007). Other recognised aspects of respiratory involvement in Fabry disease include dyspnea, wheezing and a chronic cough (Rosenberg *et al.*, 1980; Brown *et al.*, 1997). These symptoms are progressive with advancing disease (Wang *et al.*, 2008; Brown *et al.*, 1997; Magage *et al.*, 2007) in an age and gender dependent manner (Magage *et al.*, 2007).

1.3.7.5 Anaemia

Mild peripheral blood cytopenias, particularly anaemia, have been shown to be present in a large number of patients with Fabry disease as shown by data obtained from the Fabry Outcome Survey and the Fabry registry (Kleinert *et al.*, 2005; Oliveira *et al.*, 2008).

1.3.7.6 Telangiectasiae

Telangiectasiae are the second most common dermatological manifestation reported in Fabry disease and are small widened blood vessels on the skin. They occur on photodamaged areas such as the face and the 'V' of the neck (Zampetti *et al.*, 2012; Giuseppe, Daniele and Rita 2013).

1.3.7.7 Lymphoedema

Lymphoedema has been reported in Fabry disease and is caused by a blockage of the lymphatic system resulting in swelling of the arms and/or legs. In Fabry disease this blockage is most likely related to the accumulation of glycosphingolipids in the lymph vessels (Lidove, Jaussaud and Aractingi 2006).

1.3.7.8 Miscellaneous

Other less common manifestations reported in Fabry disease include arterial remodelling and intima media thickening (Boutouyrie *et al.*, 2002; Boutouyrie *et al.*, 2001; Barbey *et al.*, 2006). In a small study hypothyroidism was found in 36% of patients (Hauser *et al.*, 2005). In addition, priapism has also been reported in a small number of patients with Fabry disease (Backenroth *et al.*, 2010; Foda *et al.*, 1996; Labarthe *et al.*, 2010).

1.3.8 Diagnosis of Fabry disease

Although most patients with Fabry disease present with symptoms in early childhood, these symptoms are not necessarily specific to the disease. Hence, there is often a significant delay between the onset of symptoms before a diagnosis is confirmed and treatment can be initiated. Like all LSDs, Fabry

disease is progressive in nature and once suspected a diagnosis can be obtained relatively quickly using the appropriate biochemical and/or genetic laboratory based test(s).

1.3.8.1 Enzymatic assay

The gold standard laboratory method for confirming the diagnosis of Fabry disease in males, is the demonstration of decreased α-GAL activity in leukocytes (Mayes *et al.*, 1981). A plasma assay may also be used although there have been reports of false positive results been obtained (Hoffmann *et al.*, 2005). Enzyme activity for determination of Fabry disease in females is not a reliable indicator of disease as many females demonstrate α-GAL activity that falls within the normal range (Linthorst *et al.*, 2005). Therefore, all females suspected of having Fabry disease should have a diagnosis confirmed by mutation analysis (Germain 2010).

1.3.8.2 Globotriaosylceramide (Gb_3) measurement

Gb_3, the major metabolite that accumulates in Fabry disease (Figure 1.3), is routinely used to assess disease burden and monitor response to therapy. It has also been proposed and is currently used, as a first line screen, in the biochemical diagnosis of Fabry disease, enabling the identification of the majority of males and females with the disease (Mills *et al.*, 2005; Auray-Blais *et al.*, 2007; Auray-Blais *et al.*, 2008) However, whilst Gb_3 levels in urine have been shown to be more reliable than those in plasma, Gb_3 is not elevated in patients with certain mutations raising some concerns about the use of this biomarker in the diagnosis of Fabry disease (Young *et al.*, 2005; Mills *et al.*, 2005).

1.3.8.3 DNA analysis in the diagnosis of Fabry disease

Confirmatory diagnosis of Fabry disease in males can be obtained by mutation analysis (Froissart, Piraud and Maire 2010). In addition, a definitive diagnosis of Fabry disease by genetic analysis is required in heterozygous females, due to the often normal α-GAL activity (Caudron *et al.*, 2005; Linthorst *et al.*, 2005). Many advances have been made since genotyping became available, including developments in the technologies capable of genetic analysis as well as publication of both the complementary (Bishop *et al.*, 1986) and genomic DNA (Kornreich, Desnick and Bishop 1989) sequences of the *GLA* gene. These advances combined with the small size of the *GLA* gene has made molecular analysis to characterise mutations in Fabry disease relatively simple. Furthermore, a method that allows genotyping on DNA extracted from a dried blood spot on filter paper has recently been published. This method allows both enzymatic and confirmatory mutation analysis to be performed on a single sample (Hagège *et al.*, 2011).

1.3.9 Treatment of Fabry disease

Since the first enzyme replacement therapy (ERT) became available for Gaucher disease (Barton *et al.*, 1991) much progress has been made in the development of not only ERT for the LSDs but also in the development of novel therapies such as chaperone therapy and substrate reduction therapy.

1.3.9.1 Enzyme replacement therapy

Enzyme replacement therapy is a therapeutic approach for LSDs based on the intravenous administration of the deficient enzyme. Currently two products,

agalsidase alfa (Replagal, Shire, HGT) and agalsidase beta (Fabrazyme, Genzyme Corporation) are licensed for use as enzyme replacement therapies in Fabry disease. Agalsidase alfa is produced in a human cell line and is infused at 0.2 mg/kg over a period of forty minutes, every two weeks. Agalsidase beta is produced in a Chinese hamster ovary (CHO) cell line and is infused at a dose of 1.0 mg/kg over a period of up to four hours every two weeks. Although both glycoprotein products have the same amino acid sequences the difference in production between a human or CHO cell line results in different glycosylation at the N-linked carbohydrate attachment sites. Agalsidase alfa contains a larger proportion of complex carbohydrate compared to agalsidase beta which has a larger fraction of sialylated and phosphorylated carbohydrate. As the polypeptide sequence of the two glycoproteins is identical these differences in carbohydrate composition are thought to be solely responsible for the differences in tissue distribution and dose response of the two ERTs (Garman and Garboczi 2004).

Efficacy data from the initial randomised controlled clinical trial of agalsidase alfa after six months showed improved renal structure and function, improved cardiac conduction and decreased levels of pain and plasma Gb_3 concentrations (Schiffmann *et al.*, 2001). Likewise the initial randomised controlled clinical trial of agalsidase beta showed that after twenty weeks of treatment plasma and tissue Gb_3 levels were reduced and pain scores had improved (Eng *et al.*, 2001). Following the initial randomised controlled clinical trials a vast array of studies have been completed to assess the efficacy of both enzyme preparations. In general, these studies have demonstrated normalisation of Gb_3 levels in a variety of tissue types and biological fluids for the majority of Fabry patients. In addition, overall measures of disease burden

have been shown to be reduced (Motwani *et al.*, 2012) and occurrence of major organ involvement has been shown to be delayed (Banikazemi *et al.*, 2007). However, a recent study suggests that the long term outcome with ERT is one of limited effectiveness (Rombach *et al.*, 2013).

1.3.9.1.1 Effect of ERT on cardiac function

A progressive decrease in intraventricular septum thickness and a decrease or stabilisation in left ventricular mass has been shown following up to 24 months of ERT (Spinelli *et al.*, 2004; Hughes *et al.*, 2008). One study reported the greatest response was observed in patients who display a degree of hypertrophy at baseline (Beck *et al.*, 2004). However, Kalliokoski *et al.*, (2006) found that after 12 months of ERT patients who displayed hypertrophy at baseline showed a poorer response than those that did not. Improvements in LVH and regional myocardial function have also been observed following 12 months of therapy (Weidemann *et al.*, 2003). More recently, a long-term report following 3 years of ERT (Weidemann *et al.*, 2009) has shown significant cardiac benefits by demonstrating improved myocardial function, reduced left ventricular mass, and increased exercise capacity. In addition, long-term data from the Fabry Outcome Survey has demonstrated a sustained reduction of left ventricular mass following 5 years of ERT and a significant increase in mid-wall fractional shortening after 3 years of therapy (Mehta *et al.*, 2009a).

1.3.9.1.2 Effect of ERT on renal function

In a number of studies creatinine clearance and estimated glomerular filtration rate (eGFR) have been shown to remain stable following treatment with agalsidase alfa following up to 2 years of ERT (Beck *et al.*, 2004; Schwarting *et*

al., 2006; Choi *et al.*, 2008; Dehout *et al.*, 2003) and in another study after up to 36 months of treatment (Wilcox *et al.*, 2004). Similar findings have been reported in patients treated with agalsidase beta after 54 months of treatment (Germain *et al.*, 2007). In those patients where there is a mild to moderate degree of Fabry nephropathy ERT has been shown to slow the decline in eGFR in some patients (West *et al.*, 2009). However, for those patients with more advanced nephropathy and/or overt proteinuria (> 1 g per day) ERT has little, if any, effect (Germain *et al.*, 2007; West *et al.*, 2009). Therefore the initiation of treatment before substantial renal involvement occurs may be required in order to prevent or, at the very least delay, renal disease in patients with Fabry disease (Schiffmann *et al.*, 2009).

1.3.9.1.3 Effect of ERT on cerebrovascular events

A limited number of studies performed in small patient cohorts have resulted in conflicting evidence regarding the effect of ERT on cerebrovascular events. An initial report showed progression of white matter lesions in 2 out of 7 patients following one year of therapy (Jardim *et al.*, 2004). In contrast, Yamadera *et al.*, (2009) report amelioration of white matter lesions in a single patient with Fabry disease following ERT. In a larger study, long-term data following 25 males with Fabry disease over 4.5 years of treatment with agalsidase alfa has shown that during the time period studied 16 % of patients suffered a cerebrovascular accident or a transient ischaemic attack (Schiffmann *et al.*, 2006). Ideally, a study of patients not receiving ERT is required to establish the progression of cerebrovascular involvement in Fabry patients, only then will conclusions be able to be drawn as to the effectiveness of ERT on this clinical parameter.

1.3.9.1.4 ERT in females with Fabry disease

A number of studies looking at the effectiveness of ERT in relatively small numbers of female patients have been completed. In general, a more favourable clinical course is observed for female patients with a degree of stabilisation in renal function and a stabilisation or reduction in left ventricular mass. An overall reduction in the prevalence of body pain in females has also been documented and ERT has been shown to be well tolerated (Whybra *et al.*, 2009; Hughes *et al.*, 2011; Rombach *et al.*, 2013).

1.3.9.1.5 ERT in children with Fabry disease

Several studies have specifically documented the effects of ERT in paediatric populations. ERT has been shown to reduce pain scores, improve pain-related quality of life, increase sweat volume and reduce gastrointestinal symptoms and acroparathesia (Ries *et al.*, 2006a; Ramaswami *et al.*, 2007; Wraith *et al.*, 2008; Mills *et al.*, 2005). More recently, a study looking at the effects of ERT over a 4-year period (Schiffmann *et al.*, 2010) and the largest observational study to date (Ramaswami *et al.*, 2012) have shown similar results to those published previously. Further follow-up studies are required in order to understand fully and assess any long-term benefits of initiating treatment when there is little disease burden.

1.3.9.2 Pharmacological chaperone therapy

The aim of chaperone therapy is to use small molecules to selectively bind and stabilise target proteins in order to help normal folding. This ‘tricks’ the ER quality control system into allowing the protein to reach its final destination, the

lysosome. This results in improved intracellular trafficking and increased lysosomal enzyme activity, instead of the mis-folded but potentially catalytically active protein being exported and degraded by the proteasome. Chaperone therapy is suitable for use where small conformational changes are present but is not expected to restore the effect of mutations that cause major structural changes (van Gelder *et al.*, 2012; Valenzano *et al.*, 2011). As large gene rearrangements represent less than 10% of mutations occurring in Fabry disease pharmacological chaperone therapy could provide an attractive alternative treatment option (Ishii 2012). In addition, small molecule drugs are beneficial as they can be administered orally, they have the potential to access most cell types, they are able to cross the blood brain barrier (BBB) and access the central nervous system (CNS), and the cost of treatment is significantly lower than ERT.

A number of *in vitro* studies have demonstrated the benefits of chaperone therapy (Valenzano *et al.*, 2011) and Fabry disease became the first LSD to benefit from a clinical trial using intravenously administered galactose as the pharmacological chaperone (Frustaci *et al.*, 2001). More recently, the investigation of a small molecule drug which is a competitive inhibitor of α-GAL, 1-deoxygalactonojirimycin (DGJ, migalastat HCl, Amigal™), for use in Fabry disease both as an oral monotherapy and in combination with ERT has begun. Two phase III global studies for migalastat HCl monotherapy are currently underway following promising outcomes in preliminary studies. The first phase III trial will assess the efficacy, safety and pharmacodynamics of the oral administration of migalastat HCl in over 60 male and female Fabry patients. The second phase III clinical trial is to compare the safety and efficacy of migalastat HCl compared to ERT in over 50 patients with Fabry disease.

Preclinical studies using migalastat HCl in combination with ERT have demonstrated that the chaperone may improve the function of the α-GAL infused enzyme and be able to address some of the underlying limitations currently experienced when ERT is used alone (Benjamin *et al.*, 2012). In addition, a phase II drug-drug interaction study evaluating the co-administration of migalastat HCl and ERT has been completed and plans are currently underway for a repeat dose clinical study to be performed.

1.3.9.3 Substrate reduction therapy

Substrate reduction therapy (SRT) involves the use of drugs, often small molecules, in order to inhibit substrate synthesis thereby, reducing substrate levels and decreasing storage burden (Beck 2010; Pastores 2009; Schultz *et al.*, 2011; van Gelder *et al.*, 2012). For the glycosphingolipidoses this can be achieved by inhibiting the enzyme glucosylceramide synthase which catalyses the first step in the synthesis of glycosphingolipids and therefore subsequent molecules, including Gb_3 (Marshall *et al.*, 2010). SRT reduces the level of substrate to a point where residual enzyme activity is sufficient to prevent substrate accumulation. Ultimately, the action of these small molecules is therefore dependent on the presence of residual endogenous enzyme and as such this therapeutic option is only suitable for those patients having mutations which result in some conserved enzyme activity (Pastores 2009).

The use of N-butyldeoxynojirimycin (NB-DNJ), an imino sugar analog and glucosylceramide synthase inhibitor has been approved for use in Type I Gaucher disease. The investigation of the use of NB-DNJ in a mouse model of Fabry disease has produced promising results, including reduction of Gb_3 (Abe *et al.*, 2000; Heare *et al.*, 2007). However, NB-DNJ is associated with adverse

side effects that may compound Fabry disease symptoms, for example gastrointestinal disturbances and peripheral neuropathies, and has therefore not been approved for use (Hollak *et al.*, 2009).

The use of eliglustat tartrate (Genzyme Corporation), another inhibitor of glucosylceramide synthase, has been shown to be effective as both a monotherapy and in combination with ERT in a mouse model of Gaucher disease. This success prompted investigations of eliglustat tartrate in a mouse model of Fabry disease following which reductions in tissue Gb_3 levels were reported. The greatest effects were seen when eliglustat tartrate was used in combination with ERT (Marshall *et al.*, 2010).

Substrate reduction therapy has the potential to be used as a complementary or additive therapy to ERT, thereby improving the therapeutic management of Fabry disease. However, as the majority of male Fabry patients have very little residual enzyme activity substrate reduction therapy as a monotherapy will only be an appropriate and effective therapeutic option in a small proportion of patients (Marshall *et al.*, 2010).

1.3.10 Biomarkers in Fabry disease

The definition of a biomarker is “a characteristic that is objectively measured and evaluated as an indicator of normal biological processes, pathogenic processes or pharmacological responses to a therapeutic intervention” (Hulka 1990; Naylor 2003). In lysosomal storage disorders accumulating primary and secondary metabolites or proteins make good candidates for biomarkers (Aerts *et al.*, 2011). Currently two biomarkers globotriaosylceramide (Gb_3) (Mills *et al.*, 2005; Auray-Blais *et al.*, 2008) and globotriaosylsphingosine (lyso-Gb_3) (Aerts *et al.*, 2008) (Figure 1.3) are routinely used to assess disease burden and

monitor response to therapy in Fabry disease. Gb_3 levels can be reliably determined in urine and plasma by tandem mass spectrometry (Young *et al.*, 2005; Mills *et al.*, 2005; Mills *et al.*, 2004; Auray-Blais *et al.*, 2007). Urinary Gb_3 levels have been shown to be more useful than Gb_3 levels in plasma (Young *et al.*, 2005) however, Gb_3 has not proven to be an ideal biomarker. As Gb_3 is not significantly elevated in a large proportion of female heterozygotes this biomarker cannot be used to monitor response to treatment in patients who initially have Gb_3 levels within the normal range. In addition, falls in urinary Gb_3 in patients receiving ERT are not sustained in all cases despite clinical improvement (Mills *et al.*, 2005). A more recent study has identified a number of novel Gb_3 isoforms in the urine of Fabry patients (Auray-Blais and Boutin 2012). In the small number of untreated patients that were studied variable levels of excretion of the biomarkers was observed (Auray-Blais and Boutin 2012). Further studies are required on a larger cohort of patients to establish if measurement of these analogs will provide a better degree of correlation with disease severity, progression and response to treatment.

Lyso-Gb_3, a deacylated form of Gb_3, has also been proposed as a potentially useful diagnostic marker of Fabry disease (Aerts *et al.*, 2008). As with Gb_3, this cationic amphiphile, possesses a large polar sugar moiety making it relatively hydrophilic and water-soluble. Various hypotheses have been suggested as to the origin of lyso-Gb_3 including, its spontaneous formation from stored Gb_3, active formation by the action of a specific enzyme and formation by sequential glycosylation of sphingoid bases (Aerts *et al.*, 2008). However, as yet the origin of lyso-Gb_3 remains unknown. Following the identification of lyso-Gb_3 a number of studies have been completed to assess the level of this biomarker in both the plasma and urine of Fabry patients (Aerts *et al.*, 2008; Rombach *et al.*, 2010;

Auray-Blais *et al.*, 2010; van Breemen *et al.*, 2011). This analyte has been found to be elevated in both males and to a lesser extent in females with the disease. In addition, it appears to show a good degree of correlation with severity of disease manifestation and response to ERT (Aerts *et al.*, 2008; Auray-Blais *et al.*, 2010; Togawa *et al.*, 2010; van Breemen *et al.*, 2011; Rombach *et al.*, 2010). More recently newly defined lyso-Gb_3 analogs in plasma and urine from Fabry patients have been described (Dupont *et al.*, 2013; Auray-Blais *et al.*, 2012). Interestingly, the excretion of the majority of these analogs in urine was shown to be significantly elevated above the excretion of lyso-Gb_3 itself (Dupont *et al.*, 2013; Auray-Blais *et al.*, 2012).

Another potential biomarker having a structural resemblance to lyso-Gb_3 has been proposed recently. Sphingosine-1-phosphate (S1P) is a biologically active growth-promoting factor involved in cardiovascular remodelling in both males and females with Fabry disease (Brakch *et al.*, 2010). S1P levels in males were shown to be significantly higher than those of controls and levels in both males and females showed a good degree of correlation with left ventricular mass index and increased carotid intima media thickening (Brakch *et al.*, 2010).

The recent identification of S1P and a number of novel isoforms of both Gb_3 and lyso-Gb_3 suggests that the use of only Gb_3 and/or lyso-Gb_3 as biomarkers in Fabry disease provides a limited view of this complex disease (Auray-Blais and Boutin 2012, Auray-Blais *et al.*, 2012). This could provide an explanation as to why discrepancies in levels of these metabolites and clinical outcome have been observed. It remains to be seen if these recently identified biomarkers will indeed prove to be ideal biomarkers that provide a better correlation with disease severity, progression and response to treatment. It may be that no single biomarker is available for Fabry disease and in order to have the most

comprehensive understanding of this complex disease a panel of appropriate biomarkers is required.

Following the identification of potential biomarkers their extensive validation is required prior to use in clinical practice. The first stage of validation requires the selection of the most appropriate candidate assay, for example, the use of an ELISA based method or a mass spectrometry based assay. The next stage of validation requires both the development of the assay and subsequent experimentation to ascertain performance parameters of the method including evaluation of accuracy, precision, reproducibility, sensitivity, specificity and evaluation of the assay range (LLOQ-ULOQ). Folowing the development of an assay fitness-for-purpose testing is performed to assess the robustness of the assay and to identify any potential problems with patient sampling such as collection, storage and stability issues. Only when these parameters have been ascertained can the verification of biomarkers identified during the biomarker discovery experiments be performed. Larger cohorts of patients can now be analysed in order to confirm the validity of the biomarker/s and demonstrate links to pertinent clinical endpoints or processes. Once the validity of a biomarker/s has been proven the final stage of biomarker validation requires the assay to enter routine use, where quality control (QC) monitoring, proficiency testing and batch-to-batch QC performance parameters are required to be continually assessed to ensure the performance of the assay is maintained (Cummings *et al.*, 2010).

1.4 Mass spectrometry and biomarker discovery

Numerous advances in biological and analytical applications in recent years have led to an increasing interest in the identification and quantitation of

candidate biomarkers. Mass spectrometry (MS), when coupled with liquid chromatography (LC), is a powerful analytical technique capable of sensitive and selective detection, multi-analyte analysis and an ability to provide structural information. Owing to these attributes mass spectrometry has become increasingly important in the detection, validation and quantitation of biomarkers using both proteomic and metabolomic rationales (Ackermann, Hale, and Duffin 2006; Cravatt, Simon, and Yates 2007; Griffiths and Wang 2009).

A number of fundamental steps are required for all types of proteomic and metabolomic methodologies, these include: (i) sample preparation; (ii) sample separation by liquid chromatography; (iii) mass spectrometry analysis and; (iv) data acquisition and analysis.

1.4.1 Sample preparation

Sample preparation is a key step in proteomic and metabolomic analyses and has a direct impact on the quality of the final data obtained. By using the most appropriate preparation procedures both ion suppression and adduct formation can be minimised and the best instrument performance can be maintained (Issaq and Veenstra 2013).

1.4.2 Proteomics

Proteomics encompasses the identification and quantitation of all the expressed gene products of a cell, i.e. the proteins. The identification, structure and function of a protein is defined by a specific amino acid sequence. However, in order to sequence a protein it must first be converted into peptides, which fall within an appropriate mass range for MS analysis. This can be achieved with the use of a protease, a number of which are available. Trypsin, a sequence-

specific protease, is one of the most specific and robust proteolytic enzymes and acts by hydrolysing peptide bonds at the carboxylic groups of arginine and lysine. This protease creates positive charges at the cleavage site which is beneficial for analyses using MS. As a result, trypsin is often the protease of choice for the digestion of proteins prior to sample separation and MS analysis (Swaney, Wenger, and Coon 2010).

1.4.3 Metabolomics

Metabolomics is the characterisation of the small molecule metabolites found in an organism. Prior to analysis metabolites need to be effectively extracted from the matrix in which they are contained. For biological samples, such as urine and plasma, this is most often achieved with liquid-liquid extraction (Álvarez-Sánchez, Priego-Capote, and Castro 2010). In general, a polar aqueous solution, for example methanol, is paired with a non-polar organic solvent, such as chloroform, to create a two-phase system. When this immiscible solution is added to the biological sample compounds within the matrix distribute between the two layers based on their relative solubility. Thus permitting the separation of polar and non-polar metabolites, this chemical separation step also reduces the complexity of the analogues and reduces ion suppresion prior to subsequent chromatographic separation and analysis (Issaq and Veenstra 2013).

1.4.4 Sample separation by liquid chromatography

Prior to MS analysis the peptides and metabolites in a biological sample are required to be separated by liquid chromatography. This process also allows simultaneous desalting of the sample, which can reduce the effects of ion

suppression by salts and other co-eluting molecules. In effect, greater separation of peptides or metabolites before they enter the mass spectrometer will enable better, more robust detection and identification of both proteins and metabolites (Aebersold and Mann 2003).

1.4.5 High performance liquid chromatography

High performance liquid chromatography (HPLC) is an analytical technique used to separate components of a mixture through the mass-transfer of analytes between stationary and mobile phases. The liquid mobile phase, carrying the analytes of interest, is pumped at a high pressure (500 – 2000 psi) through the stationary phase, in the form of a HPLC column packed with particles > 2µm. Individual components of the mixture separate based on their affinity for the solid and mobile phase, with each emerging from the column at separate time points. This separation may be manipulated through different choices of stationary phase and by changing the physico-chemical properties of the mobile phase (Prichard 2003). HPLC enables the simultaneous desalting and separation of analytes, including the separation of isomers, thereby reducing ion suppression.

1.4.6 Ultra performance liquid chromatography™

Ultra performance liquid chromatography™ (UPLC™) is based on the same chromatographic principles as HPLC but uses columns packed with smaller particles (< 2µm) and which are able to withstand ultra-high pressures (up to 15,000 psi). This enables UPLC™ to separate compounds at increased speeds with superior resolution and sensitivity (Swartz 2013).

1.4.7 Reverse phase chromatography

In HPLC and UPLC™, reverse phase chromatography (RPC) is commonly used and separates compounds according to their polarity. In RPC the use of a chromatography column composed of hydrophobic alkyl chains which retain hydrophobic compounds over hydrophilic ones is employed. A solvent gradient of increasing organic content (often either acetonitrile or methanol) is used to elute the compounds in order of their hydrophobicity. The more polar a compound, the greater its affinity for the polar mobile phase, the less it will interact with the non-polar stationary phase and will thus be eluted from the column more quickly than less polar compounds. RPC allows compounds with a wide range of polarities to be separated achievable by manipulating the polarity of the mobile phase (Westermeier, Naven and Höpker 2008).

1.4.8 Liquid chromatography mass spectrometry

When HPLC or UPLC™ is coupled with mass spectrometry the separating power of liquid chromatography and the mass analysing capabilities of mass spectrometry are combined to create a powerful analytical technique amenable to automation. The separation and reduction in complexity of biological samples by liquid chromatography reduces ion suppression and enables the percentage of proteome or metabolome coverage achievable by the mass spectrometer to be considerably increased. This in turn maximises the biomarker discovery potential available using this methodology (de Hoffmann and Stroobant 2013).

1.4.9 Basic principles of mass spectrometry

Mass spectrometry is an analytical technique that separates ions according to their mass-to-charge (*m/z*) ratio (Griffiths and Wang 2009). To achieve this outcome all mass spectrometers are composed of three main components: an ion source, a mass analyser and a detector (Figure 1.7).

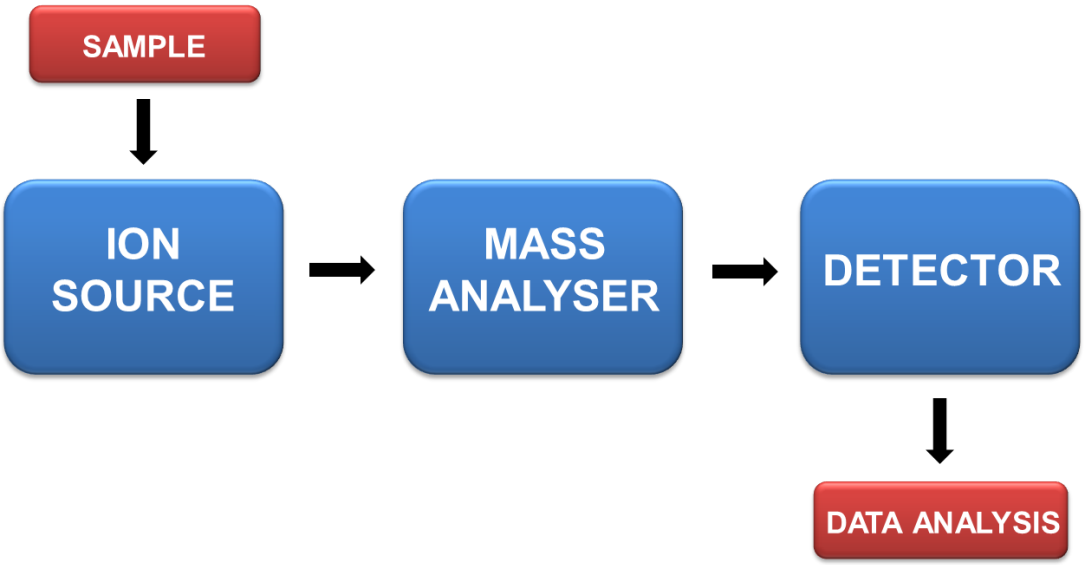

Figure 1.7 Schematic representation of the basic components of a mass spectrometer.

1.4.10 The ion source

In the ion source, the analyte of interest becomes ionised prior to analysis in the mass spectrometer. A number of ionisation techniques are available, the choice of which is dependent on the physico-chemical properties of the sample/analyte under investigation.

1.4.11 Electrospray ionisation

In 1989, John Fenn introduced electrospray ionisation (ESI), a soft ionisation technique, with the ability to ionise intact non-volatile, thermally labile biomolecules. The charged ions resulting from ESI are transferred into the gaseous phase where they can be subjected to mass analysis. The ESI process begins following the elution of biomolecules from a liquid chromatography column where they enter a static ion source through a narrow-bore metal or glass capillary tip which has a high electrical potential applied, (1.5 – 6.0 kV) relative to the counterelectrode (Fenn *et al.*, 1989). As the liquid begins to exit the capillary, the surface becomes highly charged and assumes a conical shape, referred to as the Taylor cone. At the tip of the Taylor cone, the liquid changes shape into a fine jet. This jet however, becomes unstable, breaking up into a fine mist of finely charged droplets (Figure 1.8). Once the droplets are airborne, the solvent evaporates, with the aid of nitrogen drying gas and the surface area of the charged droplet decreases until the charge density on the surface of the droplet reaches a critical limit termed the Raleigh limit. Once the Raleigh limit is surpassed the ions become so unstable they explode to form even smaller droplets in what is known as the Coulomb explosion (Chapman 2000; Ho *et al.*, 2003). Finally, the electrical field becomes large enough to allow desorption of the ions which can then be transported to the mass spectrometer through a series of focusing lenses by electrical fields and are held in a vacuum (Iribarne and Thomson 1976; Thomson and Iribarne 1979). The type of mass analyser used for analysis is dependent on the information required.

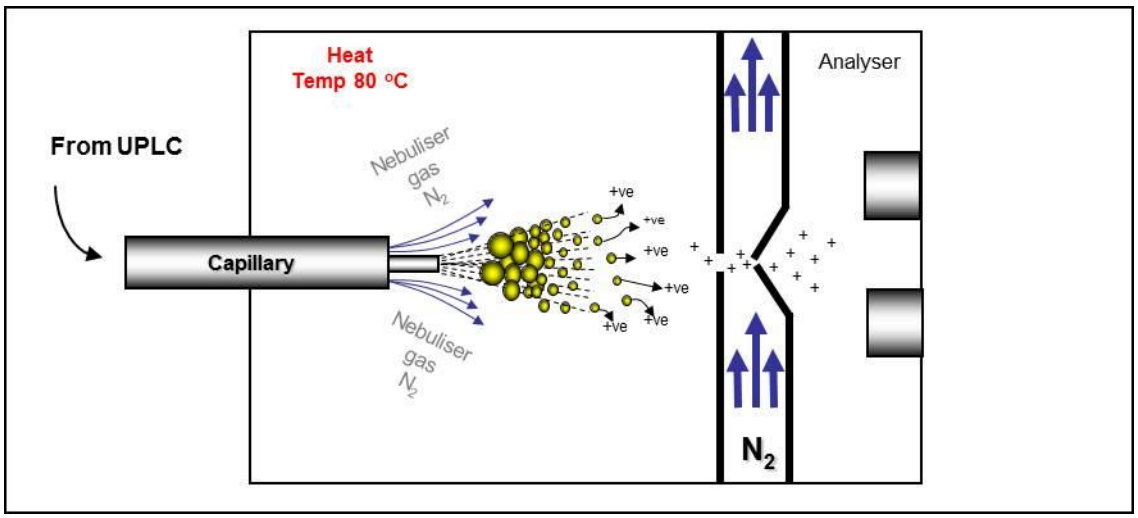

Figure 1.8 Schematic representation of an electrospray ionisation source. N_2 = nitrogen gas.

An important feature of ESI as with other soft ionisation techniques is that minimal fragmentation of the molecule of interest is produced allowing its molecular mass to be determined. When coupled to a mass spectrometer this provides a sensitive, robust and reliable tool for studying biomolecules some of which are not amenable to analysis by other conventional techniques. ESI can also be combined with UPLC™ for in-line molecular fractionation prior to mass spectrometric analysis allowing analysis of both small and large molecules of various polarities in a complex biological sample (Banerjee and Mazumdar 2012).

1.4.12 The mass analyser

The mass analyser is crucial to mass spectrometry analyses. Its key parameters include sensitivity, resolution, mass accuracy and the ability to generate spectra. A number of mass analysers are available including time-of-

flight, quadrupole time-of-flight, ion trap sector and triple quadrupole instruments. Each is different in design and performance and possesses its own strengths and weaknesses (Aebersold and Mann 2003).

1.4.13 Time-of-flight mass spectrometry

The basic principle of time-of-flight (ToF) MS is relatively simple and often used for the detection of peptides and proteins (Figure 1.9). A rapidly pulsing electrical field introduces product ions into the (field-free drift path) flight tube of the ToF mass analyser. Initially, ions are accelerated from the same position, at the same time, at identical kinetic energy. As a result, lighter ions fly faster and arrive earlier at the detector than heavier ones. The velocity of an ion is unambiguously related to its mass-to-charge (*m/z*) ratio therefore, the time it takes for an ion to travel through the flight tube and reach the detector directly indicates its mass (Gross 2011).

1.4.14 Quadrupole time-of-flight mass spectrometry

The quadrupole time-of-flight (QToF) is a hybrid mass spectrometer which combines quadrupole/collision cell technology with an orthogonally situated time-of-flight analyser (Figure 1.9). QToF instruments have been used extensively for both the detection of peptides and the identification of metabolites. Following ESI, ions enter the quadrupole mass analyser (MS1), which functions to filter/select ions based on their *m/z* ratio. The instrument consists of four parallel circular metal rods, around which an electric field is generated by applying a combination of a direct current DC (U) and a radio frequency AC (V) voltage of opposite polarities to opposite connected pairs. The field causes the ions to oscillate in x and y directions and it is alterations in both

these frequencies that allow ions, with a selected *m/z*, to pass through the mass analyser and either into a second mass analyser or a detector in a stable trajectory field. Other ions that have unstable trajectories, under that specific voltage, collide with the rods and are ejected from the quadrupole.

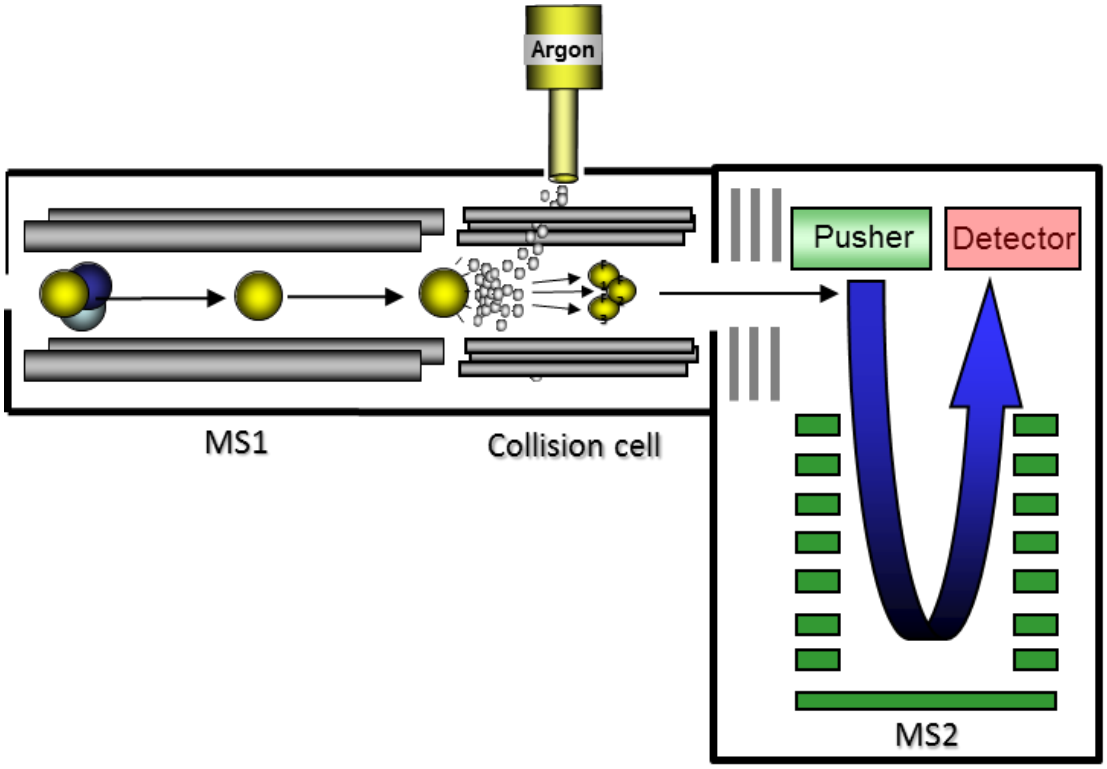

Figure 1.9 Schematic representation of a quadrupole time of flight mass spectrometer. Note: in ToF-MS the first quadrupole (MS1) is operated in scan mode and functions only to focus ions into the collision cell and second quadrupole (MS2) for subsequent detection.

Ions of a selected *m/z* (precursor ions) then enter the collision cell where they are fragmented by collision-induced dissociation using an inert gas such as argon. The fragments (product ions) are formed mainly by the cleavage of amide bonds between amino acids and can be categorised into b and y ions. The formation of b-ions occurs when the charge is retained by the amino-

terminal fragment, whereas y-ions are formed when the charge is retained by the carboxy-terminal fragment (Steen and Mann, 2004). Product ions are then introduced into the orthogonally situated flight tube of the ToF mass analyser (MS2) for detection and an MS/MS spectrum of the fragments (y- and/or b-ions) is generated (Figure 1.10). It should be noted that by operating in MS^E mode, the simultaneous fragmentation of all ions in a single LC-MS run without selecting a specific precursor ion is possible. In this mode the energy in the collision cell is alternated between low energy (MS) and higher energy (MS^E) scans. The low energy data provide information about intact precursor ions, whereas high energy data contain ion fragmentation data. The precursor and their product ions are easily linked and combined by their common retention times (Ivleva, Yu and Gilar 2010).

Ideally, the resulting MS/MS spectrum for a particular peptide ion would consist of a series of b- and y-ions, where each neighbouring fragment ion differed by one amino acid. The fact that each amino acid has a unique mass, with the exception of leucine and isoleucine, therefore allows the mass difference between neighbouring ions to be used to determine the amino acid sequence of that peptide. In effect, sequence determination by MS is based on the mass of the amino acids (de Hoffmann and Stroobant, 2002).

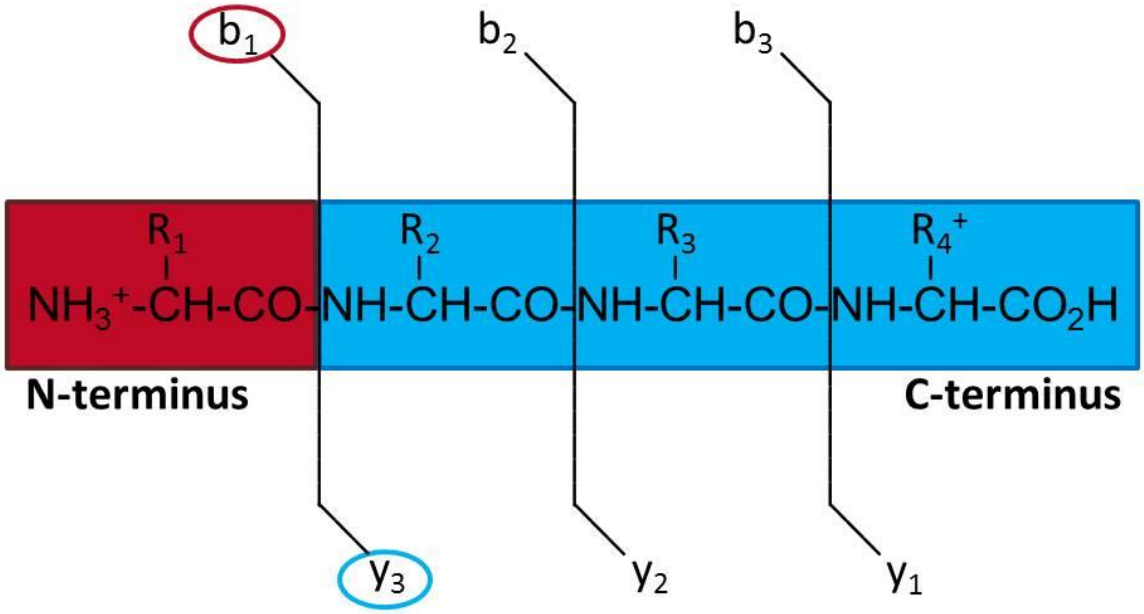

Figure 1.10 Schematic representation of fragmentation into b- and y-ions. Peptide fragments are indicated by b, if the charge is retained on the N-terminus and by y, if the charge is maintained on the C-terminus.

1.4.14.1 Label-free quantitative proteomics

The ability to profile high numbers of proteins, from multiple sets of complex biological mixtures, provides huge potential for disease biomarker discovery. Label-free quantitative proteomics is a novel adaptation of the protein sequencing method described in section 1.4.14 and allows the simultaneous identification and quantitation of proteins from complex biological samples. The process is based on the observation that the concentration of a detected ion is linearly proportional to the intensity in ESI-MS (Levin *et al*., 2007). As a result, protein samples can be spiked with known concentrations of standard proteins from an unrelated species and comparisons made between the intensities of the internal standard peptide ions. The use of nano UPLC-QToF-MS for label-free quantitative proteomics allows each sample to be analysed individually and

sequentially and puts virtually no constraint on the number of samples being compared. The relatively low cost of this methodology, in comparison to label-based methods such as iTRAQ which require expensive reagents, as well as the ability to add intact enolase prior to digestion thereby providing compensation for the trypsin efficiency, also make this an attractive analytical option. However, to be used for biomarker discovery, it is essential that reproducibility exists across multiple control samples to ensure that detected differences reflect biological and not experimental variation. Label-free quantitative proteomics provides an alternative or complementary technique to label-based proteomic methodologies and is a valuable tool in biomarker discovery with the potential to increase our understanding of the aetiology of disease.

1.4.15 Ion trap mass analysers

Ion-trap mass analysers work on the basic principle of trapping ions in circular orbit and use an electric or magnetic field to isolate molecules of specific *m/z* prior to mass spectrometric analysis.

1.4.15.1 Fourier transform ion cyclotron resonance mass spectrometry

Fourier transform ion cyclotron resonance mass spectrometry (FT-MS) determines *m/z* ratio based on the cyclotron frequency of an ion in a fixed magnetic field. Ions are first trapped where they are excited to a larger cyclotron radius by an oscillating electric field orthogonal to the magnetic field. Following the removal of the excitation field, ions rotate in “packets” at their cyclotron frequency. As these “packets” of ions pass a pair of electrodes a charge is

induced and the resultant free induction decay (FID) signal is extracted by performing a Fourier transform to produce a mass spectrum (Marshall, Hendrickson, and Jackson 1998).

The strengths of FT-MS are high sensitivity, mass accuracy, resolution and dynamic range. However, the expense, complexity and low peptide-fragmentation achievable using this technique have limited its use in mass spectral research.

1.4.15.2 Orbitrap™ mass analyser

The Orbitrap™ mass analyser is comprised of two outer electrodes and a central electrode which holds the trap together. Ions are injected into the volume between central and outer electrodes where the electrostatic attraction towards the central electrode is compensated by a centrifugal force that arises from the initial tangential velocity of ions. The electrostatic field ions are subjected to inside the Orbitrap™ causes them to move in complex spiral patterns. The axial component of these oscillations is independent of initial energy, angles and positions and can be detected as an image current on the two halves of an electrode encapsulating the Orbitrap™ (Figure 1.11). A Fourier transform is used to obtain oscillation frequencies enabling accurate *m/z* ratios to be determined (Scigelova and Makarov 2006).

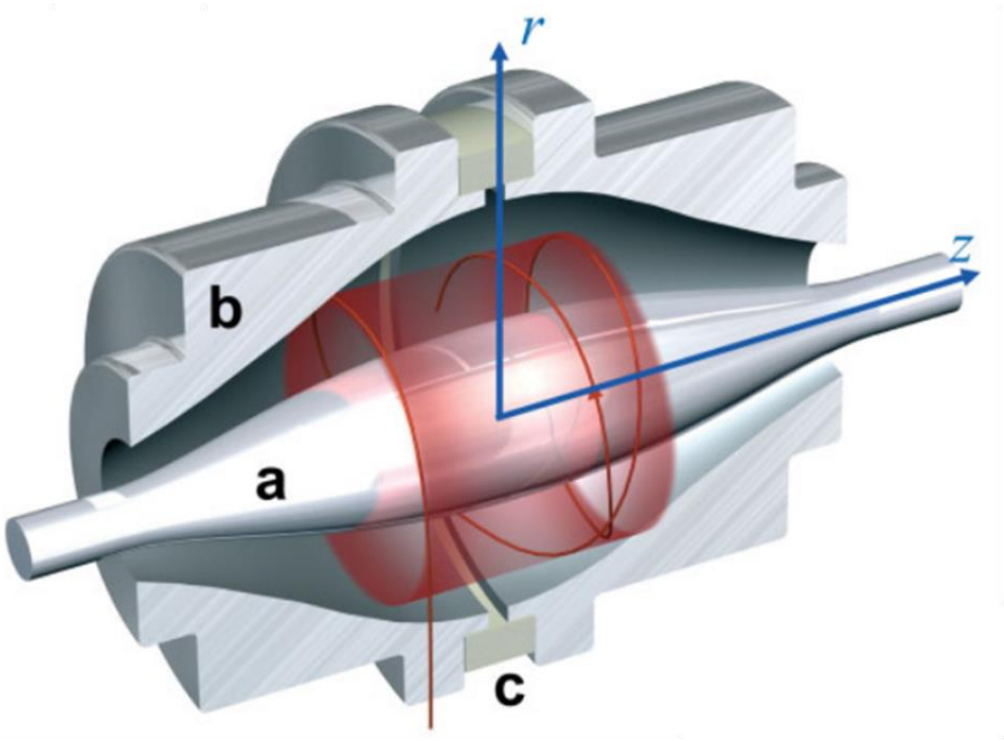

Figure 1.11 A cut-away model of an orbitrap mass analyser. Reproduced from Scigelova and Makarov 2006. Ions move in spirals around a central electrode (a). An outer electrode (b) is split in half by an insulating ceramic ring (c). An image current induced by moving ions is detected via a differential amplifier between the two halves of the outer orbitrap electrode. The *m/z* of different ions is determined from respective frequencies of oscillation after a Fourier transform.

1.4.16 Data acquisition and analysis

Following data acquisition the MS spectra obtained from both metabolomic and proteomic methodologies can be performed automatically. The analysis of metabolomic ToF-MS spectra can be achieved using a software program such as MarkerLynx XS™ to assess which metabolites represent candidate biomarkers and therefore require structural elucidation by QToF-MS. Likewise

ProteinLynx™ and Progenesis LC-MS software can be used to perform the analysis of QToF-MS spectra obtained from proteomic analyses. Following which, the peptide sequence is searched against known protein sequences in databases such as Swiss-Prot to enable protein identification.

Following the identification of a protein or metabolite, its applicability as a biomarker requires validation. Traditionally, immunoassay platforms such as western blot or ELISA have been used however, whilst this approach is suitable for the development of single biomarkers, the process becomes inefficient and costly for larger panels of multiplexed biomarkers. In addition methodologies such as these suffer from increased levels of variability and consequently increases in the coefficient of variation. The benefits of developing a tandem mass spectrometry based assay include rapid analysis times, high specificity, quantitation, ease of multiplexing and automation, making them suitable for translation for use within in clinical laboratories as functional assays.

1.4.17 Tandem mass spectrometry

The tandem mass spectrometer (MS/MS) utilises two quadrupole mass analysers coupled together in series. In a typical MS/MS analysis, ions of a selected mass (precursor or parent ions) are isolated by the first mass analyser (MS1) before transmission into a collision cell. In the collision cell ions collide with the neutral atoms of an inert gas usually argon, helium or nitrogen resulting in an increase in internal energy causing the molecule to fragment in a process called collision induced dissociation (CID). The subsequent fragments (product or daughter ion) produced are then analysed by the second mass analyser (MS2) (Figure 1.12). Tandem mass spectrometers are highly specific and sensitive instruments which enable the identification and quantification of

extremely low abundant molecules with a high degree of accuracy (de Hoffmann and Stroobant 2013).

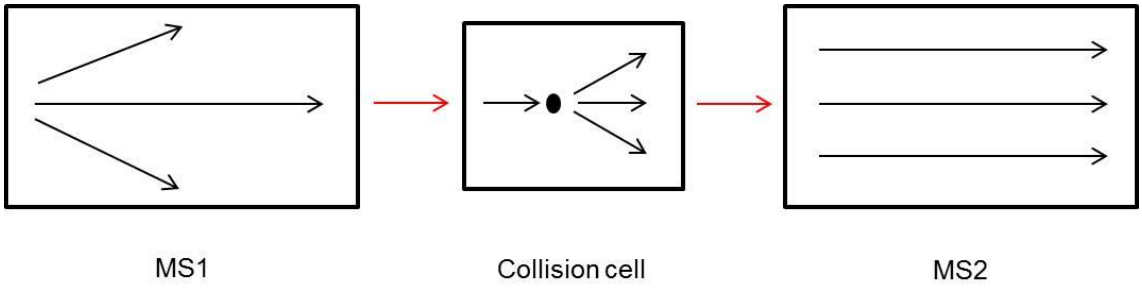

Figure 1.12 Schematic representation of a tandem mass spectrometer. Ions of a selected mass to charge (*m/z*) ratio are selected in the first quadrupole (MS1), fragmented in a collision cell and fragments separated in the second quadrupole (MS2).

1.4.17.1 Possible configurations of a tandem mass spectrometer

The first and second mass analysers (MS1 and MS2) can be operated in either fixed mass mode, whereby only ions of a certain mass are measured, or in scan mode, where ions of a range of masses are measured sequentially. By operating MS1 and MS2 in various combinations of fixed mass and scan mode, a number of different types of tandem mass spectrometric analyses are possible.

1.4.17.1.1 Straight scan mode

The tandem mass spectrometer can be operated as a simple, single quadrupole mass spectrometer by utilising only the first mass analyser in scan mode. In straight scan mode the mass analyser scans ions sequentially.

1.4.17.1.2 Product ion scan

In a product ion scan a precursor ion is selected in the first mass analyser (MS1) to be focused into the collision cell to undergo CID. The second mass analyser (MS2) is set to scan mode to analyse the characteristic fragmentation spectra of the resultant product ions.

1.4.17.1.3 Precursor ion scan

In a precursor ion scan, MS2 is fixed for a specific product ion produced by CID in collision cell. Scanning of MS1, while MS2 is fixed allows all precursor ions which fragment to give a specific product ion or class of molecules to be analysed.

1.4.17.1.4 Neutral loss scan

During a neutral loss scan both mass analysers (MS1 and MS2) are set in scan mode. However, MS2 is offset from MS1 by a mass corresponding to that of a neutral loss.

1.4.17.1.5 Selected reaction monitoring or multiple reaction monitoring

Selected or multiple reaction monitoring allows the selection of a specific precursor ion or ions in MS1 and following CID in the collision cell the selection of a specific product ion or ions in MS2. By operating both mass analysers in fixed mass mode sensitivity is dramatically increased making this configuration ideal for use in quantitative proteomic and metabolomic analyses.

1.5 Aims of thesis

The general aims of this thesis were to use proteomic and metabolic mass-spectrometry based techniques to identify potential biomarkers and disease mechanisms in Fabry disease. Specific aspects of the research were to;

(i) Use a label-free quantitative proteomic methodology to identify potential biomarkers in the urine of paediatric Fabry disease patients.

(ii) Develop and validate a rapid MRM-based tandem mass spectrometry assay for the quantitation of these potential biomarkers of lysosomal storage disorders and of pre-symptomatic kidney disease.

(iii) Use a metabolomic methodology to identify new and existing small molecule biomarkers in the plasma of Fabry disease patients.

(iv) Investigate globotriaosylceramide (Gb_3) and globotriaosylsphingosine (lyso-Gb_3) toxicity in the Fabry mouse model with particular focus on protein: glycosphingolipid interactions.

(v) Investigate mitochondrial respiratory chain enzyme activities in a Fabry mouse model.

Chapter 2

Materials and methods

Chapter 2 - Materials and methods 94

2.0 Materials and methods

2.1 Materials

2.1.1 General materials

All standard reagents were of AnalaR grade or equivalent and obtained from Sigma-Aldrich Company (Gillingham, Dorset, UK). All solvents used were LC-MS grade and were obtained from BDH Ltd. (Poole, Dorset, UK). Trypsin used was of sequencing grade and was obtained from Promega UK Ltd (Southampton, Hants, UK). Zeba™ spin desalting columns, 7 K molecular weight cut-off (MWCO), 5 ml were obtained from Thermo Scientific Pierce (Northumberland, UK). Amicon® Ultra-0.5, 30 kDa and Ultra-15, 3 kDa centrifugal filter devices, were obtained from Sigma Aldrich Company (Dorset, UK). Oasis® MCX cartridges, 30 mg, 60 µm, were obtained from Waters Corp., (Milford, MA, USA). PD_{10} desalting columns were obtained from GE Healthcare Life Sciences (Buckinghamshire, UK). RS100 ProteinChip Arrays were obtained from Bio-Rad Laboratories (Hemel Hempstead, UK). Dynabeads® M-270 Epoxy were obtained from Invitrogen (Paisley, Renfrewshire, UK). An ATP synthase enzyme activity microplate assay kit was obtained from Abcam (Cambridge, UK). Pure custom synthesised peptides were obtained from GenScript Corp (Piscataway, NJ, USA). A stable isotope labelled internal standard ("AQUA™ peptide") was obtained from Sigma-Aldrich Company (Dorset, UK). Glycosphingolipids were obtained from Biological Chemicals (Cambridge, UK) and Matreya (Pleasant Gap, PA, USA).

2.1.2 Sample materials

2.1.2.1 Ethical approval

Ethical approval was obtained from the Ethics Committees of University College London/University College London Hospital/Great Ormond Street Hospital/Institute of Child Health or the Faculty of Medicine and Health Sciences and the Centre Hospitalier Universitaire de Sherbrooke (CHUS). Written informed consent was obtained from adults, parents and children or young people where appropriate.

2.1.2.2 Urine samples

For proteomic analyses random urine samples were obtained from male paediatric Fabry disease patients (*n* = 10; age range 6 to 16 years; mean 12.5 years; for patient demographics see Table 2.1) prior to ERT, with corresponding samples collected following 12 months of treatment. Diagnosis had been confirmed by demonstrating marked enzyme deficiency in leukocytes or by mutation analysis. Urinary Gb_3 and creatinine was measured by HPLC-MS/MS (section 2.2.1 and 2.2.3, respectively) and patients classified according to their Gb_3 concentrations (see Table 2.1). For proteomic validation experiments random urine samples from male paediatric type-I diabetic patients (*n* = 10; age range 7.8 to 18.4 years; mean 12.9 years) with an average disease duration of 5 years were analysed as a positive control group. Glycosylated haemoglobin (HbA1c) was measured as part of the standard clinical appointment using the Diabetes Control and Complications Trial (DCCT) aligned Bayer 2000+ system (Siemens Healthcare Diagnostics, Inc., Deerfield, IL, USA). In addition, 10 age- and sex-matched healthy control subjects were drawn from the University

College London (UCL) Fetal Growth Study. This study consists of 1650 consecutive mothers who delivered a singleton, Caucasian baby free of pregnancy complications and whose offspring's growth had been followed for the last 10 years. For renal assay development as well as the paediatric type I diabetic patient and control groups, random urine samples from a second male paediatric Fabry disease group (*n* = 10; age range 4 to 18 years; mean 9.7 years; see Table 2.2), and an age- and sex-matched obese paediatric group were obtained. In addition, an adult male Fabry disease group (*n* = 10; age range 34 to 62 years; mean 49.4 years), an age- and sex-matched adult type II diabetic group and an age- and sex-matched adult control group were also analysed. All paediatric patient groups displayed normal glomerular filtration rates with no signs of microalbuminuria using conventional methods. All urine samples were stored at -20°C prior to analysis.

Table 2.1 Demographics of male paediatric Fabry disease patients used in the proteomic study showing total Gb_3 levels pre-treatment and 12 months post-treatment. Treatment status of patients is indicated by ↓DB for those with the least disease burden and ↑DB for those with the most disease burden.

Patient identification	**Age**	**Urinary Gb_3 pre-treatment** (µmol/mmol creatinine)	**Urinary Gb_3 post-treatment** (µmol/mmol creatinine)	**Treatment status**
1	9	0.35	0.06	↓DB
2	13	0.14	0.02	↓DB
3	15	0.18	0.15	↑DB
4	13	0.36	0.03	↓DB
5	15	0.56	0.02	↓DB
6	15	0.65	0.24	↑DB
7	14	0.47	0.04	↓DB
8	7	0.98	0.04	↓DB
9	11	0.67	0.06	↓DB
10	13	1.50	0.02	↓DB
Mean (min/max)	12.5 (7/15)	0.59 (0.14/1.50)	0.07 (0.02/0.24)	-
Normal control value	**-**	**<0.05 µmol/mmol creatinine**	**<0.05 µmol/mmol creatinine**	**-**

Table 2.2 Demographics of male paediatric Fabry disease patients used in the development of the renal assay showing total Gb_3 levels pre-treatment and following one-, two- and three-years of ERT. Treatment status of patients is indicated by ↓DB for those with the least disease burden and ↑DB for those with the most disease burden.

Patient identification	**Age at start of treatment**	**Urinary Gb_3 pre-treatment** (µmol/mmol creatinine)	**Urinary Gb_3 1 yr post-ERT** (µmol/mmol creatinine)	**Urinary Gb_3 2 yrs post-ERT** (µmol/mmol creatinine)	**Urinary Gb_3 3 yrs post-ERT** (µmol/mmol creatinine)	**Treatment status**
11	12	1.19	1.26	0.88	0.74	↑DB
12	8	1.10	0.25	0.67	0.31	↑DB
13	6	0.41	1.68	1.22	0.47	↑DB
14	6	0.58	0.29	0.41	0.41	↑DB
15	6	0.36	0.05	0.11	0.14	↑DB
16	4	0.23	0.02	0.01	0.01	↓DB
17	15	0.18	0.02	0.01	0.02	↓DB
18	6	0.35	0.07	0.08	0.01	↓DB
19	18	0.36	0.04	0.02	0.01	↓DB
20	16	0.21	0.02	0.02	0.02	↓DB
Total mean (min/max)	9.7 (4/18)	0.50 (0.18/1.19)	0.74 (0.02/1.68)	0.34 (0.02/1.22)	0.21 (0.01/0.74)	-
Mean ↑DB (min/max)	7.6 (6/12)	0.73 (0.36/1.19)	0.71 (0.05/1.68)	0.66 (0.11/1.22)	0.41 (0.14/0.74)	-
Mean ↓DB (min/max)	11.8 (4/18)	0.27 (0.18/0.36)	0.03 (0.02/0.07)	0.03 (0.01/0.08)	0.01 (0.01/0.02)	-
Normal control value	-	**<0.05 µmol/mmol creatinine**	**<0.05 µmol/mmol creatinine**	**<0.05 µmol/mmol creatinine**	**<0.05 µmol/mmol creatinine**	-

2.1.2.3 Plasma samples

For metabolomic analyses random plasma samples were collected from adult male Fabry patients (*n* = 12; age range 18 to 52 years; mean 30.5 years; see Table 2.3) and adult female Fabry patients (*n* = 12; age range 25 to 54 years; mean 39.3 years; see Table 2.4) in whom the diagnosis had been confirmed by demonstrating marked enzyme deficiency in leukocytes or by mutation analysis. Where paired urine samples were available Gb_3 and lyso-Gb_3 analyses were also performed as an additional measure to assess the level of disease burden (Tables 2.3 and 2.4). None of the patients had ever received ERT at the time of sample collection. Plasma lyso-Gb_3 and corresponding urinary Gb_3 and lyso-Gb_3 was measured by HPLC-MS/MS as described in sections 2.2.1 and 2.2.2. Creatinine was measured by HPLC-MS/MS as described in section 2.2.3. For comparison, plasma samples obtained from healthy reference control males (*n* = 8; age range 18 to 57 years; mean 37.8 years) and females (*n* = 8; age range 21 to 63 years; mean 36 years) were studied. Plasma specimens were obtained from 2 ml of blood collected in potassium ethylenediaminetetraacetic acid (EDTA) tubes and centrifuged at 10,000*g* for 5 min. All samples were stored at -20°C prior to analysis.

Table 2.3 Demographics of adult male Fabry disease patients used in the metabolomic study showing total urinary Gb_3, lyso-Gb_3 and plasma lyso-Gb_3 levels. A urine sample was not available for patient 11a.

Patient identification	**Age**	**Urinary Gb_3** (µg/mmol creatinine)	**Urinary lyso-Gb_3** (pmol/mmol creatinine)	**Plasma lyso-Gb_3** (nmol/l)
1a	36	4059	220	88
2a	40	1079	79	105
3a	35	327	159	91
4a	18	1857	95	166
5a	23	837	205	137
6a	35	507	91	107
7a	34	2452	181	90
8a	25	150	353	232
9a	20	14	149	227
10a	18	1402	38	76
11a	52	-	-	124
12a	30	92	87	172
Mean (min/max)	30.5 (18/52)	1161 (14/2452)	151 (38/353)	135 (76/227)
Normal control value	**-**	**< 25 µg/mmol creatinine**	**Not Detectable**	**Not detectable**

Table 2.4 Demographics of adult female Fabry disease patients used in the metabolomic study showing total urinary Gb_3, lyso-Gb_3 and plasma lyso-Gb_3 levels. Urine samples were not available for Gb_3 analysis for patients 6b, 7b, 8b and 11b.

Patient identification	**Age**	**Urinary Gb_3** (µg/mmol creatinine)	**Urinary lyso-Gb_3** (pmol/mmol creatinine)	**Plasma lyso-Gb_3** (nmol/l)
1b	48	51	29	11
2b	26	68	30	7
3b	45	121	15	18
4b	27	127	50	15
5b	51	725	77	15
6b	30	-	8	6
7b	25	-	29	11
8b	28	-	23	13
9b	54	7	2	3
10b	51	15	35	10
11b	48	-	48	19
12b	38	58	44	8
Mean (min/max)	39.3 (25/54)	147 (7/725)	33 (2/77)	11 (3/19)
Normal control value	-	**< 25 µg/mmol creatinine**	**Not Detectable**	**Not Detectable**

2.1.2.4 Tissue samples

For proteomic profiling analyses (Chapter 5) organs from male knock-out mice hemizygous for the *gla* gene meaning that this gene has no allelic counterparts, as well as homozygous female *gla* knock-out mice (referred to as Fabry mice; C57BL6/SVJ129) and wild-type control mice of the same genetic background were obtained as part of collaborative project with Dr Joan Keutzer, Genzyme Corporation, a Sanofi company, Cambridge, Massachusetts, USA.

For analysis of mitochondrial respiratory chain enzyme activities (Chapter 6) organs from hemizygous male *gla* knock-out mice (referred to as Fabry mice; C57BL6/SVJ129) and wild-type control mice of the same genetic background were obtained as part of a collaborative project with Dr Raphael Schiffmann, Baylor University Medical Centre, Dallas, Texas, USA. All organs were stored at -80°C until required for analysis.

For complex V enzyme activity analyses (Chapter 5) liver from male 12 week old Sprague Dawley rats were obtained from UCL Biological Services Unit, London, UK.

2.2 Methods

2.2.1 Globotriaosylceramide (Gb_3) measurement by HPLC-MS/MS

The method described by Mills *et al.*, (2005) was used to analyse Gb_3 levels in urine and tissue as follows;

2.2.1.1 Urine and tissue Gb_3 extraction

Each urine or tissue homogenate was thawed and well mixed, and 200 µl was sonicated for 10 s, at amplitude 6, using a Soniprep 150 Plus (MSE, London, UK) to fully disrupt any cellular debris or sediment. Forty microlitres of sonicate was added to 200 µl chloroform-methanol (2:1 v/v) containing 0.025 µg C17-Gb_3 internal standard (synthesised in house at the Biological Mass Spectrometry Unit, UCL Institute of Child Health, London, UK) in a 2 ml screw-cap glass vial. Urine samples were left to shake for 30 min and tissue homogenates for 60 min in a VIBRAX VXR orbital shaker (IKA, Chelmsford, UK) to extract Gb_3. Precipitated protein and any other particulate matter were removed by centrifugation at 40,000*g* for 10 min. The supernatant was removed into a 2 ml glass autosampler vial and stored at -20°C prior to analysis.

2.2.1.2 Analysis of Gb_3 in urine and tissue

An Alliance HT 2795 HPLC coupled to a Quattro Micro triple quadrupole mass spectrometer (Waters Corp, Manchester, UK) was used for the direct analysis of the eluate in section 2.2.1.1. The instrument was operated in positive ion mode. The capillary voltage was maintained at 3.7 kV, with source temperature held constant at 150°C and nitrogen used as the nebulizing gas at a flow rate of

650 l/h. A Waters Spherisorb HPLC C8-guard column (4.6 x 10 mm ID., 5 µm) was used for separation with solution A (100 % methanol; MeOH) and solution B (4 mM ammonium acetate in ddH_2O). The LC gradient is shown in Table 2.5.

Table 2.5 The liquid chromatography gradient used to analyse Gb_3 in urine

Time (min)	Solution A (%)	Solution B (%)	Curve
0	50	50	1
1	50	50	1
2	100	0	6
4	100	0	6
4.01	50	50	1
6	50	50	1

The optimum flow rate was 0.5 ml/min, with a column oven temperature of 40°C. The divert valve of the mass spectrometer was programmed to discard the HPLC effluent before (0 to 2 min) and after (5 to 6 min) the elution of Gb_3 isoforms and the C17-Gb_3 internal standard to prevent system contamination. A 35 µl injection volume was used with partial loop mode.

2.2.1.3 Quantitation of Gb_3 in urine and tissue

Multiple reaction monitoring mode was used for the measurement of Gb_3. Data were acquired over a time window of 3 min and quantitative data were taken from the Gb_3 transitions shown in Table 2.6. Quantitation was achieved using peak areas processed by QuanLynx software (Waters Corp.) and ratioing the peak areas of the native Gb_3 isoforms, shown in Table 2.6, to the peak area of the C17-Gb_3 internal standard (*m/z* 1060.90). Total Gb_3 levels (µmol) were expressed per mmol creatinine.

Table 2.6 Isoforms of Gb_3 detected by UPLC-MS/MS. The internal standard (C17-Gb_3) is shown underlined.

Gb_3 isoform	Precursor *m/z*	Cone voltage	Product *m/z*	Collision energy
Lyso-Gb_3	808.60	110	646.94	55
C16-Gb_3	1046.62	110	884.07	60
C17-Gb_3	1060.90	110	898.53	60
C18-Gb_3	1074.31	110	912.13	60
C20-Gb_3	1102.78	110	940.17	65
C22:1-Gb_3	1128.48	110	966.12	65
C22-Gb_3	1130.46	110	968.42	65
C24:2-Gb_3	1154.82	110	992.06	65
C24:1-Gb_3	1156.60	110	994.10	65
C24-Gb_3	1158.86	110	996.37	65
C24:2-OH-Gb_3	1170.68	110	1008.17	65
C24:1-OH-Gb_3	1172.69	110	1010.17	65
C24-OH-Gb_3	1174.59	110	1012.14	65
C26-Gb_3	1186.51	110	1024.18	65

2.2.2 Globotriaosylsphingosine (lyso-Gb_3) analysis in urine, plasma and tissue by HPLC-MS/MS

2.2.2.1 Lyso-Gb_3 analysis in urine

The method described by Auray-Blais *et al*., (2010) was used to analyse lyso-Gb_3 levels in urine as follows;

2.2.2.2 Sample preparation for the analysis of lyso-Gb_3 in urine

For each analysis 500 µl well mixed urine was added to 500 µl 1-β-D-glucosylsphingosine (GSG) (4 nmol/l in MeOH) internal standard (Matreya,

Pleasant Gap, PA, USA), 20 µl of 50 % acetonitrile (ACN)/0.1 % formic acid (FA)/ddH_2O and 100 µl hydrochloric acid (1 mmol/l). Solid phase extraction (SPE) was performed by transferring sample mixtures with glass pipettes to mixed-mode cation-exchange cartridges (Oasis® MCX, 30 mg, 60 µm, Waters Corp., Milford, MA, USA) preconditioned successively with 1200 µl MeOH and 1200 µl hydrochloric acid (1 mol/l). Cartridges were washed with 1200 µl 2 % FA in ddH_2O followed by 1200 µl 0.2 % FA in MeOH. Lyso-Gb_3 and GSG were then eluted into glass tubes with 600 µl 2 % ammonia in MeOH. Eluates were evaporated to dryness under nitrogen. Residues were reconstituted in 200 µl 50% ACN/0.1% FA/ddH_2O, and transferred to glass vials for LC-MS/MS analysis. A calibration curve was prepared in the same way except the patient urine sample was substituted for 500 µl of control urine, and the 20 µl of 50% ACN/0.1% FA/ddH_2O was replaced with the same volume of one of the following standard solutions: 0, 160, 400, 800, 1600, 3000 and 5000 pmol/l of lyso-Gb_3 in 50% ACN/0.1% FA/ddH_2O. The control urine used for the generation of the calibration curve contained no detectable lyso-Gb_3.

2.2.2.3 Analysis of lyso-Gb_3 in urine

An Alliance HT 2795 HPLC system coupled to a Quattro Micro triple quadrupole mass spectrometer (Waters Corp.) was used for the LC-MS/MS analysis of lyso-Gb_3. The instrument was operated in positive ion mode. The capillary voltage was maintained at 3.2 kV, with source temperature held constant at 120°C and nitrogen used as the nebulizing gas at a flow rate of 30 l/h. A Halo C_{18} column (2.1 x 50 mm ID., 2.7 µm; Advanced Materials Technology, Wilmington, DE, USA) was used for separation with solution A (0.2 % FA/ACN) and solution B (5 % ACN/0.2 % FA/ddH_2O). The gradient run was: 3 min of a

linear gradient from 20 % to 70 % of A, followed by a 4 min wash period with 70 % of A, then immediate return to initial conditions and equilibration with 20 % of A for 3 min. The optimum flow rate was 0.4 ml/min, with injector and oven temperatures of 20°C and 30°C, respectively. The divert valve of the mass spectrometer was programmed to discard the HPLC effluent before (0 to 2.8 min) and after (3.5 to 10 min) the elution of lyso-Gb_3 and GSG to prevent system contamination. A 25 µl injection volume was used with partial loop with needle overfill mode. The calibration curve was quadratic with 1/x weighing function, and the origin was excluded.

2.2.2.4 Quantitation of lyso-Gb_3 in urine

Multiple reaction monitoring (MRM) mode was used for the measurement of lyso-Gb_3. Data were acquired over a time window of 2 min and quantitative data were taken from transition 786.6>282.3 for lyso-Gb_3 and 460.5>280.3 for the GSG internal standard. Lyso-Gb_3 calibrators were measured at concentrations of 0, 160, 400, 800, 1600, 3000 and 5000 pmol/l. An example of a calibration curve generated in the analysis of lyso-Gb_3 in urine is shown in Figure 2.1. Quantitation was achieved using peak areas processed by QuanLynx software (Waters Corp.).

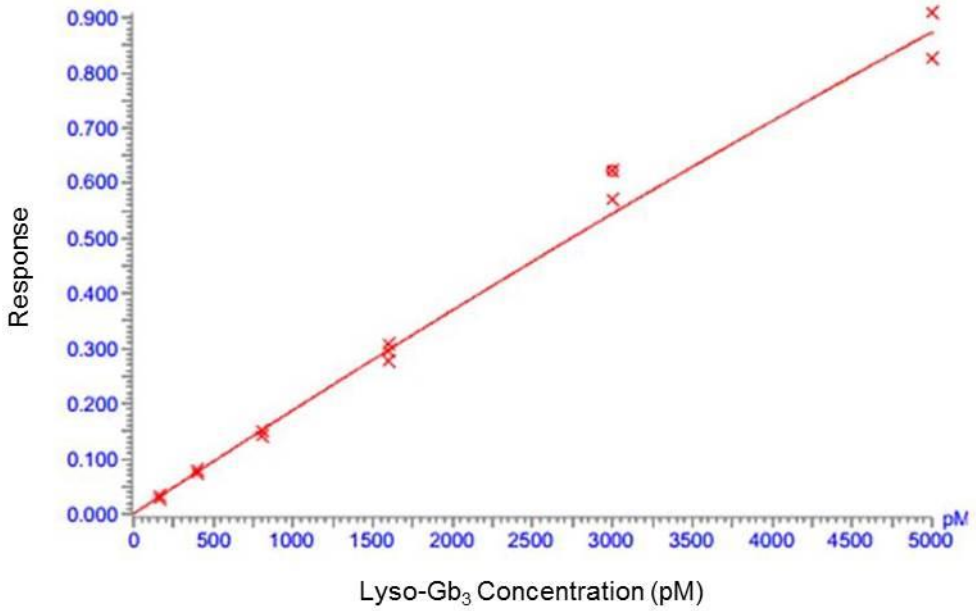

Figure 2.1 Calibration curve generated during the analysis of lyso-Gb_3 in urine. R^2 = 0.996.

2.2.2.5 Lyso-Gb_3 analysis in plasma

The method described by Boutin *et al*., (2012) was used to analyse lyso-Gb_3 levels in plasma as follows;

2.2.2.6 Sample preparation for the analysis of lyso-Gb_3 in plasma

Sample preparation for the analysis of lyso-Gb_3 in plasma was performed as described in section 2.2.2.1 with the exception that for each analysis 200 µl well mixed plasma was added to 500 µl phosphoric acid (H_3PO_4) (2 % in ddH_2O), 500 µl GSG (4 nmol/l in MeOH) internal standard, and 20 µl of 50 % ACN/0.1 % FA/ddH_2O prior to SPE. A calibration curve was prepared in the same way except the plasma sample was substituted for 200 µl of plasma stripped twice with charcoal (Bioreclamation, Hicksville, NY, USA), and the 20 µl of 50%

ACN/0.1% FA/ddH_2O was replaced with the same volume of one of the following standard solutions: 0, 4, 10, 40, 140, 400 nmol/l of lyso-Gb_3 in 50% ACN/0.1% FA/ddH_2O. The charcoal stripped plasma used for the generation of the calibration curve contained no detectable lyso-Gb_3.

2.2.2.7 Analysis of lyso-Gb_3 in plasma

Analysis of lyso-Gb_3 in plasma by HPLC-MS/MS was performed as described in section 2.2.2.3 with the following exceptions; the capillary voltage was maintained at 3.4 kV, flow rate of the nitrogen nebulizing gas 50 l/h, the gradient run was: 5 min of a linear gradient from 20 % to 100 % of A, followed by a 3 min wash period with 100 % of A, then immediate return to initial conditions and equilibration with 20 % of A for 2 min.

2.2.2.8 Quantitation of lyso-Gb_3 in plasma

Quantitation of lyso-Gb_3 in plasma by LC-MS/MS was performed as described in section 2.2.2.4 with the exception that lyso-Gb_3 calibrators were measured at concentrations of 0, 4, 10, 40, 140, 400 nmol/l. An example of a calibration curve generated in the analysis of plasma lyso-Gb_3 is shown in Figure 2.2.

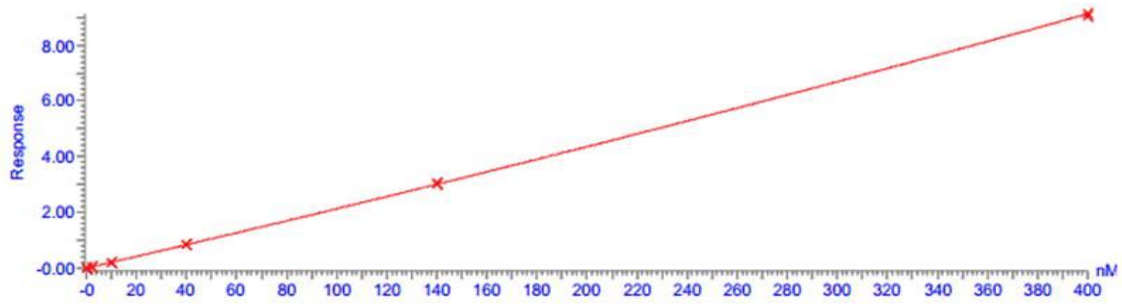

Figure 2.2 Calibration curve generated during the analysis of lyso-Gb_3 in plasma. R^2 = 0.998.

2.2.3 Creatinine analysis by HPLC-MS/MS

The method used to measure creatinine concentrations was developed in-house by the Biological Mass Spectrometry Unit at UCL Institute of Child Health, London, UK and is as follows;

2.2.3.1 Sample preparation for creatinine analysis

Each urine sample was thawed, well mixed and 200 µl centrifuged at 40,000*g* for 10 min. For each analysis, 10 µl supernatant was added to 10 µl 5 mM d_3-creatinine internal standard (synthesised in house by the Biological Mass Spectrometry Unit at UCL Institute of Child Health, London, UK) and 200 µl ddH_2O and vortexed for 30 sec. Calibration curves were constructed by spiking control urine with increasing amounts creatinine (0, 0.625, 1.25, 2.5, 5, 10 and 20 mmol/l).

2.2.3.2 Analysis of creatinine

An Alliance HT 2795 HPLC coupled to Quattro Micro triple quadrupole mass spectrometer (Waters Corp.) was used for the LC-MS/MS analysis of creatinine. The instrument was operated in positive ion mode. The capillary voltage was maintained at 3.7 kV, with source temperature held constant at 150°C and nitrogen used as the nebulizing gas at a flow rate of 50 l/h. A Discovery® HS F5 Supelguard™ column (2 x 2.1 mm ID., 5 µm) followed by a Discovery® HS F5-5 HPLC column (5 cm x 2.1 mm ID., 5 µm; Sigma Aldrich, Dorset, UK) were used for separation with solution A (100 % MeOH) and solution B (4 mM ammonium acetate in ddH_2O with 4 mM heptafluorobutyric acid). The LC gradient is shown in Table 2.7.

Table 2.7 The liquid chromatography gradient used to analyse creatinine

Time (min)	Solution A (%)	Solution B (%)	Flow rate (ml/min)	Curve
0.00	5	95	0.2	1
1.90	5	95	0.2	1
2.00	100	0	0.5	6
2.10	100	0	0.6	6
4.00	100	0	0.6	6
4.01	5	95	0.6	1
6.00	5	95	0.6	1

The column oven temperature was 20°C. The divert valve of the mass spectrometer was programmed to discard the HPLC effluent before (0 to 2 min) and after (4 to 6 min) the elution of creatinine to prevent system contamination. A 5 µl injection volume was used with partial loop mode.

2.2.3.3 Quantitation of creatinine

MRM mode was used for the measurement of creatinine. Data were acquired over a 2 min time window and quantitative data were taken from transition 113.70>43.90 for creatinine and 116.70>46.90 for the d_3-creatinine internal standard. Creatinine calibrators were measured at concentrations of 0, 0.625, 1.25, 2.5, 5, 10 and 20 mmol/l. An example of a calibration curve generated in the analysis of urine creatinine is shown in Figure 2.3. Endogenous creatinine concentrations in the control urine were determined by the intercept on the *x*-axis of the un-spiked urine (0 calibrator point) and this correction value was subtracted from each subsequent calibrator point (0.625 - 20 mmol/l). Quantitation was achieved by ratioing the peak areas obtained from QuanLynx

software (Waters Corp.) of the native creatinine to the peak area of the d_3-creatinine internal standard (*m/z* 116.70).

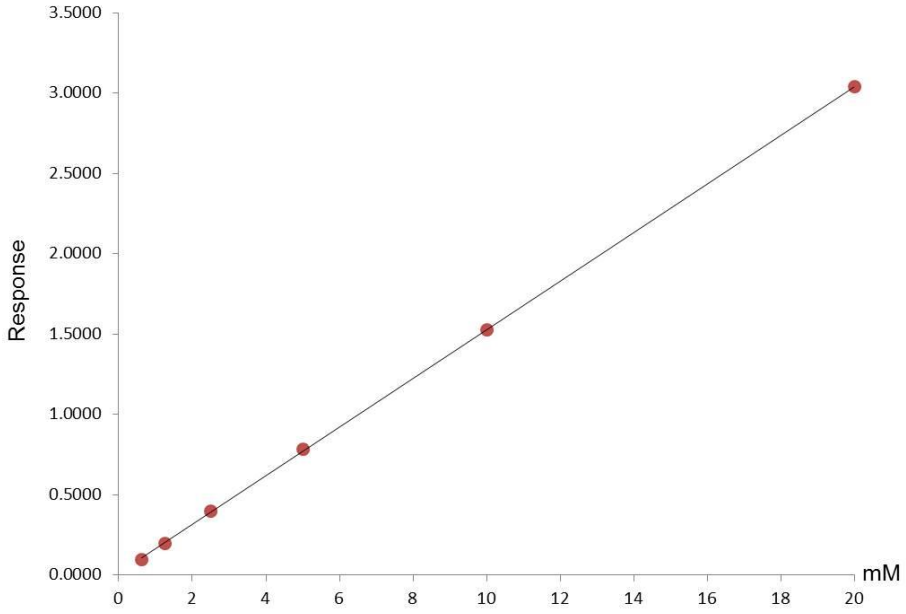

Figure 2.3 Calibration curve generated during the analysis of creatinine. $R^2 = 0.99$.

2.2.3.4 Urinary creatinine expression

In this study, urinary concentrations of compounds of interest were corrected for dilution differences by measuring the urinary creatinine concentration as creatinine is filtered but not absorbed by the kidneys.

2.2.4 Bicinchoninic acid (BCA) protein assay

A standard curve with known concentrations of bovine serum albumin (BSA) (Sigma-Aldrich, Dorset, UK) was prepared (Table 2.8). Serial dilutions of the protein sample were also prepared in the protein storage buffer and 5 µl of each dilution was mixed with 45 µl of ddH_2O. This was followed by the addition of 1

ml of bicinchoninic acid (Sigma-Aldrich, Dorset, UK) to each sample and incubated at 37°C for 10 min. Twenty microlitres of copper sulphate solution was added and incubated at 37°C for a further 20 min. The absorbance of each sample was measured with a Cecil CE 2040 spectrophotometer (Cecil Instruments, Cambridge, UK) at 562 nm and the protein concentrations (mg/ml) were calculated from the standard curve.

Table 2.8 Concentrations of BSA (stock solution 1 mg/ml) used to create a standard curve. The buffer (5 µl) that was added to each sample corresponded to the storage buffer of the protein and accounted for any background noise.

BSA conc. (mg/ml)	**BSA** (µl)	**Buffer** (µl)
0	0	50
0.05	2.5	47.5
0.1	5	45
0.2	10	40
0.4	20	30
0.6	30	20
1	50	0

2.2.4.1 Protein expression

In this study, tissue concentrations of compounds of interest were corrected for protein concentrations.

2.2.5 Proteomic analysis and method development

The methods outlined in section 2.2.5 below are used in the proteomic study described in Chapter 3 to identify and validate potential urinary biomarkers in Fabry disease.

2.2.5.1 Urine preparation prior to proteomic analysis (QToF-MS)

For each analysis, urine (Table 2.1) was desalted and the protein concentrated using Zeba™ spin desalting columns, 7 K MWCO, 5 ml (Thermo Scientific Pierce, Northumberland, UK). The Zeba™ column was centrifuged at 1,000*g* for 2 min to remove storage solution. Five ml of 50 mM ammonium bicarbonate buffer pH 7.8 was added and centrifuged at 1,000*g* for 2 min. This step was repeated 3 times and the buffer was discarded. Finally 4 ml of urine was added and collected for analysis following centrifugation at 1,000*g* for 2 min. Thereafter, 400 µg of protein was aliquoted into 1.8 ml proteomic grade vials, lyophilised and stored at -20°C until required for in-solution digestion (section 2.2.5.4) prior to analysis (section 2.2.5.5).

2.2.5.2 Urine preparation prior to proactivator polypeptide and ganglioside GM_2 activator protein analysis by UPLC-MS/MS

For each analysis 500 µl of urine was applied to an Amicon Ultra-0.5 ml centrifugal filter for protein purification and concentration (30 kDa, Sigma Aldrich, Dorset, UK) and centrifuged at 14,000*g* for 12 min. Proactivator polypeptide (prosaposin; PSAP) was distinguished from the processed saposins A, B, C and D with the use of these size exclusion filters. After centrifugation the lower fraction contained proteins < 30 kDa, which included saposins A, B, C and D (molecular weights ~ 10 kDa), and ganglioside GM_2 activator protein (GM_2AP; 21 kDa). The fraction containing proteins > 30 kDa were removed from the filter using a pipette, this fraction contained prosaposin (65 - 73 kDa). To both the > 30 kDa recovered fraction and the < 30 kDa recovered fraction, 5 µl (7.62 fmol) of a synthesised stable isotope labelled GM_2AP internal standard peptide (SEFVV[$^{13}C_6$P]DLELPSWLTTGNYRIESVL) was added ("AQUA^{TM}

peptide," Sigma-Aldrich, Dorset, UK), lyophilised and stored at -20°C until required for in-solution digestion (section 2.2.5.4) prior to analysis (section 2.2.5.7).

2.2.5.3 Urine preparation prior to renal biomarker analysis by UPLC-MS/MS

For each analysis 1 ml of urine and 2.5 µl of a 0.1 µg/µl enolase intact protein as internal standard was applied to an Amicon Ultra-1 ml centrifugal filter for protein purification and concentration (3 kDa, Sigma Aldrich, Dorset, UK) and centrifuged at 4000*g* for 50 min. The concentrate (> 3 kDa) recovered was then lyophilised and stored at -20°C until required for in-solution digestion (section 2.2.5.4) prior to analysis (section 2.2.5.8).

2.2.5.4 In-solution digestion protocol

The lyophilised protein was reconstituted in 20 µl of 100 mM Tris, pH 7.8, containing 6 M urea, and left shaking gently for 60 min at room temperature to denature the protein. Disulphide bridges were reduced by the addition of 1.5 µl of 100 mM Tris-HCl buffer, pH 7.8, containing 5 M dithioerythritol (DTE), followed by incubation at room temperature for 60 min. Free thiol groups were carboamidomethylated by incubation with 6 µl of 100 mM Tris-HCl, pH 7.8, containing 5 M iodoacetamide (IAA) for 30 min at room temperature. The reaction mixture was then diluted with 155 µl of ddH_2O and vortexed. To proteolytically digest the proteins, 1 µg of trypsin (Sigma-Aldrich, Dorset, UK) was added to the reaction mixture, followed by incubation overnight at 37°C in a water bath.

2.2.5.5 Label-free quantitation by NanoAcquity UPLC-QToF-MS

Urine and tissue proteins were identified and quantitated by direct analysis of the reaction mixtures described in sections 2.2.5.1 and 2.2.7.1.2, respectively. Prior to analysis each digest was spiked with 1 pmol of an enolase tryptic digestion (*Saccharomyces cerevisiae*). All analyses were performed using a NanoAcquity UPLC and QToF Premier mass spectrometer (Waters Corporation, Manchester, UK). Peptides were trapped and desalted prior to reverse phase separation using a Symmetry C18 5 µm, 5 mm x 300 µm pre-column. Peptides were then separated prior to mass spectral analysis using a 15 cm x 75 µm C18 reverse phase analytical column. Peptides were loaded onto the pre-column at a flow rate of 4 µl/min in 0.1 % FA for a total time of 4 min. Peptides were eluted off the pre-column and separated on the analytical column using a gradient of 3 - 40 % ACN containing 0.1 % FA over a period of 120 min and at a flow rate of 250 nl/min. The column was washed and re-generated at 300 nl/min for 10 min using a 99 % ACN containing 0.1 % FA. After all non-polar and non-peptide materials were removed, the column was re-equilibrated under the initial starting conditions for 20 min. All columns were maintained at 35ºC. Mass accuracy was maintained during the run using a lock spray of the peptide [glu1]-fibrinopeptide B delivered through the auxiliary pump of the NanoAcquity at a concentration of 500 nmol/l and at a flow rate of 300 nl/min.

Peptides were analysed in positive ion mode with the QToF operated in v-mode with a typical resolving power of 10,000 FWHM. Prior to analyses, the ToF analyser was calibrated using [glu1]-fibrinopeptide B fragments obtained using a collision energy of 25 V and over the mass range *m/z* 50 – 2000. Post-calibration of data files was corrected using the doubly charged precursor ion of

[glu1]-fibrinopeptide B (*m/z* 785.8426) with a sampling frequency of 30 s. Accurate mass LC-MS data were collected in a data-independent and alternating, low and high collision energy mode. Each low/high acquisition was 1.5 s with 0.1 s interscan delay. Low energy data collections were performed at a constant collision energy of 4 V, high collision energy acquisitions were performed using a 15 - 40 eV ramp over a 1.5 s time period and a complete low/high energy collision acquisition achieved every 3.2 s.

2.2.5.6 Data analysis by UPLC-QToF-MS

ProteinLynx Global Server version 2.4 (Waters, UK) was used to process all data acquired. Protein identifications were obtained by searching the appropriate proteome UniProt database (human or mouse) to which the sequence of P00924 yeast enolase and P00761 porcine trypsin were added manually. Protein identification from the low/high collision spectra for each sample was processed using a hierarchical approach where more than three fragment ions per peptide, seven fragment ions per protein and more than two peptides per protein had to be matched. Lock mass window was set at 0.1 Da, low and elevated energy thresholds set at 150 and 50 counts, respectively. Elution start and end times were 15 and 110 min, respectively and with chromatographic peak width set to automatic. Protein identification parameters used in the database searching included a < 10 ppm mass accuracy tolerance, fixed modifications of carboamidomethylation of cysteines, dynamic modifications of deamidation of asparagine/glutamine and oxidation of methionine, up to 3 missed cleavage sites and maximum protein mass 400 kDa. Quantitation of urinary proteins using MS^E analyses were determined as fmol of total protein in 1 l of urine and then standardized and expressed per mmol of

creatinine (fmol of protein/mmol of creatinine). Statistical differences between sample groups were analysed using Microsoft Excel and Graphpad Prism with statistical significance obtained using standard Student's *t*-test.

2.2.5.7 Development of a high-throughput UPLC-MS/MS assay for confirmation and validation of prosaposin and GM_2AP

Based on ESI-QToF analyses the peptides *m/z* 865.9681 ($EIVDSYLPVILDIIK^{2+}$) from the saposin A region of the prosaposin protein (see Figure 2.4) and *m/z* 775.6234 ($SEFVVPDLELPSWLTTGNYR^{3+}$) from GM_2AP produced the largest response and optimum product ion scans and were therefore selected as the "marker" peptides for optimization and development of a MRM-based assay.

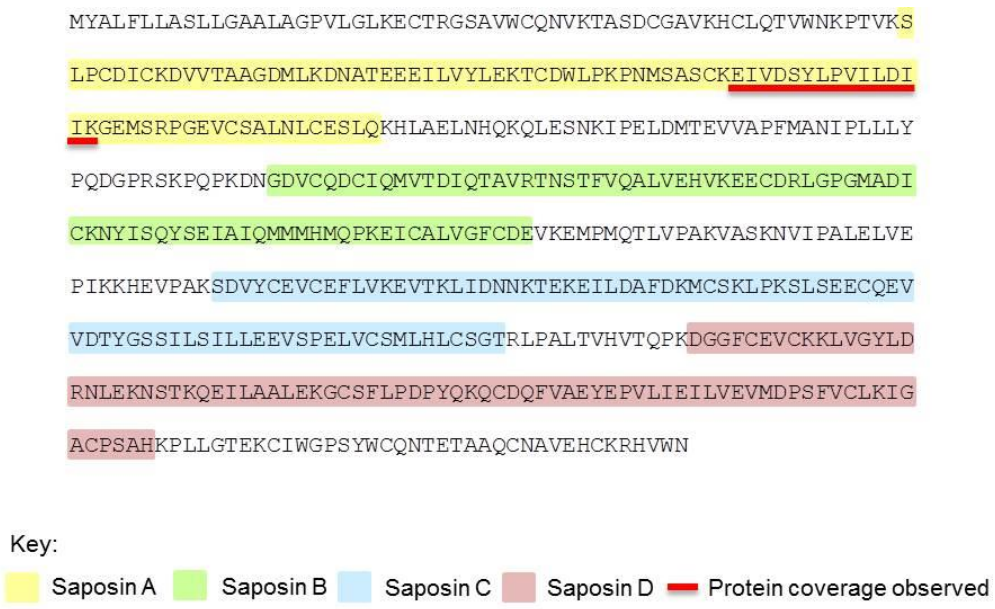

Figure 2.4 Prosaposin sequence with each mature saposin chain highlighted and the protein coverage observed in the ESI-QToF analyses underlined.

These sequences were checked for uniqueness and post-translational modifications by verification with UniProt (http://www.uniprot.org). Pure custom synthesized peptides were ordered from GenScript Corp, Piscataway, NJ, USA. A stable isotope labeled GM_2AP internal standard peptide was synthesized, which included a single missed cleavage site with a short peptide "tag" of IESVL (SEFVV[$^{13}C_6$P]DLELPSWLTTGNYRIESVL) this compensates for any inefficiencies in the trypsin protease reaction. This method has been applied previously to plasma proteins (Heywood *et al.*, 2012a) and has now been developed for urinary prosaposin and GM_2AP quantitation. Confirmation of the identification of the marker peptides for prosaposin *m/z* 865.97 and GM_2AP *m/z* 775.62 in urine was verified by comparison to their retention time with the synthesised versions of the peptides when spiked into urine. This provided a third level of identification in addition to precursor and product ion mass allowing the unequivocal identification of each peptide/protein. Quantitative data were taken from transition 865.97>215.19 for prosaposin, 775.62>213.18 for GM_2AP and 777.46>463.12 for the stable isotope labeled internal standard. Calibration curves were constructed by spiking male control urine with 7.62 fmol of the GM_2AP stable isotope labelled internal standard and increasing amounts (10, 25, 50, 75 and 100 fmol/l) of the synthesised marker peptides used to quantitate the prosaposin and GM_2AP proteins (Figure 9.1 of supplementary data, section 9.1.1). Endogenous concentrations of prosaposin and GM_2AP concentrations in the male control urine were determined by the intercept on the *x*-axis of the un-spiked urine (0 calibrator point) and this correction value was subtracted from each subsequent calibrator point (10-100 fmol/l). Quantitation of prosaposin and GM_2AP was performed by ratioing the peak area of the native peptide to the peak area of the stable isotope-labelled internal standard for GM_2AP (*m/z*

777.46). Urinary creatinine concentrations were determined as described in section 2.2.3.4. Urinary prosaposin and GM_2AP concentrations were determined relative to urinary creatinine concentrations.

A Waters Acquity UPLC coupled to a Xevo™ TQ-S triple quadrupole mass spectrometer (Waters Corp, Manchester, UK) was used for validation and clinical assay development experiments. The instrument was operated in positive ion mode. The capillary voltage was maintained at 3.7 kV, with source temperature held constant at 150°C and nitrogen used as the nebulizing gas at a flow rate of 30 l/h. For each peptide precursor ion masses were determined in scan mode with product ion masses determined following collision-induced dissociation with argon. Optimum cone and collision energies for each peptide are shown in Table 2.9. Two transitions from each peptide were selected for confirmatory purposes. A Waters ACQUITY UPLC BEH C18 column (2.1 x 100 mm ID., 1.7 µm) was used for separation with solution A (99.9% H_20 and 0.1% FA) and solution B (99.9% ACN and 0.1% FA). The flow rate was set to 0.8 ml/min and a linear gradient of 0 - 97% sol A over 7 min. The total run time was 10 min due to loading, cleaning and reconditioning. A 30 µl injection volume was used with partial loop with needle overfill mode.

Table 2.9 MRM transitions for the UPLC-MS/MS analysis of prosaposin, GM_2AP and the stable isotope-labelled GM_2AP internal standard. Ions charge is indicated by $^{2+}$ for doubly charged or $^{3+}$ for triply charged ions. Product ions underlined are those used for quantitation whilst non-underlined ions were used for confirmation only.

Protein name	Tryptic peptide sequence	Precursor *m/z*	Cone voltage	Product *m/z*	Collision energy
PSAP	EIVDSYLPVILDIIK	865.97^{2+}	70	215.19	36
		865.97^{2+}	70	538.50	40
GM_2AP	SEFVVPDLELPSWLTTGNYR	775.62^{3+}	20	213.18	44
		775.62^{3+}	20	769.64	12
AQUA peptide	SEFVV[$^{13}C_6$P]PDLELPSWLTTGNYR	777.46^{3+}	20	216.97	20
		777.46^{3+}	20	463.12	20

2.2.5.8 Development of a high-throughput UPLC-MS/MS assay for pre-symptomatic kidney disease

Suitable peptide regions, from a number of proteins of interest, were checked for uniqueness and post-translational modifications by verification with the UniProt database (http://www.uniprot.org) and selected as “marker” peptides for optimization and development of a multiple reaction monitoring (MRM)-based assay (Table 2.10). Selection of “marker” peptides was based on QToF analyses and with the use of the Global Proteome Machine (GPM; www.thegpm.org), a proteomic platform containing datasets contributed by researchers enabling the selection of peptide marker sequences based on previously tested and validated MS analyses. In addition, Skyline (MacCoss Lab, University of Washington) a targeted proteomic application for building MRM quantitative methods was used to assess optimum peptides and their

transitions. Pure custom synthesized peptides were ordered from GenScript Corp (Piscataway, NJ, USA). In addition, a yeast enolase whole protein was purchased from Sigma-Aldrich (Gillingham, Dorset, UK) to act as an internal standard to control for sample processing. Confirmation of the identification of all marker peptides in urine was verified by comparison to their retention time with the synthesised versions of the peptides when spiked into urine. This provided a third level of identification in addition to precursor and product ion mass allowing the unequivocal identification of each peptide/protein. Quantitative data for each peptide were taken from one transition, shown underlined in Table 2.10 with a second transition included for identification purposes only.

Table 2.10 MRM transitions for the UPLC-MS/MS analysis of renal proteins. Ions charge is indicated by $^{2+}$ for doubly charged or $^{3+}$ for triply charged ions. Product ions underlined are those used for quantitation whilst non-underlined ions were used for confirmation only.

Protein name	Tryptic peptide sequence	Precursor *m/z*	Cone voltage	Product *m/z*	Collision energy
Albumin	AVMDDFAAFVEK	671.82^{2+}	35	811.43	24
		671.82^{2+}	35	1041.49	24
Cubilin	DGVDSDAPILSK	609.10^{2+}	34	830.74	16
		609.10^{2+}	34	945.79	16
Endothelial protein C receptor	TLAFPLTIR	515.85^{2+}	12	215.17	26
		515.85^{2+}	12	299.82	22
Ig gamma-4 chain C region	EPQVYTLPPSQEEMTK	938.94^{2+}	52	408.37	34
		938.94^{2+}	52	436.37	28
Lysosomal α-glucosidase	AGYIIPLQGPGLTTTESR	937.46^{2+}	22	405.38	30
		937.46^{2+}	22	518.48	24
Megalin	TVLVSEGIVTPR	636.16^{2+}	44	413.44	14
		636.16^{2+}	44	858.79	22
Neutrophil gelatinase-associated lipocalin	VPLQQNFQDNQFQGK	597.61^{3+}	50	414.41	14
		597.61^{3+}	50	591.89	10
Osteopontin	AIPVAQDLNAPSDWDSR	927.90^{2+}	84	511.36	34
		927.90^{2+}	84	835.81	26
Prostaglandin-H2 D-isomerase	TMLLQPAGSLGSYSYR	872.33^{2+}	60	459.44	20
		872.33^{2+}	60	587.50	20
Retinol binding protein	WIEGDELHLEMR	509.74^{3+}	56	504.07	14
		509.74^{3+}	56	614.37	14
Sortilin	DPIYFTGLASEPGAR	797.84^{2+}	26	489.44	22
		797.84^{2+}	26	857.76	26
Vitamin D binding protein	VPTADLEDVLPLAEDITNILSK	789.54^{3+}	16	657.24	22
		789.54^{3+}	16	1053.93	20
Yeast enolase	1. SIVPSGASTGVHEALEMR 2. GNPTVEVELTTEK 3. AVDDFLISLDGTANK	614.58^{3+}	46	771.73	16
		709.06^{2+}	46	948.68	16
		790.16^{2+}	46	661.49	18

Calibration curves were constructed by spiking male control urine with 2.5 µl of 0.1 µg/µl of the yeast enolase internal standard and increasing amounts (0.1 - 150 nmol/l or 0.7 - 172 pmol/l) of each of the synthesised marker peptides used to quantitate the proteins of interest (Figures 9.2.1 and 9.2.2 of supplementary data, section 9.1.1). Endogenous concentrations of the proteins of interest in the male control urine were determined by the intercept on the *x*-axis of the un-spiked urine (0 calibrator point) and this correction value was subtracted from each subsequent calibrator point.

Quantitation of each of the proteins was performed by ratioing the peak area of the native peptide to the peak area of the yeast enolase internal standard (*m/z* 614.58 > 771.73, 709.06 > 948.68 or 790.16 > 661.49). Urinary creatinine concentrations were determined as described in section 2.2.3. Urinary concentrations of the proteins of interest were determined relative to urinary creatinine concentrations.

A Waters Acquity UPLC coupled to a Xevo™ TQ-S triple quadrupole mass spectrometer (Waters Corp, Manchester, UK) was used for validation and verification experiments. The instrument was operated in positive ion mode. The capillary voltage was maintained at 2.5 kV, with source temperature held constant at 150°C and nitrogen used as the nebulizing gas at a flow rate of 30 l/h. For each peptide precursor ion masses were determined in scan mode with product ion masses determined following collision-induced dissociation with argon. Optimum cone and collision energies for each peptide are shown in Table 2.10. Two transitions from each peptide were selected for confirmatory purposes. A Waters ACQUITY UPLC BEH C18 column (2.1 x 100 mm ID., 1.7 µm) was used for separation with solution A (99.9% dd$H_2$0 and 0.1% FA) and solution B (99.9% ACN and 0.1% FA). The flow rate was set to 0.8 ml/min and a

linear gradient of 0 - 97% sol A over 7 min. The total run time was 10 min due to loading, cleaning and reconditioning. A 25 µl injection volume was used with partial loop mode.

2.2.5.9 Data analysis

All data were analysed using MassLynx version 4.1. Statistical differences between sample groups were analysed using Microsoft Excel and Graphpad Prism with statistical significance obtained using standard Student's *t*-test.

2.2.6 Metabolomic analyses

The methods outlined in section 2.2.6 below are used in the metabolomic study described in Chapter 4 to identify new Gb_3-related biomarkers in the plasma of Fabry disease patients.

2.2.6.1 Plasma sample preparation prior to metabolomic analysis (UPLC-ToF-MS)

Plasma samples (section 2.1.2.3) were processed by liquid-liquid extraction using a method adapted from Sullards *et al.*, (2011). Two-hundred microlitres of well mixed plasma from untreated Fabry patients and healthy controls was transferred to individual glass tubes and mixed with 3 ml of MeOH and 1.5 ml of chloroform, sonicated for 30 s, and incubated for 15 hrs at 48°C. Thereafter, 450 µl of potassium hydroxide (KOH) 1M (in MeOH) was added to each tube to hydrolyse unwanted species that would interfere with the liquid-liquid extractions. After the KOH addition, the samples were vortexed for 30 s, sonicated for 30 s, and incubated for 2 hrs at 37°C. The solutions were

neutralised by the addition of 18 µl of glacial acetic acid. For the liquid-liquid extraction, 2 ml of chloroform and 4 ml of water were added and vortexed for 30 s, sonicated for 30 s, and centrifuged for 5 min at 10,000*g*. The lower organic phase was aspirated using a Pasteur pipette, taking care not to disturb the interface and transferred to new test tubes. The aqueous phase was re-extracted with a second 2 ml of chloroform. The combined lower organic phases were dried under a stream of nitrogen and re-suspended in 100 µl of MeOH/5 mM ammonium formate/0.1 % FA.

2.2.6.2 Nomenclature used in metabolomic analyses

Gb_3 isoforms: Gb_3 with different fatty acid chains coupled by amide linkage to an unmodified sphingosine moiety. The principle sphingosine species is described as d18:1, with a total of 18 carbon atoms and a single double bond (Figure 2.5).

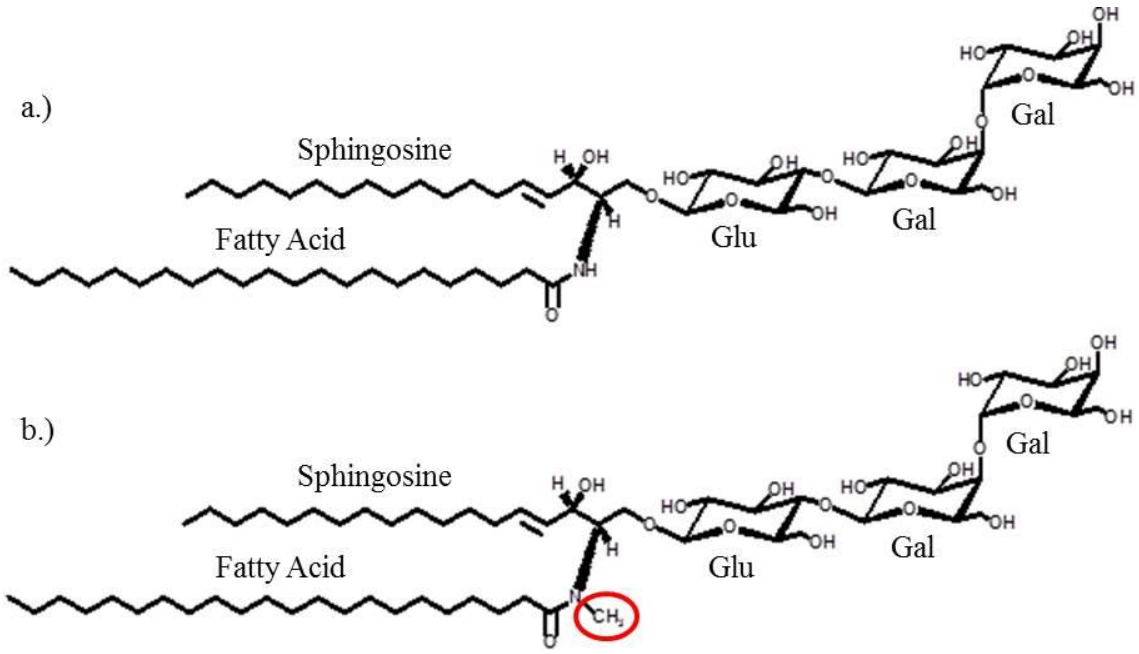

Figure 2.5 Structure of Gb_3 with behenic acid (C_{22}) fatty acid as an example; a.) Native Gb_3; b.) Methylated Gb_3.

Gb_3 analogs: Gb_3 with modified sphingosine moieties. We express the structure of Gb_3 isoforms and analogs in the following way:

$$Gb_3(dv:w)(Cx:y)Z$$

Where d = the sphingosine group; w = the number of double bonds in the sphingosine moiety; v = the number of carbons in the sphingosine moiety; C = the fatty acid group; x = the number of carbon atoms in the fatty acid moiety; y = the number of carbon-carbon double bonds in the fatty acid moiety; Z = other modifications of sphingosine structure (e.g. methylation (Me) or hydration (H_2O).

2.2.6.3 Metabolomic analysis by UPLC-ToF-MS

The ultra-performance electrospray ionization time-of-flight mass spectrometry (UPLC-ESI-ToF-MS) analyses were performed with the use of a Synapt™ (ESI-Quadrupole-ToF-MS) coupled to an ACQUITY UPLC®, both from Waters Corp. (Milford, MA). Between these two systems, a Rheodyne injection valve model MXP9900-000 from IDEX® Health and Science (Oak Harbour, WA) was installed to direct the UPLC eluent toward the mass spectrometer or to divert it to waste. The UPLC and MS methods programmed to analyse the metabolites in the plasma samples under study are shown in Table 2.11.

To increase the mass accuracy during the analysis of plasma metabolites, the “lock mass” option was activated for real-time calibration. For this purpose, a HPLC isocratic pump model 515 from Waters Corp. (Milford, MA) was used to inject the calibrating solution (500 nM terfenadine) through the reference ionisation probe during the sample analysis. The flow rate was decreased to approximately 10 µl min using a “T” splitter before its introduction into the mass spectrometer.

Table 2.11 UPLC and ESI-Tof-MS methods for the analysis of urinary metabolites.

UPLC method		**ESI-ToF-MS method**	
Column	Acquity UPLC® BEH C8	Scan mode	MS-ToF
Company	Waters Corp. (Milford, MA)	Ionisation mode	ESI
Length	50 mm	Polarity	Positive
Internal diameter	2.1 mm	Analyser mode	V
Particle diameter	1.7 µm	Dynamic range	Extended
Temperature	30 °C	Capillary voltage	3.2 kV
Flow rate	0.5 ml/min	Sampling cone voltage	20 V
Mobile phase A	MeOH/5 mM ammonium formate/0.1 % FA	Extraction cone voltage	5 V
Mobile phase B	H_2O/5 % MeOH/5 mM ammonium formate/0.1 % FA	Source temperature	120 °C
Gradient	0-1 min → 50 % A 1-6 min → 50 – 80% A 6-12 min → 80 – 100% A 12-15 min → 100 % A 15-16 min → 100 % A 16-20 min → 50 % A	Desolvation temperature	450 °C
		Cone gas flow	30 l/hr
		Desolvation gas flow	700 l/hr
		Trap collision energy	6 V
		Transfer collision energy	4 V
		Data format	Centroid
Weak wash	50 % phase A/50 % phase B	Mass range	50-2000 Da
Strong wash	MeOH/0.1 % FA	Scan time	0.1 s
Injection volume	7.5 µl	**Lock mass**	
Injection mode	Partial loop overfill	Compound	Terfenadine (500 nM)
Autosampler temperature	15 °C	Exact mass	472.3215 Da
Solvent delay	0-1 min	Solvent	H_2O/5 % ACN/0.5% FA
		Scan time	0.5 s
		Interval	5 s
		Sampling cone voltage	3 V
		Trap collision energy	6 V
		Mass window	± 0.2 Da
		Scan average	3
		Flow rate	~ 10 µl/min

2.2.6.4 Structural characterisation of Fabry disease biomarkers

For the elucidation of the structures of Fabry disease biomarkers by UPLC-ESI-QToF-MS, a 500 µl plasma aliquot from an untreated Fabry male was processed by the procedure mentioned above and re-suspended in 100 µl of phase A.

2.2.6.5 Effects of sample processing

To evaluate the potential effects of sample preparation on the structure of Gb_3 analogs and other potential biomarkers, 150 µl of a synthetic internal standard (Gb_3(d18:1)(C17:0); 0.05 mg/ml in MeOH) was processed as described above with and without the matrix (200 µl of plasma from a healthy control). The Gb_3 synthetic internal standard was chosen for its odd number of carbon atoms on the fatty acid, which is not present in human urine samples.

2.2.6.6 Data mining and multivariate data analysis

The UPLC-ESI-ToF-MS results generated during the metabolomic study were processed using MarkerLynx™ XS (Waters Corp.). This data mining software aligned the metabolites detected in different samples according to their exact mass and retention time, and also measured their peak areas. For the process, the mass range chosen was between 995 and 1200 Da, the intensity threshold was 5 counts, the mass window was 0.20 min. The results treated with MarkerLynx™ XS were downloaded into EZInfo, a software of UMETRICS (Umeå, Sweeden) integrated with the Extended Statistics Tool Box of MassLynx V4.1 (Waters Corp.) for multivariate analysis. Using EZInfo, a supervised Orthogonal Partial Least Square-Discriminant Analysis (OPLS-DA) was

performed to discriminate the 12 untreated Fabry males from the 8 healthy control males. For OPLS-DA, the Pareto scaling (Equation 2.1) was used which increases the weight of medium intensity metabolites without inflating baseline noise:

Equation 2.1:

$$Pareto = \frac{x - y}{\sqrt{\mathrm{SD}}}$$

Where x = area of the metabolite; y = mean area of the metabolite; SD = standard deviation of the area of the metabolite.

An S-plot was generated to highlight the metabolites contributing the most to the discrimination of the two groups of samples during OPLS-DA and considered to be potential Fabry disease biomarkers. The more abundant a biomarker is in patient samples and absent in control samples, the more it will be revealed by the S-Plot. For that reason, only male samples were used for the metabolomic study because, in general, the clinical, physiological and biochemical manifestations of Fabry disease are more severe for male patients compared to females.

2.2.6.7 System stability evaluation

To evaluate the system stability over the metabolomic run, a quality control plasma sample comprised of 10 µl from each Fabry and control sample was analysed 3 times at the beginning of the analytical run, then at every 6 samples and 3 times at the end of the run for a total of 9 replicates.

2.2.6.8 Structural characterisation of Fabry disease biomarkers

The biomarkers identified by multivariate statistical analysis were structurally characterised by tandem mass spectrometry. The UPLC and MS methods were the same as those shown in Table 2.11 for the identification of plasma metabolites, except that the MS mode was Quardrupole-ToF-MS instead of ToF-MS. The precursor ions were thus isolated in the quadrupole (Q), fragmented in the collision cell, and the exact mass of resulting fragments analysed in the ToF system.

2.2.6.9 Relative quantitation of Fabry disease biomarkers

The Fabry disease biomarkers identified by multivariate data analysis were quantitated relatively by integration of peak areas using the QuanLynx™ software (Waters Corp.). The Apex track integration algorithm was employed using a mass window of 0.2 Da and a retention time window of 0.2 min. For smoothing, 3 integrations of the “mean” method were used with a smoothing width of 2.

2.2.7 Investigation of Gb_3 and lyso-Gb_3 toxicity in the Fabry mouse model

The methods outlined in section 2.2.7 below are used in the study described in Chapter 5 to investigate Gb_3 and lyso-Gb_3 toxicity in the Fabry disease mouse model.

2.2.7.1 Proteomic profiling of Fabry mouse tissues

2.2.7.1.1 Tissue preparation prior to proteomic profiling (UPLC-QToF-MS)

Mouse organs (liver, kidney, heart and brain) from Fabry mice (*n* = 3) and wild-type controls (*n* = 3) (section 2.1.2.4) were homogenised in 9 ml of 50 mM ammonium bicarbonate (pH 7.4) per gram of tissue using a Potter-Elvehjem tissue grinder. Homogenates of the same tissue type were combined and a BCA protein assay performed as described in section 2.2.4. Thereafter, 400 µg of protein from each tissue type was aliquoted into 1.8 ml proteomic grade vials, lyophilised and stored at -80°C until required for in-solution digestion (section 2.2.5.4) and fractionation (section 2.2.7.1.2).

2.2.7.1.2 Fractionation of Fabry mouse tissues using high pH C18 chromatography

Following in solution digestion (section 2.2.5.5) Isolute C18 chromatography columns (50 mg/1 ml; Biotage, Hengoed, UK) were successively primed with 1 ml of 50 % ACN containing 0.1 % ammonia and 2 ml of 0.1 % ammonia. One-hundred microlitres of the tissue digest (section 2.2.7.1.1) and 100 µl of 0.2 % ammonia were combined and applied to the pre-conditioned C18 column and allowed to flow though under gravity. This breakthrough fraction was captured and re-applied to the column and the subsequent elution retained. A 500 µl solution of 0.1 % ammonia was then applied to the column and the eluting wash fraction collected and retained. Thereafter, peptides were eluted from the column with 500 µl of a solution containing an increasing percentage of ACN (3 %, 5 %, 8 %, 10 %, 12 %, 15 %, 20 % and 100 %) with 3 % ammonia and each

fraction captured. All fractions were then lyophilised and reconstituted in 30 µl of 3 % ACN containing 0.1 % trifluroacitic acid (TFA) prior to label-free quantitative analysis by UPLC-QToF-MS (section 2.2.5.5).

2.2.7.1.3 Data analysis of Fabry mouse tissues by UPLC-QToF-MS

Analysis of data acquired from all tissue fractions was processed by ProteinLynx Global Server version 2.4 as described in section 2.2.5.6. With the exception that elution start and end times were 5 and 55 min, respectively. Quantitation of mouse proteins using MS^E analyses were determined as fmol of total protein per mg of tissue. In addition, data was also analysed using Progensis LC-MS (Nonlinear Dynamics, Waters Corp.) a data analysis program which identifies and quantitates peptides and proteins detected in label-free analyses based on ion abundance. Differences between groups were assessed by identifying fold changes greater than 2.

2.2.7.2 Protein: glycosphingolipid interaction experiments

2.2.7.3 Sample preparation

Control mouse brain or kidney tissue (100 mg) was homogenised using a Potter-Elvehjem tissue grinder, in 900 µl 150 mM PBS, pH 7.2 and centrifuged for 10 min at 40,000*g* to remove particulate. Thereafter, tissue homogenate supernatant was aliquoted into Eppendorf tubes, a BCA protein assay performed as described in section 2.2.4 and aliquots stored at -80°C until required for analysis.

2.2.7.4 Glycosphingolipid preparation

Glycosphingolipids were solubilised in chloroform: methanol (2:1 v/v) and then centrifugally evaporated. Thereafter, glycosphingolipids were reconstituted in 150 mM phosphate buffered saline (PBS; pH 7.4) to a final concentration of 30 µmol/l.

2.2.7.5 ProteinChip® RS100 array technology

2.2.7.5.1 Coupling glycosphingolipids to the RS100 array surface

Five microlitres of 30 µmol/l glycosphingolipid was added to each spot on the ProteinChip array. The RS100 chip was incubated overnight at 4°C in a humidity chamber to prevent the sample from evaporating. Excess liquid was removed using a clean tissue. Any unreacted carbonyl diiamidazole sites present on the surface of the RS100 chip were blocked by the addition of 5 µl of 0.5 M ethanolamine, 50 mM Tris, pH 8.0, followed by incubation at room temperature (20°C), for 30 min in a humidity chamber. After this time, excess blocking solution was removed using a tissue and the array was washed in a conical tube containing 8 ml of PBS, pH 7.4, 0.1 % Triton X-100, which was agitated for 15 min. The RS100 chip was washed for 15 min in 8 ml PBS containing no Triton X-100, followed by a final wash with 10 ml PBS, pH 7.4 containing no Triton X-100 for 10 min. Excess PBS wash buffer was removed from the areas around the spots using a tissue. Care was taken not to touch the surface of the spots containing the bound glycosphingolipids.

2.2.7.5.2 Tissue binding and extraction

For the analysis 400 µg of mouse brain tissue homogenate supernatant (section 2.2.7.3) was applied to each binding site and aspirated several times to mix and optimise binding. The RS100 chip was then incubated for 2 hrs at room temperature (20°C) in a humidity chamber. Excess sample solution was removed from the spots and the RS100 chip was washed twice in 8 ml of PBS, pH 7.4 containing 0.1 % Triton X-100 for 15 min. The RS100 chip was transferred to a fresh tube and washed in 8 ml PBS, containing no Triton X-100, for 5 min. Bound proteins were removed from the surface of the RS100 chip by the addition of 5 µl FAPHs reagent (50 % FA, 25 % ACN, 15 % isopropyl alcohol), followed by repeated aspiration of the solution. Each wash was combined and collected in Eppendorf tubes. The protein solutions were lyophilised and stored at -20°C prior to in-solution digestion (section 2.2.5.4) and label-free quantitation by UPLC-QToF-MS (section 2.2.5.5).

2.2.7.6 Dynabeads® M-270 epoxy

2.2.7.6.1 Preparation and binding of glycosphingolipids to Dynabeads®

For each analysis 1.5 mg of Dynabeads® were prepared by washing with 1 ml 150 mM PBS, pH 7.2, vortexed for 30 sec and incubated with mixing at room temperature (20°C) for 10 min. The wash solution was removed from the beads by placing the vial on the magnet and carefully pipetting off the supernatant, leaving the beads undisturbed. This wash step was repeated 3 times.

One-hundred microlitres of 30 µmol/l lyso-Gb_3, galactosylsphingosine, sphingosine (section 2.2.7.4) or PBS was added to each aliquot of washed

beads and incubated with mixing for 18 hrs at 4°C. Following incubation glycosphingolipid bound beads were washed as previously described.

2.2.7.6.2 Tissue sample binding and extraction

The glycosphingolipid bound Dynabeads® were then incubated with 400 µg protein from mouse kidney tissue homogenate supernatant (section 2.2.7.3) with mixing for 18 hrs at 4°C. Following incubation with tissue homogenate beads were washed as previously described and after all residual liquid removed stored at -20°C prior to in-solution digestion (section 2.2.5.4) and label-free quantitation by UPLC-QToF-MS (section 2.2.5.5).

2.2.7.7 Data analysis

Data obtained from the RS100 ProteinChip array analysis and the Dynabead M-270 epoxy analysis were analysed using ProteinLynx Global Server version 2.4 as described in section 2.2.5.6. With the exception that elution start and end times were 5 and 55 min, respectively. Proteins identified were considered to interact with a glycosphingolipid if they were not detected as binding to the negative control group.

2.2.7.8 Von Frey assay to assess pain thresholds

In order to assess touch thresholds in mice following exposure to Gb_3 and lyso-Gb_3 a von Frey assay was performed by Professor John Wood, Molecular Nociception Group at UCL, as part of a collaborative project.

2.2.7.8.1 Glycosphingolipid preparation for von Frey assay

The glycosphingolipids Gb_3 and lyso-Gb_3 were solubilised in chloroform/methanol (2:1 v/v) at final concentrations of 300 µmol/l and 30 µmol/l, respectively. Compounds were lyophilised and stored at -20°C until required for analysis. Prior to analysis each lyophilised compound was reconstituted in 100 µl 150 mM PBS, pH 7.2.

2.2.7.8.2 Von Frey assay

For the von Frey assay C57BL/6 mice were used. Each subject mouse was assigned an identification key and placed into one of the following test groups; Gb_3 (n = 9) lyso-Gb_3 (n = 9) and control/PBS (n = 6). Identification keys and test groups were assigned by someone other than the test operator so as not to introduce testing bias.

2.2.7.8.3 Von Frey assay – habituation

Subject mice were placed into their assigned, specific test compartment and left to explore, undisturbed for 1 hr. After exploratory behaviour had stopped or decreased to a minimal level the test operator entered the room for 5 min before starting the test.

2.2.7.8.4 Von Frey assay – testing

Following the intraplantar injection of Gb_3, lyso-Gb_3 or saline (Figure 2.6) the von Frey assay was performed 0, 0.5, 1, 2, 4, 6 and 24 hr post injection. The first von Frey hair was applied perpendicular to the paw (Figure 2.6), until it buckled slightly and was held for 3 sec. If a response (pain behaviour) was

observed the first column of a scoring grid was marked with an “X”. If no response was observed it was marked with an “O”. It should be noted that the mouse should not be asleep or grooming during testing as this may influence the response (Callahan *et al.*, 2008). If the hair used produced a response the next lower weight hair was selected for the following use. Conversely, if the hair used failed to produce a response the next higher weight hair was selected for the following use. A minimum interval of 1 min was left between each application. Increasing or decreasing application of weighted hairs was applied and the results marked into the first column of a scoring grid until a change in response occurred – e.g., “XXXO” or simply “OX”. Once the perception threshold had been crossed, the continued application of increasing (no response) or decreasing (response) weighted hairs, for the next five applications was recorded.

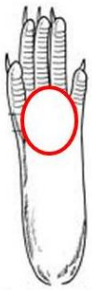

Figure 2.6 Mouse paw with the circle indicating the area of the plantar surface of the paw to be stimulated with von Frey hair as well as the site for intraplantar injection

2.2.7.8.5 Von Frey assay – threshold calculation

Using the reference table (Table 2.12) the corresponding κ value for each response series was allocated and used in equation 2.2 to calculate the 50 % threshold (grams).

Table 2.12 Von Frey kappa value reference table. The number of responses before the response threshold is crossed determines the column. The following pattern of responses determines the row. *Note that the κ value is inverted if the response series prior to threshold crossing is X.*

κ for test series whose first part is:					
	O	OO	OOO	OOOO	
XOOOO	-0.547	-0.547	-0.547	-0.547	OXXXX
XOOOX	-1.250	-1.247	-1.246	-1.246	OXXXO
XOOXO	0.372	0.380	0.381	0.381	OXXOX
XOOXX	-0.169	-0.144	0.142	-0.142	OXXOO
XOXOO	0.022	0.039	0.040	0.040	OXOXX
XOXOX	-0.500	-0.458	-0.453	-0.453	OXOXO
XOXXO	1.169	1.237	1.247	1.248	OXOOX
XOXXX	0.611	0.732	0.756	0.758	OXOOO
XXOOO	-0.296	-0.266	-0.263	-0.263	OOXXX
XXOOX	-0.831	-0.763	-0.753	-0.752	OOXXO
XXOXO	0.831	0.935	0.952	0.945	OOXOX
XXOXX	0.296	0.463	0.500	0.504	OOXOO
XXXOO	0.500	0.648	0.678	0.681	OOOXX
XXXOX	-0.043	0.187	0.244	0.252	OOOXO
XXXXO	1.603	1.917	2.000	2.014	OOOOX
XXXXX	0.893	1.329	1.465	1.496	OOOOO
	X	XX	XXX	XXXX	
- κ for test series whose first part is:					

Equation 2.2:

$$50\ \%\ threshold\ = (10^{[x+\mathrm{k}\delta]}/\ 10{,}000)$$

Where; *x* = log of the final von Frey hair used; κ = tabular value and ; δ = log of mean difference between stimuli (typically 0.224 for most von Frey sets)

2.2.7.8.6 Data analysis of von Frey assay

Statistical differences between sample groups were analysed using Microsoft Excel and Graphpad Prism with statistical significance obtained using standard Student's *t*-test.

2.2.7.9 ATP synthase (complex V) enzyme activity assay

An ATP synthase enzyme activity microplate assay kit was purchased from Abcam (Cambridge, UK).

2.2.7.9.1 Isolation of mitochondria from rat liver

Following the sacrifice of a rat (section 2.1.2.4), the liver was removed, washed with ice cold saline and the mitochondria isolated immediately. The liver was homogenised with ice cold homogenisation buffer (250 mM sucrose, 2 mM hydroxyethylpiperazine-N'-2-ethanesulfonic acid (HEPES) and 0.1 M ethylene glycol tetraacetic acid (EGTA), pH 7.4) and centrifuged at 25,000*g* for 10 min at 4°C. The supernatant (S1) was removed with care taken not to disrupt the pellet and stored on ice. To maximise mitochondrial yield the pellet was re-suspended in homogenisation buffer and the homogenisation process repeated. The supernatant was removed, combined with S1 and centrifuged at 25,000*g* for 10 min at 4°C. The supernatant was removed and the resultant mitochondrial pellet transferred to an Eppendorf tube, a BCA protein assay performed as described in section 2.2.4 and stored at -80°C until required for analysis.

2.2.7.9.2 Sample preparation for ATP synthase assay

The mitochondrial pellet was thawed and re-suspended in 4 volumes of buffer solution and the protein concentration adjusted to 5.5 mg/ml. An extraction was performed by adding 1/10 volume detergent to the sample making the final protein concentration 5 mg/ml, vortexed immediately and incubated on ice for 30 min. The sample was then centrifuged at 38,000*g* for 20 min. The supernatant was saved as sample and the pellet discarded. The sample was diluted in buffer solution to a final concentration of 1 µg/5 µl. Diluted samples were kept on ice until required for analysis.

2.2.7.9.3 ATP synthase assay

Fifty microlitres of sample was added to each individual well on the plate required for analysis. Buffer (50 µl) was added to 1 well to act as a null control or background reference. The plate was incubated at room temperature for 3 hrs.

Following incubation, during which time the bound antibody immobilises the enzyme in the wells, all liquid was removed by turning the plate over and shaking. Once emptied, 300 µl of buffer solution was added to each well in a wash step, all liquid was removed by turning the plate over and shaking. This step was repeated twice. Once the wells were empty 40 µl of a high medium or low concentration lipid of lyso-glycosphingolipid (see Table 2.13) was added to each well required for analysis and incubated at room temperature for 45 min. Following incubation 200 µl of reagent mix was added to each well. All bubbles were removed with a fine needle. The plate was then placed in an Infinite® 200 PRO plate reader (Tecan, Theale, Reading, UK) and the absorbance read at 340 nm at 1 min intervals for 120 min.

Table 2.13 Lipids and lyso-glycosphingolipids concentrations used to assess the effect on levels of ATP synthase activity.

Lipid	High	Medium	Low
Globotriaosylceramide (Gb_3)	300 µmol/l	30 µmol/l	0.3 µmol/l
Lyso-Gb_3	30 µmol/l	0.3 µmol/l	0.003 µmol/l
Sulfatide	300 µmol/l	30 µmol/l	0.3 µmol/l
Lyso-sulfatide	30 µmol/l	0.3 µmol/l	0.003 µmol/l
GM_1 ganglioside	300 µmol/l	30 µmol/l	0.3 µmol/l
Lyso-GM_1 ganglioside	30 µmol/l	0.3 µmol/l	0.003 µmol/l
Glucosylceramide	300 µmol/l	30 µmol/l	0.3 µmol/l
Lyso-glucosylceramide	30 µmol/l	0.3 µmol/l	0.003 µmol/l
Galactosylceramide	300 µmol/l	30 µmol/l	0.3 µmol/l
Lyso-galactosylceramide	30 µmol/l	0.3 µmol/l	0.003 µmol/l
Lactosylceramide	300 µmol/l	30 µmol/l	0.3 µmol/l
lyso-lactosylceramide	30 µmol/l	0.3 µmol/l	0.003 µmol/l
Cardiolipin	300 µmol/l	30 µmol/l	0.3 µmol/l

2.2.7.9.4 Data analysis

The activity of the ATP synthase enzyme is coupled to the molar conversion of NADH to NAD^+ measured as a decrease in absorbance at 340 nm. The activity rate is expressed as the change in absorbance at optical density (OD) 340 nm/min/amount loaded into the well.

Therefore, to calculate a value for ATP synthase the rate of decrease in absorbance at 340 nm over time is analysed. The rate is calculated between two time points when the fastest most linear rate of activity is seen (Figure 2.7) using equation 2.3.

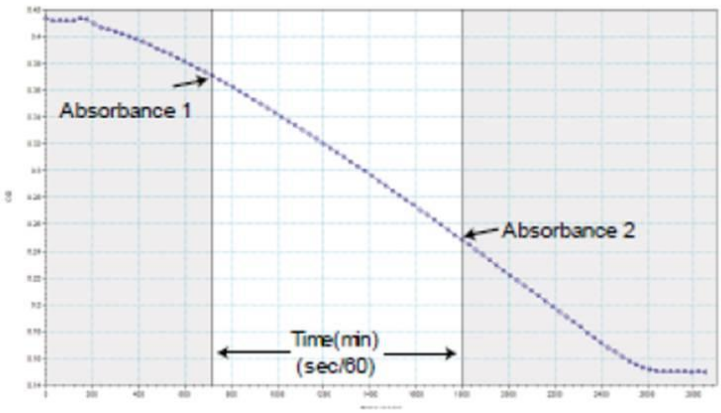

Figure 2.7 Example of a trace obtained during the analysis of ATP synthase. Indicating the time points between which rate should be calculated using equation 2.3.

Equation 2.3:

$$\text{Rate (mOD/min)} = \frac{Absorbance\ 1 - Absorbance\ 2}{Time\ (min)}$$

Statistical differences between groups were analysed using Microsoft Excel with statistical significance obtained using standard Student's *t*-test.

2.2.8 Mitochondrial respiratory chain enzymes

The methods outlined in section 2.2.8 below are used in the investigation of mitochondrial respiratory chain enzyme activities described in Chapter 6.

2.2.8.1 Sample preparation

Mouse organs (liver, kidney, heart and brain) from Fabry (*n* = 8) and wild-type control (*n* = 8) mice (see section 2.1.2.4) were homogenised using a Potter-Elvehjem tissue grinder in 9 ml of a muscle isolation buffer (320 mM sucrose, 1 mM EDTA, 10 mM Trizma-base in H_2O, pH 7.4) or a liver and kidney isolation

buffer (250 mM sucrose, 1 mM EDTA, 10 mM Trizma-base in ddH_2O, pH 7.4) per gram of tissue. Thereafter, tissue homogenates were aliquoted into Eppendorf tubes® and stored at -80°C until required for analysis.

2.2.8.2 Complex I (NADH-ubiquinone oxidoreductase) assay

The method described by Ragan *et al.*, (1987) was modified and used to measure complex I activity in tissue homogenates. This assay measures the oxidation of NADH, at the decrease in absorbance at 340 nm, during the reduction of ubiquinone to ubiquinol by complex I. The specific complex I inhibitor rotenone is used to determine the proportion of NADH oxidation which is independent of complex I.

Tissue homogenates were successively thawed and refrozen in liquid nitrogen (twice) following which, for each analysis, a sample and corresponding reference cuvette were prepared as shown in Table 2.14.

Table 2.14 Preparation of sample and reference cuvettes required for the analysis of complex I.

Reagent	**Sample** (µl)	**Reference** (µl)
25 mM potassium phosphate / 10 mM magnesium chloride (pH 7.2)	800	800
50 mg/ml bovine serum albumin (BSA)	50	50
5 mM β-NADH	30	30
100 mM potassium cyanide (KCN)	10	10
Homogenate	20	20
ddH_2O	80	90

The cuvettes were then gently mixed and placed in a Uvikon 941 spectrophotometer (Northstar Scientific, Potton, UK) and left for 2 min to reach 30 °C. The reaction was started by the addition of 10 µl 5 mM ubiquinone to the sample cuvettes only. Cuvettes were again gently mixed and the reaction was measured at 340 nm at 30 sec intervals for 5 min. After 5 min 20 µl 1 mM rotenone was added to sample cuvettes only and measurement continued for a further 5 min.

To calculate a value for complex I activity the change in absorbance at 340 nm following rotenone addition was subtracted from that before rotenone inhibition. Absorbance was converted to molar concentration using the NADH extinction coefficient 6.81 x 10^3 M^{-1} cm^{-1} (path length 1 cm, total volume 1 ml), taking account of ubiquinone, using a re-arrangement of Beer-Lambert law, equation 2.4:

Equation 2.4:

$$\frac{\Delta A}{\varepsilon} = c$$

Where ∆A is the specific change in absorbance; ε = extinction coefficient; and *c* = mole/min/ml. Results are expressed as a ratio to citrate synthase activity (section 2.2.8.5).

2.2.8.3 Complex II/III (succinate dehydrogenase cytochrome c reductase) assay

The method described by King (1967) was modified and used to measure complex II/III activity in tissue homogenates. This assay measures the

succinate dependent reduction of cytochrome c by measuring the increase in absorbance at 550 nm. The complex III inhibitor antimycin A is used to determine the proportion of cytochrome c oxidation which is independent of complex II/III activity.

Tissue homogenates were successively thawed and refrozen in liquid nitrogen (twice) following which, for each analysis, a sample and corresponding reference cuvette were prepared as shown in Table 2.15.

Table 2.15 Preparation of sample and reference cuvettes required for the analysis of complex II/III.

Reagent	**Sample** (µl)	**Reference** (µl)
166 mM Potassium phosphate (pH 7.4)	600	600
15 mM EDTA	20	20
100 mM KCN	10	10
0.8 mM Cytochrome C	125	125
Homogenate	20	20
ddH_2O	185	225

The cuvettes were then gently mixed and placed in a Uvikon 941 spectrophotometer (Northstar Scientific) and left for 2 min to reach 30 °C. The reaction was started by the addition of 40 µl 0.5 M succinate to the sample cuvettes only. Cuvettes were again gently mixed and the reaction was measured at 550 nm at 30 sec intervals for 5 min. After 7 min 10 µl 1 mM antimycin A was added to sample cuvettes only and measurement continued for a further 5 min.

To calculate a value for complex II/III activity the change in absorbance at 550 nm following antimycin A addition was subtracted from that before antimycin A inhibition. Absorbance was converted to molar concentration using Beer-Lambert law (equation 2.4; section 2.2.8.2) and the extinction coefficient of cytochrome c, 19.2 x 10^3 M^{-1} cm^{-1} (path length 1 cm, total volume 1ml). Results are expressed as a ratio to citrate synthase (section 2.2.8.5).

2.2.8.4 Complex IV (cytochrome C oxidase) assay

The method described by Wharton and Tzagoloff (1967) was modified and used to measure complex IV activity in tissue homogenates. This assay measures the reduction of cyctochrome c catalysed by complex IV.

Prior to analysis of tissue homogenates, reduced cytochrome c was prepared by the addition of a few crystals of ascorbic acid to 10 mg/ml oxidised cytochrome c in water. A PD_{10} desalting column (GE Healthcare Life Sciences, Buckinghamshire, UK) equilibrated with 10 mM potassium phosphate (pH 7.0) in ddH_2O, was then used to remove ascorbate from the reduced cytochrome c. Thereafter, 50 µl reduced cytochrome c was added to 950 µl ddH_2O in a sample and reference cuvette. The sample cuvette was blanked against the reference at 550 nm using a Uvikon 941 spectrophotometer (Northstar Scientific). Cytochrome c in the reference cuvette was then oxidised by the addition of 10 µL 100 mM ferricyanide. The absorbance was recorded after 1 min and used to determine the concentration of reduced cytochrome c using Beer-Lambert law (see equation 2.2; section 2.2.8.2) and the extinction coefficient for cytochrome c, 19.2 x 10^3 M^{-1} cm^{-1} (path length 1 cm, total volume 1 ml).

Tissue homogenates were successively thawed and refrozen in liquid nitrogen (twice) following which, for each analysis, a sample and corresponding reference cuvette were prepared as shown in Table 2.16.

Table 2.16 Preparation of sample and reference cuvettes required for the measurement of complex IV. X = volume of stock reduced cytochrome c to give a final concentration of 50 µM.

Reagent	**Sample** (µl)	**Reference** (µl)
100 mM Potassium phosphate (pH 7.0)	100	100
Cytochrome c (reduced)	**X**	**X**
ddH_2O	880-**X**	890-**X**

The cuvettes were then gently mixed and placed in a Uvikon 941 spectrophotometer (Northstar Scientific) and the sample cuvette blanked against the reference cuvette at 550 nm. Thereafter, 10 µl 100 mM ferricyanide was added to the reference cuvette to oxidise cytochrome c. The reaction was started by the addition of 20 µl homogenised tissue sample to the sample cuvette and the change in absorbance at 550 nm was recorded over 3 min at 30°C.

The reaction of complex IV with cytochrome c follows first order kinetics as it is dependent on the concentration of cytochrome c. Activity is therefore expressed as a first order rate constant (k). k is calculated by plotting the natural log of absorbance against time and determining the slope. Results are expressed as k/mol when divided by citrate synthase activity.

2.2.8.5 Citrate synthase assay

Mitochondrial citrate synthase is the first enzyme of the tricarboxylic acid cycle responsible for catalysing the condensation of acetyl-Coenzyme A and oxaloacetate to yield citric acid and CoA. Citrate synthase activity is frequently used as a mitochondrial marker and also as a measure of mitochondrial enrichment (Winder and Holloszy 1977; Fatania and Dalziel 1980; Hargreaves, Heales, and Land 1999). The method described by Shepherd and Garland (1969) was modified and used to measure citrate synthase activity in tissue homogenates.

Tissue homogenates were successively thawed and refrozen in liquid nitrogen (twice) following which, for each analysis, a sample and corresponding reference cuvette were prepared as shown in Table 2.17.

Table 2.17 Preparation of sample and reference cuvettes required for the analysis of citrate synthase

Reagent	**Sample** (µl)	**Reference** (µl)
100 mM Tris/0.1 % v/v Triton (pH 8.0)	950	960
Homogenate	20	20
Acetyl-CoA	10	10
5,5'-dithiobis-(2-nitrobenzoic acid) (DTNB)	10	10

The cuvettes were then gently mixed and placed in a Uvikon 941 spectrophotometer (Northstar Scientific). The reaction was started by the addition of 10 µl 20 mM oxaloacetate to the sample cuvettes only. Cuvettes were again gently mixed and the reaction was measured at 412 nm at 30 sec

intervals for 5 min at 30°C. After 7 min 10 µl 1 mM antimycin A was added to sample cuvettes only and measurement continued for a further 5 min. Absorbance was converted to molar concentration using Beer-Lambert law (see equation 2.4; section 2.2.8.2) and the extinction coefficient of DTNB, 13.6 x 10^3 M^{-1} cm^{-1} (path length 1 cm, total volume 1 ml).

2.2.8.6 Transformation of data

Prior to statistical analysis complex I, II/III and IV activities when expressed as a ratio to citrate synthase were transformed by the following calculation (equation 2.5):

Equation 2.5:

$$Arcsin\sqrt{(ratio)}$$

Where percentage values were first divided by 100 to give a ratio. This transformation yielded data with a normal distribution to enable statistical analysis to be performed (Gegg *et al.*, 2003).

Chapter 3

A proteomic study to identify and validate potential urinary biomarkers in Fabry disease

Chapter 3 - A proteomic study to identify and validate potential urinary biomarkers in Fabry disease 156

3.0 A proteomic study to identify and validate potential urinary biomarkers in Fabry disease

3.1 Introduction

Fabry disease is an X-linked lysosomal storage disorder caused by abnormalities in the *GLA* gene, which results in a deficiency of the enzyme α-galactosidase A (α-GAL) (Bishop, Kornreich and Desnick 1988; Zarate and Hopkin 2008). This leads to the progressive accumulation of neutral glycosphingolipids, primarily globotriaosylceramide (Gb_3, CTH or GL-3) in the lysosome of the cell. With time accumulation of Gb_3 leads to hypertrophy of the lysosome and leakage of these metabolites into the circulation. The clinical consequences of α-GAL deficiency are varied and include acroparathesia and painful crises, hypohidrosis, gastrointestinal symptoms, angiokeratoma and corneal opacities. As the disease progresses proteinuric kidney complications, the same as those experienced by diabetic patients, as well as cardiac involvement and cerebrovascular events can be life limiting (Zarate and Hopkin 2008; Schiffmann 2009; O'Mahony and Elliott 2010).

Enzyme replacement therapy (ERT) has been shown to stabilise renal function and cardiac size, as well as improve pain and quality of life (Eng *et al.*, 2001; Schiffmann *et al.*, 2001). Some reduction in frequency of occurrence of established renal failure and cardiovascular events has also been reported, but ERT cannot reverse established disease and it is not yet clear whether early treatment can prevent development of significant end organ involvement (Hughes *et al.*, 2008; Warnock *et al.*, 2012). More recently, pharmacological chaperone therapy has been developed as a therapeutic treatment for Fabry

disease. Following promising results in preclinical studies (Benjamin *et al.*, 2012; Young-Gqamana *et al.*, 2013), further clinical trials to assess the use of pharmacological chaperone therapy both as an oral monotherapy and in combination with ERT are underway.

Currently, Gb_3 is used as a biomarker to monitor response to therapy and urine and plasma Gb_3 concentrations can be measured reliably by tandem mass spectrometry (Young *et al.*, 2005; Mills *et al.*, 2004; Mills *et al.*, 2005). However, whilst it has been suggested that urinary Gb_3 concentration is more useful than Gb_3 concentration in plasma (Young *et al.*, 2005), Gb_3 has not proven to be an ideal biomarker for measuring the response to treatment in all patients; i.e., falls in urinary Gb_3 concentrations are not sustained in all cases despite clinical improvement (Mills *et al.*, 2005). More recently, plasma and urinary lyso-Gb_3, a deacylated form of Gb_3, has been proposed as a potentially useful diagnostic biomarker of Fabry disease, and studies have shown lyso-Gb_3 to exhibit a better degree of correlation with disease severity and progression (Aerts *et al.*, 2008). However, in a study by Auray-Blais *et al.*, (2010) no significant correlation between lyso-Gb_3 in urine and estimated glomerular filtration rates were found suggesting that lyso-Gb_3 is not a good predictive biomarker for kidney involvement.

Therefore, there is a growing need for additional biomarkers that can enable detection of Fabry disease at an early stage of disease progression and that are more specific for monitoring responses to treatment than urinary Gb_3 and/or lyso-Gb_3 concentrations alone. In addition, as it can take many years for detectable cardiac or renal disease to develop, it is currently very difficult to assess the efficacy of therapy in children. A biomarker that would allow

monitoring of disease burden, as chitotriosidase does in Gaucher disease (Aerts *et al.*, 2005), or glucose tetrasaccharide does in Pompe disease (Manwaring *et al.*, 2012), would provide a useful tool in guiding treatment.

In the present study a label-free proteomic methodology was used to identify potential biomarkers in the urine of paediatric Fabry disease patients. For the purpose of this study patients were identified and grouped according to their biochemical level of disease burden. Those patients having Gb_3 levels that fell to < 0.05 µmol/mmol creatinine following instigation of ERT were identified as having the least disease burden and those patients in whom Gb_3 levels remained > 0.05 µmol/mmol creatinine following instigation of ERT were identified as having the most disease burden. Following the discovery of two potential biomarkers, prosaposin and ganglioside GM_2 activator protein, independent of level of disease burden, an initial rapid multiple reaction monitoring ultra-performance liquid chromatography-tandem mass spectrometry (MRM UPLC-MS/MS) assay was developed for verification and validation purposes. Following the success of the initial assay a second MRM UPLC-MS/MS assay was developed in order to identify biomarkers capable of detecting and monitoring pre-symptomatic kidney disease in those patients most at risk.

3.2 Results

3.2.1 Biomarker discovery experiments

MS^E label-free quantitative proteomic methodologies using UPLC-QToF-MS have been used previously for the identification of novel biomarkers from a number of biological fluids and tissues (Bennett *et al.*, 2010; Bostanci *et al.*, 2010; Heywood *et al.*, 2012b). This methodology (section 2.2.5) has now been developed for the identification of urinary biomarkers for Fabry disease.

3.2.2 Proteomic profile of Fabry disease urine samples

Ten pre-treatment paediatric urine samples and the corresponding post-treatment samples (Table 2.1) following 12 months of ERT were analysed by label-free quantitative proteomics. Altogether, 191 proteins were detected using this technique, 144 proteins in pre-treatment samples and 118 in post-treatment samples. Figures 3.1 and 3.2 show an averaged profile of the urinary proteome of the proteins detected in pre-treatment urine samples. The most abundant proteins observed were uromodulin and serum albumin which constituted approximately 8 and 6 % of the total protein detected, respectively.

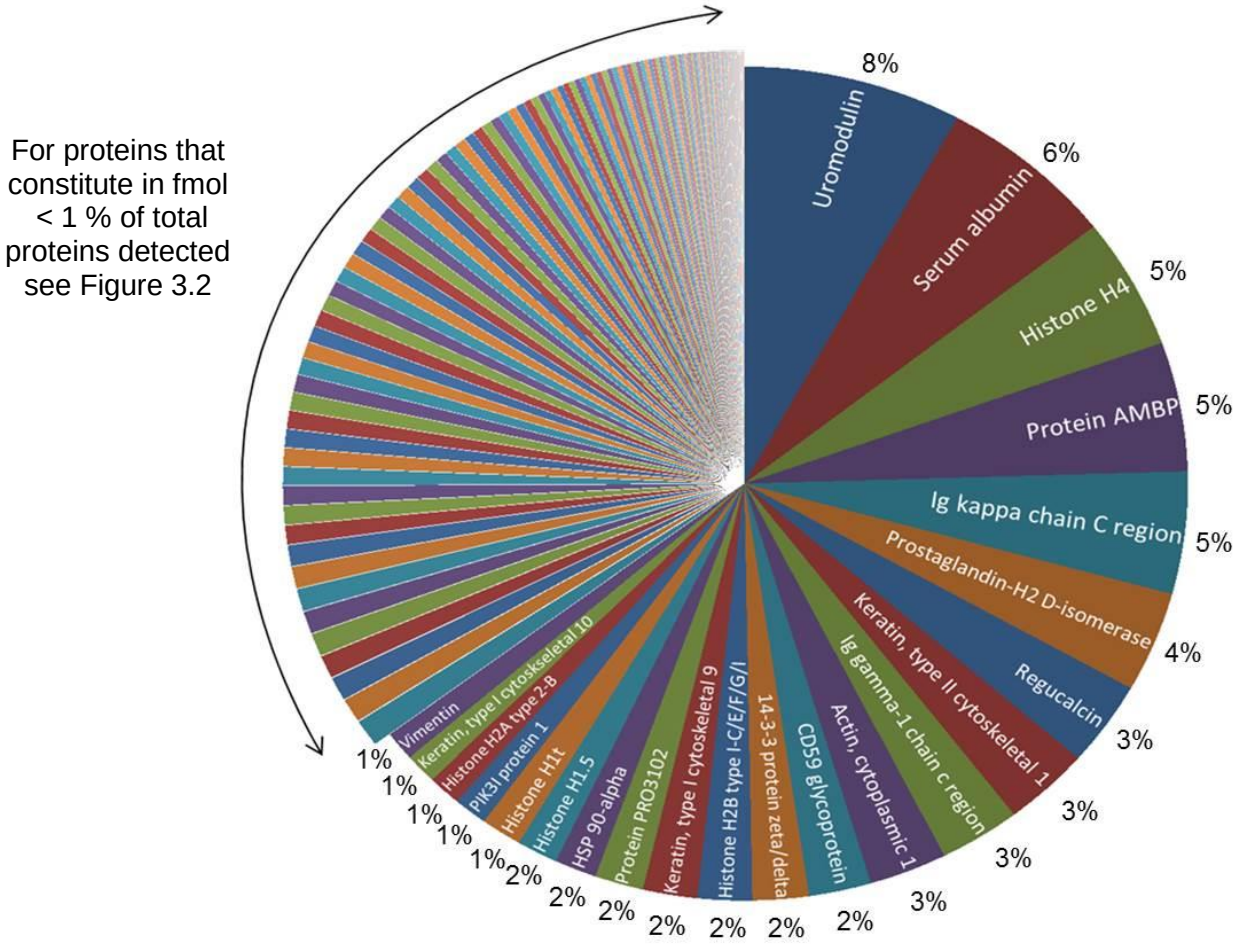

Figure 3.1. Schematic representation of a typical proteome of urine from paediatric Fabry disease patients prior to ERT. Proteins are represented as % fmol of protein of total proteins detected.

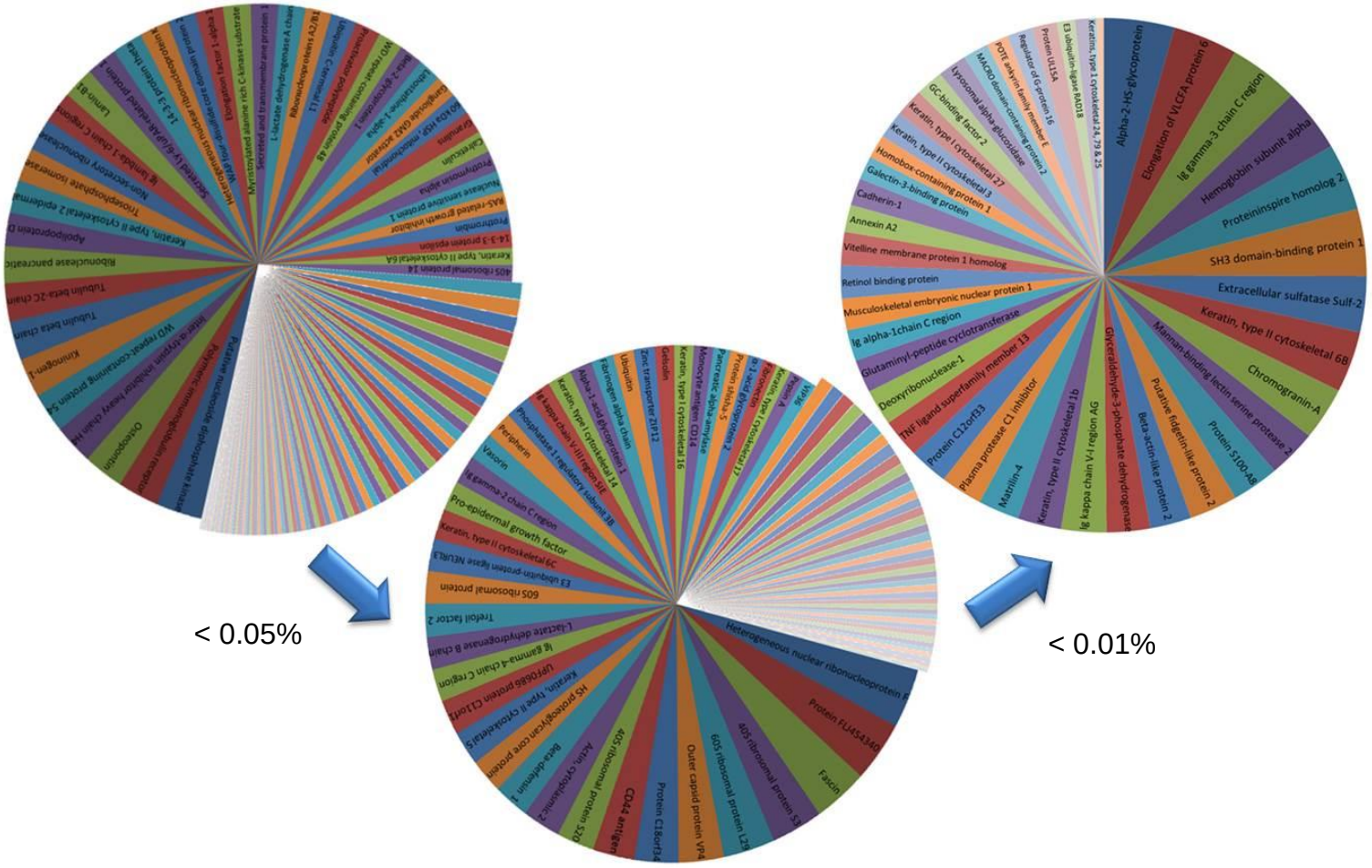

Figure 3.2. Schematic representation of lower abundance proteins. Proteins that constitute in fmol < 1% of total proteins detected in a typical proteome of urine from paediatric Fabry disease patients prior to ERT.

3.2.3 Proteins that decreased following 12 months of ERT

The concentration of the lysosomal protein prosaposin was increased significantly in the urine of Fabry patients prior to ERT. Following 12 months of treatment prosaposin was observed to be statistically decreased (p = 0.03) in both those patients with the most disease burden and those with the least disease burden (Figure 3.3). This significance was increased when patients with most disease burden were excluded from the analysis (p = 0.005).

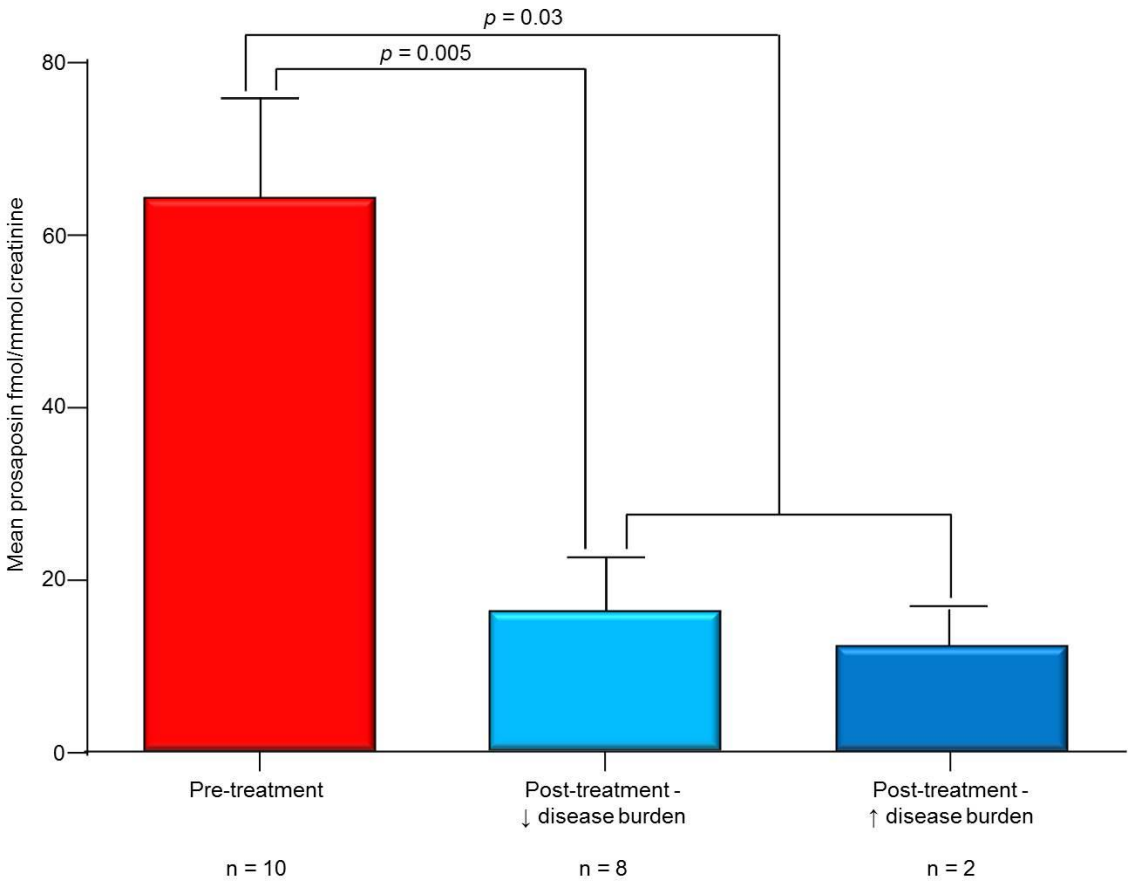

Figure 3.3. Urinary prosaposin concentrations, using QToF-MS, pre-treatment and post-treatment in patients with the least (↓) and the most (↑) disease burden. Error bars represent mean ± standard deviation (SD).

Although only one protein showed a significant and statistical change pre- and post-treatment using *t*-test analyses, the data were also reanalysed for fold changes. Using this type of analysis the concentration of 12 additional proteins showed a greater than 2-fold change following 12 months of treatment (Figures 3.4 and 3.5).

Included in these 12 proteins was another lysosomal protein and also a genetically distinct saposin, ganglioside GM_2 activator protein (GM_2AP) (Figure 3.4.1e). While this protein did not reach statistical significance using *t*-test analyses (p = 0.2) this protein had a 2.1-fold change reduction following treatment represented by a mean value of 6.58 fmol/mmol creatinine pre-treatment falling to 3.10 fmol/mmol creatinine post-treatment. Therefore, although not significant the variation shown by this protein was considered of potential importance and developed into the initial targeted MRM assay for evaluation in addition to the prosaposin molecule. By using a targeted methodological approach improved discrimination of GM_2AP and better determination of significance between patient groups may be achievable.

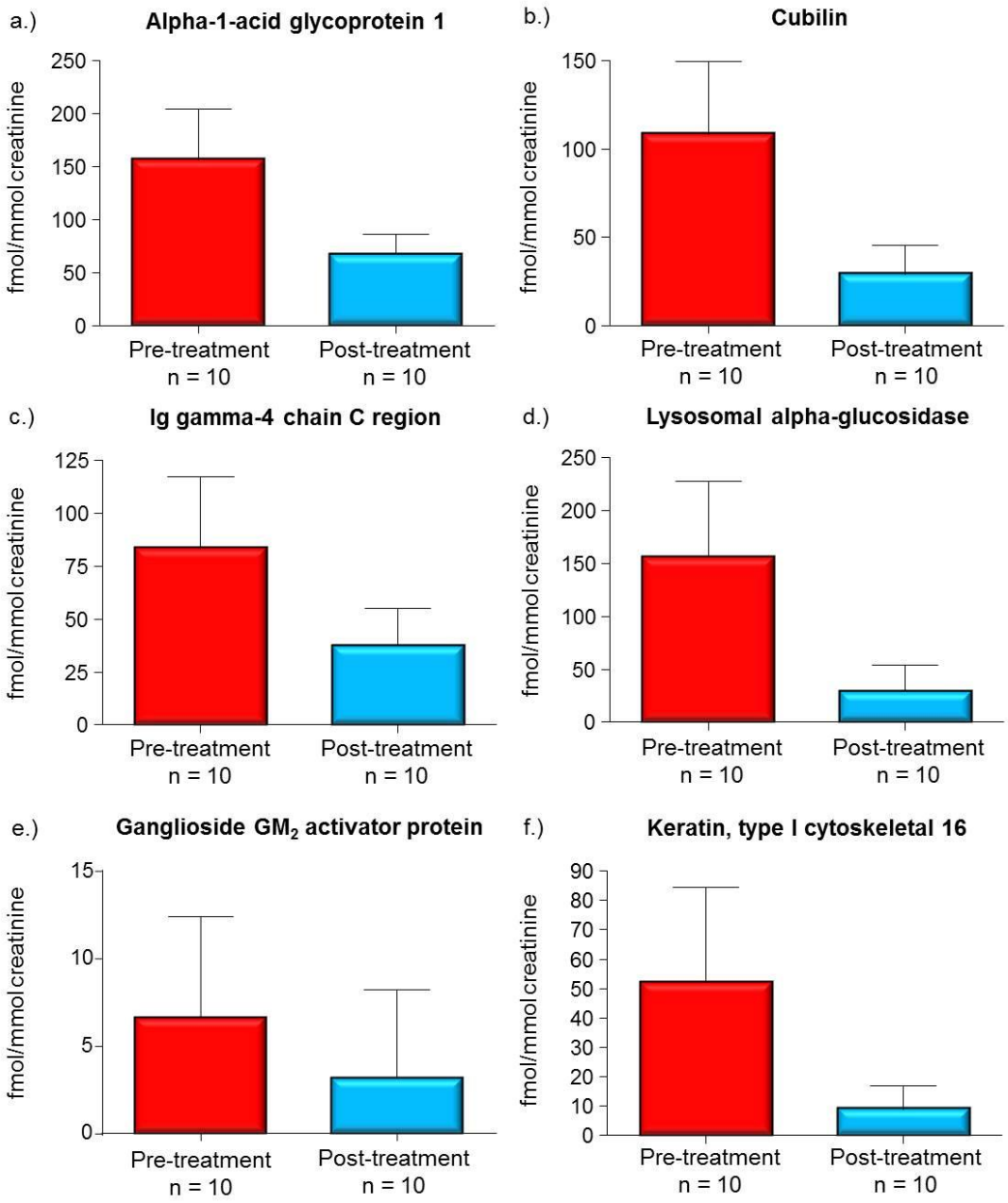

Figure 3.4.1. Urinary proteins showing a greater than two-fold decrease following 12 months of ERT, using QToF-MS; a.) Alpha-1-acid glycoprotein 1; **b.)** Cubilin; **c.)** Ig gamma-4 chain C region; **d.)** Lysosomal alpha-glucosidase; **e.)** Ganglioside GM_2 activator protein and; **f.)** Keratin, type I cytoskeletal 16. Error bars represent mean ± SD.

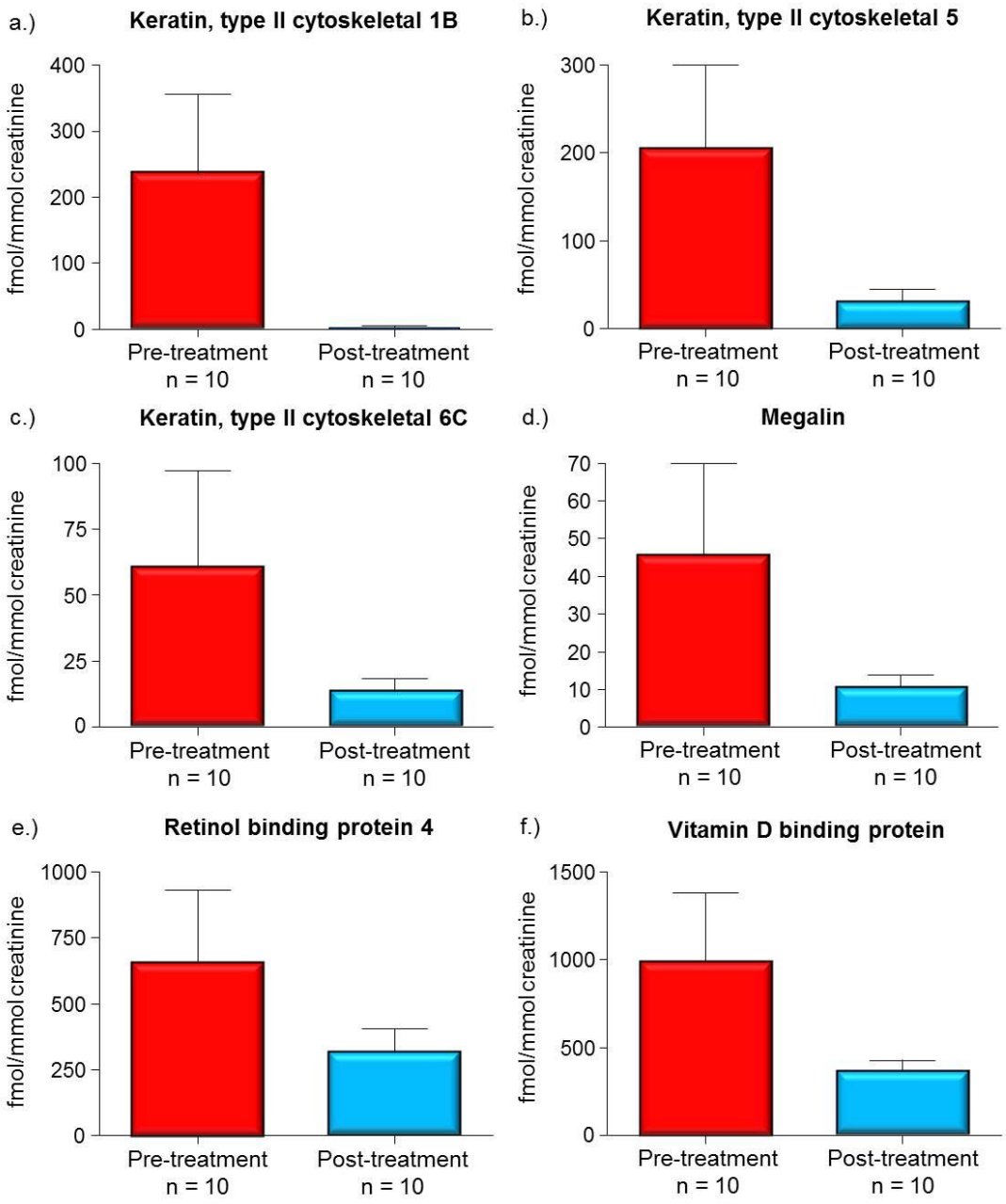

Figure 3.4.2. Urinary proteins showing a greater than two-fold decrease following 12 months of ERT, using QToF-MS; a.) Keratin, type II cytoskeletal 1B; **b.)** Keratin, type II cytoskeletal 5; **c.)** Keratin, type II cytoskeletal 6C; **d.)** Megalin; **e.)** Retinol binding protein 4 and; **f.)** Vitamin D binding protein. Error bars represent mean ± SD.

3.2.4 Proteins that increased following 12 months of ERT

Of the 118 proteins detected in post-treatment samples none were shown to be increased significantly using *t*-test analyses. However, the concentrations of 6 proteins showed a greater than 2-fold increase following 12 months of ERT (Figure 3.5).

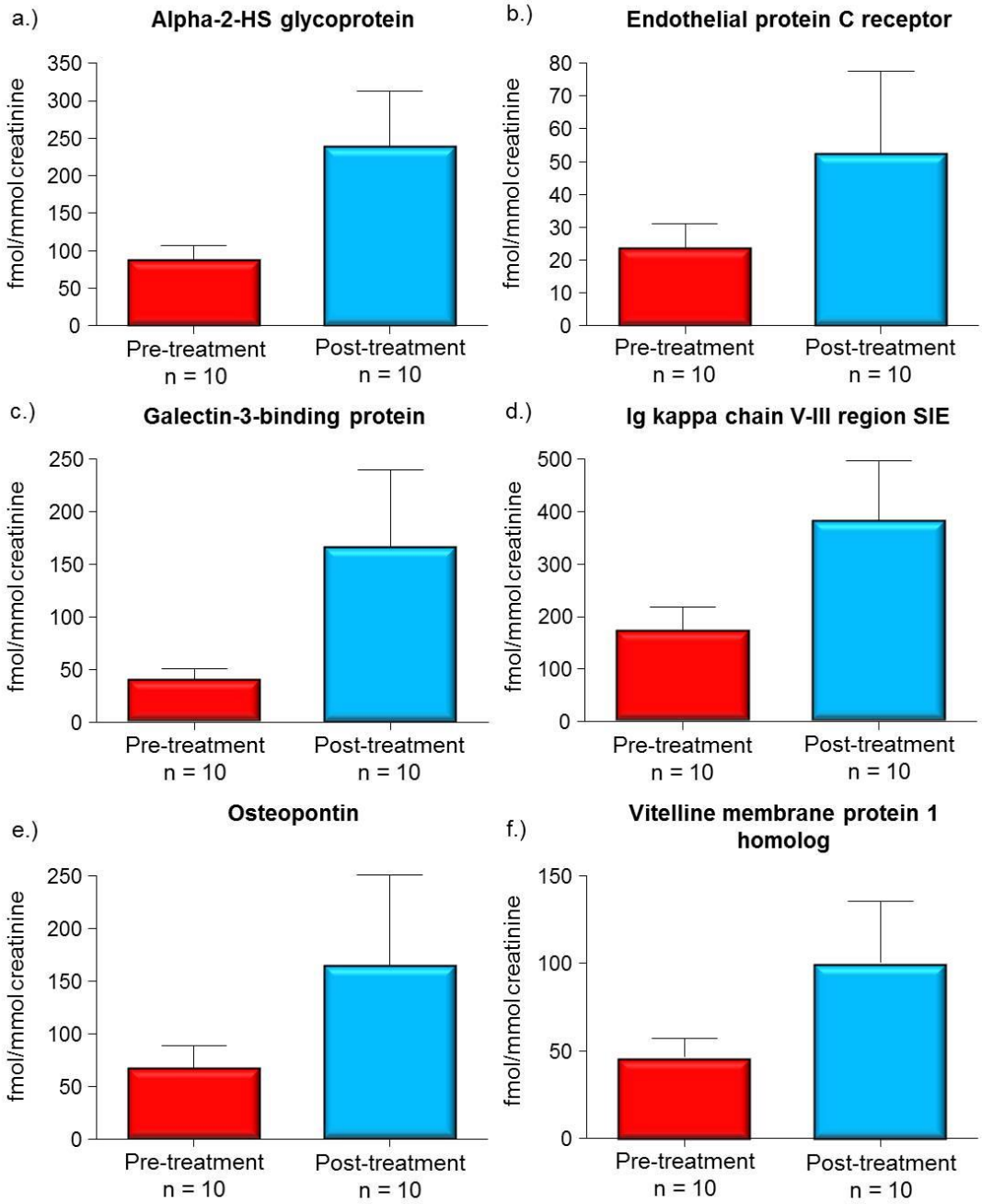

Figure 3.5 Urinary proteins showing a greater than two-fold increase following 12 months of ERT, using QToF-MS; a.) Alpha-2-HS glycoprotein; **b.)** Endothelial protein C receptor; **c.)** Galectin-3-binding protein; **d.)** Ig kappa chain V-III region SIE; **e.)** Osteopontin and; **f.)** Vitelline membrane protein 1 homolog. Error bars represent mean ± SD.

3.2.5 Verification and validation of prosaposin and GM_2AP

A rapid, 10 minute, MRM-assay using UPLC-MS/MS was developed as described in section 2.2.5.7 and used to verify prosaposin and GM_2AP concentration in urine samples from 10 pre- and corresponding post-treatment paediatric Fabry disease patients (Figure 3.6 and Table 3.1). Prosaposin concentrations were distinguished from the processed saposins A, B, C and D by the use of size exclusion filters (30 kDa). In addition to the paediatric Fabry disease patient groups, 10 age- and sex-matched diabetic samples and 10 age- and sex-matched control samples were used as positive and negative controls, respectively. Type-I diabetic patients were chosen as a positive control group due to the fact that the developing proteinuric kidney complications experienced are the same as those in Fabry disease.

Intra-batch coefficient of variation for prosaposin and GM_2AP of 5.9 and 4.3 %, respectively were determined by a repeated injection of a pooled Fabry urine sample (10 patient urines, analysed 20 times). Inter-batch coefficient of variation for prosaposin and GM_2AP of 8.3 and 6.9 %, respectively were obtained by analysing the same sample over a period of 3 consecutive days (3 x 20 analyses over 3 days).

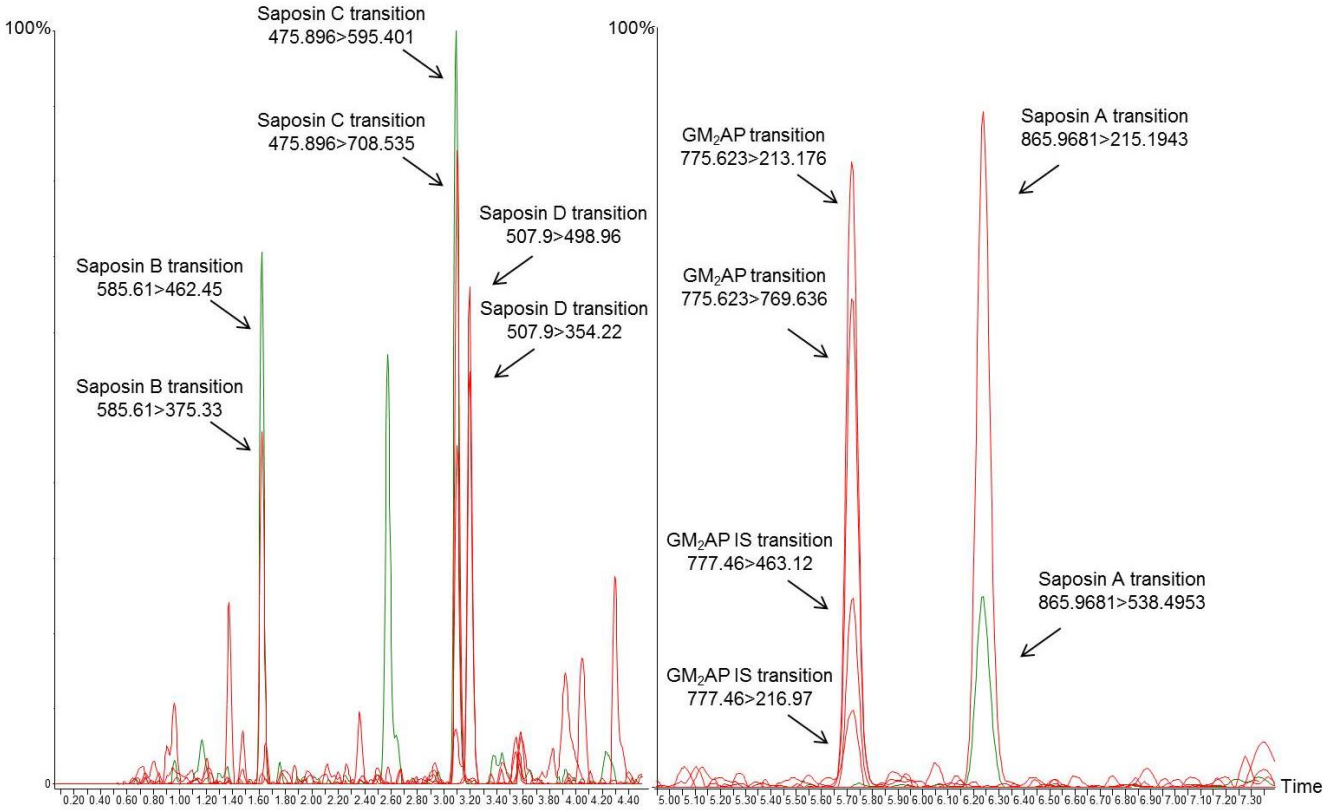

Figure 3.6 Typical UPLC-MS/MS chromatogram of the lower MW cut-off fraction from patient urine showing the 10 min assay developed for the quantitation of individual saposins A, B, C and D and GM_2AP. For each peptide and internal standard, two transitions were used, one for quantitation and one for secondary confirmation purposes.

Table 3.1. Summary of urinary prosaposin and GM_2AP results obtained by MRM UPLC-MS/MS.

Biomarker	**Fabry pre-Treatment** Mean ± SEM (min/max)	**Fabry post-Treatment** Mean ± SEM (min/max)	**Diabetic** Mean ± SEM (min/max)	**Control** Mean ± SEM (min/max)
Prosaposin (fmol/mmol creatinine)	78.3 ± 20.5 (51.4/234.6)	22.6 ± 7.1 (1.3/60.4)	25.0 ± 6.1 (6.7/64.3)	13.7 ± 2.8 (2.5/32.2)
GM_2AP (fmol/mmol creatinine)	11.09 ± 3.64 (2.1/36.3)	2.3 ± 0.7 (0.4/5.6)	7.7 ± 3.0 (0.9/24.2)	1.5 ± 0.6 (0.5/5.9)

The concentrations of prosaposin were found to be reduced statistically and significantly, between pre- and post-treatment groups (p = 0.01), between pre-treatment and diabetic groups (p = 0.009) and between pre-treatment and control groups (p = 0.002) (Figure 3.7). The significance of prosaposin was again shown to be increased when those patients with the most disease burden were excluded from the analysis (p = 0.002), data not shown.

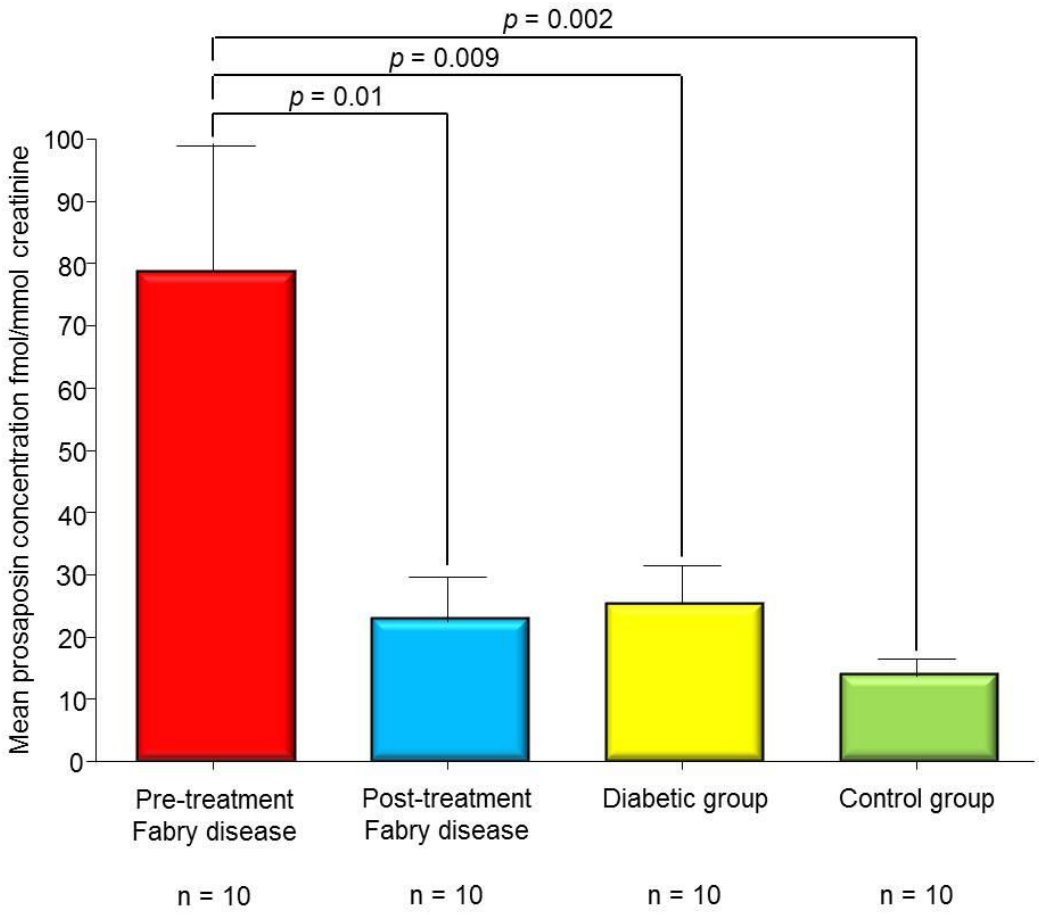

Figure 3.7 Confirmatory urinary prosaposin concentrations using a targeted MRM-UPLC-MS/MS assay in pre- and post-treatment Fabry disease patients and diabetic and control groups. Error bars represent mean ± SD.

The lower filtrate from the size exclusion experiments (< 30 kDa) which should contain the processed saposins A, B, C and D and GM_2AP were also analysed. The concentrations of GM_2AP were also found to be reduced statistically and significantly between pre- and post-treatment groups (p = 0.01) and between pre-treatment and control groups (p = 0.003). GM_2AP was also reduced significantly between diabetic and control groups (p = 0.049) (Figure 3.8).

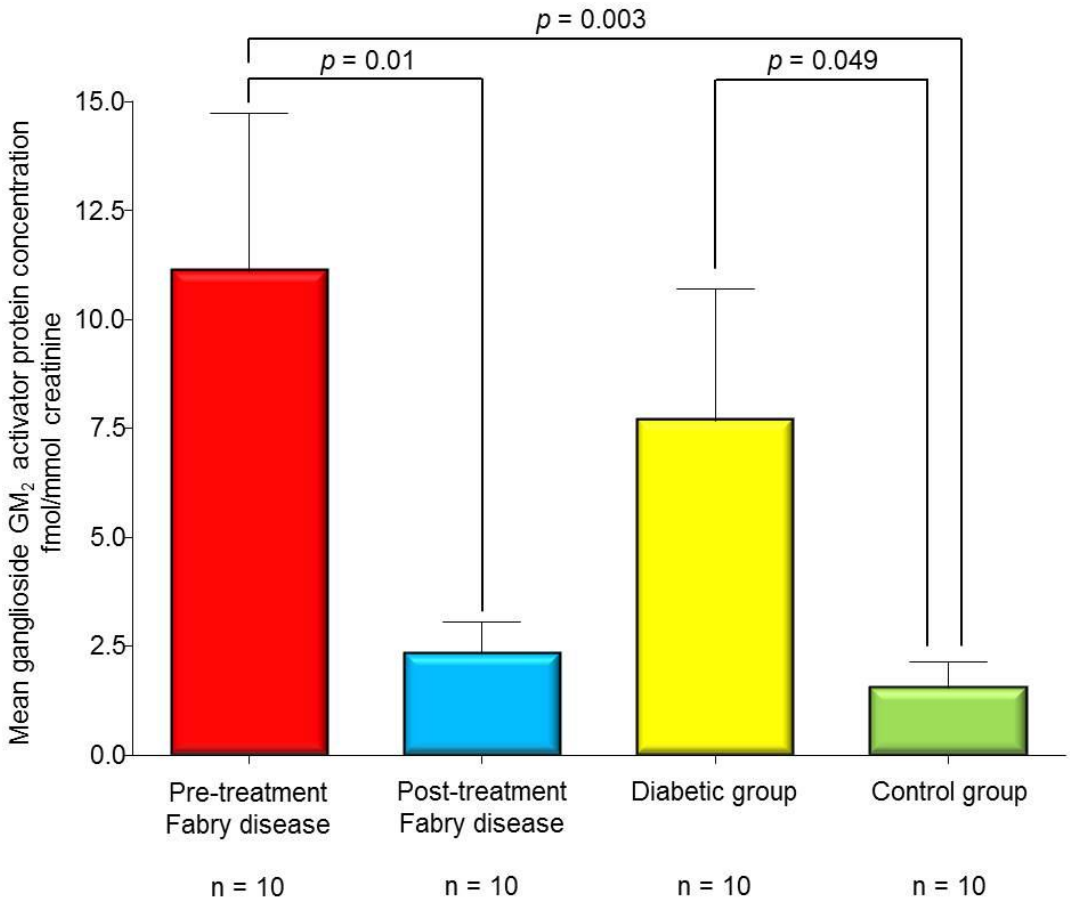

Figure 3.8 Confirmatory urinary GM_2AP concentrations using a targeted MRM-UPLC-MS/MS assay in pre- and post-treatment Fabry disease patients and diabetic and control groups. Error bars represent mean ± SD.

To assess if any correlation between urinary prosaposin or GM_2AP and the current biomarker Gb_3 existed, concentrations both pre- and post-treatment were examined. However, no significant correlation between either prosaposin and Gb_3 or GM_2AP and Gb_3 was observed (data not shown).

The urinary saposins A-D were also able to be detected in the lower filtrate in diabetic, control and Fabry pre- and post-treatment patient groups (Figure 3.6). However, while saposin A was detectable in all samples analysed, detectable

concentrations of saposin B, C and D were only present in approximately 50 % of patient samples, making statistical analysis not possible. Saposin A concentrations were found to be reduced 4-fold following treatment, with the post-treatment samples falling to within the control range, although these concentrations were not statistically significant. The mean saposin A concentrations in the diabetic cohort were observed to be 1.4-fold higher than the control group mean but were not statistically significantly raised (p = 0.6).

3.2.6 Potential biomarkers of pre-symptomatic kidney disease

Of the proteins that showed a greater than 2-fold alteration by QToF-MS during the proteomic profiling aspect of this study (Figures 3.4.1, 3.4.2 and 3.5) a number have been described previously in diseases of the kidney (Christensen and Birn 2001; Xie *et al.*, 2001; Frey *et al.*, 2008; Thrailkill *et al.*, 2011; Nozza *et al.*, 2012 Filatov *et al.*, 2012) . In addition, following a literature review (Edelstein 2010; Fassett *et al.*, 2011; Dajak *et al.*, 2011; Bolignano *et al.*, 2009; Kirsztajn *et al.*, 2002) and personal communication with Professor David Warnock (Director of the Division of Nephrology, University of Alabama at Birmingham, USA) the proteins albumin (1.3-fold decrease), retinol binding protein 4 (4.5-fold decrease), Ig gamma-4 chain C region (2.5-fold decrease), lysosomal α-glucosidase (6.3-fold decrease), osteopontin (2.6-fold increase), prostaglandin-H2 D-isomerase (1.8-fold decrease), endothelial protein C receptor (2.3-fold increase), vitamin D binding protein (2.5-fold increase), cubilin (3.9-fold decrease), megalin (4.5-fold increase), neutrophil gelatinase-associated lipocalin (not detected), and sortilin (not detected) were all considered as potential renal biomarkers. Therefore these proteins were included in the

development of a multiplex assay to assess their application as biomarkers of pre-symptomatic kidney disease.

3.2.7 Pre-symptomatic kidney disease assay

To confirm the biomarkers showing fold change alterations observed in the MS^E analyses, these proteins together with known biomarkers of kidney function were developed in a multiplex, 10 minute, MRM assay using UPLC-MS/MS as described in section 2.2.5.8. This assay was then used to assess those biomarkers with the potential to detect and monitor pre-symptomatic kidney disease in urine samples from 10 pre- and corresponding (3 year) post-treatment paediatric Fabry disease patients (see Table 2.2). In addition urine samples from 10 paediatric type I diabetic patients, 10 obese paediatric patients, 10 paediatric controls, 10 adult Fabry patients, 10 adult type II diabetic patients and 10 adult controls (section 2.1.2.2) were analysed. Urine samples were desalted and concentrated using size exclusion filters (3 kDa).

As well as the use of type I diabetic patient samples as a positive control group, an obese paediatric patient group was also used due to the fact that obesity is a major risk factor for developing kidney disease (Ejerblad et al., 2006; Gunta and Mak 2013). In addition to the paediatric cohorts, adult Fabry disease patient samples, age- and sex-matched type II diabetic patient samples and age- and sex-matched control samples were analysed as positive and negative control groups, respectively.

Twelve proteins were included in the multiplex assay for assessment (see Table 2.10 for protein details and Tables 3.2 and 3.3 for a summary of results). To identify the significant and statistical changes *t*-test analyses were performed. In

addition, the data were also examined to identify changes greater than 2-fold between patient groups.

3.2.8 The effect of ERT on potential biomarkers

The effect of ERT on the twelve proteins included in the pre-symptomatic kidney disease assay was also assessed in paediatric Fabry disease patients. Ten pre-treatment urine samples and corresponding urine samples collected one-, two-, and three-years post treatment (see Table 2.2) were analysed. The patients were again classified as those with the least disease burden (*n* = 5) or those with the most disease burden (*n* = 5) according to their Gb_3 levels (Figure 3.9; section 2.2.1).

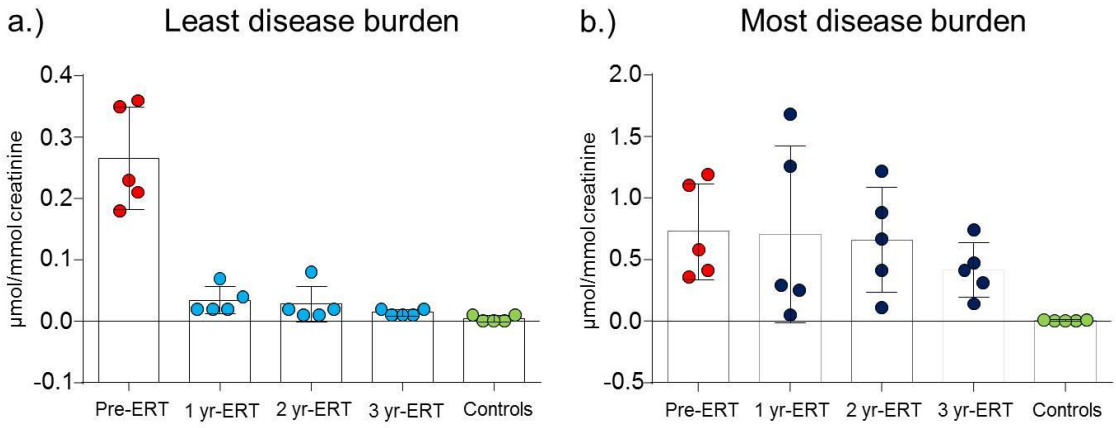

Figure 3.9 Globotriaosylceramide (Gb_3) concentrations in those patients with a.) Least disease burden and; b.) Most disease burden; pre-treatment, and one, two, and three years' post-ERT**.** Columns represent mean. Error bars represent SD.

Table 3.2 Summary of potential pre-symptomatic kidney disease biomarker results obtained by MRM UPLC-MS/MS in paediatric Fabry disease patients with the least disease burden (↓DB) and the most disease burden (↑DB) prior to ERT and following one, two and three years of treatment.

Biomarker	**Fabry pre-ERT** Mean ± SEM (min/max)	**Fabry ↓DB 1 yr ERT** Mean ± SEM (min/max)	**Fabry ↓DB 2 yr ERT** Mean ± SEM (min/max)	**Fabry ↓DB 3 yr ERT** Mean ± SEM (min/max)	**Fabry ↑DB Pre-ERT** Mean ± SEM (min/max)	**Fabry ↑DB 1 yr ERt** Mean ± SEM (min/max)	**Fabry ↑DB 2 yr ERT** Mean ± SEM (min/max)	**Fabry ↑DB 3 yr ERT** Mean ± SEM (min/max)
Albumin nmol/mmol creatinine	14.9 ± 14.0 (0.5/70.9)	14.8 ± 8.8 (0.2/39.3)	28.7 ± 23.1 (0.7/120.7)	19.8 ± 15.5 (1.2/81.4)	0.8 ± 0.2 (0.2/1.2)	9.2 ± 7.1 (0.5/37.4)	2.4 ± 1.0 (0.8/5.9)	6.2 ± 2.2 (1.4/12.6)
Vitamin D binding protein pmol/mmol creatinine	8.5 ± 2.5 (0.7/12.6)	137.7±104.5 (0.8/542.3)	30.2 ± 12.5 (2.4/66.1)	26.3 ± 10.2 (8.6/65.1)	3.7 ± 1.4 (nd/6.1)	113.2 ± 98.0 (2.5/504.4)	40.6 ± 18.8 (0.7/97.7)	21.1 ± 8.3 (0.9/49.1)
Cubilin nmol/mmol creatinine	0.1 ± 0.1 (0.01/0.5)	0.1 ± 0.1 (0.01/0.4)	0.4 ± 0.3 (0.02/1.5)	0.3 ± 0.1 (0.1/0.7)	0.1 ± 0.02 (0.01/0.1)	0.2 ± 0.1 (0.01/0.7)	0.2 ± 0.1 (0.01/0.6)	0.1 ± 0.02 (0.01/0.1)
Osteopontin nmol/mmol creatinine	54.5 ± 18.1 (28.9/124.7)	57.3 ± 14.6 (15.2/101.9)	182.0 ± 129.8 (3.4/695.9)	61.2 ± 25.2 (19.7/153.2)	72.4 ± 31.5 (11.6/185.0)	163.9 ± 101.9 (27.5/117.3)	103.1 ± 24.3 (25.2/163.4)	66.5 ± 13.4 (27.7/110.3)
Megalin nmol/mmol creatinine	0.2 ± 0.1 (0.04/0.7)	0.3 ± 0.1 (0.02/0.5)	0.5 ± 0.3 (0.1/1.7)	0.4 ± 0.1 (0.2/0.6)	0.1 ± 0.04 (0.002/0.2)	0.4 ± 0.2 (0.03/1.2)	0.2 ± 0.1 (0.005/0.3)	0.1 ± 0.02 (0.1/0.2)
Prostaglandin-H2 D-isomerase nmol/mmol creatinine	15.0 ± 8.7 (0.6/48.5)	9.4 ± 2.5 (3.9/16.6)	44.2 ± 24.5 (0.5/111.1)	22.3 ± 11.3 (2.1/51.4)	7.6 ± 2.8 (0.5/16.6)	19.0 ± 11.4 (0.5/63.4)	10.4 ± 3.7 (1.7/23.5)	13.8 ± 3.3 (5.6/24.7)
Endothelial protein C receptor nmol/mmol creatinine	1.5 ± 0.7 (0.4/4.1)	2.0 ± 1.1 (0.4/6.1)	3.4 ± 1.4 (0.5/7.5)	1.7 ± 0.3 (0.6/2.5)	0.8 ± 0.3 (0.1/1.6)	4.8 ± 4.2 (0.3/21.6)	1.2 ± 0.6 (0.2/3.1)	1.0 ± 0.4 (0.3/2.2)
Lysosomal alpha glucosidase nmol/mmol creatinine	2.1 ± 0.7 (0.5/3.8)	1.7 ± 0.4 (0.5/3.0)	3.0 ± 1.3 (0.5/7.9)	1.6 ± 0.4 (0.6/2.8)	1.4 ± 0.8 (0.2/4.3)	2.1 ± 1.1 (0.2/6.2)	1.0 ± 0.4 (nd/2.2)	0.8 ± 0.2 (0.4/1.2)

Sortilin fmol/mmol creatinine	1.4 ± 0.9 (nd/3.3)	0.2 ± 0.2 (nd/0.8)	1.0 ± 0.8 (nd/4.3)	1.4 ± 0.9 (nd/4.7)	nd n/a	nd n/a	nd n/a	Nd n/a
Retinol binding protein fmol/mmol creatinine	0.9 ± 0.5 (nd/2.7)	2.1 ± 1.0 (nd/5.4)	11.1 ± 13.4 (nd/62.4)	0.7 ± 0.5 (nd/2.7)	2.5 ± 1.6 (nd/8.6)	1.6 ± 0.6 (nd/3.5)	0.4 ± 0.8 (nd/4.2)	0.8 ± 0.3 (nd/1.4)
Ig gamma chain C region fmol/mmol creatinine	54.7 ± 33.9 (1.3/184.0)	7.2 ± 3.8 (nd/20.7)	7.6 ± 4.2 (nd/20.1)	17.9 ± 13.1 (nd/67.9)	28.3 ± 19.9 (nd/103.1)	17.3 ± 17.3 (nd/86.4)	31.4 ± 29.6 (nd/149.9)	26.5 ± 25.3 (nd/127.5)
Neutrophil gelatinase-associated lipocalin fmol/mmol creatinine	0.2 ± 0.2 (nd/0.8)	3.7 ± 2.8 (nd/14.6)	35.4 ± 14.3 (4.7/84.5)	7.8 ± 6.6 (nd/34.2)	3.1 ± 2.3 (nd/12.0)	0.3 ± 0.3 (nd/1.7)	1.2 ± 0.8 (nd/4.2)	0.9 ± 0.7 (nd/3.7)

Table 3.3 Summary of potential pre-symptomatic kidney disease biomarker results obtained by MRM UPLC-MS/MS in a paediatric type I diabetic group, a paediatric obese group, a paediatric control group, an adult Fabry disease group, an adult type II diabetic group and an adult control group.

Biomaker	**Paediatric type I diabetic group** Mean ± SEM (min/max)	**Paediatric obese group** Mean ± SEM (min/max)	**Paediatric control group** Mean ± SEM (min/max)	**Adult Fabry disease group** Mean ± SEM (min/max)	**Adult type II diabetic group** Mean ± SEM (min/max)	**Adult control group** Mean ± SEM (min/max)
Albumin nmol/mmol creatinine	66.0 ± 55.4 (0.1/562.4)	4.6 ± 1.8 (0.1/14.2)	7.4 ± 2.5 (0.3/17.0)	349.0 ± 140.5 (6.6/1450.0)	412.1 ± 152.9 (nd/1187.8)	29.9 ± 13.5 (0.2/121.2)
Vitamin D binding protein pmol/mmol creatinine	93.1 ± 40.6 (nd-347.1)	34.4 ± 14.0 (nd-146.8)	41.0 ± 11.9 (3.5-114.5)	1294.7 ± 718.5 (1.0/6967.7)	583.3 ± 160.6 (nd/1410.1)	135.7 ± 65.7 (nd/507.3)
Cubilin nmol/mmol creatinine	0.5 ± 0.2 (nd/2.3)	0.1 ± 0.03 (nd/0.3)	0.1 ± 0.02 (0.01/0.1)	0.6 ± 0.2 (0.1/1.5)	3.5 ± 1.5 (nd/12.9)	0.4 ± 0.1 (0.03/1.3)
Osteopontin nmol/mmol creatinine	128.1 ± 34.6 (6.8/397.1)	72.9 ± 14.1 (12.9/156.4)	66.3 ± 15.0 (6.0/166.5)	340.6 ± 51.9 (114.9/621.2)	2394.9 ± 757.5 (445.9/8055.1)	280.2 ± 62.0 (43.4/702.2)
Megalin nmol/mmol creatinine	0.3 ± 0.1 (nd/1.1)	0.2 ± 0.1 (0.02/1.1)	0.1 ± 0.02 (0.01/0.2)	0.8 ± 0.2 (0.001/1.8)	3.0 ± 1.0 (0.6/11.2)	0.4 ± 0.1 (0.01/0.9)
Prostaglandin-H2 D-isomerase nmol/mmol creatinine	6.8 ± 2.1 (0.04/15.5)	17.5 ± 10.3 (0.1/100.8)	3.1 ± 0.6 (0.6/5.4)	60.9 ± 23.2 (0.8/223.6)	628.2 ± 379.7 (73.9/3982.2)	10.3 ± 3.4 (0.2/29.6)

Endothelial protein C receptor nmol/mmol creatinine	4.8 ± 2.2 (0.2/22.0)	1.4 ± 0.3 (0.2/2.9)	2.0 ± 0.3 (0.7/3.9)	8.2 ± 2.5 (0.6/23.8)	34.5 ± 14.1 (nd/140.3)	8.7 ± 1.6 (1.8/17.8)
Lysosomal alpha glucosidase nmol/mmol creatinine	2.5 ± 0.9 (0.2/8.6)	1.8 ± 0.6 (0.3/4.3)	1.2 ± 0.3 (0.2/3.5)	8.6 ± 1.2 (3.3/15.2)	26.2 ± 11.8 (nd/115.8)	5.0 ± 1.2 (1.2/12.7)
Sortilin fmol/mmol creatinine	4.2 ± 2.4 (nd/23.7)	1.7 ± 0.7 (nd/7.3)	1.9 ± 0.7 (nd/4.7)	35.0 ± 25.9 (nd/264.3)	61.0 ± 27.6 (nd/291.5)	12.5 ± 6.9 (nd/64.9)
Retinol binding protein fmol/mmol creatinine	6.2 ± 2.7 (nd/24.2)	1.2 ± 0.5 (nd/4.3)	0.7 ± 0.7 (nd/6.4)	20.2 ± 9.6 (nd/83.6)	34.4 ± 16.9 (nd/146.2)	7.0 ± 4.4 (nd/46.0)
Ig gamma chain C region fmol/mmol creatinine	468.8 ± 466.1 (nd/4663.6)	148.1 ± 97.6 (nd/813.2)	25.2 ± 24.7 (nd/247.4)	283.3 ± 218.9 (nd/2234.5)	170.5 ± 120.8 (nd/1228.3)	4.1 ± 2.6 (nd/23.9)
Neutrophil gelatinase-associated lipocalin nmol/mmol creatinine	3.1 ± 2.0 (nd/17.8)	0.9 ± 0.5 (nd/4.3)	5.6 ± 2.6 (nd/20.9)	114.1 ± 91.0 (nd/922.4)	61.8 ± 31.1 (nd/275.5)	0.4 ± 0.1 (0.01/0.9)

3.2.9 Verification and validation of albumin

Albumin (Figure 3.10) was found to be statistically and significantly elevated in both adult Fabry disease patients (p = 0.04) and adult type II diabetics (p = 0.03) compared to the adult control group. Following analysis to identify fold changes, the paediatric type I diabetic group were shown to have an 8.9-fold elevation in albumin concentrations above that of the paediatric control group.

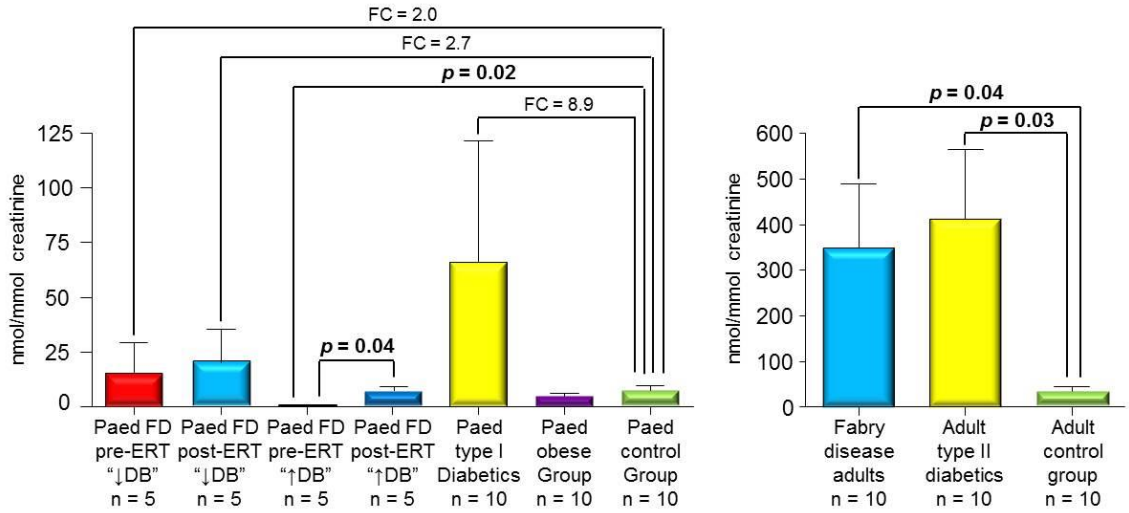

Figure 3.10 Urinary serum albumin concentrations using a targeted MRM-UPLC-MS/MS assay in paediatric and adult cohorts. Error bars represent mean ± SD. FC = fold change; FD = Fabry disease; ↓DB = least disease burden; ↑ = most disease burden.

Albumin concentrations statistically significantly below that of the control group (p = 0.02) were observed in those patients with most disease burden prior to ERT (Figure 3.10). When the effect of ERT on this protein was assessed in this patient group (Figure 3.11b) consecutive increases in albumin concentration above those of baseline pre-treatment levels were observed at all-time points studied. These elevations did not reach statistical significance following one

(12.2-fold elevation) or two years (3.2-fold elevation) of treatment however, following three years of ERT albumin concentrations became statistically and significantly elevated above those of baseline pre-treatment concentrations (p = 0.04).

Although no statistically significant alterations in albumin concentration were observed in those patients with the least disease burden, fold change elevations above that of the paediatric control group were detected at all-time points studied (Figure 3.11a). In addition, patients with the least disease burden were found to have elevated albumin concentrations above those of the patients with most disease burden at the pre-treatment (19.6-fold), two (12.0-fold) and three (3.2-fold) year post-treatment time points.

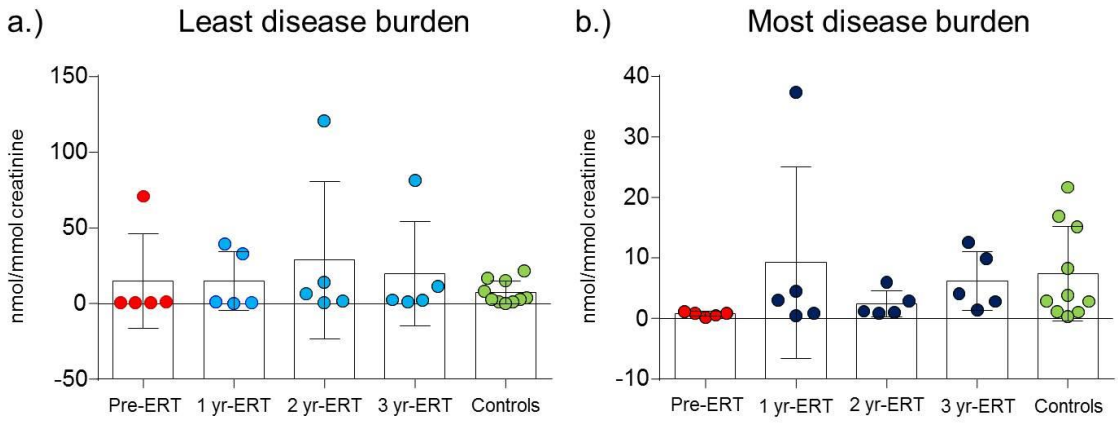

Figure 3.11 Urinary serum albumin concentrations in paediatric Fabry disease patients with a.) Least disease burden and; b.) Most disease burden; pre-treatment, and one, two, and three years' post-ERT. Columns represent mean. Error bars represent SD.

3.2.10 Verification and validation of megalin

Statistical and significant elevations were observed in the adult Fabry disease (p = 0.03) and adult type II diabetic patient groups (p = 0.03) compared to the

adult control group for the protein megalin (Figure 3.12). In addition, a 2.5-fold change in megalin concentrations in the paediatric type I diabetic group above that of the paediatric control group was observed.

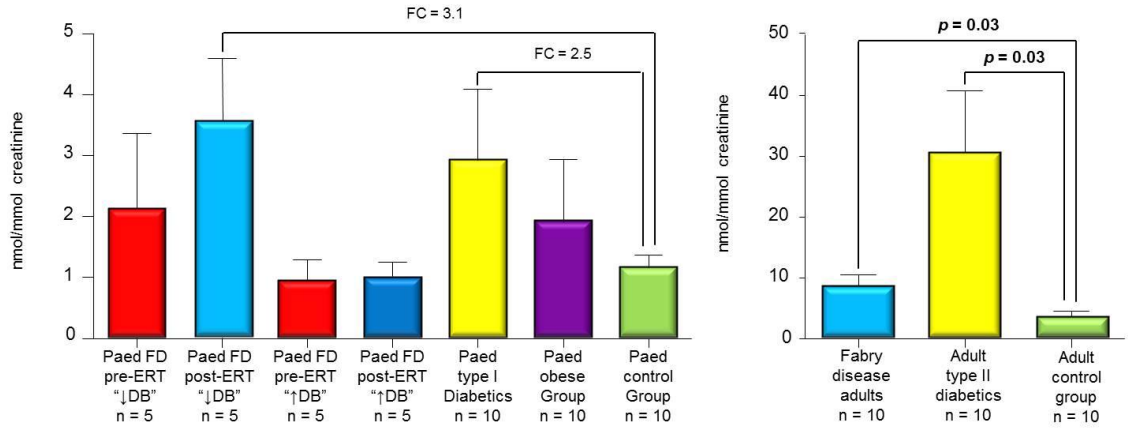

Figure 3.12 Urinary megalin concentrations using a targeted MRM-UPLC-MS/MS assay in paediatric and adult cohorts. Error bars represent mean ± SD. FC = fold change; FD = FD; ↓DB = least disease burden; ↑DB = most disease burden.

No statistically significant differences were observed in the concentrations of megalin in paediatric Fabry disease patients with either the least or the most disease burden at any time point studied (Figure 3.13). However, when the data were re-analysed to identify fold change alterations, those patients with the least disease burden were observed to have elevations in megalin concentration at the one (2.2-fold), two (4.7-fold) and three year (3.1-fold) post-treatment time points, above that of the paediatric control group. Megalin concentrations at the two-year time point also displayed a 2.6-fold elevation above that of the baseline pre-treatment levels (Figure 3.13a). Those patients with the most disease burden were found to have megalin concentrations increased 4.0-fold above baseline pre-treatment levels and 3.2-fold increased

above concentrations observed in the paediatric control group, at the one-year post-treatment time point (Figure 3.13b). However, this is as the result of a single patient displaying an elevation in megalin concentration and was not observed at any other time point studied.

The paediatric Fabry disease group with the least disease burden were also found to have megalin concentrations higher than those of the corresponding patient groups with the most disease burden at the pre-treatment (2.3-fold), two (3.2-fold) and three (3.5-fold) year post-treatment time points.

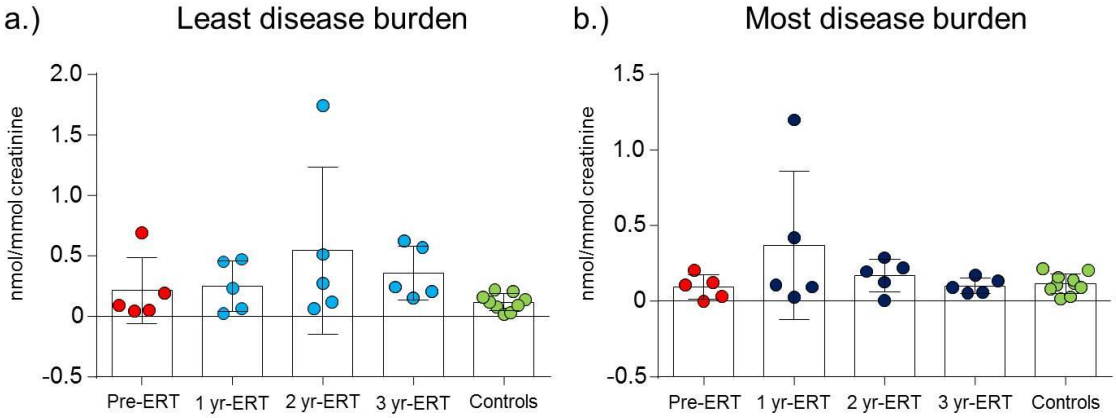

Figure 3.13 Urinary megalin concentrations in paediatric Fabry disease patients with a.) Least disease burden and; b.) Most disease burden; pre-treatment, and one, two, and three years' post-ERT. Columns represent mean. Error bars represent SD.

3.2.11 Verification and validation of vitamin D binding protein

Vitamin D binding protein (Figure 3.14) was shown to be statistically and significantly elevated in the adult type II diabetic group compared to the adult control group (p = 0.02). Concentrations of this protein were also found to be 2.3-fold elevated in the type I diabetic group compared to the paediatric control group. In addition, the adult Fabry disease patient group was shown to have

vitamin D binding protein levels 9.5-fold elevated above those of the adult control group.

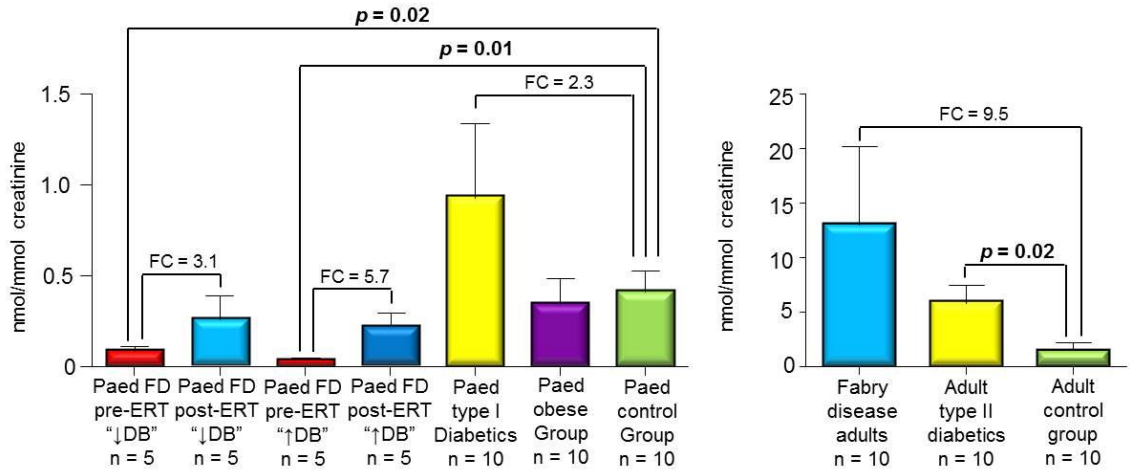

Figure 3.14 Urinary vitamin D binding protein concentrations using a targeted MRM-UPLC-MS/MS assay in paediatric and adult cohorts. Error bars represent mean ± SD. FC = fold change; FD = Fabry disease; ↓DB = least disease burden; ↑DB = most disease burden.

In the paediatric Fabry disease groups the concentrations of vitamin D binding protein were found to be statistically and significantly lower prior to the instigation of ERT in both those patients with the least disease burden (p = 0.02) and in those with the most disease burden (p = 0.01), compared to concentrations of the paediatric control group (Figures 3.14). Analysis of the data to identify fold changes also revealed greater than 2.0-fold elevations of this protein in both groups above baseline pre-treatment concentrations following the first-, second-, and third-year of ERT (Figure 3.15). However, no differences in the concentration of this protein, compared to those of the paediatric control group, were observed at these time points.

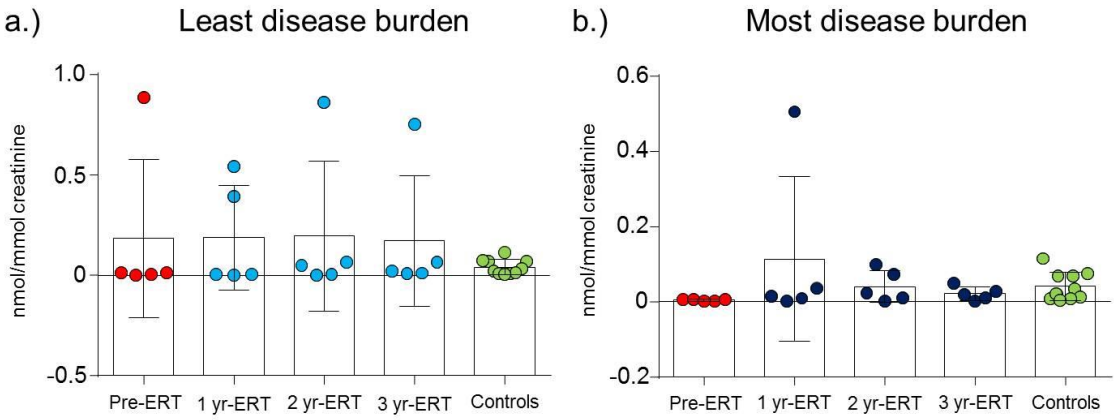

Figure 3.15 Urinary vitamin D binding protein concentrations in paediatric Fabry disease patients with a.) Least disease burden and; b.) Most disease burden; pre-treatment, and one, two, and three years' post-ERT. Columns represent mean. Error bars represent SD.

3.2.12 Verification and validation of prostaglandin-H2 D-isomerase

Prostaglandin-H2 D-isomerase (Figure 3.16) was shown to be significantly and statistically elevated in the adult Fabry disease group compared to the adult control group (p = 0.049). Following analysis to identify fold changes, the type II diabetic group was shown to have a 61.2-fold elevation compared to the adult control group however, this increase did not reach statistical significance. In addition, all paediatric groups displayed fold change elevations above that of the paediatric control group.

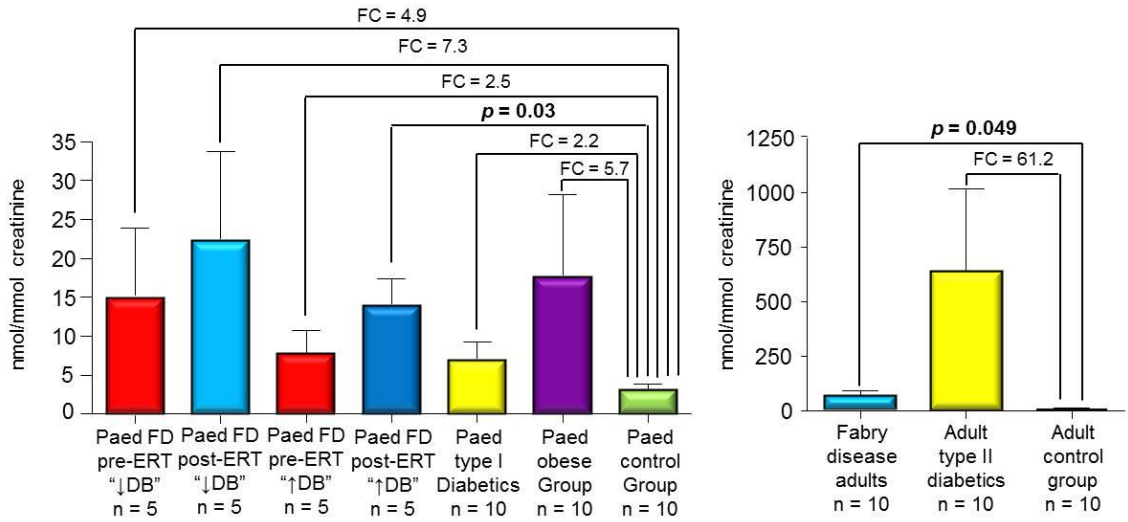

Figure 3.16 Urinary prostaglandin-H2 D-isomerase concentrations using a targeted MRM-UPLC-MS/MS assay in paediatric and adult cohorts. Error bars represent mean ± SD. FC = fold change; FD = Fabry disease; ↓DB = least disease burden; ↑DB = most disease burden.

A significant elevation (p = 0.03) in the concentrations of prostaglandin-H2 D-isomerase were also observed in the paediatric Fabry disease group with the most disease burden, following three years of treatment, above that of the control group (Figures 3.16). Following analysis to assess the effect of ERT, fold changes elevations were observed at all-time points studied in those patients with the least disease burden, and in those with the most disease burden, above the levels of the paediatric control group (Figure 3.17). In addition, those patients with the least disease burden displayed elevations in prostaglandin-H2 D-isomerase levels, both pre-treatment (2.0-fold) and following one year of treatment (4.3-fold), above those levels detected in those patients with the most disease burden at the corresponding time points. However, a 2.0-fold elevation in patients with the most disease burden,

following one-year of ERT, above that of patients with the least disease burden at the corresponding time points was also observed.

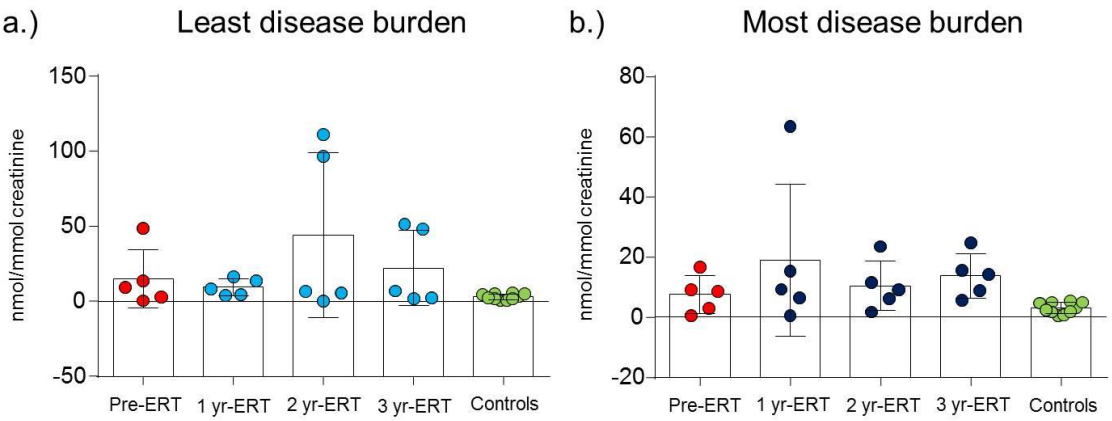

Figure 3.17 Urinary prostaglandin-H2 D-isomerase concentrations paediatric Fabry disease patients with a.) Least disease burden and; b.) Most disease burden; pre-treatment, and one, two, and three years' post-ERT. Columns represent mean. Error bars represent SD.

3.2.13 Verification and validation of lysosomal alpha-glucosidase

The adult Fabry disease group was found to have statistical and significant elevations (p = 0.049) in the protein lysosomal alpha glucosidase in comparison to the adult control group (Figure 3.18). In addition, both the type I and type II diabetic groups were shown to have fold changes of 2.1-fold and 5.3-fold respectively, above their corresponding control groups.

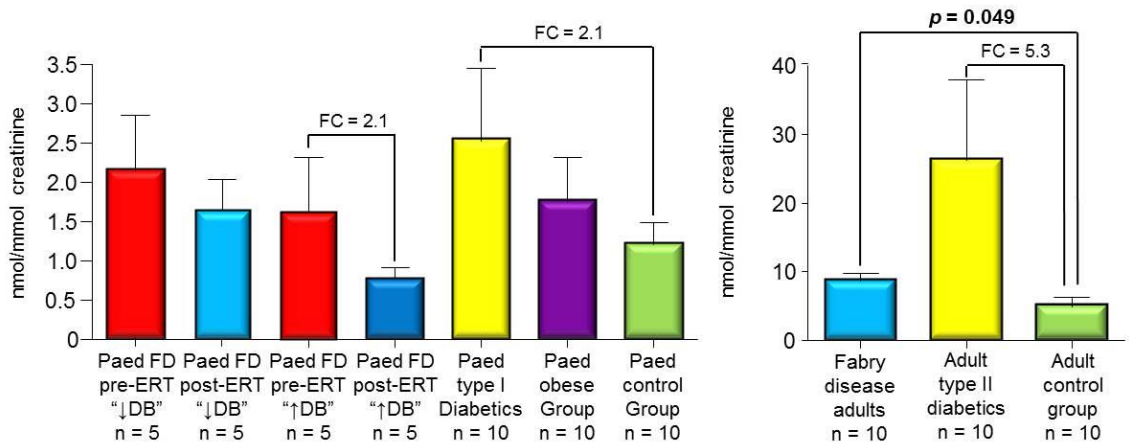

Figure 3.18 Urinary lysosomal alpha glucosidase concentrations using a targeted MRM-UPLC-MS/MS assay in paediatric and adult cohorts. Error bars represent mean ± SD. FC = fold change; FD = Fabry disease; ↓DB = least disease burden; ↑DB = most disease burden.

No statistically significant alterations were observed for the protein lysosomal alpha glucosidase in either the paediatric Fabry disease patient group with the least, or with the most, disease burden compared to those levels detected in the paediatric control group (Figure 3.19). A 2.5-fold change elevation, above that of the control group, was observed in those patients with the least disease burden following two years of ERT (Figure 3.19a). However, this was due to a single patient displaying an elevation in this protein, at this time point, and was not observed at any other time point studied. Lysosomal alpha glucosidase levels in those patients with the most disease burden (Figure 3.19b) were comparable with those of the control group throughout the duration of this study.

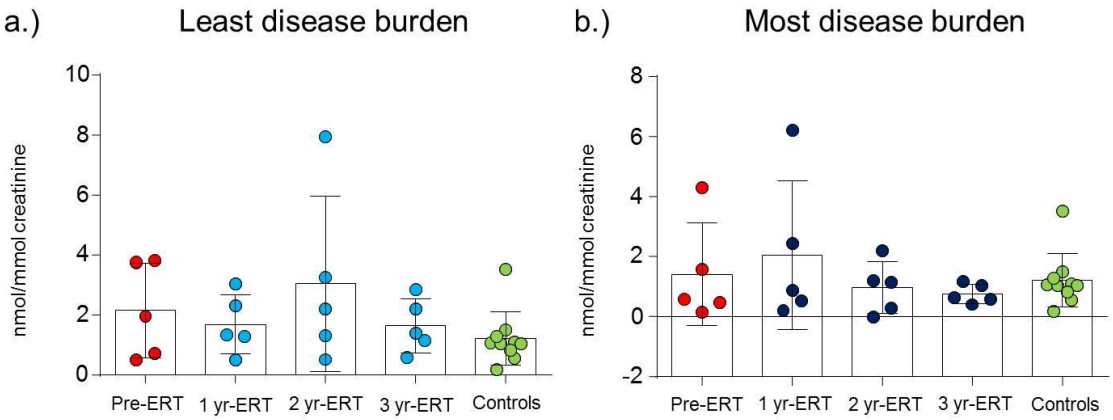

Figure 3.19 Urinary lysosomal alpha glucosidase concentrations in paediatric Fabry disease patients with a.) Least disease burden and; b.) Most disease burden; pre-treatment, and one, two, and three years' post-ERT. Columns represent mean. Error bars represent SD.

3.2.14 Verification and validation of endothelial protein C receptor

Changes in the protein endothelial protein C receptor, whilst not statistically significant, were observed in both the paediatric type I diabetic group (2.4-fold elevation) and the adult type II diabetic group (4.0-fold elevation), compared to their respective control groups (Figure 3.20).

The levels of endothelial protein C receptor in the paediatric Fabry disease patients with the most disease burden were statistically and significantly lower than those of the paediatric control group both prior to treatment (p = 0.02) and following three years of ERT (p = 0.049) (Figure 3.20). When the effect of ERT was assessed in this group of patients a 2.4-fold change increase was also observed, above that of the control group, following one year of treatment (Figure 3.21b). However, this was as the result of an elevation in this protein in a single patient at this time point and was not observed at any other time point studied. Those patients with the least disease burden (Figure 3.21a) displayed

levels comparable with those of the paediatric control group at all-time points studied.

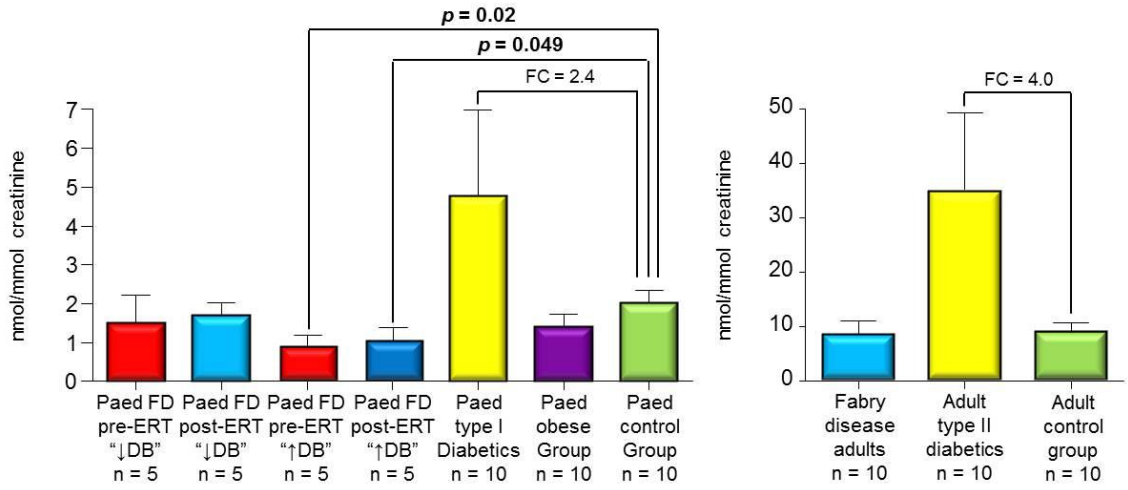

Figure 3.20 Urinary endothelial protein C receptor concentrations using a targeted MRM-UPLC-MS/MS assay in paediatric and adult cohorts. Error bars represent mean ± SD. FC = fold change; FD = Fabry disease; ↓DB = least disease burden; ↑DB = most disease burden.

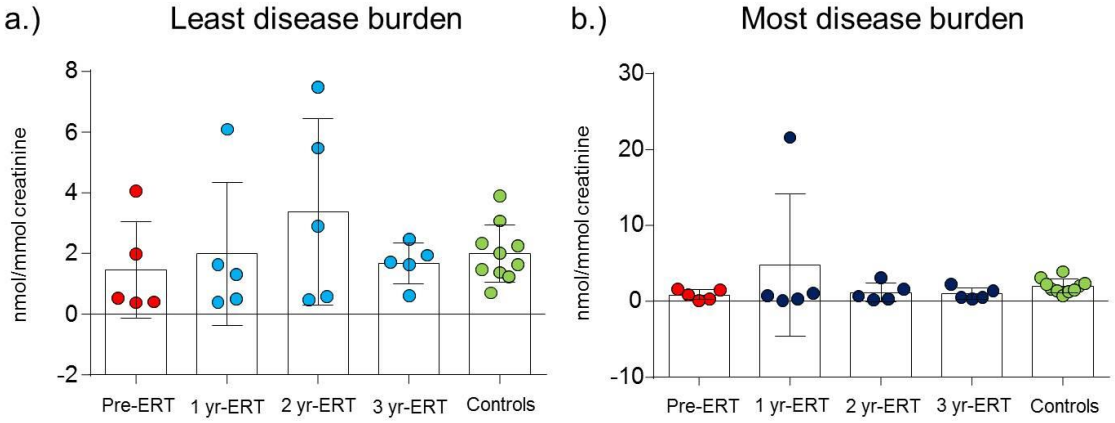

Figure 3.21 Endothelial protein C receptor concentrations in paediatric Fabry disease patients with a.) Least disease burden and; b.) Most disease burden; pre-treatment, and one, two, and three years' post-ERT. Columns represent mean. Error bars represent SD.

3.2.15 Verification and validation of osteopontin

Statistical and significant elevations were observed in the adult type II diabetic group (p = 0.02), compared to the adult control group, for the protein osteopontin (Figure 3.22). Osteopontin was also found to be 2.0-fold higher in the paediatric type I diabetic patient group compared to the paediatric control group. However, all other patient groups displayed levels comparable with those of their respective control group.

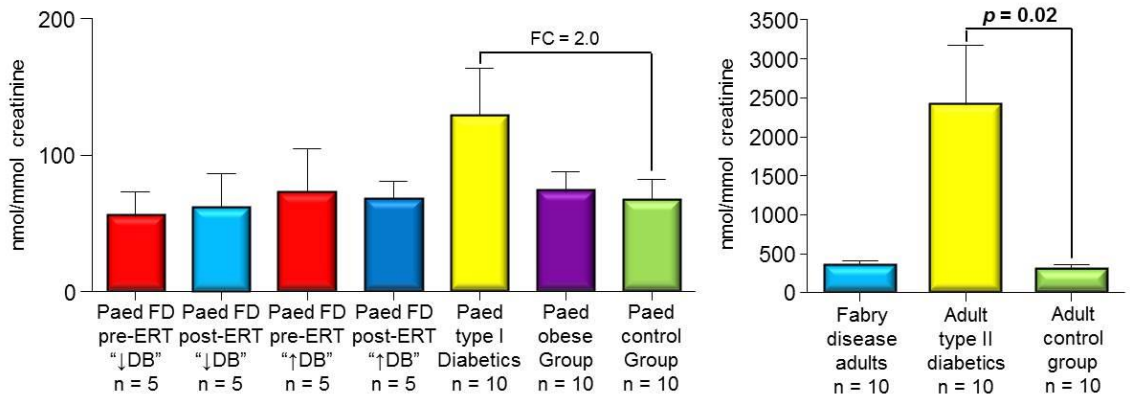

Figure 3.22 Urinary osteopontin concentrations using a targeted MRM-UPLC-MS/MS assay in paediatric and adult cohorts. Error bars represent mean ± SD. FC = fold change; FD = Fabry disease; ↓DB = least disease burden; ↑DB = most disease burden.

When the effect of ERT on osteopontin levels following one, two and three years of treatment was assessed, those patients with least disease burden displayed a fold change elevation following two years of treatment (Figure 3.23a). Whilst in those patients with most disease burden a fold change elevation following one year of treatment was observed (Figure 3.23b).

However, in both groups this fold change elevation was due to a single outlying result and no other changes were detected during the time period studied.

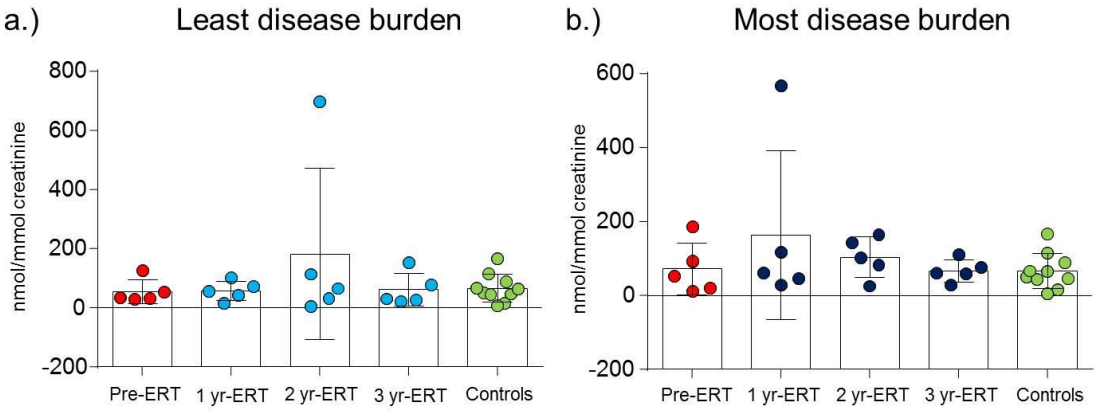

Figure 3.23 Urinary osteopontin concentrations in paediatric Fabry disease patients with a.) Least disease burden and; b.) Most disease burden; pre-treatment, and one, two, and three years' post-ERT. Columns represent mean. Error bars represent SD.

3.2.16 Verification and validation of cubilin

No statistical significant alterations were observed in the concentrations of the protein cubilin (Figure 3.24). However, an 8.5-fold elevation in the adult type II diabetic patient group and a 5.3-fold elevation in the paediatric type I diabetic group above that of their respective control groups was observed. The paediatric Fabry disease group with the least disease burden were shown to have fold change increases at the two and three year post-treatment time points, above that of the paediatric control group, when the effect of ERT was assessed (Figure 3.25a). At the two year post-treatment time point this was as the result of a single patient with an elevation in cubilin levels. However, at the three year post-treatment time point an additional patient was also displaying

elevations in cubilin excretion. Those patients with the most disease burden (Figure 3.25b) displayed increases at the one and two year post-treatment time points above both baseline pre-treatment levels (3.5-fold and 2.9-fold, respectively) and those levels observed in the control group (2.3-fold and 2.0-fold, respectively). However, this was due to elevation in cubilin excretion from different patients at these time points and if these outlying results are excluded from the analysis levels comparable with those of the control group are obtained at all-time points studied. Cubilin concentrations were also found to be higher in those patients with the least disease burden compared to those of the corresponding patients with the most disease burden at the pre-treatment (2.5-fold), two (2.4-fold) and three (3.8-fold) year time points.

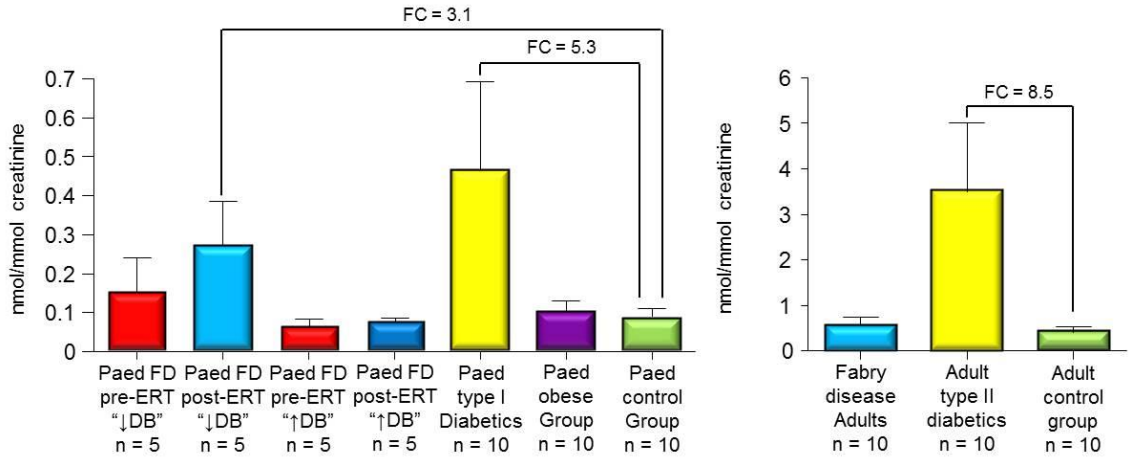

Figure 3.24 Urinary cubilin concentrations using a targeted MRM-UPLC-MS/MS assay in paediatric and adult cohorts. Error bars represent mean ± SD. FC = fold change; FD = Fabry disease; ↓DB = least disease burden; ↑DB = most disease burden.

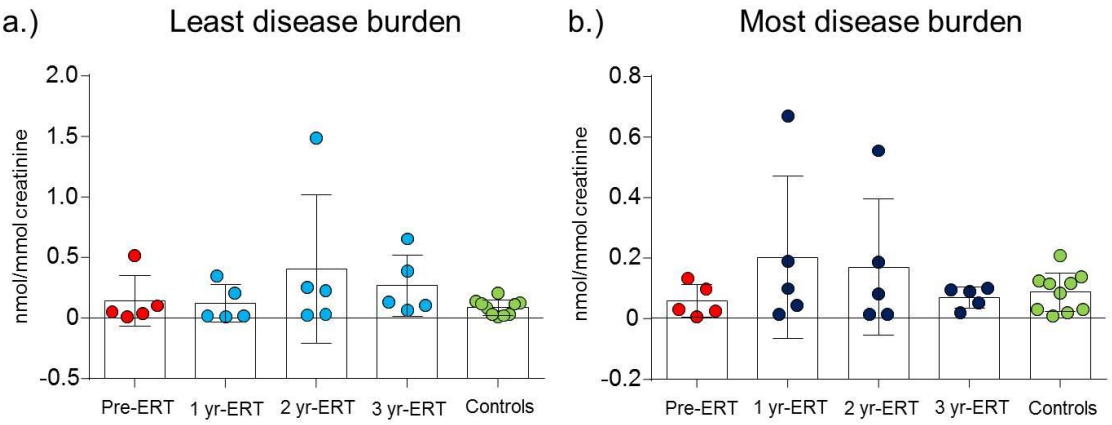

Figure 3.25 Urinary cubilin concentrations in paediatric Fabry disease patients with a.) Least disease burden and; b.) Most disease burden; pre-treatment, and one, two, and three years' post-ERT. Columns represent mean. Error bars represent SD.

3.2.17 Verification and validation of sortilin

Alterations in the levels of the protein sortilin (Figure 3.26), whilst not statistically significant, were found to be increased by fold change in both the adult Fabry disease patient group (2.8-fold) and the adult type II diabetic patient group (4.9-fold), compared to those levels observed in the adult control group. In addition, sortilin was shown to be 2.3-fold increased in the paediatric type I diabetic patients compared to the paediatric control group. No detectable levels of sortilin were present in those Fabry disease patients with the most disease burden at any time point studied resulting in statistically significant reductions (p = 0.02), compared to the paediatric control group (Figure 3.27b). In addition, sortilin concentrations in those patients with the least disease burden, at the one-year time point, were found to be reduced statistically and significantly (p = 0.03) compared to those levels observed in the paediatric control group (Figure 3.27a).

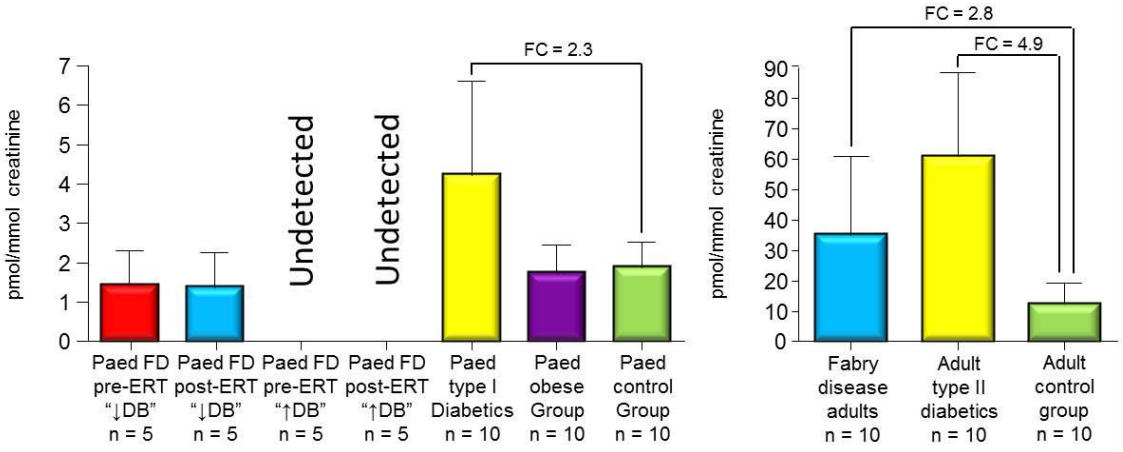

Figure 3.26 Urinary sortilin concentrations using a targeted MRM-UPLC-MS/MS assay in paediatric and adult cohorts. Error bars represent mean ± SD. FC = fold change; FD = Fabry disease; ↓DB = least disease burden; ↑DB = most disease burden.

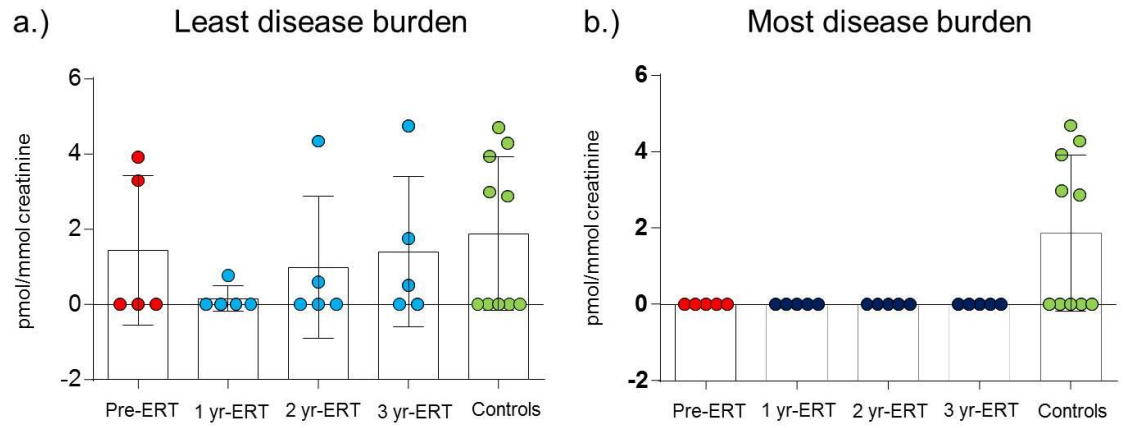

Figure 3.27 Urinary sortilin concentrations in paediatric Fabry disease patients with a.) Least disease burden and; b.) Most disease burden; pre-treatment, and one, two, and three years' post-ERT. Columns represent mean. Error bars represent SD.

3.2.18 Verification and validation of retinol binding protein

Fold change elevations were observed for retinol binding protein in the adult Fabry disease patient group (2.9-fold), the adult type II diabetic patient group (4.9-fold) and the paediatric type I diabetic patient group (6.5-fold), compared to their respective control groups (Figure 3.28).

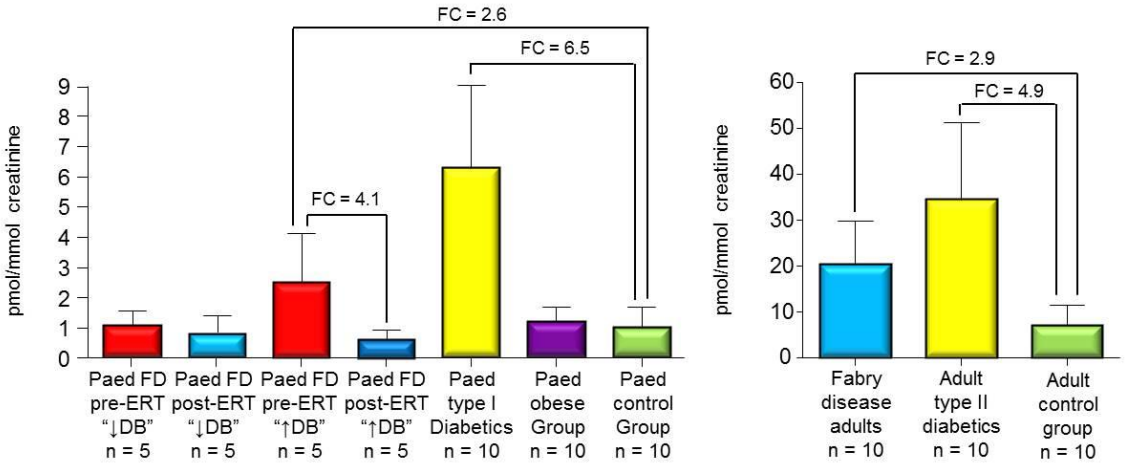

Figure 3.28 Urinary retinol binding protein concentrations using a targeted MRM-UPLC-MS/MS assay in paediatric and adult cohorts. Error bars represent mean ± SD. FC = fold change; FD = Fabry disease; ↓DB = least disease burden; ↑DB = most disease burden.

The concentrations of retinol binding protein in the paediatric Fabry disease patient group with the least disease burden (Figure 3.29a) were found to be elevated at the one- and two-year post-treatment time points above baseline pre-treatment levels (2.4-fold and 12.9-fold, respectively) and those of the paediatric control group (2.9-fold and 15.6-fold, respectively). However, at all other time points studied retinol binding protein concentrations in this group were comparable with those of the paediatric control group. In those patients with the most disease burden (Figure 3.29b) the pre-treatment retinol binding

protein concentrations were 3.5-fold higher than those of the control group. However, these levels were reduced following one- (1.5-fold), two- (5.8-fold) and three-years (3.3-fold) of treatment.

Differences between patients with the least disease burden and those with the most disease burden were also observed. Those patients with the most disease burden were found to have higher levels (2.9-fold) of retinol binding protein, than those patients with the least disease burden, prior to ERT. However, at the two year time point those patients with the least disease burden had retinol binding protein concentrations 25.7-fold higher than the corresponding patients with the most disease burden.

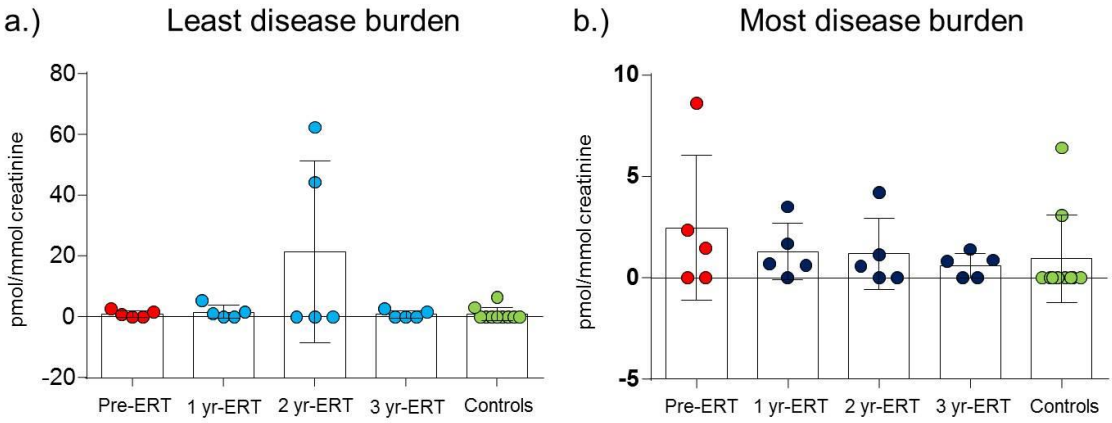

Figure 3.29 Urinary retinol binding protein concentrations paediatric Fabry disease patients with a.) Least disease burden and; b.) Most disease burden; pre-treatment, and one, two, and three years' post-ERT. Columns represent mean. Error bars represent SD.

3.2.19 Verification and validation of Ig gamma-4 chain C region

The concentrations of the protein Ig gamma-4 chain C region (Figure 3.30) were shown to be increased by fold change in the paediatric type I diabetic patient group, the obese paediatric patient group, the adult Fabry disease patient group

and the adult type II diabetic patient group by 18.6-fold, 5.9-fold, 69.8-fold and 42.0-fold respectively.

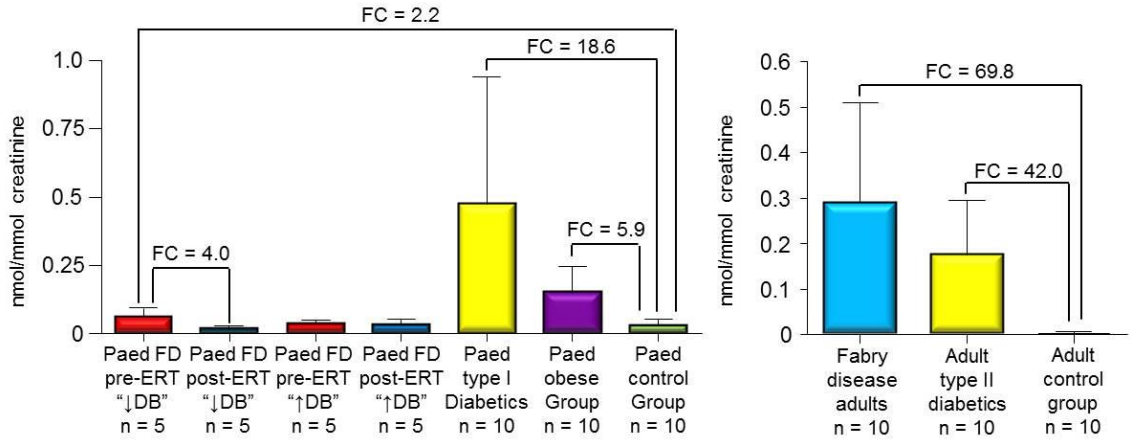

Figure 3.30 Urinary Ig gamma-4 chain C region concentrations using a targeted MRM-UPLC-MS/MS assay in paediatric and adult cohorts. Error bars represent mean ± SD. FC = fold change; FD = Fabry disease; ↓DB = least disease burden; ↑DB = most disease burden.

The paediatric Fabry disease patient group with the least disease burden (Figure 3.31a) were shown to have fold change reductions of 7.6-fold, 7.2-fold and 3.1-fold following one-, two- and three-years of ERT, below that of baseline pre-treatment concentrations. However, at the pre-treatment time point, levels of this protein were 2.2-fold higher than those of the paediatric control group. Following one- and two-years of treatment, levels in this patient group were reduced 3.5-fold and 3.3-fold below that of the paediatric control group. No differences were observed in those patients with the most disease burden compared to the paediatric control group during the time period studied. However, Ig gamma-4 chain C region concentrations were 2.4-fold and 4.1-fold higher than those of the corresponding group with the least disease burden at the one- and two-year time points, respectively.

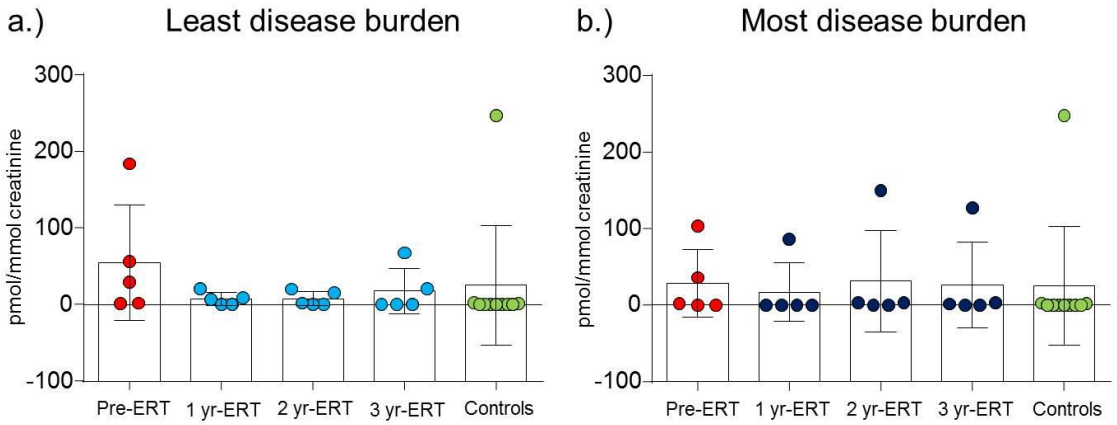

Figure 3.31 Urinary Ig gamma chain C region concentrations in paediatric Fabry disease patients with a.) Least disease burden and; b.) Most disease burden; pre-treatment, and one, two, and three years' post-ERT. Columns represent mean. Error bars represent SD.

3.2.20 Verification and validation of neutrophil gelatinase-associated lipocalin

Increases in the concentration of neutrophil gelatinase-associated lipocalin were observed in the adult Fabry disease and type II diabetic patient groups (55.8-fold and 30.2-fold, respectively) compared to the adult control group (Figure 3.32). In addition, a decrease of 6.7-fold below that of the paediatric control group was observed in the paediatric obese patient group.

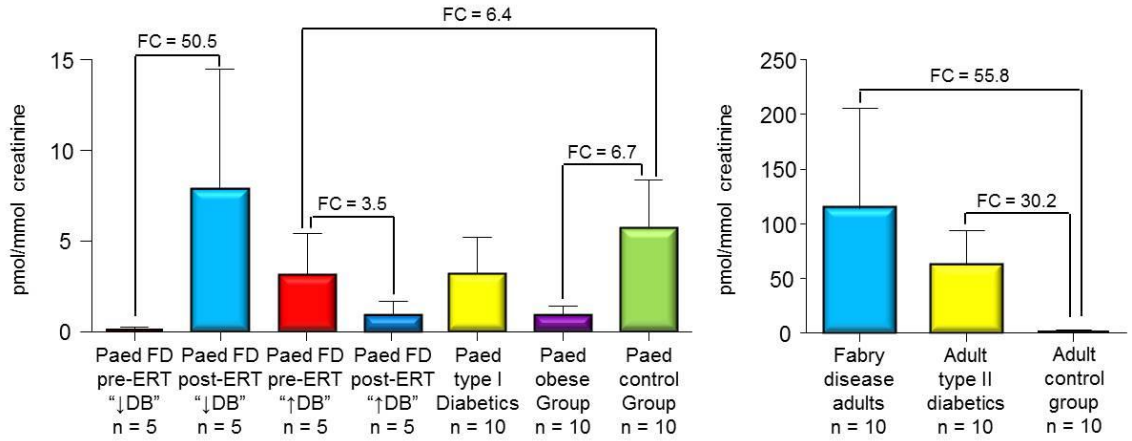

Figure 3.32 Urinary neutrophil gelatinase-associated lipocalin concentrations using a targeted MRM-UPLC-MS/MS assay in paediatric and adult cohorts. Error bars represent mean ± SD. FC = fold change; FD = Fabry disease; ↓DB = least disease burden; ↑DB = most disease burden.

A statistically significant elevation (p = 0.04) was observed in neutrophil gelatinase-associated lipocalin concentrations in the paediatric Fabry disease patient group with the least disease burden (Figure 3.33a) at the two-year time point, above that of the baseline pre-treatment concentrations. When the data were re-analysed for fold changes increases of 24.1-fold and 50.5-fold were also observed at the one- and three-year post-treatment time points compared to the baseline pre-treatment levels. The opposite was found in those patients with the most disease burden (Figure 3.33b) with 9.0-fold, 2.5-fold and 3.5-fold reductions in the concentrations of neutrophil gelatinase-associated lipocalin below those of baseline pre-treatment concentrations. An elevation in neutrophil gelatinase-associated lipocalin in one patient pre-ERT assisted the fold change reductions observed. If this single outlier is excluded from the analysis a fold change reduction in the level of this protein is still observed at the one year post-ERT time point however, pre-treatment and two and three year post-ERT

levels become comparable with pre-treatment concentrations. Levels at the one-, two- and three-year post treatment levels in those patients with most disease burden are also lower than those of the control group by 16.6-fold, 4.6-fold and 6.4-fold, respectively.

Neutrophil gelatinase associated lipocalin was also found to be increased 19.8-fold in those pre-treatment patients with the most disease burden compared to those patients with the least disease burden at the same time period. However, at the one-, two- and three-year time points this protein was 10.9-fold, 29.2-fold and 8.9-fold reduced in those patients with most disease burden compared to patients with the least disease burden at the corresponding time points.

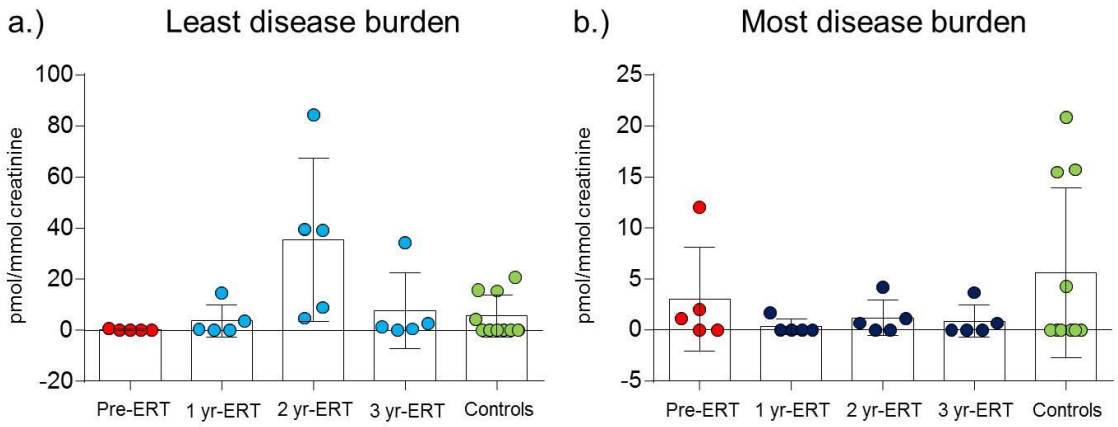

Figure 3.33 Urinary neutrophil gelatinase-associated lipocalin concentrations in paediatric Fabry disease patients with a.) Least disease burden and; b.) Most disease burden; pre-treatment, and one, two, and three years' post-ERT. Columns represent mean. Error bars represent SD.

3.3 Discussion

Urine has been used for decades for the diagnosis and assessment of disease. Recent advances in proteomic profiling techniques have demonstrated that urine contains an appreciable number of proteins and peptides making it an attractive medium for biomarker discovery studies (Decramer *et al.*, 2008). Among the advantages of using urine for analyses are that it requires non-invasive collection and allows repeated sampling for disease monitoring. In addition, the urinary proteome content is very stable for a number of years when stored under optimum conditions (-80°C).

Using label-free quantitative proteomics a number of alterations in urinary proteins were identified following 12 months of ERT in Fabry disease patients. Using MS^E, prosaposin was the only protein reduced statistically and significantly (p = 0.03) following treatment (Figure 3.3). However, another lysosomal protein of interest, GM_2AP, also demonstrated a 2.1-fold change decrease following treatment (Figure 3.4.1e). As an initial pilot study to verify the results, a rapid MRM-based UPLC-MS/MS assay was developed to quantitate prosaposin and GM_2AP in the urine of these patients as well as in a positive diabetic and negative control group. This confirmed that prosaposin was reduced significantly (p = 0.01) following treatment in Fabry disease patients (Figure 3.7). In addition, a significant difference was also observed between pre-treatment Fabry disease patients, and diabetic (p = 0.009) and control (p = 0.002) patient groups (Figure 3.7).

Prosaposin is the precursor protein for sphingolipid activator proteins (SAPs) A, B, C and D, which are four small, heat stable glycoproteins. All four mature saposins are structurally similar and have specific roles in activating their respective lysosomal hydrolases, which are required for the metabolism of

various sphingolipids (Kishimoto, Hiraiwa, and O'Brien 1992) (see Figure 1.2). Prosaposin has been shown to be secreted into body fluids, whereas the mature saposins are located within the lysosome, and unsurprisingly accumulation of the mature saposins has been reported previously in the plasma (Chang *et al.*, 2000) and tissue (Morimoto *et al.*, 1990) of various lysosomal storage disorders. Following identification and confirmation of prosaposin, the protein of interest, we attempted to identify the mature saposin chains in the filtrate fraction containing proteins < 30 kDa obtained from the size exclusion protein purification columns. While we were able to identify saposin A in all samples analysed, saposins B, C and D were not detectable in all patient samples analysed in this study. There could be a number of reasons for this such as endogenous concentrations lower than the limit of detection for this method or that the ion suppression is too great. However, we also considered perturbation of prosaposin processing into the mature saposin forms resulting in disrupted transport to the lysosome. Hiraiwa *et al.*, (1997) have reported the involvement of cathepsin D in the hydrolysis of prosaposin into a 48 kDa product containing two trisaposins including a domain for saposins A, B and C and a domain for saposins B, C and D and a 29 kDa product containing two disaposins including a domain for saposins A and B and a domain for saposins C and D. Cathepsin D then further processes the disaposins into mature saposin A and small fragments containing saposins B, C and D with portions of interdomain sequences. These small fragments then require processing by other proteases to obtain mature saposins B, C and D within the lysosome. In view of this the effect of Gb_3 and lyso-Gb_3 on cathepsin D activity was assessed. However, no inhibition of cathepsin D activity was observed by either Gb_3 or lyso-Gb_3 (data not shown).

As well as saposins A – D derived from prosaposin, encoded by the PSAP gene, the known saposins include the genetically distinct GM_2AP, encoded by the GM_2A gene. GM_2AP is larger, has a different secondary structure and is responsible for the breakdown of ganglioside GM_2 and glycolipid GA_2 by beta hexosaminidase A (Bradová *et al.*, 1993; Schuette *et al.*, 2001). GM_2AP was found to be reduced following treatment in Fabry disease patients (2.1-fold change) using label-free quantitative proteomics (Figure 3.4.1e). This protein was combined into the initial MRM UPLC-MS/MS assay for verification and confirmed that GM_2AP was reduced following treatment. By using this highly sensitive and specific technique, the reduction was shown to be significant both between pre- and post-treatment Fabry disease patients (p = 0.01) and between pre-treatment and control groups (p = 0.003) (Figure 3.8). The majority of research of GM_2AP investigates its role as a cofactor of β-hexosaminidase A to catalyse the degradation of ganglioside GM_2 and a deficiency of which results in the lysosomal storage disorder GM_2 gangliosidosis, AB variant. However, GM_2AP has also been reported to bind to and act in transport of, a wide variety of lipids including phosphatidylcholine, in addition to binding to platelet activating factor (PAF) within β-cup and hydrolysing it to inactive lyso-PAF (Rigat *et al.*, 2009). Increased concentrations of platelet activating factor have been associated with a number of clinical conditions including stroke, myocardial infarction, colitis and multiple sclerosis (Lindsberg, Hallenbeck and Feuerstein 1991; Frangogiannis, Smith and Entman 2002; Callea *et al.*, 1999). To our knowledge this is the first study to investigate GM_2AP concentrations in Fabry disease. The relevance of elevated GM_2AP concentrations in pre-treatment Fabry disease patients and their correction following 12 months of ERT requires further investigation. However, the reduction of lysosomal proteins

prosaposin and GM_2AP following ERT may be indicative of improved lysosomal function.

GM_2AP was also found to be increased significantly (p = 0.049) in diabetic patients compared to a control group (Figure 3.8), this differs from our finding in prosaposin concentrations where no significant difference was observed between diabetic and control groups (p = 0.2). Higashi *et al.*, (2011) demonstrated that administration of GM_2AP *in vivo*, significantly lowered blood glucose concentrations and stimulated insulin secretion. HbA1c concentrations provide a measure of circulating glucose over a 2 – 3 month period and can be used as a simple and reliable marker of insulin resistance. In view of this GM_2AP concentrations in this paediatric diabetic patient group were compared with HbA1c concentrations to establish if there was any correlation. However, an R^2 value of 0.3 was observed in this small sample group indicating no correlation between urinary GM_2AP concentrations and HbA1c levels in blood (data not shown). The elevation of GM_2AP in both untreated Fabry and diabetic patients may suggest that GM_2AP is a sensitive marker of pre-symptomatic kidney disease.

The population prevalence of chronic kidney disease (CKD) exceeds 10% rising to over 50% in at risk populations including those with diabetes, high blood pressure and obesity. This is a recognised major public health burden (Eckardt *et al.*, 2013). Renal involvement is also a major contributor to morbidity in Fabry disease and it has been suggested that at present biopsy is required in order to detect changes in the glomerular and vascular architecture indicative of renal disease that are evident even before detectable proteinuria in these patients (Tøndel *et al.*, 2008). Therefore a panel of biomarkers with the ability to detect pre-symptomatic kidney disease would provide a vital, non-invasive tool for the

identification of those patients most ‘at risk’ and enable therapies and/or lifestyle changes to be instigated before the occurrence of irreversible CKD. To assess whether a number of the proteins identified in the initial label-free experiment, as well as known or previously described biomarkers of kidney disease, could detect pre-symptomatic kidney disease a larger multiplex MRM UPLC-MS/MS assay was developed. This assay was then used to assess the ability of these proteins to detect pre-symptomatic kidney disease in samples from a number of ‘at risk’ patient groups. Included in the study was a paediatric Fabry disease patient group categorised for the purpose of this study into those patients with the least disease burden and those with the most disease burden, with samples collected pre-treatment and following one-, two- and three-years of therapy. Also included in the study was a paediatric type I diabetic patient group, an obese paediatric patient group and a paediatric control group. In addition, samples from an adult Fabry disease patient group, an adult type II diabetic patient group and an adult control group were also analysed.

Serum albumin was included in the pre-symptomatic kidney disease assay as it is currently the principal biomarker used to monitor kidney function in a number of clinical conditions. Albumin is a serum protein manufactured by the liver that functions as both a building block and a carrier molecule (Lehman 2009). In healthy kidneys albumin is filtered in renal glomeruli but, the large molecular weight of this protein prevents it from passing through the glomerulus and instead it is effectively reabsorbed in the proximal tubule by endocytosis (Gekle 1998). However, when the glomerulus is damaged increasing amounts of albumin pass freely through this barrier and can be detected in the urine. The degree of albumin present is reflective of the degree of damage (Nayak and Nayak 2007).

Albumin was the second most abundant protein detected in the label-free proteomic experiment representing 6 % of the total protein detected in pre-treatment Fabry disease patients (Figure 3.1). Although the mean levels of albumin increased in post-treatment Fabry disease patients this change was not statistically or significantly elevated (p = 0.4) and represented a fold change of 1.3. Following analysis by UPLC-MS/MS albumin concentrations were found to be increased statistically and significantly between both adult Fabry disease patient (p = 0.04) and adult type II diabetic patient (p = 0.03) groups, compared to the adult control group (Figure 3.10). Microalbuminuria was not evident in the paediatric patient cohorts using conventional methods and whilst no statistically significant elevations in albumin concentration above that of the control group were observed, fold change elevations were observed. Fabry disease patients with the least disease burden both pre-treatment and following three years of ERT and the type I diabetic patient group displayed >2-fold elevations above the control group, inferring that kidney function may already be reduced, at this early stage, in these patient groups. Albumin concentrations in those patients with most disease burden showed significant reductions (p = 0.02) below those of the control group. However, a significant elevation (p = 0.04) was seen following three years of ERT resulting in mean concentrations of this group comparable with the control group. Although albumin concentrations in those patients with the least disease burden were consistently elevated above those patients with the most disease burden and those of the control group no elevations were observed above baseline pre-treatment levels suggesting that ERT may be halting the progression of further kidney involvement in this patient group. Contrastingly, in those patients with the most disease burden elevations above baseline pre-treatment levels were seen at each time point studied

suggesting that ERT may not be as effective in this patient group. During this study the consecutive elevation in albumin levels at each time point resulted in albumin concentrations comparable with those of the control group. However, if this pattern continued exponentially levels would rapidly become increased above those of the control group.

The multi-ligand endocytic receptors megalin and cubilin were selected for inclusion in the pre-symptomatic kidney disease assay due in part to the role they play in the normal tubular reabsorption of proteins, including albumin and vitamin D binding protein. Megalin is heavily expressed in the renal proximal tubule and in addition to acting as a receptor, studies suggest that megalin also plays a role in the metabolism and homeostasis of essential vitamins (Christensen and Birn 2001). In this study, significant and statistical elevations were observed in megalin excretion in both the adult Fabry disease (p = 0.03) and type II diabetic (p = 0.03) groups compared to the control group (Figure 3.12). Whilst no statistically significant changes were observed in the paediatric cohorts, a 2.5-fold elevation in megalin was observed between the type I diabetic and control group. The concentrations of megalin in those patients with least disease burden (Figure 3.13a) displayed fold change elevations above baseline pre-treatment levels and those of the control group following one-, two- and three-years of ERT. However, megalin concentrations in those patients with most disease burden (Figure 3.13b), despite a slight elevation following one year of ERT, remained stable during the time frame studied with levels comparable to those of the control group.

Cubilin is co-expressed with megalin in the renal proximal tubule and although structurally very different, cubilin possesses many similar features and shares many ligands with megalin (Christensen and Birn 2001). However, in this study

whilst statistically significant results were obtained for megalin the same was not true for cubilin, although similar patterns were observed in some patient groups. Increases of 5.3-fold and 8.5-fold above their control groups were observed for the type I and type II diabetic groups, respectively (Figure 3.24). However, whilst significant elevations in megalin concentrations were observed in the adult Fabry disease group, cubilin concentrations in this group were comparable with those of the control group. The concentrations of cubilin in the group of patients with least disease burden (Figure 3.25a), like megalin, displayed fold change elevations above baseline pre-treatment levels and those of the control group following two- and three-years of ERT. Megalin concentrations in the group of patients with most disease burden (Figure 3.25b) again, despite slight elevations following one- and two-years of ERT, remained mostly stable during the time frame studied with levels comparable to those of the control group following three-years of ERT.

Vitamin D binding protein is a multifunctional protein found in a number of biological fluids and belongs to the albumin gene family. Increases in vitamin D binding protein have been reported previously in patients with chronic kidney disease and tubulointerstitial damage (Mirković *et al.*, 2013). Urinary vitamin D binding protein has also been shown to increase with increasing severity of diabetic nephropathy (Thrailkill *et al.*, 2011). Findings in this study are in agreement with previous reports with a statistical and significant elevation observed in urinary vitamin D binding protein concentrations in type II diabetic patients (p = 0.02) (Figure 3.14). Vitamin D binding protein was also shown to be increased by fold change in Fabry disease adults and paediatric type I diabetic patients (9.5-fold and 2.3-fold, respectively). Vitamin D binding protein concentrations behaved in a similar way in the groups of patients with the least

and the most disease burden (Figure 3.15). Levels of both those patients with the least disease burden and those with the most disease burden were statistically and significantly lower than those of the control group prior to ERT. A slight elevation was observed in both groups following one year of ERT however, this normalised at the two and three year time points resulting in stable values consistent with those of the control group. These findings may suggest that there is little tubulointerstitial damage in those Fabry disease patients who develop renal involvement. This is in agreement with previous studies where no change in tubulointerstitial damage was detected following ERT (Branton, Schiffmann, and Kopp 2002; Schiffmann *et al.*, 2001).

Prostaglandin-H2 D-isomerase is an enzyme involved in controlling smooth muscle contraction/relaxation, is a potent inhibitor of platelet aggregation and catalyses the conversion of prostaglandin H2 to prostaglandin D2. Prostaglandin-H2 D-isomerase also binds small non-substrate lipophilic molecules such as bilirubin and may act as a scavenger for harmful hydrophobic molecules. The use of urinary and serum prostaglandin-H2 D-isomerase levels have been suggested previously as a sensitive indicator of renal damage in diabetes mellitus, chronic kidney disease and hypertension (Dajak *et al.*, 2011; Hirawa *et al.*, 2001). In this study a statistically significant elevation in prostaglandin-H2 D-isomerase levels (p = 0.049) was found in the adult Fabry patient group (Figure 3.16). However, although a 61.2-fold change was apparent in the adult type II diabetic group this change was not statistically significant. Prostaglandin-H2 D-isomerase concentrations behaved similarly in both Fabry disease groups with the least and the most disease burden (Figure 3.17) displaying elevations above the control group at baseline and at each consecutive time point evaluated. Following three-years of treatment this level

had reached a statistically significant increase above the control group in those patients with most disease burden (p = 0.03). Elevations in prostaglandin-H2 D-isomerase were also detected in all other paediatric patient cohorts. Prostaglandin-H2 D-isomerase was the only protein included in the pre-symptomatic kidney disease assay where elevations in all paediatric and adult patient groups, above those of their respective control group, were observed. However, whether this protein is in fact a very sensitive indicator or renal damage requires further investigation.

The lysosomal protein lysosomal alpha glucosidase is essential for the degradation of glycogen to glucose within lysosomes and a statistically significant elevation of this protein was observed in adult Fabry patients (p = 0.05), above those of the control group (Figure 3.18). However, in the paediatric Fabry disease patients with the least and the most disease burden pre-treatment levels were only elevated marginally above those of the control group (Figure 3.19). Apart from a 2.5-fold increase observed in those patients with least disease burden following two years of ERT, levels in both groups were lower than those of the baseline pre-treatment concentrations following three-years of treatment resulting in levels comparable with those of the control group. Whilst elevations in lysosomal alpha glucosidase may not be indicative of pre-symptomatic kidney disease the statistically significant increase observed only in the adult Fabry disease patient group may represent a degree of impaired lysosomal function (Figure 3.18). It is possible that this may be corrected by ERT when instigated at an early stage of disease progression as demonstrated by the finding that no statistically significant alterations in either the paediatric Fabry disease patients with the least or the most disease burden, compared to that of the control group, were apparent (Figure 3.19). In addition

both type I and type II diabetic patients had 2.1-fold and 5.3-fold elevations compared to their respective control groups (Figure 3.18). This could be as a direct response to increased glucose and/or perturbation of the lysosomal system resulting in downstream effects such as impairment of the transduction mechanism for glucose-induced insulin release. (Salehi *et al.*, 1999; Moheimani *et al.*, 2012).

Membrane bound endothelial protein C receptor plays an important role within the protein C pathway in regulating coagulation and inflammation. Following cleavage by a protease endothelial protein C receptor is also found as a soluble protein and provides a sensitive indicator of endothelial damage (Nozza *et al.*, 2012). In addition, urinary levels have been suggested as a biomarker to detect the rejection of renal transplantation (Lattenist *et al.*, 2013). In this study, endothelial protein C receptor concentrations were significantly lower in the paediatric Fabry disease patients with most disease burden compared to the control group both prior to treatment and following three-years of ERT (Figure 3.21). However, levels observed in the paediatric Fabry disease group with least disease burden and adult Fabry patient groups were comparable with those of their respective control groups. Fold change elevations were however seen in endothelial protein C receptor concentrations in both the type I and type II diabetic patient groups above those of their respective control groups (Figure 3.20). This may indicate that these patients possess a degree of endothelial damage, a complication often seen in diabetic patients, which is a risk factor for progression of atherosclerosis and in turn has been shown to accelerate progression to retinopathy, nephropathy and neuropathy (Garcia *et al.*, 2001; Calles-Escandon and Cipolla 2001).

Osteopontin is a multifunctional secreted, phosphorylated glycoprotein expressed in bone, macrophages, T lymphocytes and NK cells. Osteopontin is present in the loop of Henle and distal nephrons in healthy kidneys and studies have shown that kidney cells produce high levels of this protein following an insult suggesting that osteopontin could play an important role in kidney injury (Xie *et al.*, 2001; Zhang *et al.*, 2010). A statistically significant elevation was observed in type II diabetic patients (p = 0.02) compared to the adult control group and a 2.0-fold increase was also observed in type I diabetic patients (Figure 3.22). However, levels of osteopontin in all other patient groups were comparable to those of their respective control groups suggesting that these patients have sustained comparatively less kidney injury than those patients of a similar age with diabetes.

Sortilin is a multifunctional protein that in addition to its role as a multi-ligand receptor for neuropeptides including neurotensin has been shown to mediate lysosomal trafficking of several enzymes and non-enzymatic proteins (Coutinho, Prata and Alves 2012) including prosaposin, GM_2AP (Lefrancois *et al.*, 2003), acid sphingomyelinase (Ni, Canuel and Morales 2006) and cathepsins D and H (Canuel *et al.*, 2008). Increases in sortilin concentration were observed in both the type I and type II diabetic patient groups as well as the ERT naïve adult Fabry disease group in this study (Figure 3.26). However, concentrations of this protein in the paediatric Fabry disease group with least disease burden were comparable to those of the control group pre-treatment and during the three-years following instigation of ERT (Figure 3.27). Interestingly, sortilin wasn't detectable in those patients with most disease burden either pre-treatment or at any of the consecutive time points analysed. A recent study by Prabakaran *et al.*, (2012) identified mannose 6-phosphate receptor and sortilin as alpha

galactosidase A receptors in cultured renal endothelial cells. The study went on to show that in addition to mannose 6-phosphate, sortilin is able to internalise circulating recombinant alpha-galactosidase A during ERT. This finding combined with the absence of sortilin in those patients with most disease burden in the present study may provide some explanation as to the inability of ERT to reduce or stabilise the Gb_3 concentrations in this subset of patients.

Neutrophil gelatinase-associated lipocalin (NGAL) is a ubiquitous lipocalin iron carrying protein (Bolignano *et al.*, 2009) expressed in the tubular epithelial cells of the distal nephron and has shown to be released from tubular epithelial cells following acute kidney injury (Fassett *et al.*, 2011). In the present study statistically significant elevations above baseline pre-treatment levels were found two-years post-ERT with fold change elevations at all other time points studied in the paediatric Fabry disease patients with least disease burden (Figure 3.33a). Interestingly, decreases in neutrophil gelatinase-associated lipocalin were detected in those patients with most disease burden following treatment (Figure 3.33b). Fold change increases above the adult control group were found in both the adult Fabry disease and type II diabetic groups (Figure 3.32). Urinary neutrophil gelatinase-associated lipocalin concentrations have been documented previously in non-diabetic patients with chronic kidney disease (Malyszko *et al.*, 2009) as well as in a diabetic patient group (Bolignano *et al.*, 2009) suggesting that this protein may play an important role in the pathophysiology of renal adaptation and associated nephropathy (Fassett *et al.*, 2011).

Statistically significant results were not obtained in, or between, any patient group analysed for the proteins Ig gamma-4 chain c region or retinol binding protein. Retinol binding protein was identified previously in the label-free

quantitative proteomic initial study as having a >2-fold decrease between pre-treatment and one year post-treatment Fabry disease groups. Using the pre-symptomatic kidney disease assay this finding was also observed in the paediatric Fabry disease patients with most disease burden (Figure 3.29b). Concentrations of retinol binding protein in this group were 3.5-fold higher than those of the control group prior to treatment. However, consecutive reductions from baseline pre-treatment levels were seen at each time point analysed resulting in retinol binding protein concentrations comparable with those of the control group. In the paediatric Fabry disease patients with least disease burden, apart from a fluctuation at the two-year post-ERT time point, levels comparable with those of the control group were apparent at each time point studied. However, elevations of retinol binding protein were seen in the paediatric type I diabetic group and the adult Fabry and type II diabetic groups. (Figure 3.28) Retinol binding protein is the transporter of retinol and is often found bound to transthyretin but a small unbound fraction passes through glomerular membranes and is reabsorbed by the renal proximal tubule cells where it is catabolised. Due to extensive tubular reabsorption, under normal conditions very little filtered retinol binding protein appears in the final excreted urine. Therefore, an increase in the excretion of retinol binding protein indicates proximal tubule damage and/or impaired proximal tubule function (Kirsztajn *et al.*, 2002). The decrease in retinol binding proteins in the paediatric Fabry disease patients with most disease burden following instigation of treatment may therefore indicate that ERT, when instigated at an early point of disease progression, may have a beneficial effect on proximal tubule damage.

3.4 Conclusion

Label-free quantitative proteomics identified a number of potential biomarkers, in the urine of paediatric Fabry disease patients. The development of an initial targeted and rapid peptide based assay to validate these findings confirmed that prosaposin and GM_2AP were reduced significantly following one year of ERT in Fabry disease patients. The addition of age- and sex- matched type I diabetic patients, as a positive control group, demonstrated that whilst prosaposin levels were comparable with those of the control group, the levels of GM_2AP were increased significantly. The increase in GM_2AP levels in both the paediatric Fabry disease and type I diabetic patients suggested that this protein may be a sensitive indicator of pre-symptomatic kidney disease. This protein was therefore incorporated with other biomarkers of kidney disease into a rapid, 10 minute, multiplex MRM UPLC-MS/MS, to assess if this group of biomarkers had the ability to detect pre-symptomatic kidney disease in those patients most at risk.

The inclusion of albumin, the current gold standard biomarker for monitoring kidney disease, demonstrated that this assay has the ability to detect pre-symptomatic kidney disease as alterations in these paediatric patient groups were detectable before any abnormal results were obtained using conventional methods. In addition, other known biomarkers of established kidney disease displayed alterations in these ‘at risk’ patient groups. However, although there are some common pathways to kidney disease progression, there are many primary causes, each with its own specific pathophysiological mechanism and this may go some way in explaining some of the variations observed within these patient groups for each protein.

The effect of ERT on the proteins included in the pre-symptomatic kidney disease assay requires interpretation with care and in order to draw informative conclusions, the investigation of these proteins in a paediatric patient group not receiving ERT would be required. In this way an assessment as to the levels and rates of progression of these proteins in patients not receiving ERT could be made and therefore establish to what degree ERT is able to reduce kidney involvement. This study may however demonstrate that differences exist between those patients in whom Gb_3 levels fall following instigation of treatment (those with least disease burden) and those in who they do not (those with most disease burden).

The detection of pre-symptomatic kidney disease in order to instigate concomitant therapies at an early stage of the disease is becoming more important to not only prevent development to end stage renal disease but also to alleviate the burden to health services worldwide. A panel of biomarkers, such as those investigated during this study, detectable by MRM UPLC-MS/MS a technique which has the ability to allow the panel to be expanded may be what is required. However, to fully understand the meaning and implications of these results further investigation and longitudinal observational studies are required in order to fully validate these biomarkers prior to their routine use.

Chapter 4

A metabolomic study to identify new globotriaosylceramide-related biomarkers in the plasma of Fabry disease patients

Chapter 4 - A metabolomic study to identify new globotriaosylceramide-related biomarkers in the plasma of Fabry disease patients 220

4.0 A metabolic study to identify new globotriaosylceramide-related biomarkers in the plasma of Fabry disease patients

4.1 Introduction

In the study described in the previous chapter a proteomic approach was used to identify a number of protein biomarkers in the urine of Fabry disease patients. However, to study smaller molecules requires the use of metabolomics which enables the characterisation and cataloguing of small molecule metabolites (Griffiths and Wang 2009). In the present study a targeted metabolomic approach was used to identify new and existing Gb_3-related biomarkers in the plasma of Fabry disease patients.

The study and characterisation of small molecule metabolites has evolved significantly in the last decade with advances in both the tools required to perform analyses and with the development of the necessary bioinformatic software to analyse the wealth of data acquired. With continuing advances in these areas our knowledge of the metabolome continues to grow. Metabolites are the intermediates and products of metabolism and are sensitive to short temporal variations making them ideal candidates for biomarkers. Mass spectrometry based metabolomics has proven to be the analytical tool of choice in the search and identification of such biomarkers due to the high sensitivity, specificity and robustness achievable using this methodology (Griffiths and Wang 2009; Milne *et al.*, 2013).

Currently, two metabolite biomarkers for Fabry disease, globotriaosylceramide (Gb_3) and globotriaosylsphingosine (lyso-Gb_3) (Figure 1.3) are recognised as important diagnostic tools and are used in high-risk urinary screening studies of Fabry patients. In addition, these metabolites are routinely used to assess

disease burden and monitor response to therapy. Recently, the presence of newly defined Gb_3-related analogs and isoforms in urine (Auray-Blais and Boutin 2012) and lyso-Gb_3 related analogs and isoforms in urine (Auray-Blais *et al.*, 2012) and plasma (Dupont *et al.*, 2013) has been demonstrated. Following the development of a methodology to measure plasma lyso-Gb_3 analogs and isoforms in urine by Boutin *et al.*, (2012) the excretion of the majority of these analogs was found to be above the level of lyso-Gb_3 itself. This observation combined with the reduction of these analogs following enzyme replacement therapy suggests that measurement of these novel biomarkers may provide further information as to disease status and response to treatment than the analysis of simply Gb_3 and/or lyso-Gb_3 alone (Auray-Blais *et al.*, 2012; Dupont *et al.*, 2013).

In the present study, a metabolomic approach was used to identify potential biomarkers in plasma from twelve untreated Fabry males and eight age- and sex-matched controls using time-of-flight mass spectrometry (ToF-MS). Whilst Gb_3 levels in plasma haven't proven to be an ideal biomarker (Mills *et al.*, 2005) as elevations in plasma Gb_3 concentrations are not observed in a large proportion of female heterozygotes, this study aimed to identify and assess the levels of structural isoforms and potential analogs of Gb_3 by focusing on mass-to charge (*m/z*) ratios between 995 and 1200 Da. In addition, following the identification of Gb_3-related analogs and isoforms the levels of these biomarkers were assessed in plasma from ten untreated Fabry females. Finally, findings from this study were compared and correlated with a previous study in urine to draw conclusions regarding the presence of these metabolites in the biological fluids of Fabry patients.

4.2 Results

4.2.1 Effects of sample processing

A control plasma sample was spiked with a synthetic standard (Gb_3(d18:1)(C17:0)) to ensure that the Gb_3 analogs detected in this study were not generated by sample processing (section 2.2.6.5). This was clearly demonstrated as no chemical modifications such as methylation, addition of a double bond or hydration were observed on the synthetic standard after processing procedures.

4.2.2 System stability evaluation

Quality controls were analysed throughout the metabolomic run (section 2.2.6.7) and used to evaluate the reproducibility of the mass and retention time, thus determining the smallest mass (0.05 Da) and retention time window (0.2 min), to ensure good alignment in MarkerLynx™.

4.2.3 Data mining and multivariate analysis

Following analysis of the UPLC-ESI-ToF-MS metabolomic results of plasma samples obtained from twelve untreated Fabry males and eight healthy controls with MarkerLynx™ (as described in section 2.2.6.6), a total of 14,514 markers aligned according to their exact masses and retention time. Using these markers, an OPLS-DA score plot (Figure 4.1) was created and showed clear differentiation between the two sample groups.

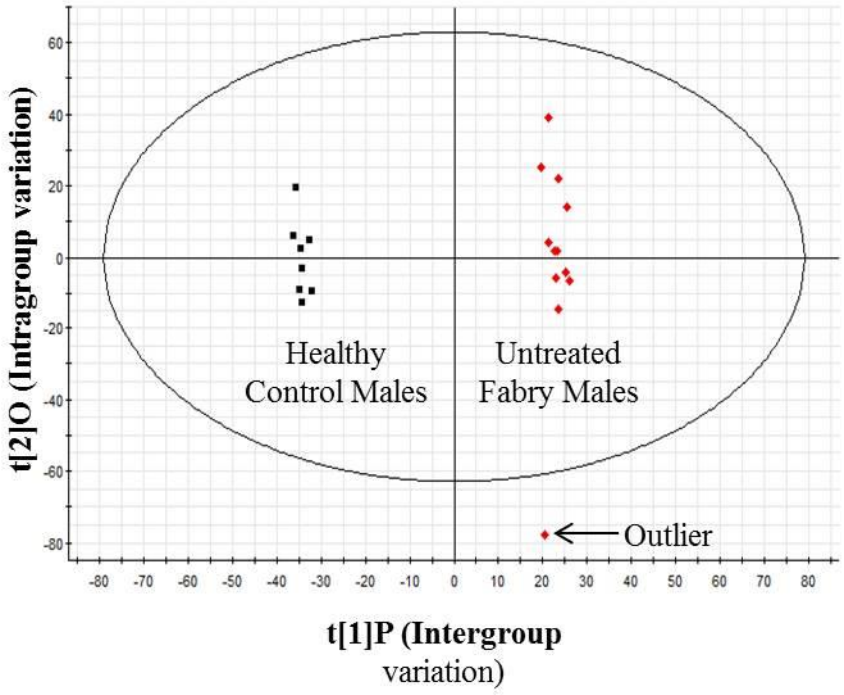

Figure 4.1 OPLS-DA score plot derived from the UPLC-ESI-ToF-MS metabolomic analysis of plasma samples from untreated Fabry males (*n* = 12) and healthy control males (*n* = 8). The ellipse corresponds to the Hotelling T^2 range with a significance level of $p = 0.05$. The statistical analysis revealed a $R^2 = 0.815$, a Q2 = 0.383, and a root mean square error of validation (RMSEV) = 0.77.

Each symbol in the plot corresponds to one sample. The x-axis represents the intergroup variation and the y-axis represents the intragroup variation. The ellipse corresponds to the Hotelling T^2 range with a significance level of 95 % ($p = 0.05$). The Fabry sample (Patient 12, Table 2.3) was outside the Hotelling T^2 ellipse. This sample was thus considered an outlier and excluded from the analysis. Further statistical analyses performed produced an R^2 value of 0.815, a Q2 value of 0.383 and an RMSEV value of 0.77 for this data set.

This data was then used to create an S-plot (Figure 4.2A) where each point corresponds to a marker as defined by MarkerLynx™. The S-plot shows the reliability (y-axis) as a function of covariance (x-axis) for each metabolite. The more a metabolite is located at the top right or at the bottom left of the graph, the greater the influence on the discrimination of the sample groups in the OPLS-DA score plot. Metabolites located at the top right corner of the S-plot were found at a higher concentration in the Fabry patient group compared to the control group, and the metabolites at the bottom left were found at a lower concentration in the Fabry patient group compared to the control group. Fabry disease metabolites are considered as potential biomarkers if they are present in Fabry patient samples but not in normal control samples. The S-plot in Figure 4.2B shows a zoomed image of the potential metabolite biomarkers. Of the potential biomarkers of interest, seventeen had previously been identified in urine as isoforms or analogs of Gb_3 (Auray-Blais and Boutin 2012), these are highlighted in red and annotated with a lower case initial on the S-plot. The remaining seven markers were considered as potential new biomarkers and are shown highlighted in blue on the S-plot and annotated with a number. These new potential biomarkers required further investigations for structural elucidation and characterisation.

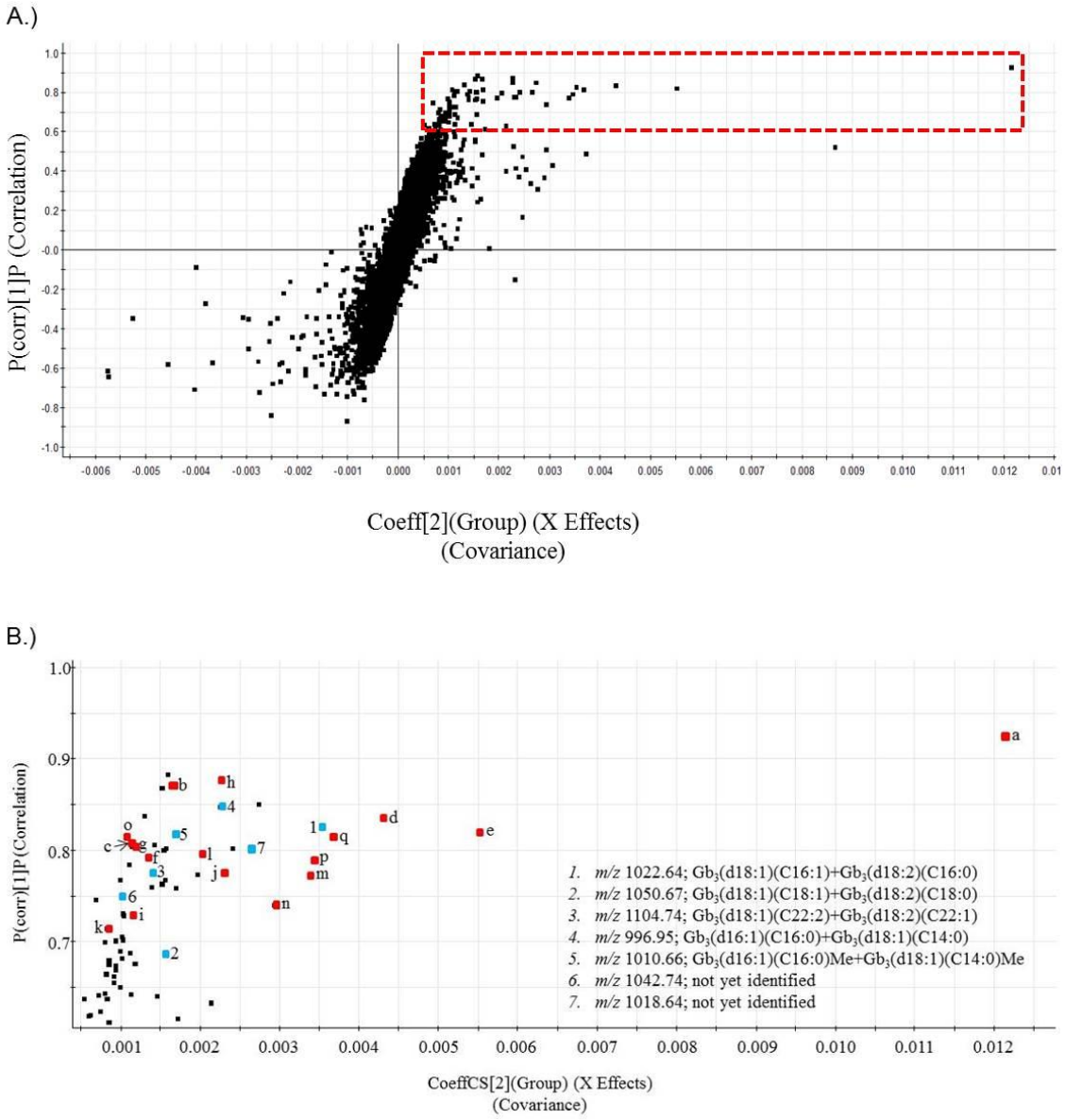

Figure 4.2 (A) S-plot showing the correlation in function of the covariance for the metabolites used to discriminate the two sample groups in the OPLS-DA score plot. (B) Zoom of the section of the S-plot where the Fabry disease biomarkers are shown. Those highlighted in red are previously described Gb_3 analogs or isoforms with the letter corresponding to the analog or isoform in Table 4.1 Those highlighted in blue and annotated with numbers are newly discovered potential Fabry disease biomarkers.

4.2.4 Plasma Gb_3-related metabolites in Fabry patients

The nomenclature used in metabolomic analyses to describe Gb_3-related isoforms and analogs is outlined in section 2.2.6.2. Identification and relative area counts of the new Gb_3-related analogs and isoforms and the Gb_3-related analogs and isoforms previously described in urine (Auray-Blais and Boutin 2012) and now identified during this study in plasma were obtained using QuanLynx™ (as described in section 2.2.6.9). Table 4.1 summarises the data obtained for Gb_3-related analogs and isoforms detected in this study in plasma and also data for those Gb_3-related analogs and isoforms previously detected in urine. The majority of these Gb_3-related analogs and isoforms were also revealed in the multivariate analysis and are shown in the S-plot (Figure 4.2B). Previously identified biomarkers are highlighted in red and annotated with a lowercase letter corresponding to their Gb_3-related analog/isoform displayed in Table 4.1. As expected, the relative area counts for plasma Gb_3-related analogs and isoforms were found to be higher in Fabry patients compared to controls.

Table 4.1 Retention time and relative abundance of the biomarkers in plasma from the current study revealed by the S-plot (Figure 4.2) in untreated Fabry males and healthy control males. Corresponding information for biomarkers in urine from a previous study (Auray-Blais and Boutin 2012) is also supplied for comparison. Those biomarkers depicted in bold are novel biomarkers detected in this study. AUC: Area under the ROC curve for plasma. *These biomarkers were not revealed by the S-plot but were detected by extracted ion chromatogram. nd: not detectable; na: not applicable.

Category	**Biomarkers**	**S-plot ID**	**Retention time (min)**	**Fabry males mean (min-max)**		**Control males mean (min-max)**		**AUC**	***t*-test**	
			Urine and plasma	Plasma [Area]	Urine Area/[creat.]	Plasma [Area]	Urine Area/[creat.]	Plasma	Fabry plasma *vs* control plasma	Fabry plasma *vs* Fabry urine
1	Gb_3(d18:1)(C16:0)	a	8.8	81.8 (69.2-94.5)	5.4 (0.3-25.5)	21.0 (15.5-27.8)	0.01 (nd-0.1)	1	$p < 0.001$	$p < 0.001$
1	Gb_3(d18:1)(C18:0)	b	9.2	8.8 (4.9-15.2)	3.2 (0.1-13.3)	1.7 (1.1-2.2)	nd	1	$p < 0.001$	$p < 0.001$
1	Gb_3(d18:1)(C20:0)	c	9.7	5.4 (3.7-8.4)	7.4 (0.30-31.73)	1.4 (0.7-2.3)	0.01 (nd-0.1)	1	$p < 0.001$	$p < 0.4$
1	Gb_3(d18:1)(C22:0)	d	10.1	8.3 (4.7-12.2)	28.2 (1.6-68.3)	1.5 (1.2-1.7)	0.2 (nd-0.8)	1	$p < 0.001$	$p < 0.004$
1	Gb_3(d18:1)(C24:0)	e	10.4	11.5 (7.5-16.4)	59.8 (2.5-214.2)	1.7 (1.2-2.3)	0.4 (0.1-1.2)	1	$p < 0.001$	$p < 0.001$
1	Gb_3(d18:1)(C26:0)	f	10.7	0.8 (0.5-1.3)	2.4 (0.4-8.7)	0.1 (0.01-0.2)	0.01 (nd-0.1)	1	$p < 0.001$	$p < 0.01$
2	Gb_3(d18:1)(C16:0)Me	g	9.0	0.3 (0.1-0.5)	0.3 (nd-1.3)	nd	nd	1	$p < 0.001$	$p < 0.74$

2	Gb_3(d18:1)(C18:0)Me	*	9.5	nd	0.2 (nd-0.9)	nd	nd	na	na	na
2	Gb_3(d18:1)(C20:0)Me	h	9.9	1.0 (0.7-1.7)	1.7 (0.1-4.2)	0.4 (0.2-0.6)	0.03 (nd-0.2)	1	$p < 0.001$	$p < 0.03$
2	Gb_3(d18:1)(C22:1)Me	i	9.9	1.6 (1.1-2.5)	1.3 (0.1-4.4)	0.2 (0.04-0.3)	nd	1	$p < 0.001$	$p < 0.3$
2	Gb_3(d18:1)(C22:0)Me	j	10.3	3.3 (2.2-5.1)	6.1 (0.3-17.6)	0.9 (0.7-1.3)	0.01 (nd-0.1)	1	$p < 0.001$	$p < 0.03$
2	Gb_3(d18:1)(C24:1)Me	*	10.2	0.5 (0.3-0.6)	0.8 (nd-2.4)	0.2 (0.04-1.0)	nd	1	$p < 0.001$	$p < 0.04$
2	Gb_3(d18:1)(C24:0)Me	k	10.5	1.2 (0.7-1.8)	2.2 (nd-6.4)	nd	nd	1	$p < 0.001$	$p < 0.03$
3	**Gb_3(d18:1)(C16:1) + Gb_3(d18:2)(C16:0)**	**1**	**8.4**	**10.6 (7.8-13.0)**	**nd**	**2.2 (1.7-3.5)**	**nd**	**1**	***p* < 0.001**	**na**
3	**Gb_3(d18:1)(C18:1) + Gb_3(d18:2)(C18:0)**	**2**	**8.9**	**3.3 (2.1-5.0)**	**nd**	**0.7 (0.5-1.1)**	**nd**	**1**	***p* < 0.001**	**na**
3	Gb_3(d18:1)(C20:1) + Gb_3(d18:2)(C20:0)	l	9.4	3.5 (2.3-4.6)	0.9 (0.02-4.1)	1.0 (0.7-1.8)	nd	1	$p < 0.001$	$p < 0.001$
3	Gb_3(d18:1)(C22:1) + Gb_3(d18:2)(C22:0)	m	9.8	10.2 (7.1-16.0)	4.5 (0.1-18.4)	3.6 (2.2-5.3)	nd	1	$p < 0.001$	$p < 0.003$
3	Gb_3(d18:1)(C24:1) + Gb_3(d18:2)(C24:0)	n	10.1	11.3 (7.2-15.3)	41.7 (2.1-133.5)	3.2 (2.4-4.3)	0.3 (nd-1.5)	1	$p < 0.001$	$p < 0.001$
3	Gb_3(d18:1)(C26:1) + Gb_3(d18:2)(C26:0)	o	10.5	nd	1.1 (0.2-3.6)	nd	nd	na	na	na
4	Gb_3(d18:0)(C24:1)H_2O	p	9.9	1.5 (1.0-2.1)	2.1 (0.2-8.0)	0.5 (0.2-0.7)	nd	1	$p < 0.001$	$p < 0.27$
5	**Gb_3(d18:1)(C22:2) + Gb_3(d18:2)(C22:1)**	**3**	**9.5**	**1.3 (0.8-1.7)**	**nd**	**0.4 (0.1-0.8)**	**nd**	**0.989**	***p* < 0.001**	**na**

5	Gb_3(d18:1)(C24:2) + Gb_3(d18:2)(C24:1)	q	9.9	11.9 (8.5-16.5)	5.7 (0.2-27.0)	4.1 (3.1-6.6)	nd	1	$p < 0.001$	$p < 0.002$
6	**Gb_3(d16:1)(C16:0) + Gb_3(d18:1)(C14:0)**	**4**	**8.3**	**3.0 (2.1-4.8)**	**nd**	**0.6 (0.4-0.9)**	**nd**	**1**	***p* < 0.001**	**na**
7	**Gb_3(d16:1)(C16:0)Me + Gb_3(d18:1)(C14:0)Me**	**5**	**8.5**	**2.9 (2.2-3.7)**	**nd**	**0.6 (0.4-0.9)**	**nd**	**1**	***p* < 0.001**	**na**
-	Not yet identified (*m/z* 1042.74)	6	8.5	1.1 (0.7-1.4)	nd	0.2 (0.1-0.4)	nd	1	$p < 0.001$	na
-	Not yet identified (m/z 1018.64)	7	8.3	1.9 (1.4-3.2)	nd	0.3 (0.01-0.5)	nd	1	$p < 0.001$	na

The biomarkers detected during this study have been classified into categories. The majority of biomarkers detected were able to be classified into one of the five existing categories described by Auray-Blais and Boutin (2012). However, two additional categories have been created specifically for plasma Gb_3-related analogs/isoforms, resulting in the following seven categories: **1)** Gb_3-related isoforms with saturated fatty acids; **2)** Methylated Gb_3-related isoforms; **3)** Gb_3-related isoforms/analogs with one double bond; **4)** Gb_3 analogs with an hydrated sphingosine; **5)** Gb_3-related isoforms/analogs with two double bonds; **6)** Short chain Gb_3-related isoforms/analogs; and **7)** Short chain methylated Gb_3-related isoforms/analogs.

Area under the ROC curve (AUC) data were also calculated for each Gb_3-related analog and isoform detected in plasma from untreated Fabry males and values are displayed in Table 4.1. For the majority of Gb_3-related analogs/isoforms an AUC value of 1 was obtained. Only one biomarker displayed an AUC value of less than 1, this biomarker in category 5, Gb_3(d18:1)(C22:2)+Gb_3(d18:2)(C22:1), obtained an AUC value of 0.989.

4.2.5 Gb_3-related metabolites present in plasma that have previously been identified in urine

Within the first five categories of biomarker, seventeen had previously been identified in urine (Auray-Blais and Boutin 2012). In category 1, one saturated Gb_3 isoform Gb_3(d18:1)(C16:0) was highly excreted compared to the excretion of all other Gb_3 isoforms with saturated fatty acids. In category 2, the extent of methylation was greatest for the isoform Gb_3(d18:1)(C22:0)Me. No detectable levels of methylation were observed for the isoform Gb_3(d18:1)(C18:0)Me previously identified in urine and the least amount of methylation was observed

on the isoform Gb_3(d18:1)(C16:0)Me, the most excreted saturated Gb_3 isoform in category 1. The structural isomer mixture Gb_3(d18:1)(C24:1) + Gb_3(d18:2)(C24:0) was the most highly excreted in category 3 whilst the lowest levels of excretion in plasma were observed for the structural isomer Gb_3(d18:1)(C26:1) + Gb_3(d18:2)(C26:0). In categories 4 and 5, the Gb_3 hydrated at the sphingosine level and the mixture of isoforms with two double bonds Gb_3(d18:1)(C24:2) + Gb_3(d18:2)(C24:1) present in urine were both also detected in plasma.

All biomarkers were shown to be statistically and significantly elevated (p <0.001) in plasma from untreated Fabry males as compared to healthy control reference plasma specimens following *t*-test analyses (Table 4.1). In addition, statistical and significant differences were also observed in the extent of excretion of the biomarkers between plasma and urine in Fabry patients. The excretion of the biomarkers, Gb_3(d18:1)(C16:0), Gb_3(d18:1)(C18:0), Gb_3(d18:1)(C20:1) + Gb_3(d18:2)(C20:0), Gb_3(d18:1)(C22:1) + Gb_3(d18:2)(C22:0) and Gb_3(d18:1)(C24:2) + Gb_3(d18:2)(C24:1) was significantly higher in plasma compared to urine. Whereas the biomarkers, Gb_3(d18:1)(C22:0), Gb_3(d18:1)(C24:0), Gb_3(d18:1)(C26:0), Gb_3(d18:1)(C20:0)Me, Gb_3(d18:1)(C22:0)Me, Gb_3(d18:1)(C24:1)Me, Gb_3(d18:1)(C24:0)Me, Gb_3(d18:1)(C24:1) + Gb_3(d18:2)(C24:0) were significantly higher in urine compared to plasma.

4.2.6 Structural characterisation of novel Fabry disease biomarkers in plasma

In addition to the seventeen previously described Gb_3-related analogs/isoforms detected in this study, seven new plasma Fabry disease biomarkers, not

detected in urine, were revealed by the S-plot (Figure 4.2B). These are shown highlighted in blue and annotated with a number. Data corresponding to the relative abundance of the biomarkers is shown in Table 4.1. To elucidate the structure of these seven new biomarkers, tandem mass spectrometry analyses were performed on a 500 µl plasma sample from an untreated Fabry male (as described in section 2.2.6.8). Of these seven potential new biomarkers, five showed fragmentation profiles similar to Gb_3 and were therefore considered to be structurally related to Gb_3. Exact mass and empirical formula of Gb_3 analogs and fragments are shown in Figures 4.3 – 4.6. Of the seven newly detected biomarkers two, at *m/z* 1018.64 and *m/z* 1042.74, did not show fragmentation profiles similar to Gb_3 and are therefore not considered to be related to Gb_3. However, their abundance was too low to obtain a sufficient number of characteristic fragments with accurate mass measurements to allow their structural elucidation. The S-plot revealed six biomarkers belonging to category 3, corresponding to Gb_3 with an extra double bond. Among these, four had previously been detected in urine (C20 to C26). The two remaining biomarkers with *m/z* 1022.6701 (point 1 on the S-plot, Figure 4.2B) and *m/z* 1050.6637 (point 2 on the S-plot, Figure 4.2B) correspond to Gb_3 with C16 and C18 fatty acid chains, respectively. Figure 4.3 presents the fragmentation spectrum and Table 4.2 presents the exact mass and empirical formula of the peaks detected for the biomarker with the C16 fatty acid. This biomarker presents a mixture of two structural isomers, one with the extra double bond on the sphingosine (Gb_3(d18:2)(C16:0)) and the other with the extra double bond on the fatty acid (Gb_3(d18:1)(C16:1)).

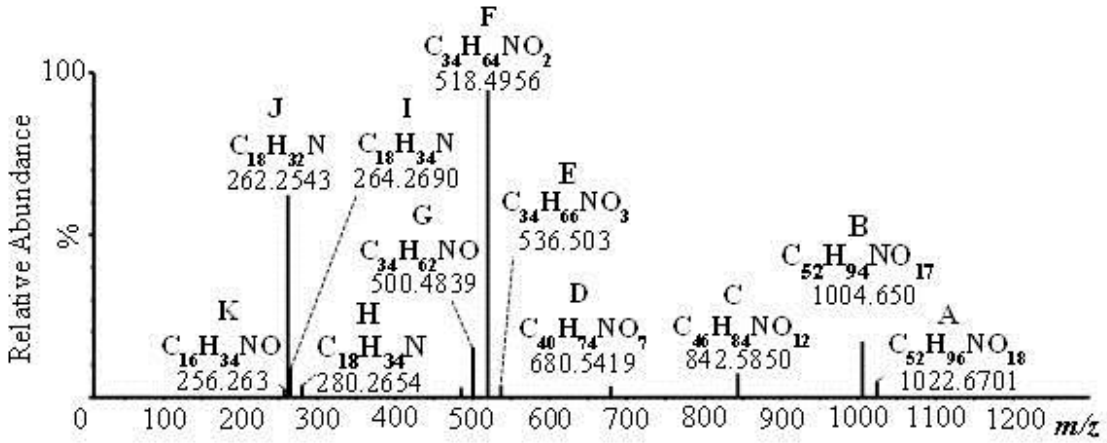

Figure 4.3 ESI-QToF-MS fragmentation spectra of Gb_3(d18:2)(C16:0) + Gb_3(d18:1)(C16:1)

Table 4.2 Exact mass and empirical formula of Gb_3(d18:2)(C16:0) + Gb_3(d18:1)(C16:1). Fragments observed in Figure 4.3.

Fragment	Formula	Calculated Mass Da	Measured Mass Da	Δ Mass ppm
A	$C_{52}H_{96}NO_{18}$	1022.6627	1022.6701	7.2
B	$C_{52}H_{94}NO_{17}$	1004.6522	1004.6504	-1.8
C	$C_{46}H_{84}NO_{12}$	842.5994	842.5850	-17.1
D	$C_{40}H_{74}NO_7$	680.5465	680.5419	-6.8
E	$C_{34}H_{66}NO_3$	536.5043	536.5037	-1.1
F	$C_{34}H_{64}NO_2$	518.4937	518.4956	3.7
G	$C_{34}H_{62}NO$	500.4831	500.4839	1.6
H	$C_{18}H_{34}NO$	280.2640	280.2654	5.0
I	$C_{18}H_{34}N$	264.2691	264.2690	-0.4
J	$C_{18}H_{32}N$	262.2535	262.2543	3.1
K	$C_{16}H_{34}NO$	256.2640	256.2632	-3.1

In Figure 4.3 peak A corresponds to the molecular ion and peak B the dehydrated molecular ion. Peaks B, C, D and F are each separated by 162 Da

($C_6H_{10}O_5$) corresponding to the consecutive loss of the three sugar units (galactose, galactose, glucose) to generate the dehydrated ceramide (peak F). This fragmentation profile was also observed for all the other fragmentation spectra shown in Figures 4.4 – 4.6, and will thus not be further described. The fragment corresponding to the ceramide (peak E) in Figure 4.3 then undergoes two consecutive dehydrations to generate peaks F and G. Peak H corresponds to the sphingosine with an extra double bond (d18:2). Unfortunately, the sensitivity was not sufficient enough to allow the observation of the d18;1 sphingosine. In the mass spectrum, the presence of the two structural isomers is revealed by peaks J and I. These peaks separated by 2 Da, correspond respectively to dehydrated sphingosine with one extra double bond (d18:2-H_2O) and regular dehydrated sphingosine (d18:1-H_2O). Peak K corresponds to the saturated C16:0 fatty acid which is the counterpart of sphingosine with an extra double bond (d18:2). However, the sensitivity was not sufficient to observe the fatty acid with the extra double bond (C16:1), the counterpart of regular sphingosine (d18:1).

The S-plot also revealed two biomarkers belonging to category 4, corresponding to Gb_3 isoforms with two extra double bonds. The first (point p in Figure 4.2B) was previously observed in urine (Auray-Blais and Boutin 2012) and corresponds to the mixture of two structural isomers: one with one extra double bond on the sphingosine and one extra double bond on the fatty acid (Gb_3(d18:2)(C24:1)), and the other with both extra double bonds on the fatty acid (Gb_3(d18:1)(C24:2)). One Gb_3 isoform with two extra double bonds and a C22 fatty acid was observed in plasma during this study but had not previously been detected in urine (point 3 in Figure 4.2B), the fragmentation profile of

which is shown in Figure 4.4 and the exact mass and empirical formulas of each detected peak are shown in Table 4.3.

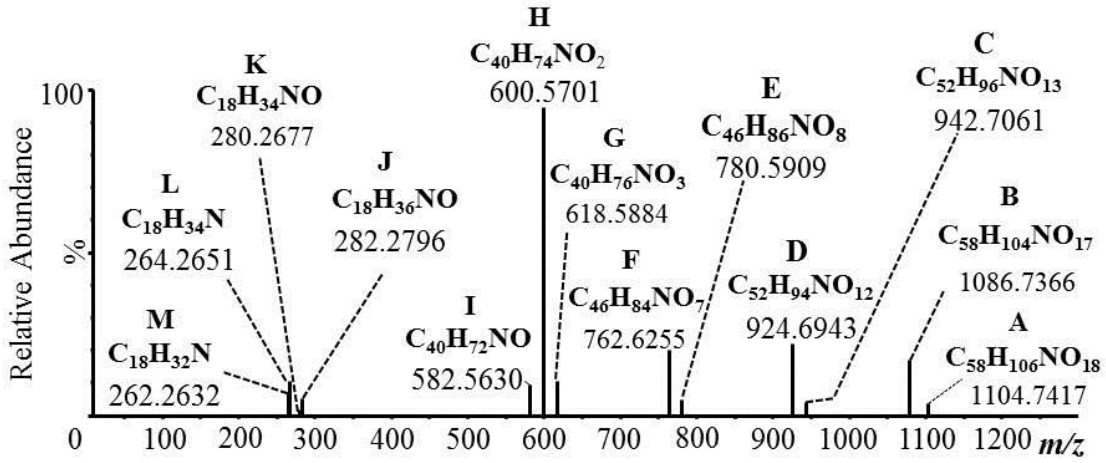

Figure 4.4 ESI-QToF-MS fragmentation spectra of Gb_3(d18:1)(C22:2) + Gb_3(d18:2)(C22:0)

Table 4.3 Exact mass and empirical formula of Gb_3(d18:1)(C22:2) + Gb_3(d18:2)(C22:0). Fragments observed in Figure 4.4.

Fragment	Formula	Calculated Mass Da	Measured Mass Da	Δ Mass ppm
A	$C_{58}H_{106}NO_{18}$	1104.7410	1104.7417	0.6
B	$C_{58}H_{104}NO_{17}$	1086.7366	1086.7366	0.0
C	$C_{52}H_{96}NO_{13}$	942.6882	942.7061	19.0
D	$C_{52}H_{94}NO_{12}$	924.6776	924.6943	18.1
E	$C_{46}H_{86}NO_8$	780.6353	780.5909	-56.9
F	$C_{46}H_{84}NO_7$	762.6248	762.6255	0.9
G	$C_{40}H_{76}NO_3$	618.5825	618.5884	9.5
H	$C_{40}H_{74}NO_2$	600.5720	600.5701	-3.2
I	$C_{40}H_{72}NO$	582.5614	582.5630	2.7
J	$C_{18}H_{36}NO$	282.2797	282.2796	-0.4
K	$C_{18}H_{34}NO$	280.2640	280.2677	13.2
L	$C_{18}H_{34}N$	264.2691	264.2651	-15.1
M	$C_{18}H_{32}N$	262.2535	262.2632	37.0

Peaks J and K in Figure 4.4 correspond to regular sphingosine (d18:1) and to sphingosine with one extra double bond (d18:2), respectively. Peaks L and M correspond to their dehydrated counterparts (d18:1-H_2O and d18:2-H_2O, respectively). Unfortunately the mass spectrum was not sufficiently sensitive to observe the peaks corresponding to the mono- and di-unsaturated fatty acid. However, the mass difference between the ceramide fragment (peak G) and the sphingosine fragments (d18:2) (peak K) and (d18:1) (peak J) allows the calculation of their fatty acid counterparts (C22:1) and (C22:2), respectively.

Figure 4.5 shows the fragmentation profile and Table 4.4 displays the exact mass and empirical formula of the peaks obtained for the biomarker (point 4, Figure 4.2B) which corresponds to a mixture of two structural isomers: the first with a d16:1 sphingosine and a C16:0 fatty acid (Gb_3(d16:1)(C16:0)) and the other with a d18:1 sphingosine and a C14:0 fatty acid (Gb_3(d18:1)(C14:0)). These two isomeric biomarkers were considered as a short chain Gb_3-related analog/isoform (Category 6).

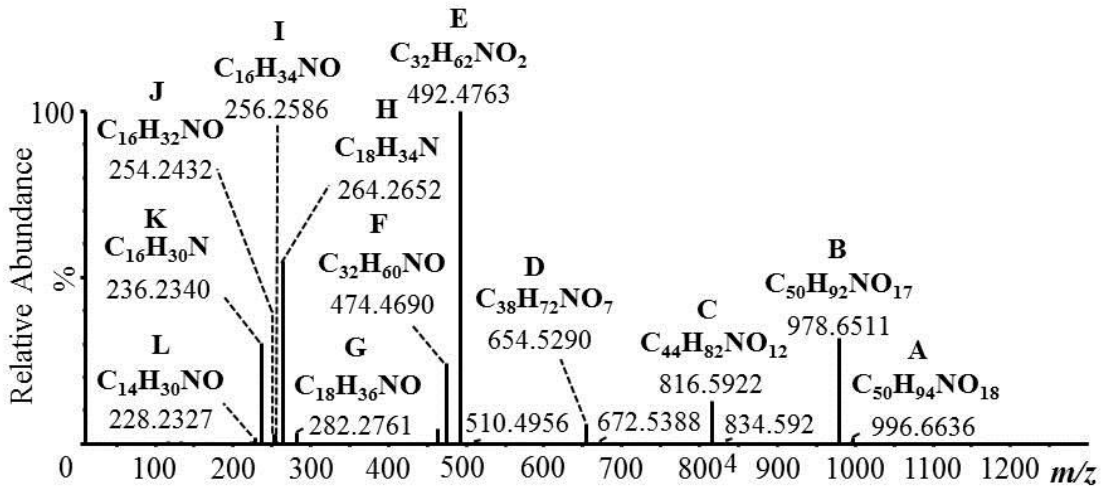

Figure 4.5 ESI-QToF-MS fragmentation spectra of Gb_3(d16:1)(C16:0) + Gb_3(d18:1)(C14:0).

Table 4.4 Exact mass and empirical formula of Gb_3(d16:1)(C16:0) + Gb_3(d18:1)(C14:0). Fragments observed in Figure 4.5.

Fragment	Formula	Calculated Mass Da	Measured Mass Da	Δ Mass ppm
A	$C_{50}H_{94}NO_{18}$	996.6741	996.6636	-16.6
B	$C_{50}H_{92}NO_{17}$	978.6365	978.6511	14.9
C	$C_{44}H_{82}NO_{12}$	816.5837	816.5922	10.4
D	$C_{38}H_{72}NO_7$	654.5309	654.5290	-2.9
E	$C_{32}H_{62}NO_2$	492.4781	492.4763	-3.7
F	$C_{32}H_{60}NO$	474.4675	474.4690	3.2
G	$C_{18}H_{36}NO$	282.2797	282.2761	-12.8
H	$C_{18}H_{34}N$	264.2691	264.2652	-14.8
I	$C_{16}H_{34}NO$	256.2640	256.2586	-21.1
J	$C_{16}H_{32}NO$	254.2484	254.2432	-20.5
K	$C_{16}H_{30}N$	236.2378	236.2340	-16.1
L	$C_{14}H_{30}NO$	228.2327	228.2358	13.6

In Figure 4.5 peaks I, J and K correspond to the fatty acid fragment (C16:0), the sphingosine fragment (d16:1) and the dehydrated sphingosine fragment (d16:1-H_2O) of Gb_3(d16:1)(C16:0), respectively. The peaks G, H and L correspond to the sphingosine fragment (d18:1), the dehydrated sphingosine fragment (d18:1-H_2O), and the fatty acid fragment (C14:0) of Gb_3(d18:1)(C14:0), respectively.

The Gb_3(d16:1)(C16:0) analog shown in Figure 4.5 is also present in its methylated form. This biomarker is thus classified as a methylated short chain Gb_3-related isoform/analog and falls into category 7. The Gb_3(d16:1)(C16:0)Me fragmentation spectrum is shown in Figure 4.6 and the exact mass and empirical formulas of those peaks detected are shown in Table 4.5.

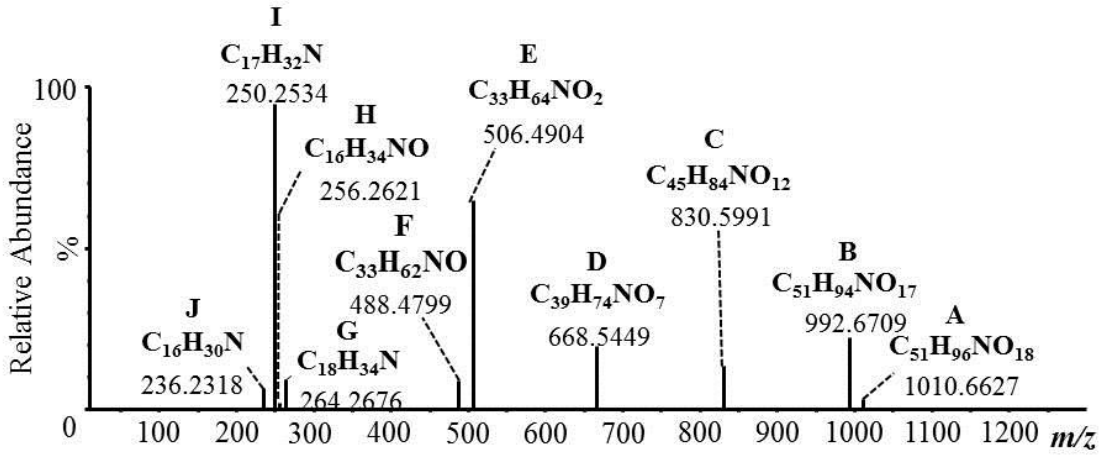

Figure 4.6 ESI-QToF-MS fragmentation spectra of Gb_3(d16:1)(C16:0)Me + Gb_3(d18:1)(C14:0)Me

Table 4.5 Exact mass and empirical formula of Gb_3(d16:1)(C16:1)Me + Gb_3(d18:1)(C14:0)Me. Fragments observed in Figure 4.6.

Fragment	Formula	Calculated Mass Da	Measured Mass Da	Δ Mass ppm
A	$C_{51}H_{96}NO_{18}$	1010.6833	1010.6627	-20.4
B	$C_{51}H_{94}NO_{17}$	992.6522	992.6709	18.8
C	$C_{45}H_{84}NO_{12}$	830.5994	830.5991	-0.4
D	$C_{39}H_{74}NO_7$	668.5465	668.5449	-2.4
E	$C_{33}H_{64}NO_2$	506.4937	506.4904	-6.5
F	$C_{33}H_{62}NO$	488.4831	488.4799	-6.6
G	$C_{18}H_{34}N$	264.2691	264.2676	-5.7
H	$C_{16}H_{34}NO$	256.2640	256.2621	-7.4
I	$C_{17}H_{32}N$	250.2535	250.2534	-0.4
J	$C_{16}H_{30}N$	236.2378	236.2318	-25.4

Peak I of Figure 4.6 corresponds to dehydrated methylated sphingosine (d16:1)Me-H_2O) which loses its methyl group to generate the d16:1-H_2O sphingosine (peak J), peak H corresponds to the C16:0 fatty acid fragment. The

peak at *m/z* 264.2746 is not attributed to the Gb_3(d16:1)(C16:0)Me biomarker. It probably arises from another structural isomer. However, no other fragments from that molecule are present on the spectrum preventing the elucidation of its structure.

4.2.7 Gb_3-related metabolites present in plasma from untreated Fabry females

Following the identification of Gb_3-related analogs and isoforms in plasma from untreated Fabry males, the levels of these biomarkers were assessed in ten untreated Fabry females. Identification and relative area counts of all Gb_3-related analogs and isoforms were obtained using QuanLynx™. A summary of the data obtained is shown in Table 4.6. Of the Gb_3-related analogs/isoforms previously detected in urine from untreated Fabry males, six were not detectable in plasma from untreated Fabry females. Of these two, Gb_3(d18:1)(C18:0)Me and Gb_3(d18:1)(C26:1) + Gb_3(d18:2)(C26:0) were also undetectable in plasma from untreated Fabry males. All five of the newly identified Gb_3-related isoforms/analogs detected in this study in plasma from untreated Fabry males were also identified in plasma from Fabry females. Four of these showed statistically significant elevations in excretion ($p < 0.05$) compared to an age- and sex-matched control group. One, Gb_3(d16:1)(C16:0) + Gb_3(d18:1)(C14:0) which showed the lowest levels of excretion was the only analog not found to be statistically and significantly elevated compared to the control group. AUC data were also calculated for each Gb_3-related analog and isoform resulting in values ranging from 0.633 to 0.883.

Table 4.6 Retention time and relative abundance of the biomarkers in plasma from untreated Fabry females and healthy control females. Those biomarkers depicted in bold are novel biomarkers detected in this study. AUC: Area under the ROC curve for plasma. nd: not detectable; na: not applicable.

Category	**Biomarkers**	**Retention time (min)**	**Fabry females mean (min-max)**	**Control females mean (min-max)**	**AUC**	***t*-test**
		Plasma	Plasma [Area]	Plasma [Area]	Plasma	Fabry females *vs* female control
1	Gb_3(d18:1)(C16:0)	8.8	23.2 (18.1-30.6)	20.8 (16.9-25.0)	0.675	$p < 0.16$
1	Gb_3(d18:1)(C18:0)	9.2	2.9 (2.4-3.7)	2.4 (1.8-2.9)	0.800	$p < 0.007$
1	Gb_3(d18:1)(C20:0)	9.7	2.3 (1.7-3.6)	1.7 (1.2-2.5)	0.758	$p < 0.02$
1	Gb_3(d18:1)(C22:0)	10.1	2.5 (1.7-4.5)	2.1 (1.5-2.8)	0.633	$p < 0.15$
1	Gb_3(d18:1)(C24:0)	10.4	2.6 (1.8-3.9)	2.1 (1.5-3.1)	0.750	$p < 0.06$
1	Gb_3(d18:1)(C26:0)	10.7	nd	nd	na	na
2	Gb_3(d18:1)(C16:0)Me	9.0	nd	nd	na	na
2	Gb_3(d18:1)(C18:0)Me	9.5	nd	nd	na	na
2	Gb_3(d18:1)(C20:0)Me	9.9	0.5 (0.2-0.9)	0.3 (nd-0.6)	0.742	$p < 0.02$
2	Gb_3(d18:1)(C22:1)Me	9.9	nd	nd	na	na
2	Gb_3(d18:1)(C22:0)Me	10.3	1.6 (1.0-3.6)	0.1 (0.8-1.4)	0.783	$p < 0.04$
2	Gb_3(d18:1)(C24:1)Me	10.2	nd	nd	na	na

2	Gb_3(d18:1)(C24:0)Me	10.5	0.4 (0.1-1.1)	0.1 (nd-0.4)	0.850	$p < 0.01$
3	**Gb_3(d18:1)(C16:1) + Gb_3(d18:2)(C16:0)**	**8.4**	**5.2 (2.9-14.6)**	**2.9 (1.6-4.7)**	**0.858**	***p* < 0.05**
3	**Gb_3(d18:1)(C18:1) + Gb_3(d18:2)(C18:0)**	**8.9**	**1.5 (0.8-3.0)**	**0.9 (0.6-1.1)**	**0.883**	***p* < 0.01**
3	Gb_3(d18:1)(C20:1) + Gb_3(d18:2)(C20:0)	9.4	1.8 (1.3-2.9)	1.4 (0.9-2.2)	0.792	$p < 0.03$
3	Gb_3(d18:1)(C22:1) + Gb_3(d18:2)(C22:0)	9.8	6.1 (4.3-8.9)	4.1 (3.0-5.8)	0.875	$p < 0.003$
3	Gb_3(d18:1)(C24:1) + Gb_3(d18:2)(C24:0)	10.1	3.9 (2.4-8.3)	2.7 (1.9-4.0)	0.742	$p < 0.07$
3	Gb_3(d18:1)(C26:1) + Gb_3(d18:2)(C26:0)	10.5	nd	nd	na	na
4	Gb_3(d18:0)(C24:1)H_2O	9.9	0.7 (0.4-1.3)	0.5 (0.3-0.7)	0.717	$p < 0.06$
5	**Gb_3(d18:1)(C22:2) + Gb_3(d18:2)(C22:1)**	**9.5**	**0.6 (0.3-1.1)**	**0.4 (0.1-0.6)**	**0.817**	***p* < 0.01**
5	Gb_3(d18:1)(C24:2) + Gb_3(d18:2)(C24:1)	9.9	1.0 (0.3-1.1)	4.2 (3.0-6.4)	0.817	$p < 0.01$
6	**Gb_3(d16:1)(C16:0) + Gb_3(d18:1)(C14:0)**	**8.3**	**1.3 (0.5-3.2)**	**0.9 (0.6-1.3)**	**0.650**	***p* < 0.14**
7	**Gb_3(d16:1)(C16:0)Me + Gb_3(d18:1)(C14:0)Me**	**8.5**	**1.2 (0.5-2.9)**	**0.7 (nd-1.2)**	**0.758**	***p* < 0.04**
-	Not yet identified (*m/z* 1042.74)	8.5	0.3 (nd-0.5)	0.2 (0.1-0.4)	0.717	$p < 0.15$
-	Not yet identified (m/z 1018.64)	8.3	0.9 (0.5-1.4)	0.7 (0.3-1.2)	0.758	$p < 0.06$

4.3 Discussion

Using a mass-spectrometry based metabolomic methodology 14,514 markers were detected from the plasma of twelve untreated Fabry males and eight age- and sex-matched healthy controls. The creation of an OPLS-DA score plot demonstrated that one male Fabry patient (Patient 12, Table 2.3) fell outside the Hotelling T^2 ellipse, this patient was thus considered an outlier and excluded from the multivariate statistical analysis. This patient displayed both low urinary Gb_3 and lyso-Gb_3 excretion (Table 2.3) therefore, low Gb_3-related biomarker excretion would be expected. Further statistical analyses of this data set revealed a goodness of fit value approaching unity (R^2 = 0.815). However, the predicted variation value obtained (Q2 = 0.383) was low compared to the goodness of fit which may be due to the presence of some extreme values within the data set.

Of the potential biomarkers of interest identified by the S-plot (Figure 4.2), the majority had previously been identified in the urine of Fabry patients (Auray-Blais and Boutin 2012). However, seven potential new biomarkers were also detected and following structural elucidation and characterisation, five were found to be Gb_3-related analogs/isoforms and assigned to one of seven categories.

All biomarkers within category 1 had been identified previously in urine. However, the excretion profiles observed for these saturated Gb_3 isoforms differs significantly between urine and plasma. The saturated Gb_3 isoform Gb_3(d18:1)(C16:0) was the most highly excreted in plasma, from both males and females with Fabry disease, compared to the excretion of all other Gb_3 isoforms with saturated fatty acids. This differs from the urinary Gb_3 profile of Fabry patients where Gb_3(d18:1)(C22:0) and Gb_3(d18:1)(C24:0) are the most

highly excreted. The excretion of all saturated Gb_3 isoforms in plasma from Fabry males was shown to be statistically and significantly elevated compared to an age- and sex-matched control group. However, in Fabry females, only the excretion of the saturated Gb_3 isoforms Gb_3(d18:1)(C18:0) and Gb_3(d18:1)(C20:0) reached statistical significance. Differences in excretion profiles in Fabry patients have previously been described and the findings in this study are in accordance with the literature (Kitagawa *et al.*, 2005).

In category 2, the levels of excretion of the methylated Gb_3-related isoforms are statistically and significantly elevated in urine from Fabry males compared to the excretion levels detected in plasma from Fabry males, for all but the Gb_3(d18:1)(C22:1)Me isoform. However, the excretion profiles observed for the two biological matrices are similar. The extent of methylation observed in plasma from both Fabry males and females was greatest for the isoform Gb_3(d18:1)(C22:0)Me, the same as that observed in urine (Auray-Blais and Boutin 2012). The least amount of methylation in plasma from Fabry males was observed for the Gb_3(d18:1)(C16:0)Me isoform, with no detectable levels of excretion for this isoform in Fabry females, however, this is the most excreted saturated Gb_3 isoform in both males and females in category 1. This shows that the level of methylated Gb_3 is not proportional to the level of its un-methylated counterpart. No detectable levels of excretion were observed in plasma from Fabry males or females for the methylated Gb_3-related isoform Gb_3(d18:1)(C18:0)Me, which also displayed the lowest levels of excretion in urine (Auray-Blais and Boutin 2012). In addition, no detectable levels of excretion were observed in plasma from Fabry females for Gb_3(d18:1)(C22:1) or Gb_3(d18:1)(C24:1).

Two new biomarkers detected in this study, Gb_3(d18:1)(C16:1) + Gb_3(d18:2)(C16:0) and Gb_3(d18:1)(C18:1) + Gb_3(d18:2)(C18:0), which were not previously identified in urine were assigned to category 3. One of these structural isomer mixtures, Gb_3(d18:1)(C16:1) + Gb_3(d18:2)(C16:0) was among the most highly excreted in this category as well as the structural isomer mixtures, Gb_3(d18:1)(C22:1) + Gb_3(d18:2)(C22:0) and Gb_3(d18:1)(C24:1) + Gb_3(d18:2)(C24:0), the latter of which was also the most highly excreted in urine. The structural isomer mixture Gb_3(d18:1)(C26:1) + Gb_3(d18:2)(C26:0) showed the lowest levels of excretion in plasma from Fabry males whilst it was undetectable in Fabry females. This differs to findings in urine where Gb_3(d18:1)(C20:1) + Gb_3(d18:2)(C22:0) showed the least amount of excretion.

In category 4, the Gb_3 hydrated at the sphingosine level, Gb_3(d18:0)(C24:1)H_2O, identified previously and which showed moderate excretion in urine, showed similar levels of excretion in plasma from Fabry males whilst lower levels of excretion were observed in plasma from Fabry females. This biomarker was shown to be statistically elevated in plasma from Fabry males ($p < 0.0001$) compared to an age- and sex-matched control group however, levels in Fabry females failed to reach statistical significance ($p < 0.06$).

Another biomarker detected during this study which comprised a mixture of isoforms with two double bonds, Gb_3(d18:1)(C22:2) + Gb_3(d18:2)(C22:1), was added to category 5. Although this biomarker displayed low levels of excretion in plasma from both male and female Fabry patients, levels were statistically and significantly elevated above their respective age- and sex-matched control groups. It was however, the other biomarker in this category, Gb_3(d18:1)(C24:2)

+ Gb_3(d18:2)(C24:1), that had been previously identified in urine which displayed the highest levels of excretion in plasma.

The identification during this study of two new biomarkers, Gb_3(d16:1)(C16:0) + Gb_3(d18:1)(C14:0) and its methylated counterpart, required the creation of two additional categories, category 6) short chain Gb_3-related isoforms/analogs and category 7) short chain methylated Gb_3-related isoforms/analogs. Whilst previous studies have demonstrated the presence of lyso-Gb_3 with d16:1 sphingosine in the urine (Auray-Blais *et al.*, 2012) and plasma (Dupont *et al.*, 2013) of Fabry patients this is the first study to report a Gb_3 analog with a d16:1 sphingosine moiety. Gb_3 analogs with a d16:1 sphingosine moiety or a C14:0 fatty acid were not detected in the urine of Fabry patients (Auray-Blais and Boutin 2012). In the case of the structural isomer mixture Gb_3(d16:1)(C16:0) + Gb_3(d18:1)(C14:0), the Gb_3(d16:1)(C16:0) isomer becomes significantly more abundant compared to Gb_3(d18:1)(C14:0) due to the fact that the C16:0 fatty acid was found to be considerably more abundant than the C14:0 fatty acid.

The short chain methylated Gb_3-related analog/isoform, Gb_3(d16:1)(C16:0)Me + Gb_3(d18:1)(C14:0)Me was also detected during this study. Although the fragmentation spectra generated was limited, confirmation of the structure of this biomarker was obtained due to the fact that in nature, an even number of carbons are present in the fatty acid backbone and therefore in the sphingosine backbone, which is constructed from fatty acids. Owing to this, the presence of the methylation was additionally confirmed by the detection of the methylated ceramide fragment containing an odd number of carbons in its empirical formula ($C_{33}H_{64}NO_2$).

Whilst the Gb_3 analog with a d16:1 sphingosine moiety was only found to be significantly elevated in the plasma of Fabry males, its methylated counterpart

was statistically and significantly elevated in the plasma of both male (p < 0.0001) and female (p < 0.04) Fabry patients compared to their respective control groups.

Area under the curve (AUC) values were obtained for each of the Gb_3-related analogs and isoforms in both untreated Fabry males and females. An AUC of 1 indicates complete discrimination between patients and controls whereas 0.5 indicates no discrimination. Complete discrimination was observed for the majority of biomarkers detected in the untreated Fabry males. Only one biomarker, Gb_3(d18:1)(C22:2) + Gb_3(d18:2)(C22:1), displayed an AUC value of less than 1 (AUC = 0.989). The AUC values obtained for the Gb_3-related analogs and isoforms in Fabry females showed a more variable discrimination with complete discrimination between patients and controls unachievable in any of the biomarkers (AUC values ranging from 0.633 to 0.883). This variability further confirms that women are often less severely affected than their male counterparts.

4.4 Conclusion

This metabolomic study has used time-of-flight mass spectrometry focusing on Gb_3 isoforms/analogues with *m/z* ratios between 995 and 1200 Da to identify new and existing biomarkers in the plasma of Fabry disease patients. Seventeen biomarkers revealed by the S-plot were isoforms/analogues of Gb_3 that had been previously detected in the urine of Fabry patients (Auray-Blais and Boutin 2012). This enabled relative concentrations of these biomarkers in plasma to be obtained and statistical analyses performed. Statistical and significant elevations in the excretion of all of these biomarkers were observed in the plasma of treatment naïve male Fabry disease patients compared to an age- and sex-matched control group. In addition, significant differences in the levels of excretion of these biomarkers between the biological matrices, urine and plasma, are apparent.

Five novel biomarkers were also identified and characterised as analogues/isoforms of Gb_3. Three of these new biomarkers correspond to Gb_3 having an extra double bond on the sphingosine chain (d18:2) with C16:0, C18:0 and C22:1 fatty acids. The fourth biomarker corresponds to a mixture of two structural isomers, the first with a d16:1 sphingosine and a C16:0 fatty acid and the second with a d18:1 sphingosine and a C14:0 fatty acid. This is the first time that a Gb_3 analogue with a d16:1 sphingosine moiety has been reported. In addition, this Gb_3 analogue was also present in its methylated form. Further studies are needed in order to better understand the underlying metabolic process occurring in Fabry patients. However, considering the presence and also the important variation in the relative quantification of these biomarkers in plasma compared to urine, assessment and monitoring could provide further insights than measurement of Gb_3 and/or lyso-Gb_3 alone.

Chapter 5

Investigation of globotriaosylceramide and globotriaosylsphingosine toxicity in the Fabry mouse model

Chapter 5 - Investigation of globotriaosylceramide and globotriaosylsphingosine toxicity in the Fabry mouse model 250

5.0 Investigation of globotriaosylceramide (Gb_3) and globotriaosyl-sphingosine (lyso-Gb_3) toxicity in the Fabry mouse model

5.1 Introduction

In the study described in Chapter 4, a number of new and existing Gb_3-related biomarkers were identified in the plasma of Fabry disease patients using a metabolomic methodology. In Fabry disease a deficiency of the enzyme α-galactosidase A (α-GAL) results in the accumulation of Gb_3 as the primary metabolite. However, in a number of patients the level of stored Gb_3 does not always correlate with the presenting clinical symptoms (Mills *et al.*, 2004; Linhart 2006). Therefore, this study aimed to identify proteins which interact with Gb_3 in order to gain a better understanding of the underlying disease mechanisms associated with disease pathology.

Authentic animal models are required for studies to enable progression in our understanding of the underlying pathological mechanisms associated with Fabry disease that, for ethical and practical reasons, are not able to be completed in humans. In nature, lysosomal storage disorders are known to occur in both dogs and cats, inherited in an autosomal recessive manner, as they are in humans. However, to date no large animal model for Fabry disease has been discovered (Haskins, Giger and Patterson 2006). This has resulted in the development of a knockout mouse model for Fabry disease which displays a complete lack of α-GAL activity (Ohshima *et al.*, 1997). However, in contrast to the painful small-fibre peripheral neuropathy, renal, cerebral and cardiovascular dysfunction that are experienced in humans as a result of the absence of α-GAL, Fabry knockout mice appear clinically normal and have a normal adult lifespan (Ohshima *et al.*, 1997; Ohshima *et al.*, 1999). Studies

have however, demonstrated an accumulation of Gb_3 and lyso-Gb_3 in the urine, plasma and tissues of these mice (Ohshima *et al.*, 1997; Ohshima *et al.*, 1999; Ioannou *et al.*, 2001; Shiozuka *et al.*, 2011; Durant *et al.*, 2011). In addition, lamellar inclusions have been observed in the lysosomes of Kupffer cells and also hepatocytes of affected mice. Increased numbers of lamellar bodies within proximal and distal tubular cells, as well as within glomerular epithelial cells and peripheral tubular capillary endothelial cells have also been reported (Haskins, Giger, and Patterson 2006).

In the present study, a label-free proteomic methodology was used to create a proteomic profile of Fabry mice tissues (liver, kidney, heart and brain). Data obtained during the label-free study was analysed, using two different software platforms, and a number of proteins that were identified as altered by both analysis methods were selected for further investigation. Protein interactions with molecules in the glycosphingolipid biosynthetic pathway and with particular interest on Gb_3 were also investigated. The results of this aspect of the study led to the assessment of touch thresholds in mice following exposure to Gb_3 and lyso-Gb_3. In addition, the effect of glycosphingolipids and their deacylated counterparts on ATP synthase activity has been investigated.

5.2 Results

5.2.1 Gb_3 and lyso-Gb_3 analyses in the tissues of a Fabry mouse model

Gb_3 and lyso-Gb_3 analyses were performed on all male, female and control mouse tissue samples (liver, kidney, heart and brain) as described in Section 2.2.1. Both Gb_3 (Figure 5.1) and lyso-Gb_3 (Figure 5.2) concentrations were found to be significantly elevated ($p < 0.05$) in all tissue types compared to their respective control group.

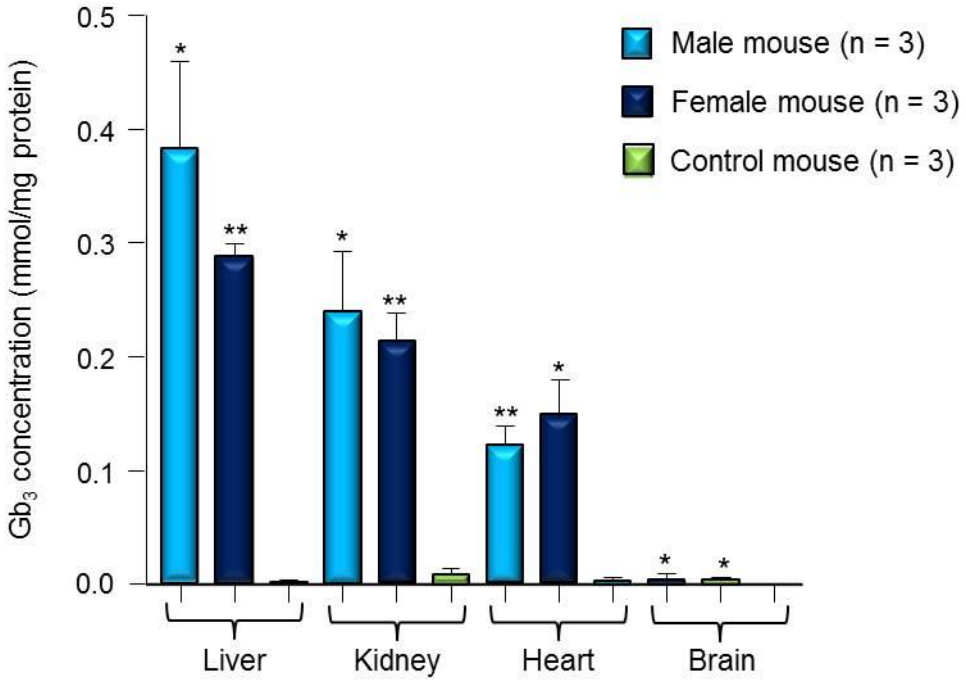

Figure 5.1 Globotriaosylceramide (Gb_3) concentrations in male, female and control mouse, liver, kidney, heart and brain tissue. Data expressed as mean ± SD. * $p < 0.05$; ** $p < 0.01$.

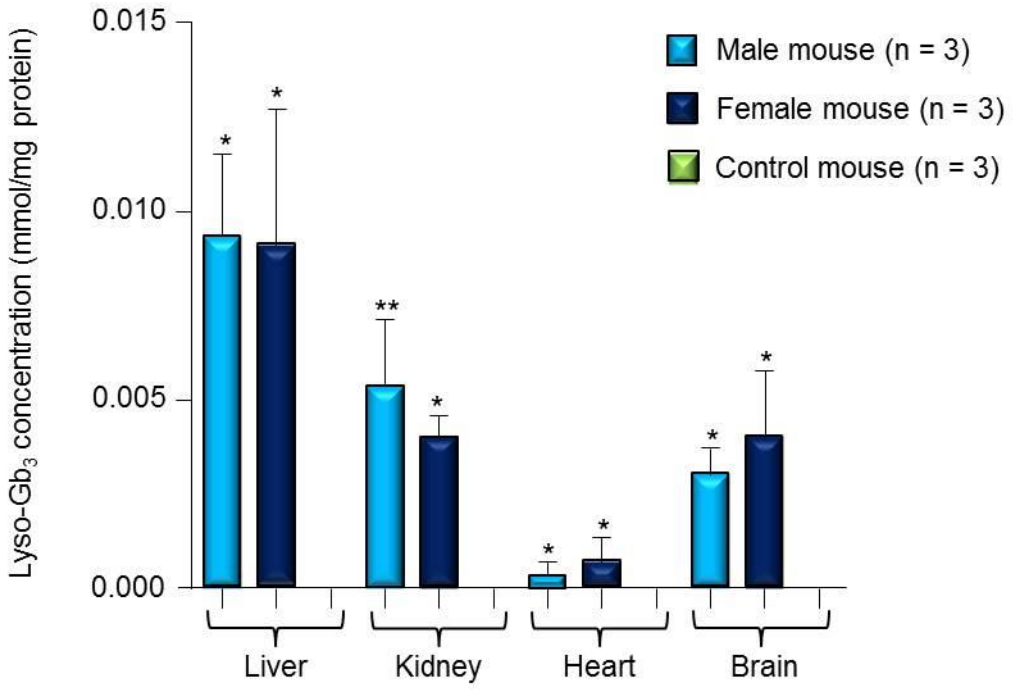

Figure 5.2 Globotriaosylsphingosine (lyso-Gb_3) concentrations in male, female and control mouse, liver, kidney, heart and brain tissue. Data expressed as mean ± SD. * $p < 0.05$; ** $p < 0.01$.

5.2.2 Proteomic profiling of tissues from a Fabry mouse model

The liver, kidney, heart and brain of three Fabry mice were homogenised as described in section 2.2.7.1.1. In order to reduce biological variation, homogenised tissue samples were pooled and subsequently fractionated to achieve the highest possible proteome coverage (see section 2.2.7.1.2). A MS^E label-free quantitative proteomic methodology using UPLC-QToF-MS (section 2.2.5.6) was used to analyse all tissue fractions and data acquired was processed by ProteinLynx Global Server version 2.4 (ProteinLynx; Waters Corp.) as described in section 2.2.7.1.3. Using this methodology a total of 5280 proteins were detected in Fabry and/or control mouse tissues. In addition, the data was also analysed using Progenesis LC-MS (Nonlinear Dynamics, Waters

Corp.), a data analysis program which identifies and quantifies peptides and proteins detected in label-free analyses based on ion abundance (see section 2.2.7.1.3). This software uses a ‘quantify-then-identify’ approach which promotes identification of low abundance proteins. Using this technique 3950 proteins were identified in the tissues from Fabry and/or control mice. Differences between groups were assessed by identifying fold changes greater than two.

5.2.2.1 Analysis of liver tissues from a Fabry mouse model

Data analysis with ProteinLynx identified a total of 1060 proteins in liver tissues from Fabry and/or control mice. Twenty-three of the 1060 proteins detected were found to have a greater than two-fold alteration in both male and female Fabry mice compared to levels observed in the control group (Table 5.1). Of these 23 proteins, 7 were found to have levels greater than two-fold increased and 16 proteins were found to have levels greater than two-fold decreased.

The levels of 1037 of the 1060 proteins detected using ProteinLynx displayed no fold change alterations between both the male and female Fabry and control mice groups.

Table 5.1 Proteins detected as altered by a fold change greater than two in liver tissues of male and female Fabry mice by ProteinLynx. FM = Fabry mice

Description	**Control** fmol/mg protein	**Male FM** fmol/mg protein	**Fold change**	**Female FM** fmol/mg protein	**Fold change**	**↑ or ↓**
28S ribosomal protein S10, mitochondrial	1.3	0.0	Infinity	0.0	Infinity	↓
60S acidic ribosomal protein P2	5.6	0.0	Infinity	0.0	Infinity	↓
Agmatinase, mitochondrial	193.9	34.0	5.71	19.5	10.0	↓
Alcohol dehydrogenase 1	137.5	0.0	Infinity	0.0	Infinity	↓
Aldehyde dehydrogenase family 8 member A1	227.0	0.0	Infinity	30.9	7.3	↓
Arginase-1	18.3	715.8	39.11	219.7	12.0	↑
Aspartate aminotransferase, mitochondrial	0.0	92.0	Infinity	51.9	Infinity	↑
ATP-binding cassette sub-family D member 3	13.6	6.7	2.03	0.0	Infinity	↑
ATP synthase subunit beta, mitochondrial	0.0	63.3	Infinity	40.5	Infinity	↑
Cbp/p300-interacting transactivator 4	2.4	0.0	Infinity	0.0	Infinity	↓
Coiled-coil domain-containing protein 45	26.8	0.0	Infinity	0.0	Infinity	↓
Fructose-1, 6-bisphosphatase 1	126.0	0.0	Infinity	0.0	Infinity	↓
Fumarylacetoacetase	0.0	37.0	Infinity	104.1	Infinity	↑
Glutamate dehydrogenase1, mitochondrial	0.0	7.6	Infinity	8.8	Infinity	↑
Glyceraldehyde-3-phosphate dehydrogenase	32.3	0.0	Infinity	9.7	3.3	↓
Kinesin-1 heavy chain	1.7	0.0	Infinity	0.0	Infinity	↓
NADH dehydrogenase [ubiquinone] flavoprotein 1, mitochondrial	171.0	0.0	Infinity	0.0	Infinity	↓
Ornithine aminotransferase, mitochondrial	0.0	97.6	Infinity	12.8	Infinity	↑
Pyruvate dehydrogenase protein X component, mitochondrial	7.8	0.0	Infinity	0.0	Infinity	↓
Ribonuclease UK114	10.6	205.4	19.41	137.8	13.0	↑
Ribosomal protein, large, P0	10.9	0.0	Infinity	0.0	Infinity	↓
S-adenosylmethionine synthetase isoform type-1	28.2	0.0	Infinity	0.0	Infinity	↓
Ubiquitin subunit 1	10.4	0.0	Infinity	0.0	Infinity	↓

When data were analysed using the Progenesis LC-MS software a total of 720 proteins were detected in liver tissue from Fabry and/or control mice. Of the 720 proteins detected, 9 were found to have greater that two-fold alterations in the average normalised abundance detected in both male and female Fabry mice, compared to those levels detected for the control group (Table 5.2). Of the 9 proteins found to be altered in both male and female Fabry mice, a greater than two-fold elevation was detected in 4 proteins and a greater than two-fold reduction was detected in 5 proteins.

The average normalised abundance of 711 of the 720 proteins detected by Progenesis LC-MS did not display fold change alterations between both the male and female Fabry and control mice groups.

Table 5.2 Proteins detected as altered by a fold change greater than two in liver tissues of male and female Fabry mice by Progenesis LC-MS. FM = Fabry mice; ANA = Average normalised abundance

Description	**Control** ANA	**Male FM** ANA	**Fold change**	**Female FM** ANA	**Fold change**	**↑ or ↓**
Agmatinase, mitochondrial	3069.9	1240.4	2.5	1036.2	3.0	↓
ATP synthase subunit beta, mitochondrial	3315.2	6989.6	2.1	7388.7	2.2	↑
Calcium-binding mitochondrial carrier protein Aralar2	63.2	0.0	Infinity	0.5	131.8	↓
Catalase	347.7	1133.0	3.3	2131.0	6.1	↑
Elongation factor 1-alpha 1	630.1	0.0	Infinity	8.8	71.8	↓
Inositol polyphosphate 5-phosphatase K	1159.8	215.6	5.4	250.7	4.6	↓
L-lactate dehydrogenase A chain	24.8	49.8	2.0	241.2	9.7	↑
Mitofusin-1	87.2	25.0	3.5	0.0	Infinity	↓
Ribonuclease UK114	7985.8	17100.0	2.1	16600.0	2.1	↑

When results obtained from liver tissues using ProteinLynx and Progenesis LC-MS were cross referenced 3 proteins were confirmed by both analysis methods as showing fold change alterations. Of these 3 proteins, ATP synthase subunit beta (mitochondrial) and ribonuclease UK114, were detected to have greater than two-fold increases in both male and female Fabry mice compared to that of the control group (Figure 5.3). ATP synthase subunit beta (mitochondrial), which together with the alpha subunit forms the catalytic core in the F_1 portion of ATP synthase (Figure 5.23), was not detected in control tissue by the ProteinLynx software but was detected in both male and female Fabry mice. Using Progenesis LC-MS this protein was detected to be increased 2.1-fold and 2.2-fold in male and female Fabry mice liver tissues, respectively. Ribonuclease UK114 is an endoribonuclease responsible for inhibiting translation by cleaving mRNA and this protein was also found to be increased by both analysis methods. Using ProteinLynx increases of 19.4-fold in male and 13.0-fold in female Fabry mice were detected. Using Progenesis-LC/MS the same protein was found to be increased in male Fabry mice 2.1-fold with increases of 2.1-fold detected in female Fabry mice.

Agmatinase (mitochondrial), which is responsible for the hydrolysis of agmatine to putrescine and urea, was the only protein found to be decreased in liver tissues of both male and female Fabry mice by both analysis methods. Using ProteinLynx reductions of 5.7-fold in male and 10.0-fold in female Fabry mice were detected. Using Progenesis LC-MS, agmatinase (mitochondrial) was found to be 2.5-fold and 3.0-fold reduced in male and female Fabry mice, respectively.

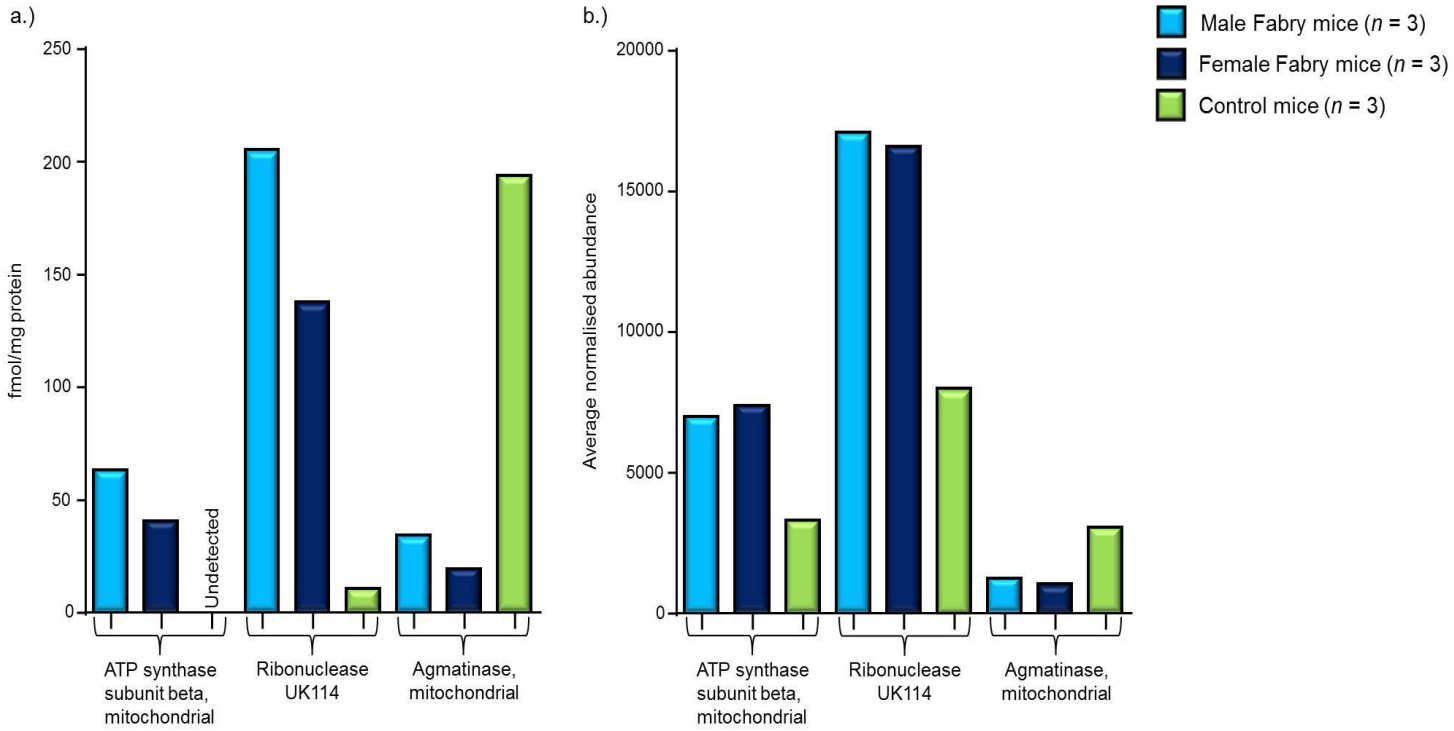

Figure 5.3 Proteins detected as showing a greater than two-fold alteration in pooled liver tissues from both male Fabry mice (*n* = 3) and female Fabry mice (*n* = 3) by a.) ProteinLynx and; b.) Progenesis LC-MS

5.2.2.2 Analysis of kidney tissues from a Fabry mouse model

Data analysis of kidney tissues with ProteinLynx identified a total of 353 proteins in Fabry and/or control mice. Of the 353 proteins detected in kidney tissue, 8 were found to have levels displaying a greater than two-fold alteration in both male and female Fabry mice, compared to levels detected in the control group (Table 5.3). Increases greater than two-fold above levels detected in control mice were detected in 3 proteins, with 5 proteins having levels greater than two-fold decreased below that of the control group.

The levels of 345 of the 353 proteins detected using ProteinLynx displayed no fold change alterations between both the male and female Fabry and control mice groups.

Table 5.3 Proteins detected as altered by a fold change greater than two in kidney tissues of male and female Fabry mice by ProteinLynx. FM = Fabry mice

Description	**Control** fmol/mg protein	**Male FM** fmol/mg protein	**Fold change**	**Female FM** fmol/mg protein	**Fold change**	**↑ or ↓**
ATP synthase subunit beta, mitochondrial	17.9	36.6	2.0	55.6	3.1	↑
Beta-actin FE-3	27.8	59.0	2.1	105.9	3.8	↑
Dyslexia susceptibility 1 candidate gene 1 protein homolog	7.3	0.0	Infinity	0.0	Infinity	↓
Epidermal growth factor receptor	1.1	0.0	Infinity	0.0	Infinity	↓
GRAM domain-containing protein 1B	61.0	0.0	Infinity	0.0	Infinity	↓
Lmo7 protein	38.5	0.0	Infinity	0.0	Infinity	↓
Ribonuclease UK114	11.8	36.4	3.1	44.5	3.8	↑
Serine protease inhibitor A3K	8.0	0.0	Infinity	0.0	Infinity	↓

Following analysis with the Progenesis LC-MS software 171 proteins were detected in kidney tissue from Fabry and/or control mice. Of the 171 proteins detected, 10 were found to have greater than two-fold increases in the average normalised abundance of both male and female Fabry mice compared to those levels observed in the control group (Table 5.4). No protein was found to display a greater than two-fold decrease in both male and female Fabry mice compared to the control group.

The average normalised abundance of 161 of the 171 proteins detected by Progenesis LC-MS did not display fold change alterations between both the male and female Fabry and control mice groups.

Table 5.4 Proteins detected as altered by a fold change greater than two in kidney tissues of male and female Fabry mice by Progenesis LC-MS. FM = Fabry mice; ANA = average normalised abundance.

Description	**Control** ANA	**Male FM** ANA	**Fold change**	**Female FM** ANA	**Fold change**	**↑ or ↓**
Actin, aortic smooth muscle	64.3	3595.2	56.0	2321.8	36.1	↑
ATP synthase subunit alpha, mitochondrial	25.2	2010.5	79.9	558.1	22.2	↑
ATP synthase subunit beta, mitochondrial	0.0	328.1	Infinity	481.5	Infinity	↑
Complement component 1 Q subcomponent-binding protein, mitochondrial	0.0	291.2	Infinity	49.4	Infinity	↑
Fructose-1,6-bisphosphatase 1	0.0	315.1	Infinity	132.3	Infinity	↑
Fumarylacetoacetase	0.0	73.2	Infinity	57.2	Infinity	↑
Myelin proteolipid protein	0.0	90.6	Infinity	44.6	Infinity	↑
Myosin-9	0.0	16.1	Infinity	189.1	Infinity	↑
Ribonuclease UK114	2358.1	12300.0	5.2	6056.1	2.6	↑
Sodium/potassium-transporting ATPase subunit alpha-2	0.0	464.3	Infinity	89.6	Infinity	↑

When data obtained from ProteinLynx and Progenesis LC-MS analyses were cross-referenced two proteins, ATP synthase subunit beta (mitochondrial) and ribonuclease UK114, were detected as having fold change increases in both male and female Fabry mice compared to levels observed in the control group (Figure 5.4). Interestingly, these proteins were the same proteins detected as showing increases in liver tissues from both male and female Fabry mice. In kidney tissues elevations in ATP synthase subunit beta (mitochondrial) of 2.0-fold in male and 3.1-fold in female Fabry mice were detected using ProteinLynx. Using Progenesis LC-MS the same protein was not detectable in control kidney tissue but was detected in both male and female Fabry mice. Ribonuclease UK114 was also found to be increased, elevations of 3.1-fold in male and 3.8-fold in female Fabry mice were detected with ProteinLynx whilst the same protein showed elevatations of 5.2-fold in male and 2.6-fold in female Fabry mice with Progenesis LC-MS.

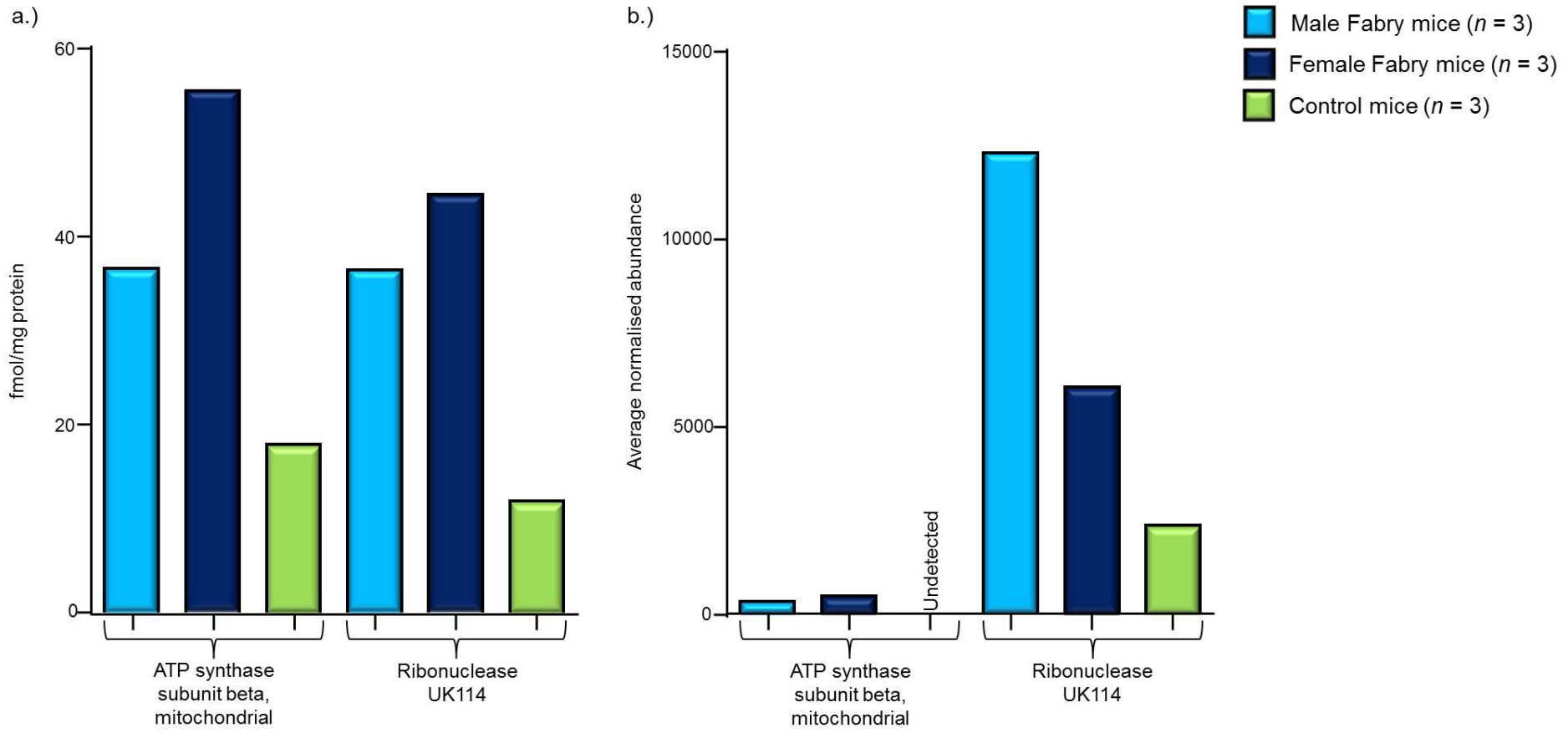

Figure 5.4 Proteins detected as showing a greater than two-fold alteration in pooled kidney tissues from both male Fabry mice (*n* = 3) and female Fabry mice (*n* = 3) by a.) ProteinLynx and; b.) Progenesis LC-MS

5.2.2.3 Analysis of heart tissues from a Fabry mouse model

Following analysis with ProteinLynx, a total of 960 proteins were detected in heart tissue from Fabry and/or control mice. Twenty-two proteins were found to be altered by a fold change greater than two in both male and female Fabry mice compared to levels observed in the control group (Table 5.5). Of these 22 proteins, 2 were shown to have levels greater than two-fold increased and 20 proteins were shown to have levels greater than two-fold decreased.

The levels of 938 of the 960 proteins detected using ProteinLynx displayed no fold change alterations between both the male and female Fabry and control mice groups.

Table 5.5 Proteins detected as altered by a fold change greater than two in heart tissues of male and female Fabry mice by ProteinLynx. FM = Fabry mice

Description	**Control** fmol/mg protein	**Male FM** fmol/mg protein	**Fold change**	**Female FM** fmol/mg protein	**Fold change**	**↑ or ↓**
Alpha-cardiac actin	699.7	0.0	Infinity	0.0	Infinity	↓
Alpha-globin	165.1	0.0	Infinity	17.2	9.6	↓
ATP synthase subunit alpha, mitochondrial	28.9	3142.3	108.7	997.9	34.5	↑
Beta-actin-like protein 2	1.4	0.0	Infinity	0.0	Infinity	↓
Calcium-binding protein p22	4.2	0.0	Infinity	0.0	Infinity	↓
Creatine kinase S-type, mitochondrial	308.7	0.0	Infinity	0.0	Infinity	↓
Desmin	114.5	0.0	Infinity	0.0	Infinity	↓
Dihydropyrimidinase-related protein 4	6.6	0.0	Infinity	0.0	Infinity	↓
Elongation factor - alpha 1	21.4	0.0	Infinity	0.0	Infinity	↓
Hemoglobin subunit alpha	291.1	0.0	Infinity	0.0	Infinity	↓
Kallikrein 1-related peptidase b8	5.8	0.0	Infinity	0.0	Infinity	↓
Long chain specific acyl-CoA dehydrogenase, mitochondrial	23.5	0.0	Infinity	0.0	Infinity	↓
Myosin-7B	0.0	7.9	Infinity	9.5	Infinity	↑
Myosin, heavy polypeptide 1, skeletal muscle, adult	8.6	0.0	Infinity	0.0	Infinity	↓
Myosin, heavy polypeptide 8, skeletal muscle, perinatal	2.1	0.0	Infinity	0.0	Infinity	↓
NADH dehydrogenase [ubiquinone] 1 alpha subcomplex subunit 9, mitochondrial	2.6	0.0	Infinity	0.0	Infinity	↓
NADH dehydrogenase [ubiquinone] iron-sulfur protein 3, mitochondrial	8.1	0.0	Infinity	0.0	Infinity	↓
Rab40b, member RAS oncogene family	9.2	0.0	Infinity	0.0	Infinity	↓
Sarcoplasmic/endoplasmic reticulum calcium ATPase 2	18.5	0.0	Infinity	0.0	Infinity	↓
Transcription termination factor 2	3.5	0.0	Infinity	0.0	Infinity	↓
Tripartite motif-containing protein 72	9.6	0.0	Infinity	0.0	Infinity	↓
Tropomyosin alpha-1 chain	34.9	0.0	Infinity	0.0	Infinity	↓

When data were analysed with the Progenesis LC-MS software a total of 729 proteins were detected in heart tissue from Fabry and/or control mice. Of the 729 proteins detected, 5 were found to have greater than two-fold alterations in the average normalised abundance detected in both male and female Fabry mice compared to those levels detected in the control group (Table 5.6). Of the 5 proteins found to be altered in both male and female Fabry mice, a greater than two-fold elevation was detected in 4 proteins, with a greater than two-fold reduction observed in only a single protein.

The average normalised abundance of 724 of the 729 proteins detected by Progenesis LC-MS did not display fold change alterations between both the male and female Fabry and control mice group.

Table 5.6 Proteins detected as altered by a fold change greater than two in heart tissue of male and female Fabry mice by Progenesis LC-MS. FM = Fabry mice; ANA = average normalised abundance

Description	**Control** ANA	**Male FM** ANA	Fold change	**Female FM** ANA	**Fold change**	↑ **or** ↓
ATP synthase subunit alpha, mitochondrial	0.7	380.2	551.0	80.2	116.3	↑
Baz2a protein	1.3	21.0	15.8	23.1	17.4	↑
Long-chain specific acyl-CoA dehydrogenase, mitochondrial	533.2	11.0	48.7	8.0	66.3	↓
Myosin light chain 1/3, skeletal muscle isoform	0.0	77.1	Infinity	1.1	Infinity	↑
Tropomyosin alpha-3 chain	97.6	632.4	6.5	691.7	7.1	↑

When results obtained from ProteinLynx and Progenesis LC-MS were cross referenced 2 proteins, ATP synthase subunit alpha (mitochondrial) and long chain specific acyl-CoA dehydrogenase (mitochondrial) were confirmed by both analysis methods as having greater than two-fold alterations (Figure 5.5). Using ProteinLynx, ATP synthase subunit alpha (mitochondrial), which together with the beta subunit forms the catalytic core in the F_1 portion of ATP synthase (Figure 5.23), was found to be increased by 108.7-fold in male Fabry mice and by 34.5-fold in female Fabry mice, compared to levels observed in the control group. When the data were analysed using Progenesis LC-MS the same protein was found to be increased 551.0-fold in male Fabry mice and 116.3-fold in female Fabry mice. Long chain specific acyl-CoA dehydrogenase (mitochondrial), is one of the four enzymes that catalyse the initial step of mitochondrial beta-oxidation of straight chain fatty acids and was found to be decreased in heart tissues from both male and female Fabry mice, by both analysis methods. This protein was detected in only control tissues using ProteinLynx with no detectable levels observed in either male or female Fabry mice. Using Progenesis LC-MS, long chain specific acyl-CoA (mitochondrial) was found to be 48.7-fold reduced in male Fabry mice and 66.3-fold reduced in female Fabry mice.

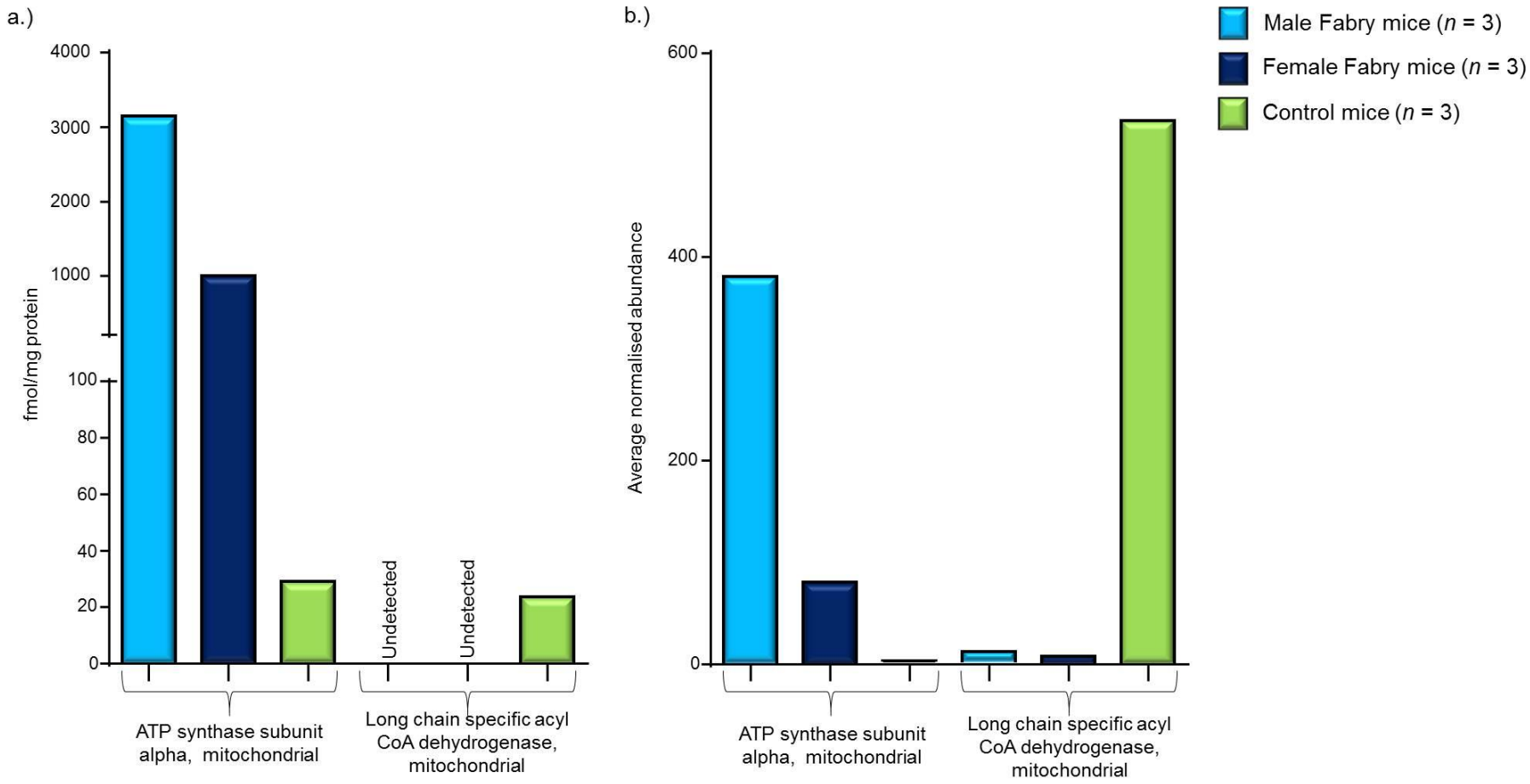

Figure 5.5 Proteins detected as showing a greater than two-fold alteration in pooled heart tissues from both male Fabry mice (*n* = 3) and female Fabry mice (*n* = 3) by a.) ProteinLynx and; b.) Progenesis LC-MS

5.2.2.4 Analysis of brain tissues from a Fabry mouse model

Data analysis with ProteinLynx identified a total of 2917 proteins in brain tissue from Fabry and/or control mice. Of the 2917 proteins detected in brain tissues, 13 were found to have levels displaying a greater than two-fold alteration in both male and female Fabry mice, compared to levels detected in the control group (Table 5.7). Of these 13 proteins, 4 were found to have levels greater than two-fold increased and 9 were found to have levels greater than two-fold decreased. The levels of 2904 of the 2917 proteins detected using ProteinLynx displayed no fold change alterations between both the male and female Fabry and control mice groups.

Table 5.7 Proteins detected as altered by a fold change greater than two in brain tissues of male and female Fabry mice by ProteinLynx. FM = Fabry mice

Description	**Control** fmol/mg protein	**Male FM** fmol/mg protein	**Fold change**	**Female FM** fmol/mg protein	**Fold change**	↑ **or** ↓
14-3-3 protein epsilon	45.5	275.0	6.0	145.0	3.2	↑
Actin-related protein 3	694.4	304.5	2.3	310.2	2.2	↓
Alpha-synuclein	78.2	28.9	2.7	31.3	2.5	↓
Aspartate aminotransferase, mitochondrial	3.6	38.3	10.6	33.4	9.3	↑
ATP-binding cassette sub-family B member 8, mitochondrial	59.4	0.0	Infinity	0.0	Infinity	↓
Calcium/calmodulin-dependent protein kinase II subunit beta	859.3	117.1	7.3	48.4	17.8	↓
Dihydropyrimidinase-related protein 2	0.0	170.1	Infinity	81.5	Infinity	↑
Guanine nucleotide-binding protein G(I)/G(S)/G(T) subunit beta-2	2657.8	647.7	4.1	666.4	4.0	↓
Interferon-stimulated 20 kDa exonuclease-like 2	22.2	5.1	4.4	3.2	7.0	↓
Microtubule-associated protein 4	542.6	196.1	2.8	155.7	3.5	↓
Nascent polypeptide-associated complex subunit alpha, muscle-specific form	126.2	58.8	2.2	36.1	3.5	↓
OXR1 short isoform C7C	2.6	41.5	16.1	22.4	8.7	↑
Tubulin alpha-4A chain	4848.3	786.2	6.2	612.8	7.9	↓

Following analysis with the Progenesis LC-MS software a total of 2340 proteins were detected in brain tissues from Fabry and/or control mice. Of the 2340 proteins detected, 12 were found to have greater than two-fold alterations in their average normalised abundance, compared to the average normalised abundance of the control group (Table 5.8). Of these 12 proteins, 4 were found to have a greater than two-fold increase and 8 proteins were detected as having greater than two-fold decreases.

The average normalised abundance of 2328 of the 2340 proteins detected using Progenesis LC-MS displayed no fold change alterations between both the male and female Fabry and control mice groups.

Table 5.8 Proteins detected as altered by a fold change greater than two in brain tissue of male and female Fabry mice by Progenesis LC-MS. FM = Fabry mice; ANA = average normalised abundance

Description	**Control** ANA	**Male FM** ANA	**Fold change**	**Female FM** ANA	**Fold change**	↑ or ↓
Actin-related protein 2/3 complex subunit 4	2.6	41.4	16.2	41.9	16.4	↑
Alpha-actinin-2	18.9	52.7	2.8	57.7	3.1	↑
Alpha-synuclein	859.3	117.1	7.3	48.4	17.8	↓
ATPase, Ca++ transporting, plasma membrane 3	192.8	86.5	2.3	83.7	2.3	↓
ATP-binding cassette sub-family B member 8, mitochondrial	2657.8	647.7	4.1	666.4	4.0	↓
Calm4 protein	694.4	304.5	2.3	310.2	2.2	↓
Cell cycle exit and neuronal differentiation protein 1	22.2	5.1	4.4	3.2	7.0	↓
Elongation factor 1-alpha 1	62.9	238.6	3.8	193.4	3.1	↑
Exocyst complex component 7	2507.6	887.9	2.8	595.7	4.2	↓
Heat shock 70 kDa protein 14	395.9	129.1	3.1	68.9	5.8	↓
L-asparaginase	0.0	62.7	Infinity	52.3	Infinity	↑
MKIAA4098 protein	4848.3	786.2	6.2	612.8	7.9	↓

When results obtained from ProteinLynx and Progenesis LC-MS were cross referenced 2 proteins, alpha-synuclein and ATP-binding cassette sub-family B member 8 (mitochondrial), were confirmed by both analysis methods as showing greater than two-fold reductions in male and female Fabry mice (Figure 5.6). Using ProteinLynx alpha-synuclein, a pre-synaptic neuronal protein with a genetic and neuropathological link to Parkinson's disease was found to be 2.7-fold reduced and 2.5-fold reduced in brain tissues of male and female Fabry

mice, respectively. Using Progenesis LC-MS the same protein was found to be reduced 7.3-fold in male and 17.8-fold in female Fabry mice. ATP-binding cassette sub-family B member 8 (mitochondrial) is an ATP-dependent transporter that may mediate the passage of organic and inorganic molecules out of the mitochondria and was also found to be reduced. This protein was not detectable in male or female Fabry mice brain tissues using ProteinLynx but was found in the control group. Using Progenesis LC-MS this protein was found to be 4.1-fold reduced in male and 4.0-fold reduced in female Fabry mice.

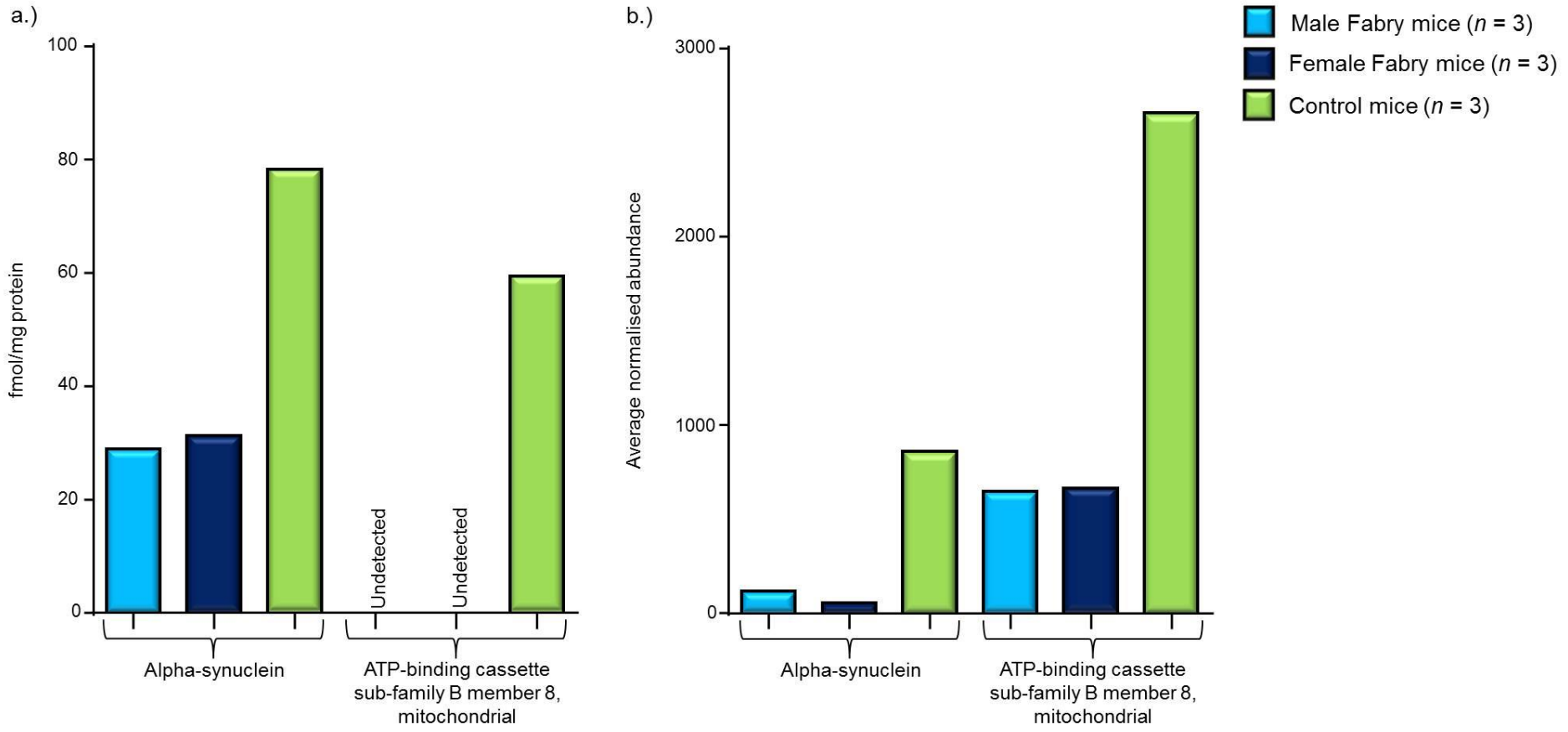

Figure 5.6 Proteins detected as showing a greater than two-fold alteration in pooled brain tissues from both male Fabry mice (*n* = 3) and female Fabry mice (*n* = 3) by a.) ProteinLynx and; b.) Progenesis LC-MS

5.2.2.5 Classification of proteins showing alterations in Fabry mouse tissues using the Gene Ontology annotation system

Those proteins that were shown to have alterations by both ProteinLynx and Progenesis LC-MS in Fabry mouse tissues were investigated with the Gene Ontology (GO) annotation system using the PANTHER website. The GO annotation system classifies proteins according to their molecular functions, biological processes and biological pathways this enables common features between proteins of interest to be grouped and identified.

5.2.2.6 Molecular functions associated with proteins that show alterations in Fabry mouse tissues

Six molecular functions were shown to be associated with proteins identified as having alterations during the proteomic profiling aspect of the study (Figure 5.7). ATP synthase subunits alpha (increased in the heart) and beta (increased in the liver and kidney), were shown to have a role in five of the six molecular functions. This suggests that an increase in these proteins could affect a variety of functional activities performed at the molecular level.

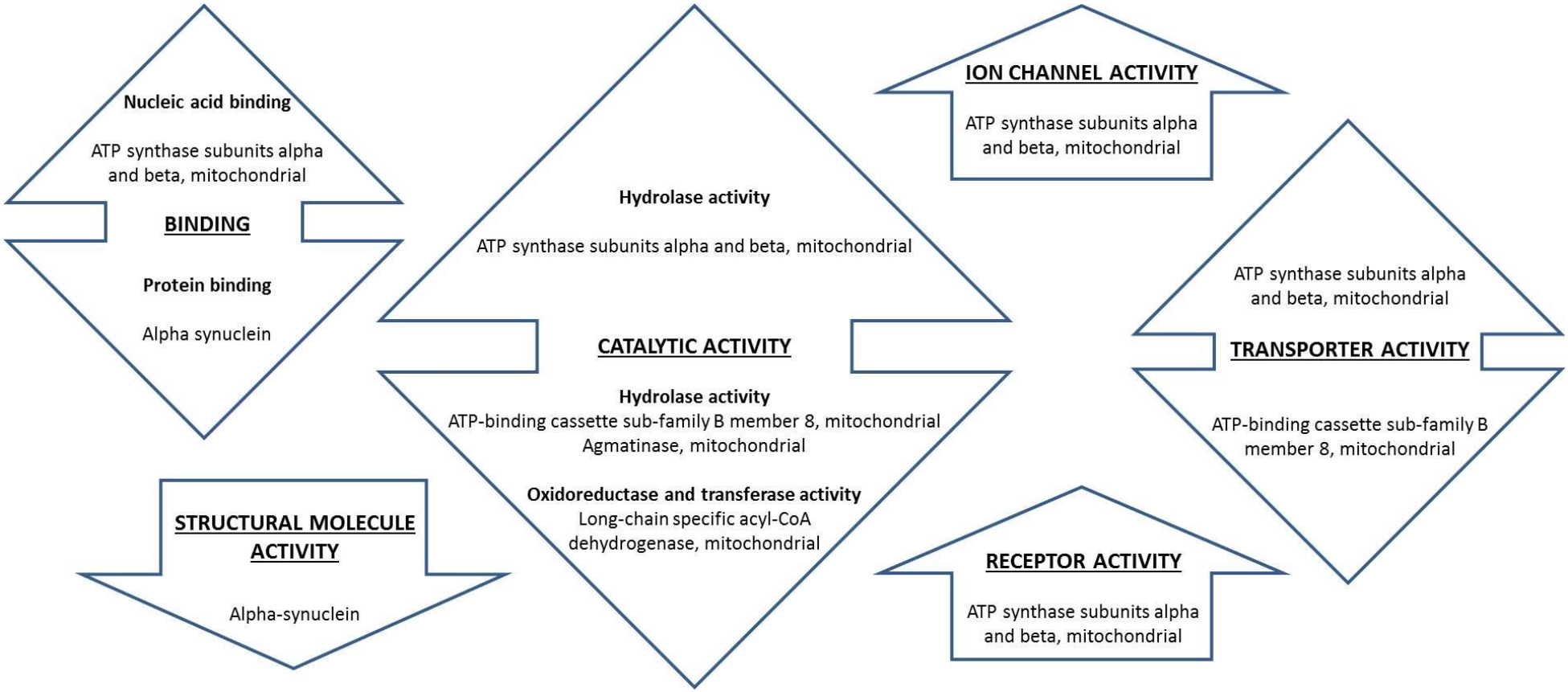

Figure 5.7 Molecular functions associated with proteins identified as showing alterations by both ProteinLynx and Progenesis LC-MS in Fabry mouse tissues during the proteomic profiling study. Arrowed boxes indicate an increase or decrease of the detected protein.

5.2.2.7 Biological processes associated with proteins that show alterations in Fabry mouse tissues

Nine biological processes were revealed to be associated with proteins shown to have an alteration during the proteomic profiling study (Figure 5.8). Interestingly, all biological processes were associated with at least one protein that was found to be decreased during the proteomic profiling study. A biological process by definition involves more than one distinct step. A disease-related perturbation affecting any or all of these steps, for example an alteration of a vital protein such as those shown to be altered in this study, could therefore result in abnormal execution of a number of biological processes.

5.2.2.8 Biological pathways associated with proteins that show alterations in Fabry mouse tissues

Only three of the proteins showing alterations in the proteomic profiling study were shown to be associated with biological pathways using the GO annotation system. Of the three proteins two, ATP synthase subunits alpha and beta (mitochondrial) which were found to be increased in heart and liver and kidney tissues respectively, were shown to be involved in ATP synthesis. The third protein, alpha synuclein, has a well-established roll in the Parkinson's disease pathway. This protein was found to be reduced in Fabry mouse brain tissues.

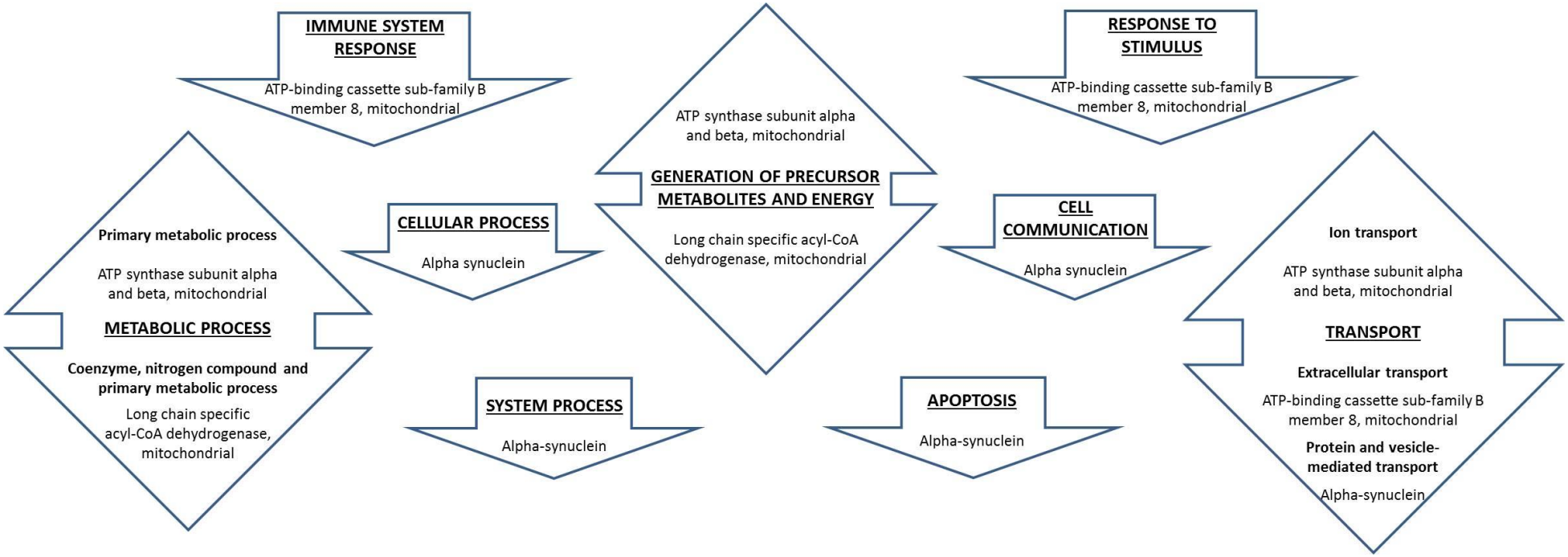

Figure 5.8 Biological processes associated with proteins identified as showing alterations by both ProteinLynx and Progenesis LC-MS in Fabry mouse tissues during the proteomic profiling study. Arrowed boxes indicate an increase or decrease of the detected protein.

5.2.3 Identification of protein: glycosphingolipid interactions

In this aspect of the study two complementary technologies were used to identify proteins that interact with a number of lipids in the glycosphingolipid biosynthetic pathway with particular interest on Gb_3. These complementary strategies were used in order to evaluate the best method for performing lipid-binding experiments.

5.2.3.1 RS100 ProteinChip array technology for the study of protein: glycosphingolipid interactions

RS100 technology is a type of ProteinChip Array that has been used previously to study antibody-antigen interactions (Mills *et al*., 2006). RS100 ProteinChip arrays are pre-activated with carbonyl diimidazole active groups present on large C12-linker arms bound to the chip surface. These active groups bind covalently to free primary amine groups of amino acids present on the exterior of antibodies/proteins, while maintaining their active conformation and biological activity. Potential binding proteins/antigens can be used as 'bait' and can capture proteins, which can then subsequently be analysed and identified by mass spectrometry.

In the present study, a novel method based on RS100 technology was developed to investigate proteins captured using Gb_3 as the target. In addition, to distinguish those proteins that bind exclusively to Gb_3, with those proteins that interact non-selectively with glycosphingolipids, interactions with GM_1 ganglioside were also investigated in brain tissues from a control mouse. In order to bind the glycosphingolipids to the surface of the RS100 ProteinChip, deacylated versions of each glycosphingolipid which possess a primary free amine group were used. The covalent bond that is formed via the free amine

group of the deacylated glycosphingolipid and the C12-linker arm on the surface of the chip effectively restores each glycosphingolipid to its acylated form (Figure 5.9). In addition, to ensure the specificity of the interactions with the glycosphingolipids, non-specific binding to the chip surface was detected with the use of phosphate buffered saline (PBS), which blocks the C12-linker arm and therefore acts as a negative control.

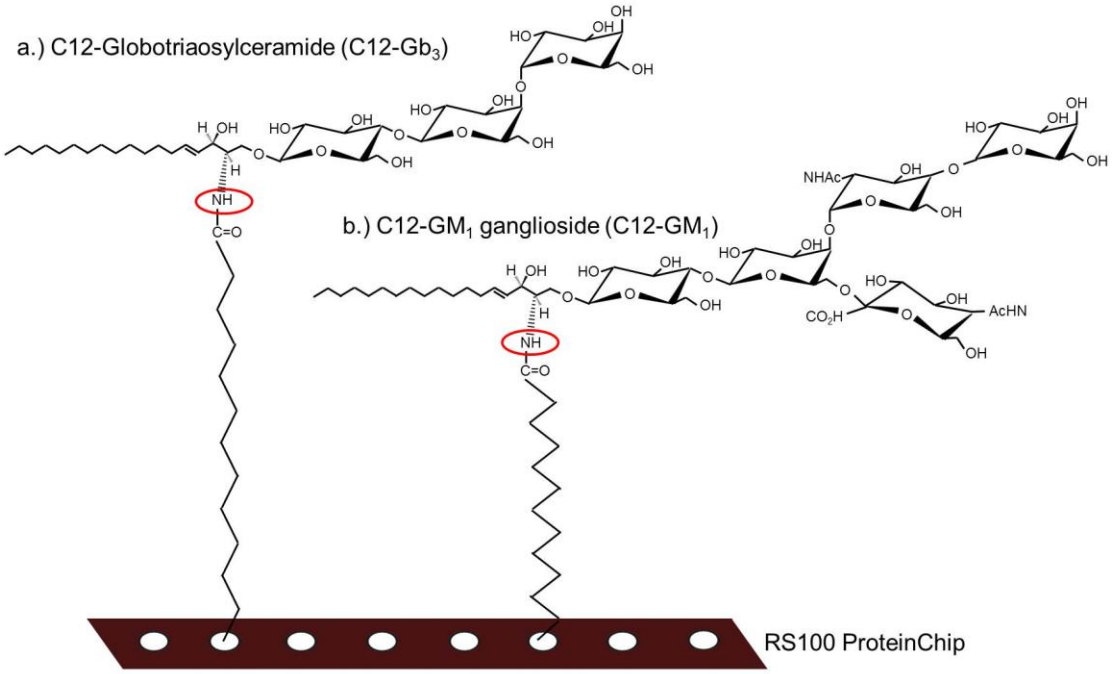

Figure 5.9 Schematic representation of how deacylated sphingolipids bind to the surface of the RS100 ProteinChip through the primary amine group, (shown circled in red) to form a.) C12-globotriaosylceramide; b.) C12-GM_1 ganglioside.

5.2.3.2 The interaction of proteins with Gb_3 when immobilised on a RS100 ProteinChip

Following the extraction of proteins which interacted with Gb_3 and GM_1 ganglioside when bound to the surface of the RS100 ProteinChip and subsequent analysis by UPLC-QToF-MS, a total of 157 proteins were identified using ProteinLynx. Following the exclusion of those proteins that displayed non-specific binding, a total of 62 proteins were identified that bound to Gb_3 in mouse brain tissue (Figure 5.10).

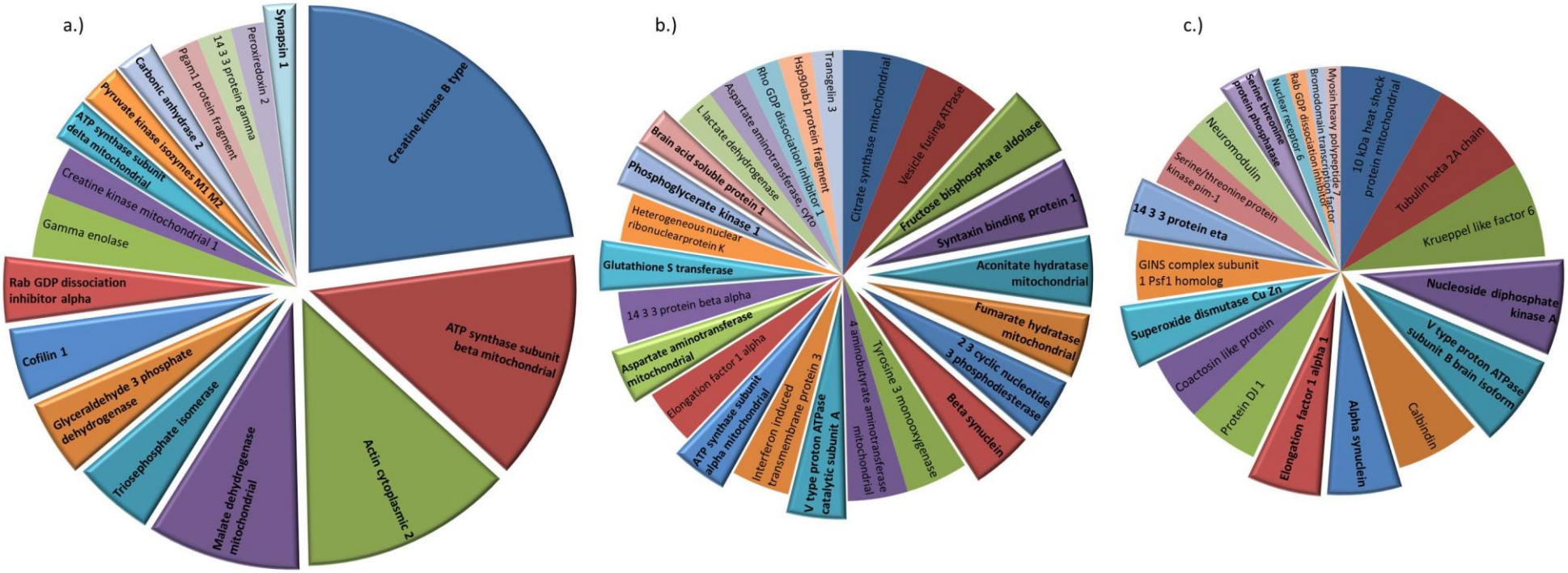

Figure 5.10 Schematic representation of proteins that interact with Gb_3 in mouse brain tissue a.) proteins that constitute > 30 fmol protein; b.) proteins that constitute 30 - 10 fmol protein and c.) proteins that constitute < 10 fmol protein. Those sections of the pie chart which are extracted were also shown to interact with GM_1 ganglioside.

5.2.3.3 The interaction of proteins with GM_1 ganglioside when immobilised on a RS100 ProteinChip

Of the 157 proteins that were identified in mouse brain by ProteinLynx as binding to the RS100 ProteinChip, 101 proteins were found to interact with GM_1 ganglioside (Figure 5.11).

5.2.3.4 The interaction of proteins with Gb_3 and GM_1 ganglioside when immobilised on a RS100 ProteinChip

Thirty-two of the 157 proteins that were identified by ProteinLynx as binding to the RS100 ProteinChip were detected binding to both Gb_3 and GM_1 ganglioside, shown as the extracted segments of the pie charts in Figures 5.10 and 5.11. It is most likely that these 32 proteins recognise the sphingosine portion of the molecule, common to both Gb_3 and GM_1 ganglioside and not the sugar portion of the molecule which is unique to each glycosphingolipid.

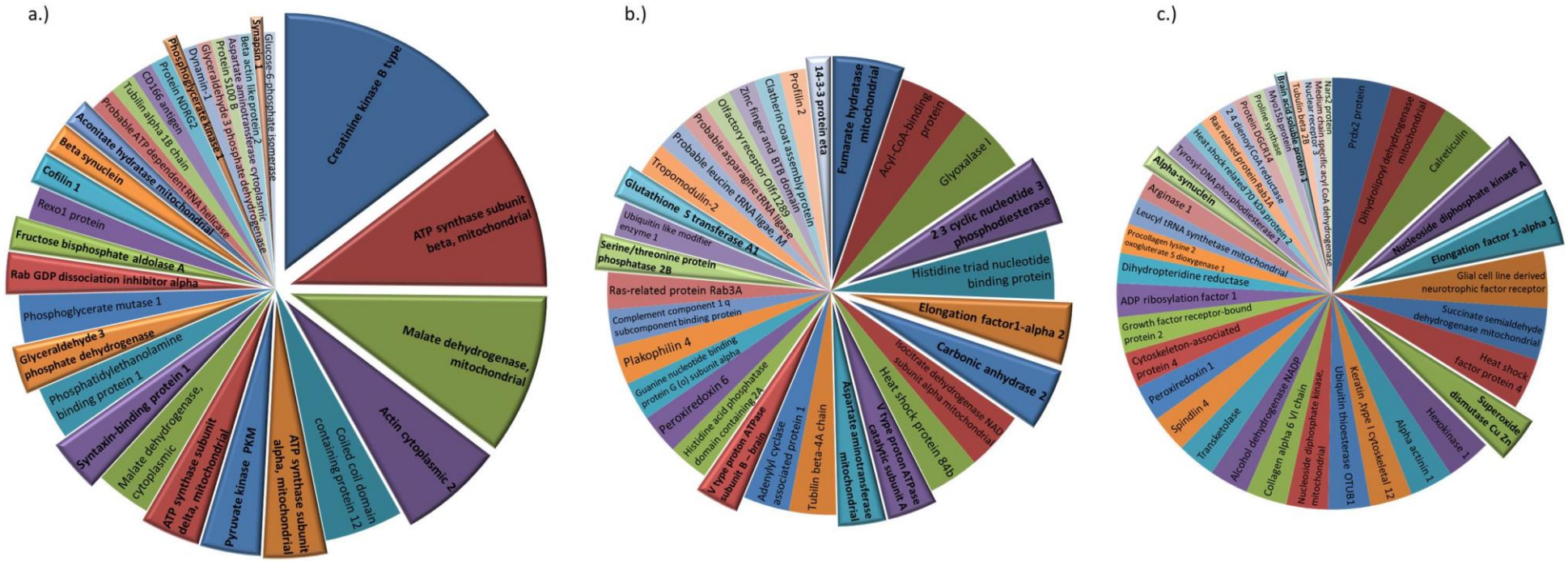

Figure 5.11 Schematic representation of proteins that interact with GM_1 ganglioside in mouse brain tissue a.) proteins that constitute > 30 fmol protein; b.) proteins that constitute 30 - 10 fmol protein and c.) proteins that constitute < 10 fmol protein. Those sections of the pie chart which are extracted were also shown to interact with Gb_3.

5.2.3.5 Classification of proteins interacting with glycosphingolipids

In order to identify common molecular functions, biological processes and pathways associated with the proteins identified as binding to Gb_3 and GM_1 ganglioside, interactions were investigated with the GO annotation system using the PANTHER website. Of the 131 protein identifications entered into the PANTHER website 24 proteins could not be detected using this software. Of those proteins that were identified a large proportion were found to be located in the mitochondria or to possess catalytic activity involving ATP. This suggests that those proteins that interact with Gb_3 and/or GM_1 ganglioside may have a role in mitochondrial energy production which may be affected by binding to a glycosphingolipid.

5.2.3.6 Molecular functions associated with proteins that interact with Gb_3 and GM_1 ganglioside

Two molecular functions, catalytic activity and protein binding, were found to be the molecular functions that the most proteins interacting with Gb_3 and/or GM_1 ganglioside shared. Of the 131 proteins detected as binding with Gb_3 and/or GM_1 ganglioside, 62 proteins were detected as having catalytic activity. Further investigation was able to subdivide these proteins into those with RNA splicing factor, helicase, hydrolase, isomerase, ligase, lyase, oxidoreductase, and transferase activities (Figure 5.12). Of these subcategories, the highest number of proteins (18 proteins) were detected to possess hydrolase activity. In addition, many proteins were found to possess transferase (16 proteins) and oxidoreductase (15 proteins) activities. Thirty-one of the 131 proteins detected were also identified as having binding capability. This category was further subdivided into those protein binding, calcium ion binding, chromatin ion binding

and nucleic acid binding proteins (Figure 5.10). The most proteins were identified as protein binding proteins with 18 proteins falling into this subcategory.

Other common molecular functions associated with proteins that interact with Gb_3 and GM_1 ganglioside in mouse brain tissue are shown in Figure 5.12.

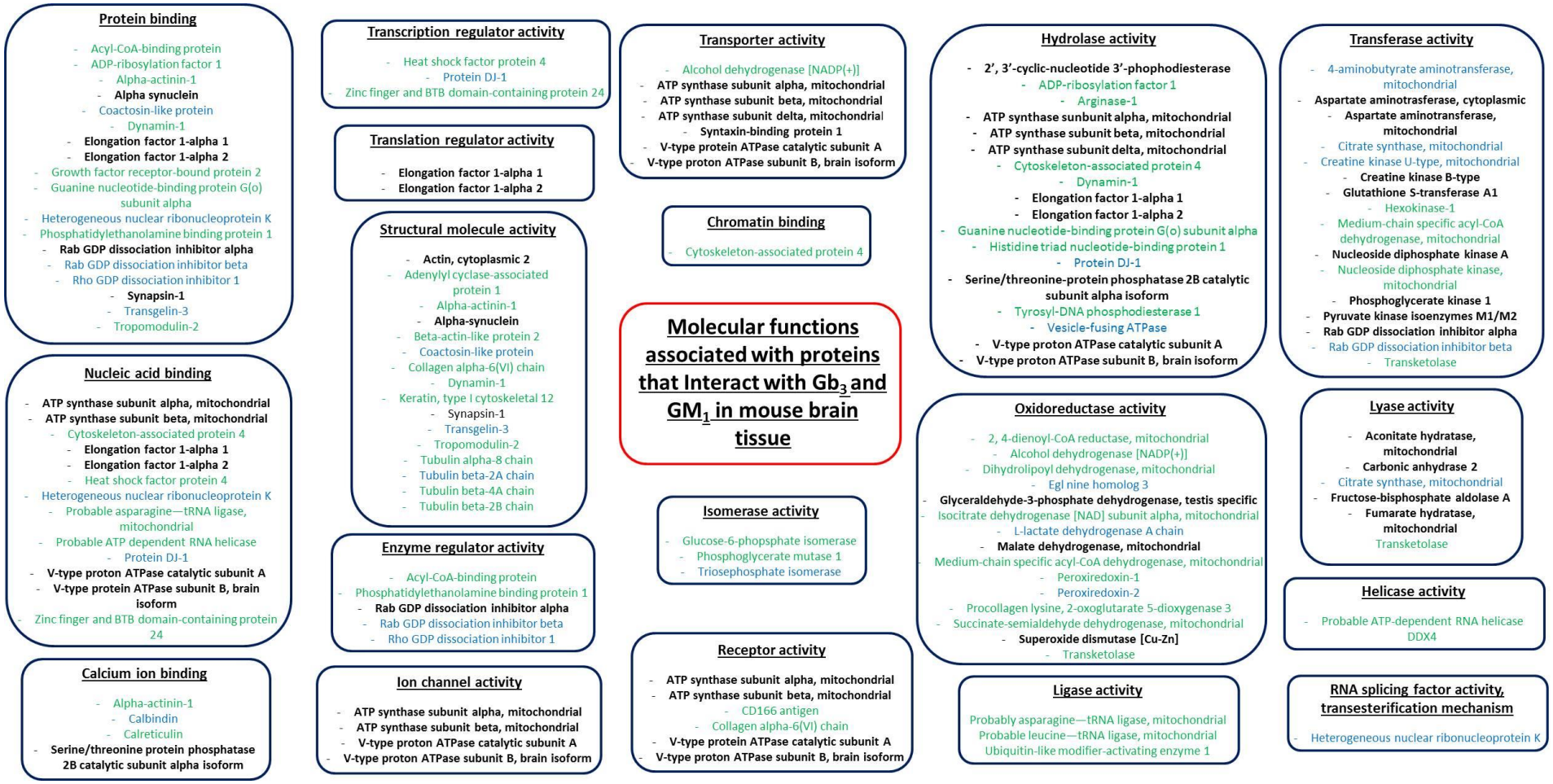

Figure 5.12 Molecular functions associated with proteins found to interact with Gb_3 and/or GM_1 ganglioside (shown in black and bold). Those proteins that interact with Gb_3 only (shown in blue) and those that interact with GM_1 ganglioside only (shown in green).

5.2.3.7 Biological processes associated with proteins that interact with Gb_3 and GM_1 ganglioside

The proteins that were found to interact with Gb_3 and/or GM_1 ganglioside were also investigated to establish if any common biological processes existed. Fifty-one proteins found to interact with Gb_3 and GM_1 ganglioside were grouped by the GO annotation system as having 'primary metabolic processes' as their biological function. This classification was further subdivided into carbohydrate, cellular amino acid and derivative, lipid, protein and nucleobase, nucleoside, nucleotide and nucleic acid, metabolic processes (Figure 5.13). Following sub-classification 18 proteins were found to have nucleobase, nucleoside, nucleotide and nucleic acid metabolic processes as their biological function. Carbohydrate and protein metabolic processes were also common biological processes shared by proteins binding to Gb_3 and GM_1 ganglioside with 16 and 14 proteins in each of these categories, respectively.

Other biological processes that many proteins interacting with Gb_3 and GM_1 ganglioside were found to share were cellular processes, transport and cell communication with 33, 24 and 20 proteins assigned to these categories, respectively. All biological processes associated with the proteins detected as interacting with Gb_3 and GM_1 ganglioside in mouse brain tissue as defined by the GO annotation system are shown in Figure 5.13.

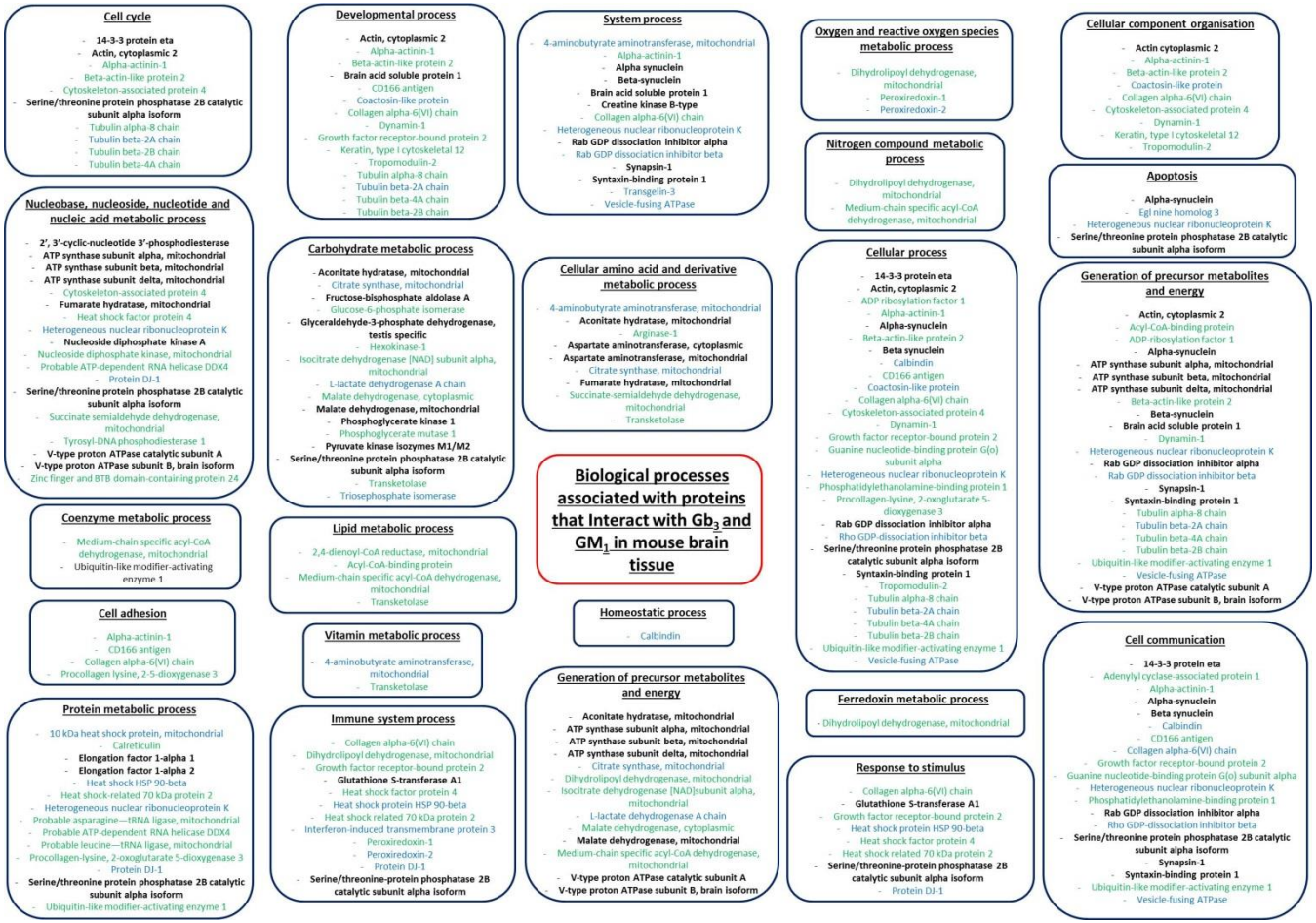

Figure 5.13 Biological processes associated with proteins found to interact with Gb_3 and/or GM_1 ganglioside (shown in black and bold). Those proteins that interact with Gb_3 only (shown in blue) and those that interact with GM_1 ganglioside only (shown in green).

5.2.3.8 Biological pathways associated with proteins that interact with Gb_3 and GM_1 ganglioside

In total 51 biological pathways were identified by the GO annotation system as having involvement with one or more protein which binds to Gb_3 and/or GM_1 ganglioside. Figure 5.14 shows only those biological pathways that have two or more proteins assigned that were detected as interacting with Gb_3 and/or GM_1 ganglioside. Of the 51 biological pathways indentified, the Huntington's disease and glycolysis pathways involved the most proteins. A total of 7 proteins were identified as interacting with Gb_3 and/or GM_1 ganglioside in each of these biological pathways. Huntington's disease is a progressive neurodegenerative disorder which leads to extensive degeneration of the basal ganglia (Bard *et al.*, 2014). Whilst neurodegeneration is not a prominent feature of Fabry disease, both Fabry and Huntington diseases are associated with protein mis-folding (Chaudhuri and Paul 2006). Furthemore, 6 of the 7 proteins involved in the Huntington's disease pathway were found to interact with GM_1 ganglioside. Accumulation of GM_1 ganglioside in the basal ganglia is a prominent feature of GM_1 gangliosidosis and is thought to be responsible for the neurologic picture (Campdelacreu *et al.*, 2002). Interestingly, 3 biological pathways, tyrosine, phenylalanine and asparagine and aspartate were only assosicated with proteins that bound to both Gb_3 and GM_1 ganglioside. The pentose pathway was also the only biological pathway containing only proteins that bound GM_1 ganglioside. Other common biological pathways associated with proteins that interact with Gb_3 and/or GM_1 ganglioside in mouse brain tissue are shown in Figure 5.14.

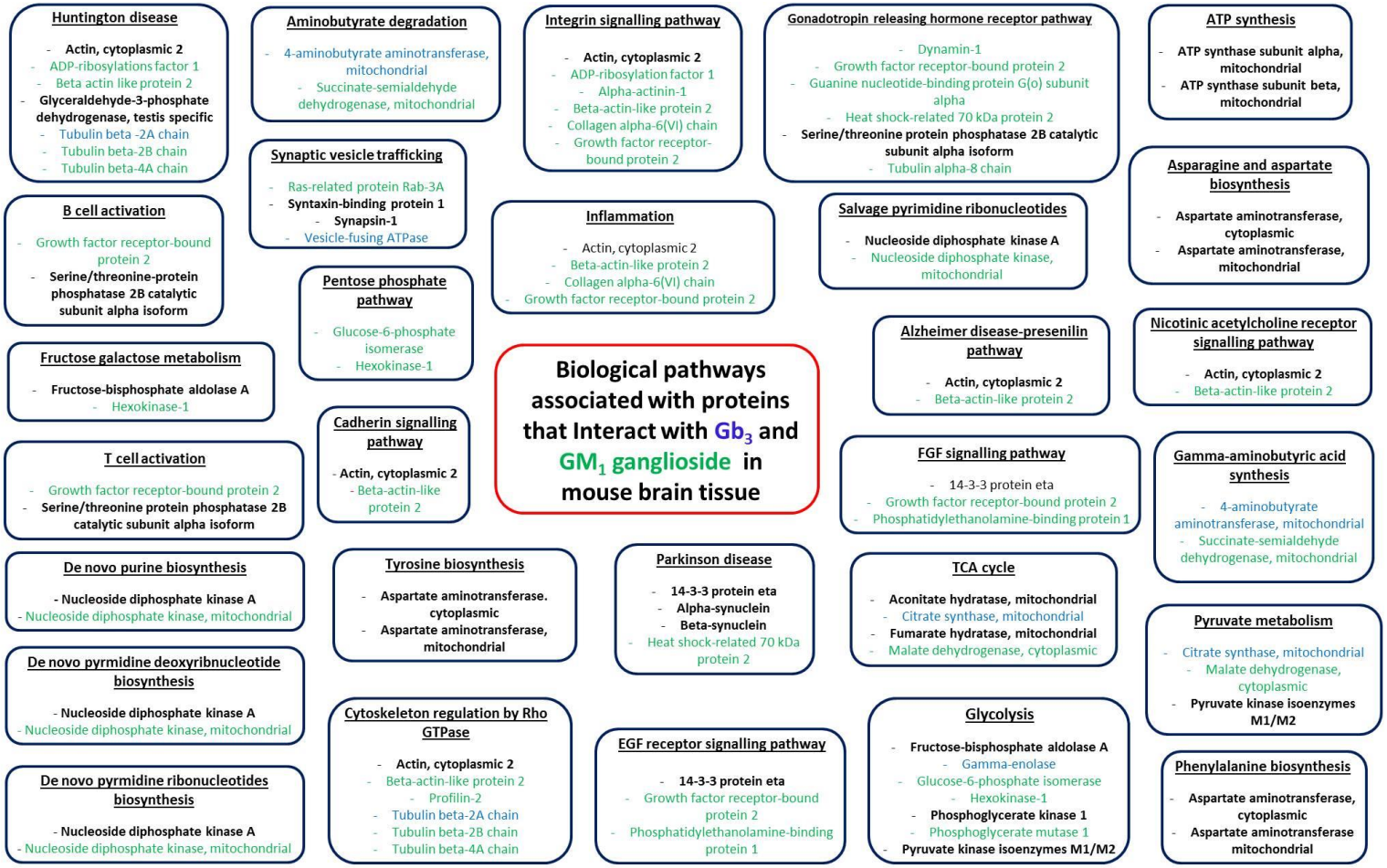

Figure 5.14 Biological pathways associated with proteins found to interact with Gb_3 and/or GM_1 ganglioside (shown in black and bold). Those proteins that interact with Gb_3 only (shown in blue) and those that interact with GM_1 ganglioside only (shown in green).

5.2.3.9 The use of Dynabeads® M-270 Epoxy for the study of protein: glycosphingolipid interactions

An alternative strategy to the RS100 ProteinChip array technology was also used to study protein: glycosphingolipid interactions. This additional analysis, using Dynabeads® M-270 Epoxy, was performed not only to evaluate the best method for performing lipid binding experiments but also to compare the effect of differing acyl-chain lengths on observed interactions. Dynabeads® M-270 Epoxy are superparamagnetic hydrophilic beads coated with surface epoxy groups to allow the direct covalent binding of primary amino and sulfhydryl groups present in proteins and peptides. This allows the coupling of a desired ligand to the beads which can then be used as 'bait' to capture proteins. Captured proteins are separated, washed and eluted using a DynaMag™ magnet and the magnetic separation properties of the Dynabeads®. Eluted proteins can then subsequently be analysed and identified by mass spectrometry.

In this aspect of the study Dynabead® technology was used to investigate proteins captured using Gb_3 as the target. In addition, interactions of proteins with the glycosphingolipids GM_1 ganglioside, galactosylceramide and ceramide were investigated as further controls to identify those proteins which interact solely with the protein of interest, Gb_3, and those which also interact with other glycosphingolipids in mouse kidney tissues. In order to bind the glycosphingolipids to the Dynabeads®, again deacylated versions of each glycosphingolipid possessing a primary free amine group were used. The covalent bond that is formed via the free amine group of the deacylated glycosphingolipid and the C5-linker arm of the epoxy group coating the surface of the Dynabeads® effectively restores each glycosphingolipid to its acylated

form (Figure 5.15). In addition, to ensure the specificity of the interactions with the glycosphingolipids, non-specific binding to the ‘bead’ surface was detected with the use of PBS, which blocks the C5-linker arm and therefore acts as a negative control.

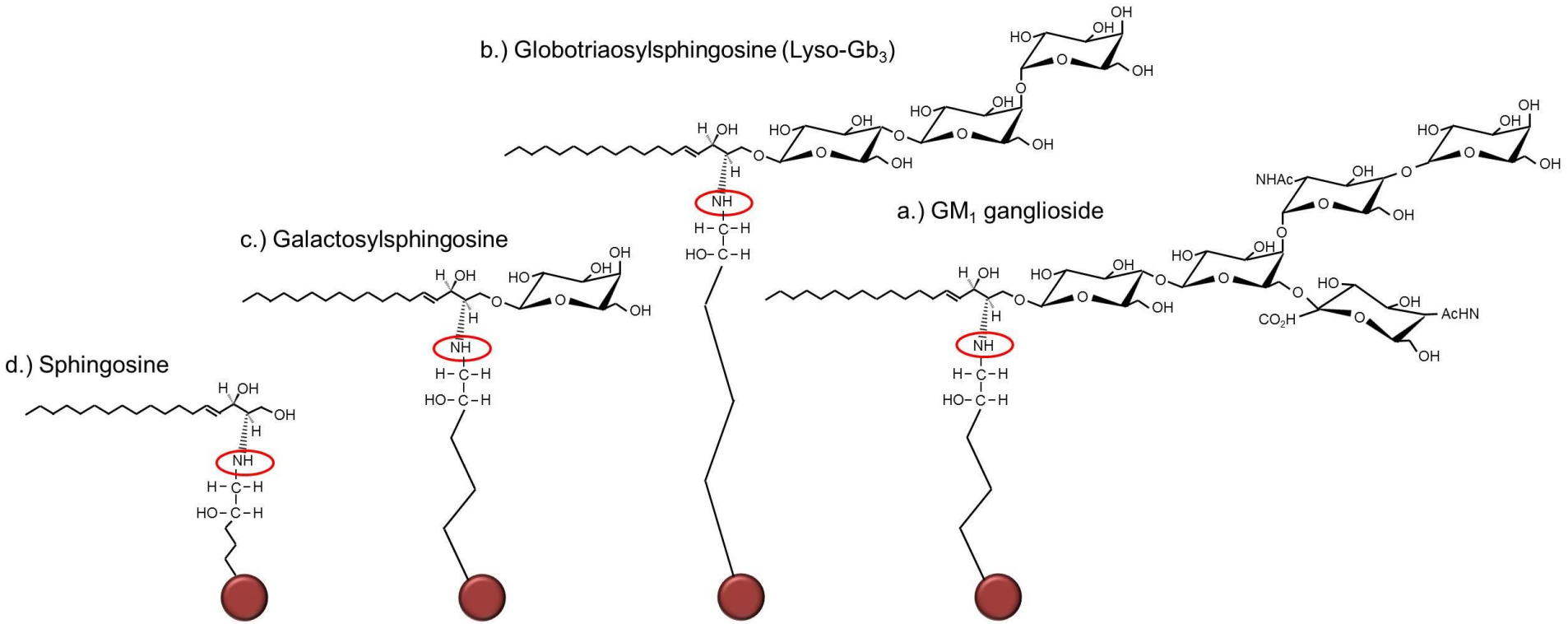

Figure 5.15 Schematic representation of how the deacylated sphingolipids a.) Lyso-GM_1 ganglioside (Lyso-GM_1); b.) Globotriaosylsphingosine (Lyso-Gb_3); c.) Galactosylsphingosine and d.) Sphingosine bind to Dynabeads® M-270 Epoxy through the primary amine group, shown circled in red.

5.2.3.10 The interaction of proteins with glycosphingolipids when bound to Dynabeads®

Following the extraction of proteins which interacted with those glycosphingolipids bound to Dynabeads® and analysis by UPLC-QToF-MS, a total of 100 proteins were identified using ProteinLynx Global Server version 2.4. Following the exclusion of those proteins that displayed non-specific binding, a total of 22 proteins were identified that bound to one or more of the glycosphingolipids (Figure 5.16).

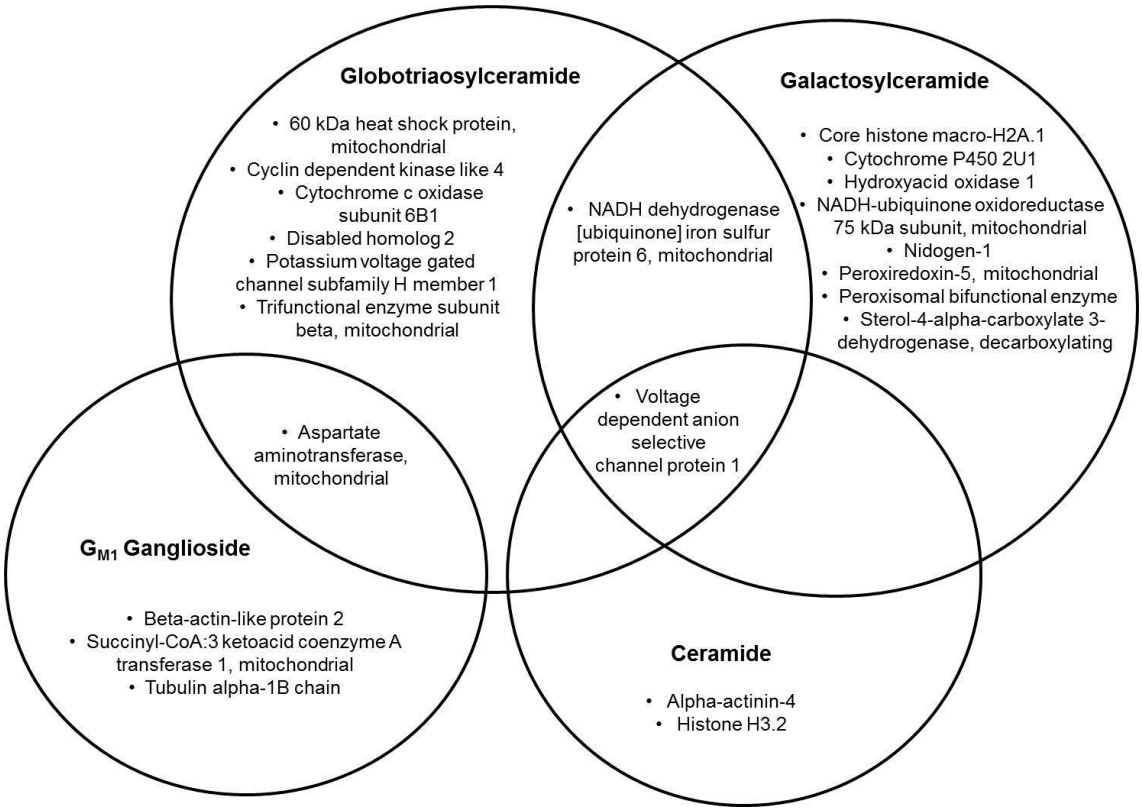

Figure 5.16 A modified Venn diagram showing proteins that interact with globotriaosylceramide (Gb_3), GM_1 ganglioside, galactosylceramide and ceramide.

5.2.3.11 Classification of proteins interacting with glycosphingolipids

In order to identify common molecular functions, biological processes and pathways associated with the proteins identified as binding to Gb_3, GM_1 ganglioside, galactosylceramide and/or ceramide, interactions were investigated with the GO annotation system, using the PANTHER website.

5.2.3.12 Identification of proteins that bind only to Gb_3

Six proteins were detected that interacted with only the glycolipid of interest, Gb_3 (Figure 5.16). Further analysis of these proteins using the GO annotation system revealed that 2 of the 6 proteins, 60 kDa heat shock protein (mitochondrial) and cyclin-dependant kinase like-4, possessed the molecular function to interact selectively and covalently with ATP. A further association was identified with a third protein, cytochrome C oxidase subunit 6B1, for which the biological function has a role in the respiratory electron transport chain from which ATP is generated.

5.2.3.13 Identification of proteins that bind only to the control GM_1 ganglioside array

Three proteins were detected binding solely to GM_1 ganglioside (Figure 5.16). Further analysis using the GO annotation system did not reveal any common biological processes, pathways or molecular functions associated with the identified proteins. However, all three proteins were again found to be involved in energy metabolism.

5.2.3.14 Identification of proteins that bind only to the control galactosylceramide array

The most protein interactions were detected binding to the glycosphingolipid galactosylceramide. In total 8 proteins were identified which interacted with galactosylceramide (Figure 5.16). Functional analysis revealed that 6 of the 8 proteins identified possessed oxidoreductase activity as one of, or their sole, molecular function. In addition, 3 of the proteins, hydroxyacid oxidase 1, peroxiredoxin-5 and peroxisomal bifunctional enzyme were all shown to be located in the peroxisome.

5.2.3.15 Identification of proteins that bind only to the control ceramide array

The least amount of protein interactions were detected when the glycosphingolipid ceramide was bound to the surface of the beads. Two proteins were identified, alpha-actinin-4 and histone H3.2. Unfortunately due to the limited amount of interactions detected and their non-specific nature functional analysis was not able to reveal any common biological processes, pathways or molecular functions associated with the identified proteins (Figure 5.16).

5.2.3.16 Identification of proteins that bind to more than one glycosphingolipid when bound to Dynabeads® M-270 Epoxy

Although no protein was identified that bound to all four glycosphingolipids, one protein was detected that bound to Gb_3, galactosylceramide and ceramide. This protein, voltage dependent anion selective channel protein 1 (Figure 5.16),

partly functions to form a channel through the mitochondrial outer membrane to allow the diffusion of small hydrophilic molecules. Another ion channel, potassium-voltage gated channel subfamily H member 1, was also detected in this study and was found to interact exclusively with Gb_3. One protein, NADH dehydrogenase [ubiquinone] iron sulfur protein 6 (mitochondrial), was also identified that bound to both Gb_3 and galactosylceramide. This protein shares a common molecular function and/or biological process with proteins that were detected interacting individually with either Gb_3 or galactosylceramide as it displays both oxidoreductase activity and is essential to the mitochondrial electron transport chain. In addition a single protein, aspartate aminotransferase (mitochondrial), was detected that bound to both Gb_3 and GM_1 ganglioside. This protein is important for metabolite exchange between the mitochondria and the cytosol and in addition facilitates the cellular uptake of long-chain free fatty acids.

5.2.3.17 Comparison of RS100 ProteinChip and Dynabead® M-270 Epoxy methods for the study of protein: glycosphingolipid interactions

The study of protein: glycosphingolipid interactions using complementary RS100 ProteinChip and Dynabeads® methods revealed the proteins beta-actin-like protein 2 and tubulin alpha-1B chain to interact solely with GM_1 ganglioside. In addition, aspartate aminotransferase (mitochondrial) was found to bind to both Gb_3 and GM_1 ganglioside using both analysis techniques. Although only a small number of proteins were confirmed to bind to Gb_3 and/or GM_1 ganglioside using both analysis methods a variety of mitochondrial proteins were also revealed to interact with the glycosphingolipids using both methods. Of these proteins the mitochondrial ATP synthase subunits alpha, beta and delta were

detected binding to both Gb_3 and GM_1 ganglioside when immobilised on the RS100 ProteinChip. This confirmed results observed in the proteomic profiling aspect of the study where ATP synthase subunit beta was found to be increased in both Fabry mouse liver and kidney tissues and ATP synthase subunit alpha was found to be increased in Fabry mouse heart tissues. A number of proteins with the ability to interact selectively and covalently to ATP were also identified binding to Gb_3 during the protein: glycosphingolipid interaction study when using Dynabeads®. As a result the effect of various glycosphingolipids and their deacylated counterparts on ATP synthase activity were investigated (section 5.2.4).

5.2.4 ATP synthase activity

A functional assay to assess ATP synthase activity was performed as described in section 2.2.7.9. As well as Gb_3 a number of other glycosphingolipids involved in the glycosphingolipid biosynthetic pathway (GM_1 ganglioside, sulfatide, lactosylceramide, glucosylceramide, and galactosylceramide) were also assessed with regards to their effect on ATP synthase activity. In addition cardiolipin, a lipid which has been shown previously to affect the supramolecular organisation of ATP synthase in mitochondria, was included for comparison. The effect of the lyso-glycosphingolipids lyso-Gb_3, lyso-GM_1 ganglioside, lyso-sulfatide, lyso-lactosylceramide, lyso-glucosylceramide, and lyso-galactosylceramide were also evaluated. Three concentration levels of each glycosphingolipid and lyso-glycosphingolipid were evaluated on the effect of ATP synthase activity. The high level consisted of glycosphingolipids at 300 µmol/l a concentration based on plasma Gb_3 levels in Fabry patients with a severe disease phenotype. High level lyso-glycosphingolipids were ten times

less concentrated than their acylated counterparts at 30 µmol/l. The medium level comprised glycosphingolipids at a concentration of 30 µmol/l based on plasma Gb_3 levels in Fabry patients with a mild disease phenotype. Medium level lyso-glycosphingolipids were one-hundred times less concentrated than their acylated counterparts at 0.3 µmol/l. The low level consisted of glycosphingolipids at a concentration of 0.3 µmol/l based on plasma Gb_3 levels in a healthy control group. The low level lyso-glycosphingolipids were one-hundred times less concentrated than their acylated counterparts at 0.003 µmol/l. A control sample was also analysed, this was prepared in the same way as all samples (section 2.2.7.9) but without the addition of any lipid or lyso-glycosphingolipid.

5.2.4.1 The effect of glycosphingolipids on ATP synthase activity

Following the analysis of the effect of seven lipids at three concentration levels on ATP synthase activity, using students *t*-test statistically significant increases were observed with the highest concentrations of cardiolipin ($p < 0.01$), GM_1 ganglioside ($p < 0.007$), Gb_3 ($p < 0.006$), sulfatide ($p < 0.04$) and lactosylceramide ($p < 0.006$) (Figure 5.17). Statistically significant increases in ATP synthase activity were also observed with the medium concentration level of cardiolipin ($p < 0.002$), GM_1 ganglioside ($p < 0.0003$) and lactosylceramide ($p < 0.003$). In addition, a statistically significant increase was observed with the lowest level of cardiolipin ($p < 0.01$), this was the only compound to cause a statistically significant increase at the low concentration.

5.2.4.2 The effect of lyso-glycosphingolipids on ATP synthase activity

Following analysis of the effect of six lyso-glycosphingolipids at three concentration levels on ATP synthase activity, a number of statistical and significant increases were observed (Figure 5.18). The highest concentration of lyso-glycosphingolipids displayed the most effect on ATP synthase activity with statistical and significant increases observed with lyso-GM_1 ganglioside ($p < 0.00007$), lyso-Gb_3 ($p < 0.003$), lyso-sulfatide ($p < 0.0003$), lyso-lactosylceramide ($p < 0.0001$) and lyso-glucosylceramide ($p < 0.009$). Statistical and significant increases were also observed with the medium level lyso-GM_1 ganglioside ($p < 0.001$), lyso-Gb_3 ($p < 0.002$) and lyso-glucosylceramide ($p < 0.01$). No statistically significant increases were observed with any of the lowest level lyso-compounds.

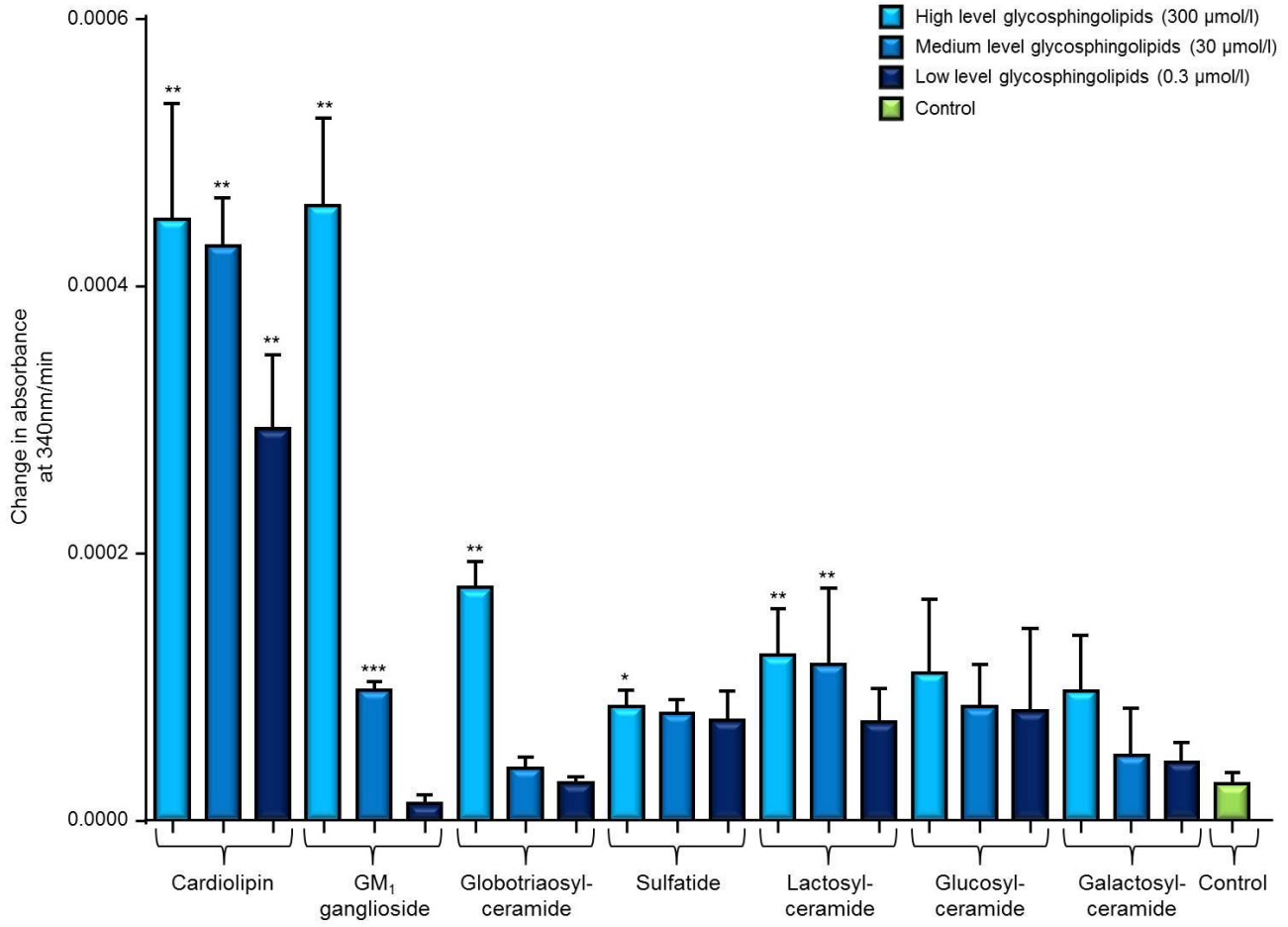

Figure 5.17 The effect of various lipids at high, medium and low concentrations on ATP synthase activity in a mitochondrial preparation from rat liver. Data expressed as mean ± standard deviation. * $p < 0.05$, ** $p < 0.01$, *** $p < 0.001$

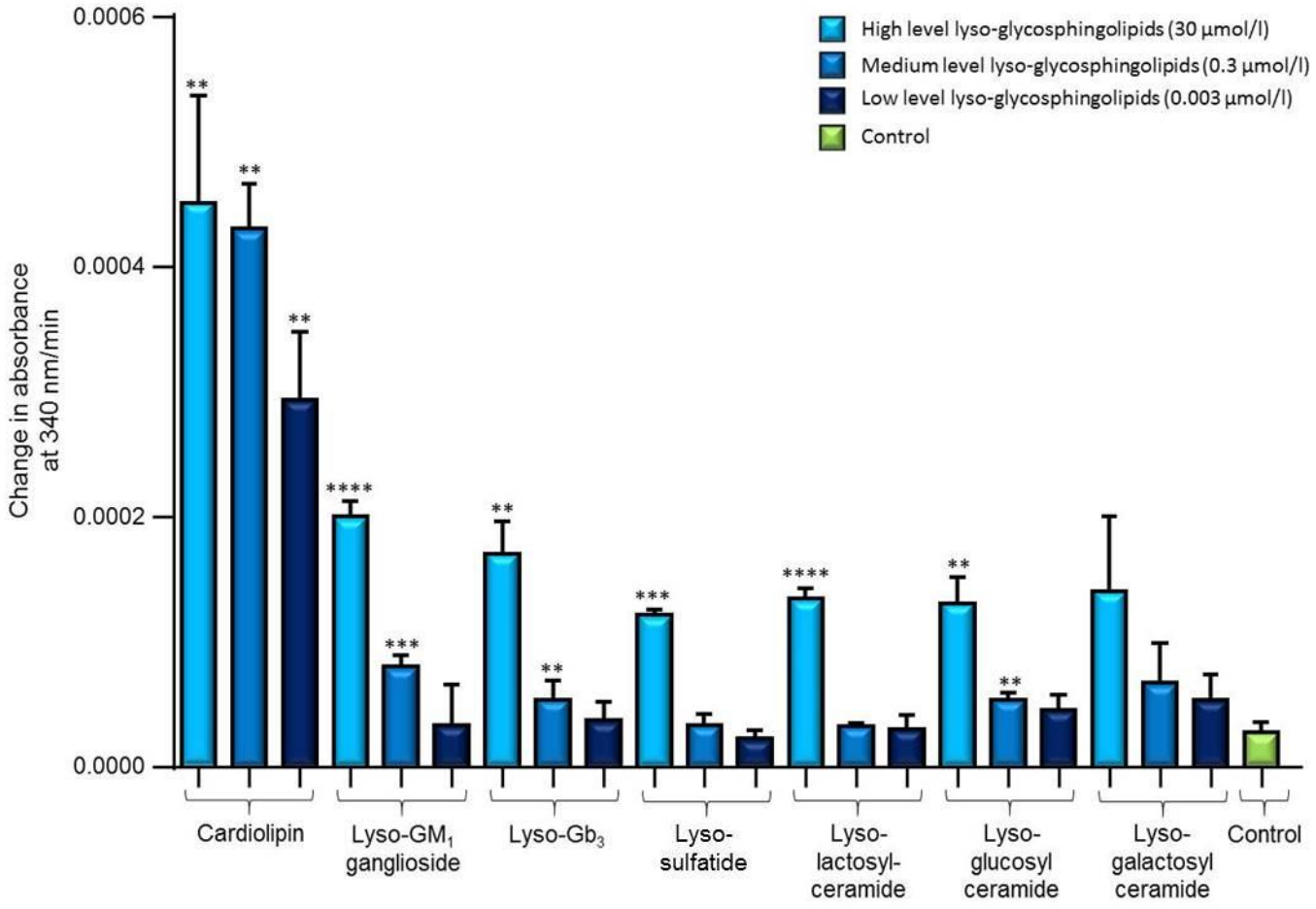

Figure 5.18 The effect of various lyso-glycosphingolipids at high, medium and low concentrations on ATP synthase activity in a mitochondrial preparation from rat liver. Data expressed as mean ± standard deviation. ** $p < 0.01$, *** $p < 0.001$, **** $p < 0.0001$

5.2.4.3 The effect of high level glycosphingolipids on ATP synthase activity in comparison to their deacylated counterparts

When the effect of high level glycosphingolipids are compared with that of high level lyso-glycosphingolipids (Figure 5.19), it appears that with the exception of GM_1 ganglioside and sulfatide and their deacylated counterparts, that most high level compounds induce similar increases in ATP synthase activity. GM_1 ganglioside and cerebroside however, were shown to exhibit a 4.6-fold and 2.7-fold greater effect on ATP synthase activity than their deacylated counterparts. In addition, GM_1 ganglioside was the only glycosphingolipid to affect ATP synthase activity to a similar extent as shown by cardiolipin. When interpreting these results consideration must however be made to the fact that the high level of glycosphingolipids assessed in this study was ten times more concentrated than that of the corresponding high level of lyso-glycosphingolipids.

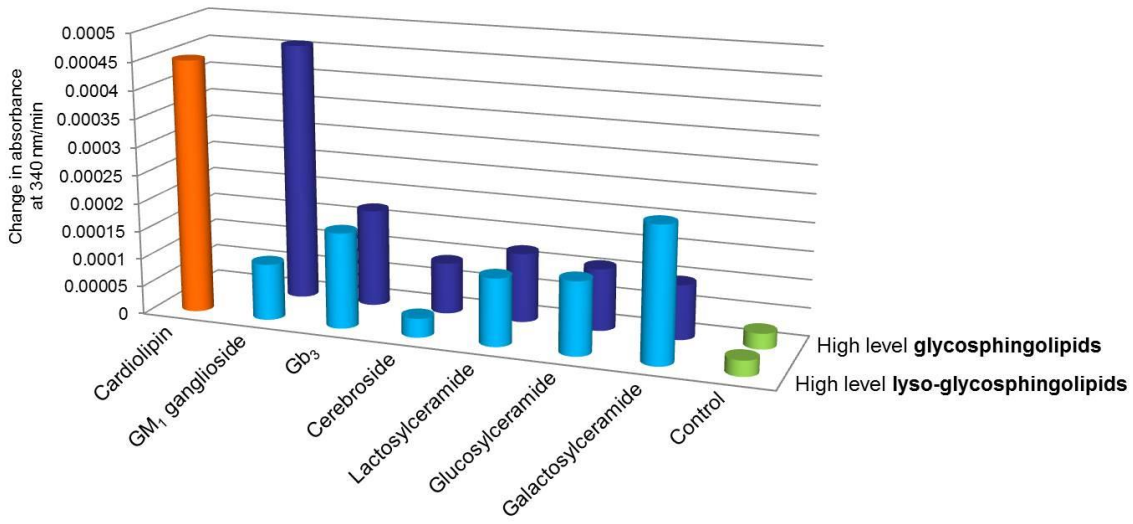

Figure 5.19 A graph showing the effect of high level glycosphingolipids (back row) on ATP synthase activity in comparison to high level lyso-glycosphingolipids (front row).

5.2.4.4 The effect of medium level glycosphingolipids on ATP synthase activity in comparison to their deacylated counterparts

When the effect of medium level glycosphingolipids on ATP synthase activity were compared against the effect of medium level lyso-glycosphingolipids (Figure 5.20), lyso-Gb_3 and lyso-galactosylceramide were shown to produce more of an effect on ATP synthase activity than their acylated counterparts. In contrast lactosylceramide was shown to increase ATP synthase activity 3.5-fold more than its deacylated counterpart. It is of interest that at the medium level GM_1 ganglioside did not exhibit as great an effect on ATP synthase activity as cardiolipin, as observed at the high concentration. Consideration must again be made to the fact that the medium level glycosphingolipids used in this study were one-hundred times more concentrated than the medium level lyso-glycosphingolipids.

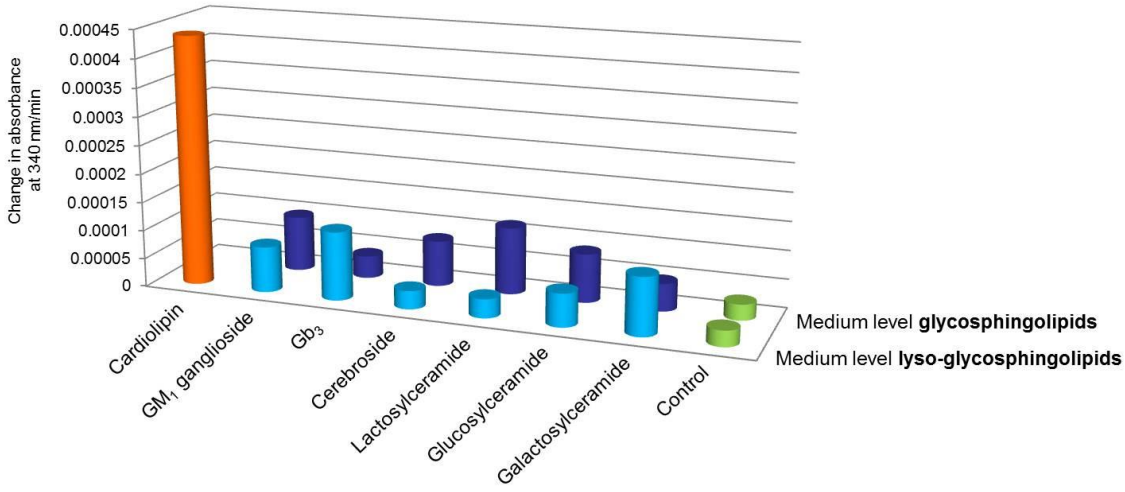

Figure 5.20 A graph showing the effect of medium level glycosphingolipids (back row) on ATP synthase activity in comparison to medium level lyso-glycosphingolipids (front row).

5.2.4.5 The effect of low level glycosphingolipids on ATP synthase activity in comparison to their deacylated counterparts

Although no significant differences between the low level glycosphingolipids or their acylated counterparts and the control were observed some differences between the acylated and deacylated groups were noted. Lyso-GM_1 and lyso-Gb_3 were shown to have a greater than 2.0-fold increase on ATP synthase activity compared to their acylated counterparts. This was not so for lactosylceramide where a 3.3-fold increase in ATP synthase activity was seen compared to that of lyso-lactosylceramide. This pattern was the same as that observed at the medium concentration for this compound. It should be noted that the low level concentration of glycosphingolipids were one-hundred times more concentrated than that of the low level lyso-glycosphingolipids.

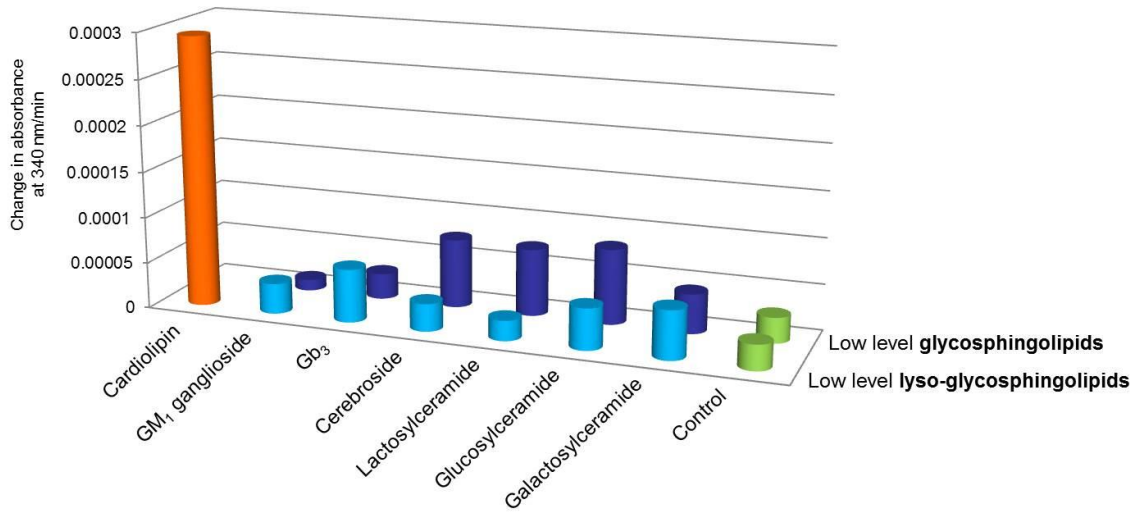

Figure 5.21 A graph showing the effect of low level glycosphingolipids (back row) on ATP synthase activity in comparison to low level lyso-glycosphingolipids (front row).

5.2.5 The effect of glycosphingolipids on behavioural measures of pain thresholds in mice

Of particular interest during the protein: glycosphingolipid interaction study was the discovery that voltage dependent anion selective channel protein 1 bound to three glycosphingolipids (Gb_3, galactosylceramide and ceramide). In addition, one protein potassium voltage-gated channel subfamily H, member 1 was detected to bind exclusively to Gb_3. As voltage-gated potassium channels have been associated with neuropathic pain (Wood *et al.*, 2004) and patients with Fabry disease are afflicted with neuropathic pain from an early stage of disease progression, the effect of Gb_3 and lyso-Gb_3 on behavioural measures of pain thresholds was investigated in a mouse model using a von Frey assay (section 2.2.7.4).

5.2.5.1 Von Frey nociception assay

Subject mice were assigned an identification key and placed into a test group (section 2.2.7.8.2). The Gb_3 test group (n = 9) received a 300 µmol/l solution injection of Gb_3, which is the equivalent of Gb_3 plasma concentrations observed in patients with a severe disease phenotype. The lyso-Gb_3 test group (n = 9) received a 30 µmol/l solution injection of lyso-Gb_3 and the control test group (n = 6) received an injection of saline. All injections were received into the plantar surface of the right hind paw of the mouse. Following the injection of Gb_3 or lyso-Gb_3, or the injection of saline as a control the reactions of the mice were monitored immediately and then 0.5, 1, 2, 4, 6 and 24 hr post-injection (Figure 5.22).

Following analysis using students *t*-test statistically significant differences were

observed between the Gb_3 and control group at the 0.5 ($p < 0.02$), 2 hr ($p < 0.004$) and 4 hr ($p < 0.03$) post injection time points. Statistically significant differences were also observed between the lyso-Gb_3 and control group at the 0.5 ($p < 0.01$), 1 hr ($p < 0.03$), 2 ($p < 0.0003$) and 4 ($p < 0.002$) hr post injection time points. No differences were observed between the Gb_3 and lyso-Gb_3 groups. These results demonstrate that the mechanical nociceptive threshold of mice, following injection with 300 µmol/l Gb_3 or 30 µmol/l lyso-Gb_3, is reduced statistically and significantly compared to that of a control group. This results in the mice becoming more sensitive to the pain of the applied mechanical stimulus.

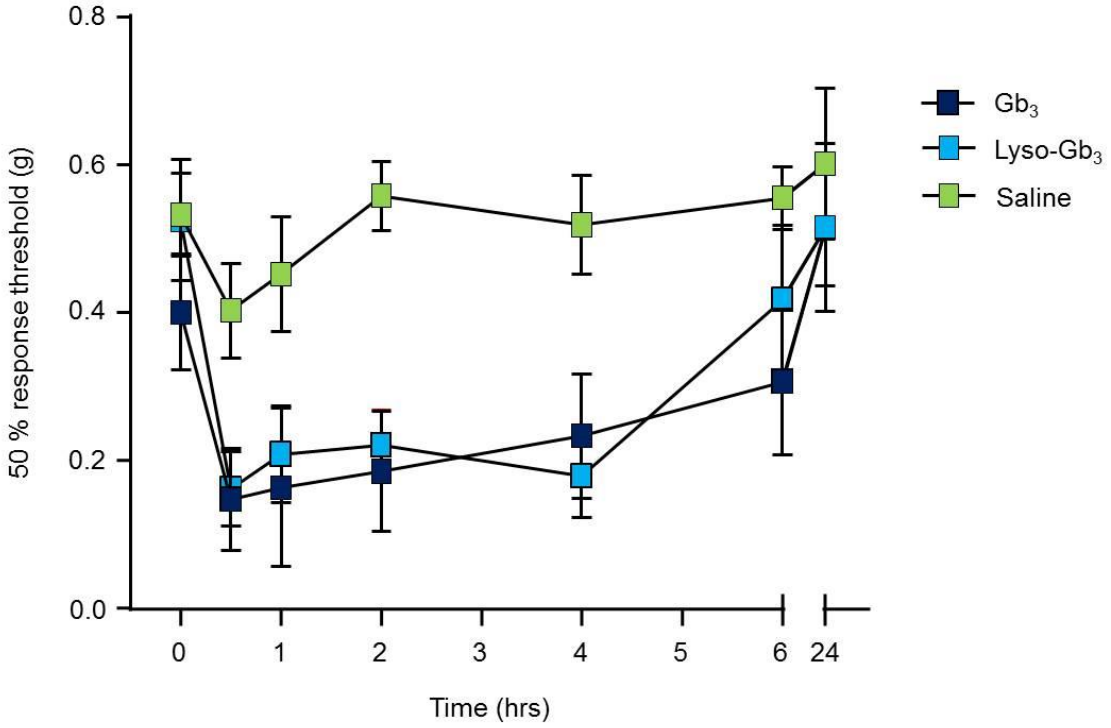

Figure 5.22 The effect of Gb_3 and lyso-Gb_3 on behavioural measures of pain thresholds as assessed by the von Frey assay.

5.3 Discussion

In recent years much progress has been made in defining the molecular basis of genetic diseases in humans. However, in some diseases, such as Fabry disease, this has not translated into an appreciable increase in the understanding of the underlying mechanisms associated with disease pathology. The use of authentic animal models is required to enable studies to expand our knowledge of the underlying pathological mechanisms associated with disease. Although the phenotype exhibited by Fabry mice is discreet, this has not prevented its use in a number of preclinical studies (Ioannou *et al.*, 2001) where assessment of Gb_3 concentrations in plasma and various tissue types, and its reduction following treatment, have provided the predominant outcome measures (Marshall *et al.*, 2010; Choi *et al.*, 2010; Ogawa *et al.*, 2009).

Using a UPLC-MS/MS method statistically significant increases in the concentrations of Gb_3 and lyso-Gb_3 in liver, kidney, heart and brain tissues obtained from male and female Fabry knockout mice was demonstrated (Figure 5.1 and 5.2). This confirmed that an accumulation of these toxic metabolites was present and hence the organs were suitable for subsequent investigations in this study. Interestingly, the ratio of Gb_3 to lyso-Gb_3 was higher in liver (27:1), kidney (40:1) and heart (54:1) tissues. However, in the brain the concentration of lyso-Gb_3 was higher than that detected in other tissue types resulting in a ratio of 1:1 with Gb_3. Various hypotheses have been suggested as to the origin of lyso-Gb_3 including, its spontaneous formation from stored Gb_3, active formation by the action of a specific enzyme and formation by sequential glycosylation of sphingoid bases (Aerts *et al.*, 2008). However, as yet the origin of lyso-Gb_3 remains unknown despite numerous studies to identify the ‘elusive

deacylase'. The higher Gb_3 to lyso-Gb_3 ratio as seen in liver, kidney and heart in this study may be suggestive of a lower 'deacylase' activity or availability in these organs. Alternatively, the increased levels of lyso-Gb_3 observed in brain tissue compared to other tissues analysed in this study may support the findings of Kobayashi *et al.*, (1992) which suggest, based on the analysis of sphingoid base composition in brain tissue from patients with GM_1 or GM_2 gangliosidosis, that elevated levels of lysosphingolipids might originate from biosynthesis and not from deacylation of corresponding sphingolipids. In addition, biosynthesis of galactosylsphingosine from sphingosine has also been reported (Cleland and Kennedy 1960; Vanier and Svennerholm 1976).

Following the proteomic profiling of Fabry mouse tissues using label-free quantitative proteomics, a number of protein alterations were detected in the tissues of male and female Fabry mice. These alterations were confirmed with the use of two data analysis software platforms. The first software used was "ProteinLynx" and provides absolute quantitation based on the peak intensities of identified proteins and their comparison to the peak intensities of an added known peptide acting as an internal standard. The second software package "Progenesis LC-MS", provides relative quantification based on the ion intensities recorded in the MS data. Differences in the identification of proteins obtained during this study are most likely due to differences in the processing parameters available from the software packages as well as thresholds and cut-off values used in the data analysis. An advantage of using ProteinLynx to obtain identifications is that absolute quantitation of data is achievable compared to relative quantitation obtained with Progenesis LC-MS. Both analysis methods enable quantification of peptide ions without MS/MS data, this is achieved by analysing data at the LC-MS rather than the MS/MS level to

locate peaks exhibiting significant expression change between experiment groups. However, Progenesis LC-MS is designed to avoid 'missing data' thereby minimising the technical error and improving quantitative precision. Each software package uses different methods of inferring the protein quantitation from the peptide ions in order to calculate the numeric and ultimately, there are pros and cons associated with using both software programs. Therefore, in this study proteins that were found to be altered by each methodology were cross-referenced revealing those proteins found to be altered using both software platforms, and therefore providing an enhanced level of confidence in the identification, to be selected for further investigation.

Of the proteins detected to be altered in male and female Fabry mice by both software platforms, ATP synthase subunit beta (mitochondrial) was found to be increased in both liver and kidney tissues. Another subunit of ATP synthase, ATP synthase subunit alpha (mitochondrial) was also found to be increased in heart tissue. ATP synthase (complex V; Figure 5.23) is a highly complex enzyme responsible for the synthesis of ATP from ADP in the mitochondrial matrix using the energy provided by the proton electrochemical gradient which is generated by complexes I, III and IV of the electron transport chain. ATP synthase consists of two functional domains, F_1 which contains the extramembraneous catalytic core, and F_0 which contains the membrane proton channel. The two domains are linked together by a central and peripheral stalk. The catalytic domain F_1 is composed of three copies of each alpha and beta subunit, both of which were detected as elevated in Fabry disease mouse tissues during the proteomic profiling study. During catalysis, ATP synthesis in the F_1 domain, is coupled via a rotary mechanism of the central stalk subunits (gamma, delta and epsilon) to proton translocation. Rotation of the central stalk

against the surrounding alpha and beta subunits leads to hydrolysis of ATP in three separate catalytic sites on the beta subunits. The inner mitochondrial membrane phospholipid, cardiolipin, binds tightly to complex V and is essential for its catalytic and structural operation. This reaction is however reversible and when the H^+ gradient across the mitochondrial inner membrane decreases ATP synthase can utilise ATP hydrolysis in the F_1 domain to induce the rotation of the F_0 rotor in the reverse direction thereby driving proton pumping (Orriss *et al.*, 1998; Stock, Leslie and Walker 1999; Walker and Dickson 2006).

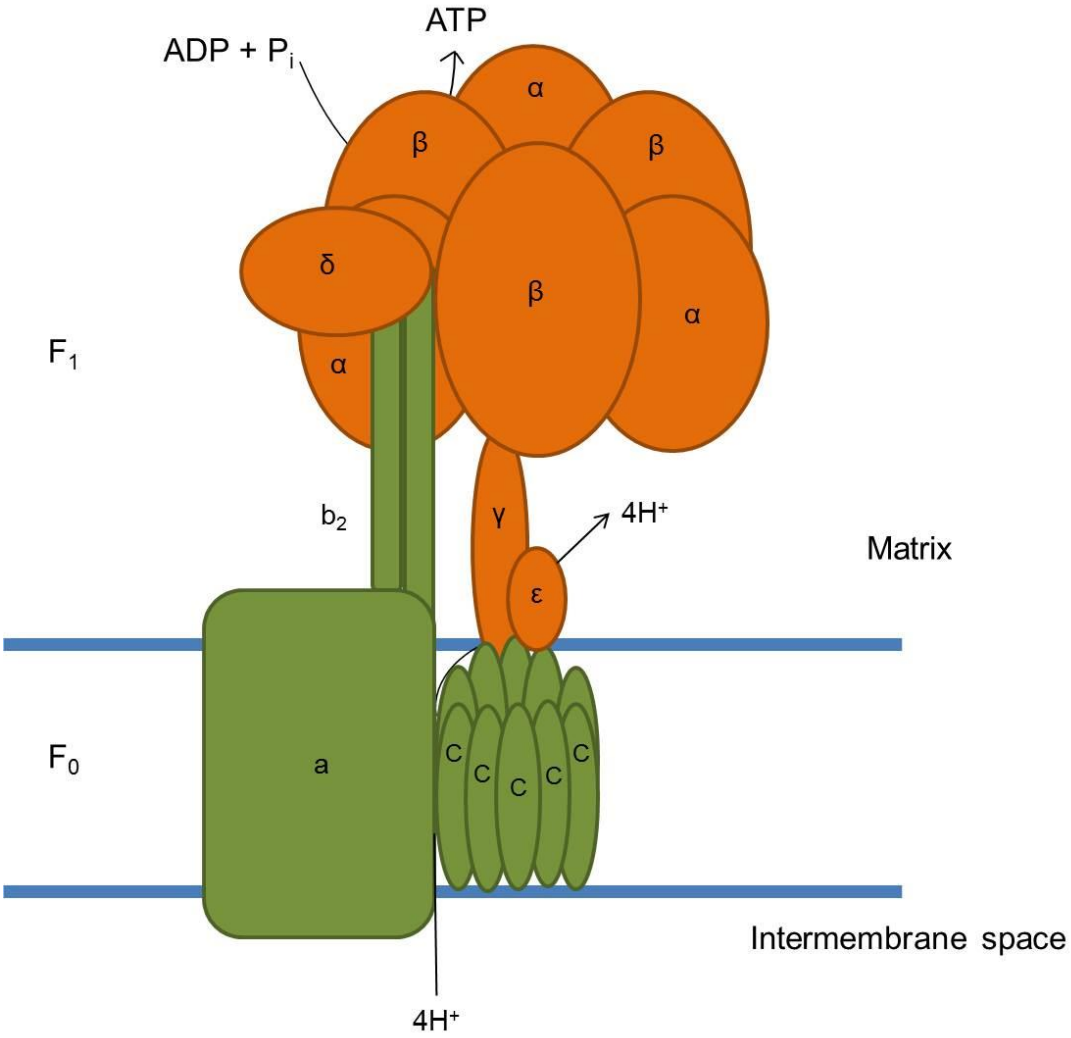

Figure 5.23 A schematic representation of mitochondrial ATP synthase (complex V) showing the architecture and subunit composition.

The only other protein found to be increased during the proteomic profiling study was ribonuclease UK114. This protein was found to be increased in both male and female Fabry mouse liver and kidney tissues, where it is reported to be expressed predominantly. Ribonuclease UK114 is an endoribonuclease that functions to inhibit translation by cleaving mRNA. This enzyme is also responsible for the cleavage of phosphodiester bonds in single stranded RNA and the inhibition of cell-free protein synthesis. Levels of ribonuclease UK114 have also been shown to be reduced in human hepatocellular carcinoma leading to the suggestion that this protein may be an important biomarker for hepatic carcinoma (Chong *et al.*, 2008).

In contrast to the increases detected in the levels of the mitochondrial proteins ATP synthase subunit alpha and ATP synthase subunit beta (mitochondrial), the other mitochondrial proteins of interest detected during this study, agmatinase, ATP-binding cassette, sub-family B, member 8 and long chain specific acyl CoA dehydrogenase, were found to be reduced. Agmatinase (mitochondrial) was reduced in the liver tissue of both male and female Fabry mice. This protein is responsible for the hydrolysis of agmatine to putrescine and urea. Reduced levels of this enzyme may therefore result in a build-up of agmatine which has been reported to stimulate hepatic fatty acid oxidation (Nissim *et al.*, 2006).

Long chain specific acyl CoA dehydrogenase (mitochondrial; LCAD) is one of the four enzymes that catalyses the initial step of mitochondrial beta-oxidation of straight chain fatty acids in mice (Chegary *et al.*, 2009) and this enzyme was found to be reduced in heart tissues of both male and female Fabry mice. Mitochondrial dysfunction has been shown to result in a reduction of the enzymes involved in beta-oxidation and importantly reduced cardiac fatty acid

oxidation has been proposed as a consequence of pathological left ventricular hypertrophy (Ingwall 2009; Ellis *et al.*, 2011), the most common cardiac abnormality experienced in patients with Fabry disease. In addition, in a mouse model of LCAD deficiency, 10% of male adult mice were shown to develop cardiomyopathy. Furthermore sudden death was observed in 3% of LCAD deficient mice (Kurtz *et al.*, 1998). This underlines the vital role of mitochondrial fatty acid oxidation and LCAD *in vivo*. The finding in this study that LCAD is reduced significantly in Fabry mice requires further investigation to establish if this enzyme could play a role in the underlying pathological mechanism of cardiomyopathy in Fabry disease.

The third mitochondrial protein shown to be altered, ATP-binding cassette sub-family B member 8, was found to be reduced in brain tissue and as yet the function of this ATP-dependent transporter has not been fully elucidated. However, it has been postulated to be involved in the transport of both organic and inorganic molecules out of the mitochondria. In a mouse model with loss of function for the related gene that encodes for this protein, a disruption of iron homeostasis between the mitochondria and cytosol has been demonstrated (Allikmets *et al.*, 1996).

Alpha-synuclein was also found to be reduced in male and female Fabry mouse brain tissue. This protein is highly abundant in brain and whilst the exact function of alpha-synuclein remains unclear it is known to be the major component in Lewy bodies and Lewy neurites (Marques and Outeiro 2012; Olanow and Brundin 2013). In contrast to the reduction of alpha-synuclein observed in this study, Nelson *et al.*, (2014) have reported an accumulation of an aberrant phosphorylated form of α-synuclein in the brain of α-Gal A deficient mice. Further studies are therefore required in order to validate these findings

before conclusions as to the implications for the neuropathology of Fabry disease can be made. Loss of alpha-synuclein, as detected in this study, has been observed in the aging mouse brain with one study suggesting that alpha-synuclein could contribute to, or be a marker of, synaptic dysfunction (Mak *et al.*, 2009). Synaptic dysfunction has been associated with depression (Duman and Aghajanian 2012), which is a frequent but under-recognised finding in Fabry disease, however as yet there are no reports linking synaptic dysfunction with depression in Fabry disease.

Further to the label-free proteomic profiling of Fabry mouse tissues those proteins of interest, i.e. those proteins shown by both analysis platforms as having alterations, were interrogated with the GO annotation system using the PANTHER website. By analysing the data in this way the molecular functions, biological processes and/or biological pathways that each protein is connected to is revealed thereby enabling common links between proteins to be established. Following this analysis six molecular functions were revealed to be associated with the proteins of interest. Three of these, catalytic activity, binding and transporter activity, were shown to involve proteins found to be increased, as well as proteins that were shown to be decreased, in the tissue in which they were detected. A possible explanation for this is the fact that each organ has a specific function and therefore a generalised increase or decrease in a molecular function such as transporter activity is unlikely. However, identifying increases or decreases in proteins associated with a molecular function and a specific tissue type could help elucidate underlying molecular mechanisms. Five of the six molecular functions revealed by the GO annotation system were shown to involve ATP synthase subunits alpha and beta (mitochondrial), both of which were found to be increased during the label-free analysis. This illustrates

what a critical role these proteins perform and reinforces the suggestion that increases in the levels of these proteins will most likely have an effect on molecular function. Interestingly, two molecular functions, ion channel and receptor activity, were shown to be associated with only the ATP synthase subunits, of the proteins of interest detected in the label-free study. Potential increases in these molecular functions could influence cellular and functional activities performed at the molecular level and potentially have a role in the underlying molecular mechanism of Fabry disease.

Nine biological processes were revealed from the GO annotation analysis to be associated with one or more of the proteins of interest detected during the label-free proteomic aspect of the study. Each biological process is a collection of multiple molecular events pertinent to the correct functioning of cells, tissues and organs. The proteins alpha synuclein and ATP-binding cassette, sub-family B, member 8 (mitochondrial), both of which were found to be decreased in Fabry mouse brain tissue, were shown to be involved in seven of the nine biological processes revealed. A number of these biological processes including immune system response, cell communication and response to stimulus have been shown to be involved with the nervous system (Kawli, He and Tan 2010; Susuki K 2010). A number of neurological manifestations including peripheral and central nervous system involvement have been described in patients with Fabry disease (Schiffmann and Moore 2006) and therefore it seems probable that a decrease in a protein involved in one or multiple steps of a biological process will have an effect on the optimal operation of that process resulting in biological consequences.

Of the seven proteins of interest identified during the label-free analysis three were found to be involved in biological pathways using the GO annotation

system. ATP synthase subunits alpha and beta (mitochondrial) are heavily involved in the ATP synthesis pathway and the role that these subunits have within ATP synthase (complex V) and ATP synthesis has been discussed. The third protein, alpha synuclein, was shown to be involved in the Parkinson's disease pathway. This protein was found to be decreased in Fabry mouse brain tissue and could support the observations that neurodegeneration is not a prominent feature in Fabry disease, unlike some of the other lysosomal storage disorders (Jeyakumar *et al.*, 2005). However, a common factor that these diseases do share is that both are associated to be protein-misfolding disorders (Garman 2007). The literature describes only two patients with both Fabry disease and Parkinson's disease (Orimo *et al.*, 1994; Buechner *et al.*, 2006) nevertheless one of these studies postulates that Fabry disease may provoke Parkinsonism as a result of some of the common neurological manifestations observed in Fabry disease including lacunas in the basal ganglia and Gb_3 accumulation in the substantia nigra (Buechner *et al.*, 2006). These suggestions may be supported by Nelson *et al.*, (2014) where in a recent study the accumulation of aberrant phosphorylated-α-synuclein in the brains of α-Gal A deficient mice was demonstrated. However, further investigations are required to fully understand the implications of these findings not only on the neuropathology associated with Fabry disease but also before any potential links between Fabry disease and the pathogenesis of age-related neurodegenerative disorders such as Parkinson's disease can be made.

Following the proteomic profiling aspect of this study two novel protein: glycosphingolipid interaction methodologies were used in order to identify proteins that interact solely with Gb_3 and also proteins that interact with a group of glycosphingolipids to gain an understanding of the underlying disease

mechanisms associated with Fabry disease and other lysosomal storage disorders in the glycosphingolipid biosynthetic pathway (Figure 1.2). The first methodology used a novel method based on RS100 ProteinChip technology to bind deacylated or 'lyso' versions of the glycosphingolipid of interest through a C12-linker arm. The second, Dynabead® M-270 epoxy methodology, uses similar principles to bind deacylated glycosphingolipids to beads, rather than a ProteinChip, and through a C5 rather than a C12-linker arm. Thus, the classes of proteins binding to each array differ by their affinities to the hydrophobicities of the acyl moiety of the glycosphingolipids (C5 versus C12). Both methodologies effectively restore the deacylated glycosphingolipids to their acylated counterparts. However, it should be noted that in both protein: glycosphingolipid methodologies an inherent limitation of binding the glycosphingolipids to the surface of the chip/beads through the fatty acid group is that the number of interactions available with this portion of the molecule are limited. Consequently, some interactions will not be able to be formed and subsequently detected. However, the carbohydrate region which is unique to each of the molecules and the sphingosine moiety, which is common to each of the molecules, are readily available for interaction. In this study, many more protein interactions were identified using the RS100 ProteinChip than the Dynabead® M-270 epoxy methodology. There could be a number of reasons for this including the fact that the RS100 ProteinChip binds through a C12 rather than a C5-linker arm, as used in the Dynabeads® M-270 Epoxy methodology. This may suggest that binding interactions are more readily formed when a longer acyl moiety is available. Other possibilities for the differences between the two methodologies may be that control mouse brain tissue was used with the RS100 ProteinChip and control mouse kidney tissue was used with the

Dynabeads®, and therefore a direct comparison of the interactions observed with each methodology may be inappropriate. Furthermore, although PBS was used to control for any for non-specific binding with both methodologies, the high number of interactions identified with the RS100 ProteinChip suggests that a more stringent wash procedure may be required with this methodology. Unfortunately, due to time constraints optimisation of binding conditions in order to minimise non-specific binding was not possible for the purpose of this thesis. However, before further experimentation using this methodology is performed optimum binding conditions should be established.

Following the exclusion of those proteins displaying non-specific binding, using both analysis methods, three common interactions were detected. The proteins beta-actin-like protein 2 and tubulin alpha-1B chain were detected to bind only to GM_1 ganglioside and aspartate aminotransferase (mitochondrial) was detected to bind to both Gb_3 and GM_1 ganglioside. In addition, a number of mitochondrial proteins were revealed to interact with the glycosphingolipids using both methods. Interestingly, no lysosomal proteins (e.g. saposins) and associated lysosomal pathways were detected during the protein: glycosphingolipid binding experiments. This suggests that in order to identify these interactions may require experimentation under acidic conditions representative of that of the lysosome.

During the RS100 ProteinChip analysis, proteins that interacted with Gb_3 and/or GM_1 ganglioside in control mouse brain tissue were identified. Of the 157 proteins detected in total as binding to Gb_3 and/or GM_1 ganglioside during the study, 32 proteins were found to interact with both glycosphingolipids. Interestingly, 3 proteins detected during the proteomic profiling study, ATP synthase subunit alpha (mitochondrial), ATP synthase subunit beta

(mitochondrial) and alpha-synuclein were also found to bind to both Gb_3 and GM_1 ganglioside. All proteins that interact with Gb_3 and/or GM_1 ganglioside were subsequently classified according to the GO annotation system using the PANTHER website to enable proteins to be grouped according to common functions, processes or pathways. This analysis identified the most common molecular functions associated with proteins that bind to Gb_3 and/or GM_1 ganglioside to be catalytic activity and binding. Following further interrogation of the catalytic activity category most proteins were found to possess hydrolase, transferase and/or oxidoreductase activities. Proteins that bound to Gb_3 and/or GM_1 ganglioside and possessed binding activity were also able to be further subdivided showing that most proteins detected were protein binding proteins.

When the biological processes associated with the proteins identified as binding to Gb_3 and/or GM_1 ganglioside were defined, the most proteins detected were found to be associated with metabolic processes. When this category was further sub-divided, the most common sub-category was nucleobase, nucleoside, nucleotide and nucleic acid metabolic processes. Other common metabolic processes associated with the proteins that bind to Gb_3 and/or GM_1 ganglioside included carbohydrate and protein metabolism. It is not unexpected that proteins responsible for these metabolic processes would interact with glycosphingolipids that accumulate as a result of a deficiency of a lysosomal enzyme as in addition to these lipids the lysosome is responsible for the catabolism of various proteins, carbohydrates and nucleic acids via a variety of acid hydrolases. Interestingly, three categories of biological processes, nitrogen compound metabolic processes, lipid metabolic processes and cell adhesion were all found to contain proteins that bound only to GM_1 ganglioside.

The proteins identified as binding to Gb_3 and/or GM_1 ganglioside were found to be associated with a large number of biological pathways, with most proteins detected found to be connected to the Huntington disease biological pathway. Huntington's disease is a progressive neurodegenerative disorder and recently a link between lysosomal dysfunction and neurodegenerative diseases such as Huntington's, as well as Parkinson's disease and Alzheimer's disease, has been shown (Usenovic and Krainc 2012). In addition, similaraties also exist between the dyshomeostasis of Ca^{2+} and/or the mitochondrial stress that is involved in Huntington's disease with that observed in lysosomal storage disorders (Giacomello, Hudec and Lopreiato 2011). Interestingly, like Fabry disease and Parkinson's disease, Huntington's disease is also associated with protein mis-folding (Garman 2007). Of the proteins detected to be involved in the Huntington's disease pathway more were found binding to GM_1 ganglioside than Gb_3. The age of onset of GM_1 gangliosidosis type III and some of the clinical features including dystonia and parkinsonian features are the same as that experienced in Huntington's disease (Roze *et al.*, 2005; Louis *et al.*, 1999).

Another biological pathway involving a number of proteins was glycolysis. The free energy released during glycolysis is used to form ATP and NADH and as many proteins that interact with Gb_3 and/or GM_1 ganglioside have been identified as mitochondrial proteins or possessing catalytic activity involving ATP it is unsuprising that this biological pathway is one which most proteins are commonly assigned to by the GO annotation system.

A second, complimentary protein: glycosphingolipid interaction study used Dynabeads® M-270 epoxy to identify proteins that interacted with Gb_3 and a wider range of glycosphingolipids in control mouse kidney tissue. Of the proteins identified binding to Gb_3 using this methodology a common association

with ATP was revealed with two proteins found to interact selectively and covalently with ATP and another functioning in the mitochondrial respiratory chain from which ATP is generated. In a study by Lücke *et al.*, (2004) mitochondrial respiratory chain enzyme activities were investigated in fibroblasts from Fabry patients. This study demonstrated disruption of the mitochondrial respiratory chain enzymes (investigated and discussed in Chapter 6) but no significant alteration in ATP production was shown.

The glycosphingolipid that most proteins were detected binding to was galactosylceramide and of the proteins detected binding to this glycosphingolipid, three were found to be peroxisomal proteins. This was of particular interest as in a study by Khan *et al.*, (2005), in which the effects of galactosylceramide on peroxisomal function and the relationship with reactive oxygen species were investigated, peroxisomal beta-oxidation was shown to be inhibited and very long chain fatty acids and free radicals were shown to be increased in cells treated with galactosylceramide. The study concluded that inhibition of peroxisomal function and increased free radical production by galactosylceramide may be partly be responsible for the oligodendrocyte and myelin loss observed in Krabbe's disease (Khan *et al.*, 2005).

Whilst the proteins found to interact with GM_1 ganglioside were limited, a common connection involving all three proteins with energy metabolism was established however, no other common connections could be determined. Unfortunately the limited number of proteins detected to interact with ceramide was not sufficient to establish any further relationship between functions, processes or pathways beyond that of both proteins possessing binding capacity.

Of the proteins detected as interacting with more than one glycosphingolipid using the Dynabeads® one, aspartate aminotransferase (mitochondrial) was found to interact with both Gb_3 and GM_1 ganglioside. This protein was also detected to bind to both Gb_3 and GM_1 ganglioside when these glycosphingolipids were immobilised on an RS100 ProteinChip. Aspartate aminotransferase is responsible for the catalysis and irreversible transamination of the L-tryptophan metabolite, L-kynurenine to form kynurenic acid. In addition, this protein is involved in amino acid metabolism, metabolite exchange between the mitochondria and the cytosol and facilitates the cellular uptake of long-chain fatty acids (Zhou *et al.*, 1998). Aspartate aminotransferase levels are frequently used to diagnose myocardial infarction and viral hepatitis. Increases in aspartate aminotransferase levels have been reported in a small number of patients with Fabry disease treated with the ERT preparation Fabrazyme (Genzyme Corporation) (eHealthMe 2004). However, in a preclinical efficacy and safety study of 1-deoxygalactonojirimycin in mice for Fabry disease, levels of aspartate aminotransferase were unchanged (Ishii *et al.*, 2009). Likewise a study by Ohshima *et al.*, (1999) found no changes in aspartate aminotransferase levels in Fabry mice. Interestingly, activities of aspartate aminotransferase have also been shown to be increased in the cerebrospinal fluid (CSF) of dogs with GM_1 gangliosidosis, leading to the suggestion that it be used as a biomarker to assess central nervous system degeneration in this animal model (Satoh *et al.*, 2007).

Another protein was found to interact with two glycosphingolipids, NADH dehydrogenase [ubiquinone] iron sulfur protein 6 (mitochondrial), interacted with both Gb_3 and galactosylceramide. This protein is an accessory subunit of the mitochondrial respiratory chain enzyme, complex I but is not believed to be

involved in catalysis. Complex I activity has been shown to be reduced significantly in fibroblasts from Fabry patients (Lücke *et al.*, 2004). In addition, galactosylsphingosine has been shown to inhibit complex I by interacting at this site and causing a change in the lipid environment of the membrane which is ultimately responsible for the mitochondrial dysfunctions observed to be induced by galactosylsphingosine (Tapasi, Padma, and Setty 1998).

Although no protein was found to bind to all four glycosphingolipids when bound to the Dynabeads®, one protein, voltage dependent anion selective channel protein 1 (VDAC1), was found to interact with Gb_3, galactosylceramide and sulfatide. This protein forms a channel through the mitochondrial membrane to allow the diffusion of small hydrophilic molecules and also through the plasma membrane where it is involved in regulation of cell volume and apoptosis. In addition, VDAC has been shown to be involved in the transport of ATP, ADP, pyruvate and other metabolites. A number of ATP-dependent enzymes have all been found to bind VDAC (Törnroth-Horsefield and Neutze 2008). VDAC is also an important regulator of Ca^{2+} transport in and out of the mitochondria (Báthori *et al.*, 2006).

Another ion channel, potassium-voltage gated channel subfamily H member 1, was found to bind explicitly to Gb_3. Voltage-gated ion channels are associated with neuronal excitability and voltage-gated potassium channels (K_V) have been shown to be important regulators of membrane potentials, action potential shape and firing adaptation in excitable tissues including nociceptive sensory neurons. Injury and inflammation of peripheral nerves has been shown to reduce the densities of potassium-voltage gated channels implicating them in the development of neuropathic/inflammatory pain (Takeda *et al.*, 2011). As neuropathic pain is one of the most frequent, early and debilitating clinical

manifestations experienced in patients with Fabry disease and this K_V channel was found binding explicitly to Gb_3, the effect of Gb_3 and in addition lyso-Gb_3, on pain thresholds in mice was assessed using a von Frey assay. This assay was performed by Professor John Woods molecular nociception group at UCL as part of a collaborative project.

The results of this study demonstrated that the injection of either Gb_3 or lyso-Gb_3 into the hind paw of a mouse results in a significant increase in sensitivity to mechanical stimuli. Statistically significant increases in sensitivity were obtained using students *t*-test, 0.5, 1, 2 and 4 hrs post injection, with the highest degree of sensitivity observed at the 2 hr post injection time point. Increases in sensitivity continued to be observed 6 hrs post injection, although not to the point of statistical significance and sensitivity 24 hrs post injection had reverted back to almost baseline/control responses. No difference in the effect on sensitivity between injection with Gb_3 or lyso-Gb_3 was observed when each metabolite was injected at a high concentration level. The high Gb_3 concentration level used in this study is the equivalent to those levels observed in the plasma of Fabry patients with a severe disease phenotype. However, in order to assess sensitivity, using this methodology, required the injection of lyso-Gb_3, at levels although one-hundred times less concentrated than that of Gb_3 are significantly more concentrated than lyso-Gb_3 levels observed *in vivo*. Injection at these concentrations resulted in almost identical pain thresholds between the two metabolites suggesting that lyso-Gb_3 is one-hundred times more potent in creating a pain response than Gb_3. However, it is unlikely that lyso-Gb_3 levels *in vivo* would ever reach concentrations as high as those used in this study. Therefore, this finding may suggest that *in vivo* Gb_3 is responsible

for the nociceptive pain experienced in Fabry disease however, this requires further investigation.

Of particular interest during this study was the observation that ATP synthase subunits alpha and beta (mitochondrial) were increased in either the heart or liver and kidney tissues from male and female Fabry mice. In addition, these subunits were found to bind to both Gb_3 and GM_1 ganglioside when immobilized on the RS100 ProteinChip. As a result the effect of several glycosphingolipids in the glycosphingolipid biosynthetic pathway and their corresponding deacylated or 'lyso' counterparts, were assessed regarding their effect on ATP synthase activity. In addition, as a comparison the effect of cardiolipin, a complex phospholipid found almost exclusively in the inner mitochondrial membrane and required to maintain ATP synthase (complex V) structure and function was also assessed as a positive control molecule (Lee 1995).

Following the assessment of all lipids on complex V activity at high, medium and low concentrations the phospholipid cardiolipin, as expected, was shown to produce the most pronounced effect. Statistically significant increases in ATP synthase activity were observed at all concentration levels tested which are most likely as a result of the phospholipids high binding affinity for complex V.

At the highest concentration level assessed the glycosphingolipids GM_1 ganglioside, Gb_3, sulfatide and lactosylceramide were all shown to increase significantly ATP synthase activity. In addition, all lyso-glycosphingolipids, with the exception of lyso-galactosylceramide, were also shown to increase significantly ATP synthase activity. When the effect of high level glycosphingolipids were compared with the effects of high level lyso-glycosphingolipids on ATP synthase activity most high level compounds were shown to induce similar effects on ATP synthase activity. The exceptions to this

were the glycosphingolipids GM_1 ganglioside and sulfatide which were shown to increase ATP synthase to a greater extent than their deacylated counterparts. Furthermore, at this high concentration level GM_1 ganglioside was the only glycosphingolipid to effect ATP synthase activity to a similar extent as that shown by cardiolipin. Interestingly, this was only observed at the high concentration level and not at the medium or low concentration levels used in this study.

When the medium concentration level of compounds were assessed, only GM_1 ganglioside and lactosylceramide were shown to increase significantly ATP synthase activity. Of the lyso-glycosphingolipids, lyso-GM_1, lyso-Gb_3, and lyso-glucosylceramide were also found to increase significantly ATP synthase activity. On comparison of the effects of glycosphingolipids and their deacylated counterparts lyso-Gb_3 and lyso-galactosylceramide were shown to have more of an effect on ATP synthase activity. However, the opposite was so for lactosylceramide, with this glycosphingolipid producing more of an effect on ATP synthase activity that its deacylated counterpart.

No significant increases in ATP synthase activity were demonstrated using any glycosphingolipid or lyso-glycosphingolipid at the lowest concentration level assessed. However, lyso-Gb_3 and lyso-GM_1 were shown to increase ATP synthase activity to a greater extent than their acylated counterparts. As observed at the medium concentration level lactosylceramide produced more of an effect on ATP synthase activity than lyso-lactosylceramide.

As the levels of lyso-glycosphingolipids used to assess the effect on ATP synthase activity were significantly less concentrated than those of the corresponding levels of glycosphingolipids this, as observed in the von Frey nociception assay, supports the hypothesis that lyso-Gb_3 is more toxic than

Gb_3. However, in this study the concentrations of the high, medium and low level glycosphingolipid concentrations are based on plasma Gb_3 levels described in patients with severe Fabry disease, mild Fabry disease and those with no detectable disease, respectively. In comparison the levels of lyso-glycosphingolipids, although considerably less concentrated, are still higher than those levels observed in a diseased state. In fact, in an assessment of Fabry patients the low concentration level of lyso-glycosphingolipids was found to be the equivalent of physiological levels observed in plasma. At this level the lyso-glycosphingolipids did not produce any effect on ATP synthase activity. Therefore it is most likely that it is the glycosphingolipids and not their deacylated counterparts that are affecting ATP synthase activity *in vivo*.

One hypothesis to account for the increase in ATP synthase activity shown by some glycosphingolipids could be that in lysosomal storage disorders where glycosphingolipids accumulate, the extra availability of certain glycosphingolipids are able to displace cardiolipin and bind to ATP synthase in its place. Further evidence to support this, is the finding demonstrated in this study, that ATP synthase subunits alpha and beta were shown to bind to the glycosphingolipids Gb_3 and GM_1 ganglioside when immobilised on a RS100 ProteinChip. However, the observation that increased concentrations of pure glycosphingolipids and their deacylated counterparts increase ATP synthase activity may not be concomitant with an increase in ATP or indeed any noticeable disruption to this pathway *in vivo.* In fact, a single study analysing complex V activity in fibroblasts from three Fabry patients has shown a significant decrease in complex V (Lücke *et al.*, 2004). However as mitochondria isolated from control rat liver were used to perform this experiment assumptions relating to the findings obtained from the study by Lücke *et al.*,

(2004) may not be appropriate. Mitochondria isolated from control rat liver tissue were used as the starting material in this study as a limitation of the ATP synthase assay used was incompatibility with mouse tissues. The analysis of tissues from Fabry mice utilising a different methodology is required in order to confirm the findings in this study and also to provide more information as to ATP synthase activity and ATP production *in vivo*. Only these further analyses will enable a more in-depth understanding of the complex mechanism associated with this essential pathway to be obtained and conclusions to be drawn regarding its role in Fabry disease.

5.4 Conclusion

This study has used a number of complimentary rationales to investigate the toxicity of Gb_3 and lyso-Gb_3 in the Fabry mouse model in order to gain a better understanding of the underlying disease mechanisms associated with Fabry disease pathology. Following an initial label-free quantitative proteomic study to create a proteomic profile of Fabry mouse tissues a number of proteins were found to have fold change alterations by the software platforms ProteinLynx and Progenesis LC-MS. Two of these proteins, ATP synthase subunit alpha and ATP synthase subunit beta (mitochondrial) were of particular interest and were selected for further investigation. Subsequently a number of glycosphingolipids and their deacylated counterparts were assessed as to their effect on ATP synthase activity. The results obtained from this aspect of the study showed that a number of these compounds significantly alter ATP synthase activity and suggest that in environments where there are increased levels of some glycosphingolipids e.g. Gb_3 as in Fabry disease, the glycosphingolipid could theoretically displace the cofactor cardiolipin, which is required for the optimal operation of ATP synthase and binds to the enzyme in its place. Further studies are required to confirm this hypothesis and also to ascertain what, if any, downstream consequences result from an increase in ATP synthase activity.

Following the proteomic study protein interactions with a number of proteins in the glycosphingolipid biosynthetic pathway, with particular interest on Gb_3, were investigated using two complementary binding methodologies. This aspect of the study demonstrated that many of the proteins that interact with the glycosphingolipids are involved in a number of vital molecular functions, biological processes and biological pathways. In addition, a number of these proteins were found to have a role in energy production which consequently

may be affected by binding to a glycosphingolipid when an accumulation occurs such as in a lysosomal storage disorder.

In addition to those proteins found to bind non-selectively to glycosphingolipids, some proteins were found to bind exclusively to a specific glycosphingolipid demonstrating an affinity for the sugar portion of the molecule, unique to each glycosphingolipid. One such protein was potassium-voltage gated channel subfamily H member 1, which was found to bind explicitly to Gb_3. This prompted the investigation of touch thresholds in mice following exposure to Gb_3 or lyso-Gb_3. Interestingly, this aspect of the study demonstrated that high levels of both Gb_3 and lyso-Gb_3 increase significantly the sensitivity to an applied mechanical stimulus. However, due to the concentration levels used in this study it is postulated that it is Gb_3 and not lyso-Gb_3 that is responsible for nociceptive pain *in vivo* in Fabry disease. However, ultimately before conclusions can be drawn this requires further investigation.

In conclusion, this study has investigated the toxicity of Gb_3 and lyso-Gb_3 in a Fabry mouse model which has led to the identification of a number of potential mechanisms responsible for the underlying pathology associated with Fabry disease. Whilst further investigations are required to both confirm and expand aspects of this work, this study has highlighted a number of important avenues for investigation that have as yet received little or no attention in Fabry disease. It is only once all these avenues have been investigated that we will be able to fully understand this complex disease.

Chapter 6

The investigation of mitochondrial respiratory chain enzyme activities in a Fabry mouse model

Chapter 6 - The investigation of mitochondrial respiratory chain enzyme activities in a Fabry mouse model 334

6.0 The investigation of mitochondrial respiratory chain enzyme activities in a Fabry mouse model

6.1 Introduction

In the study described in Chapter 5, a number of interactions between Gb_3 and different mitochondrial proteins were detected. Of these proteins one, ATP synthase, was of particular interest and further targeted investigations found ATP synthase activity was increased in the presence of increasing concentrations of both Gb_3 and lyso-Gb_3. ATP synthase is part of the oxidative phosphorylation (OXPHOS) system, located in the mitochondrial inner membrane. In addition to ATP synthase, the OXPHOS system comprises four multi-subunit mitochondrial respiratory chain complexes, as well as the mobile electron carriers, cytochrome c and ubiquinone (Figure 6.1). Together these components of the mitochondrial respiratory chain are responsible for electron transport and contribute to the generation of the proton gradient in the mitochondrial intermembrane space that drives the synthesis of ATP by ATP synthase (Fernández-Vizarra, Tiranti and Zeviani 2009).

The first and largest enzyme in the mitochondrial respiratory chain and OXPHOS system is complex I (nicotinamide adenine dinucleotide (NADH): ubiquinone oxidoreductase). The L-shaped structure of Complex I is composed of 45 subunits, 7 of which are encoded by the mitochondrial DNA (mtDNA) with the remaining 38 subunits encoded by the nuclear genome (Carroll *et al.*, 2006). Complex I is responsible for the oxidation of NADH from the tricarboxylic acid cycle and beta oxidation, the two electrons produced during this reaction are transferred via flavin mononucleotide and iron-sulfur prosthetic groups and are subsequently used in the reduction of ubiquinone to ubiquinol (Baradaran *et al.*, 2013; Hirst 2009; Hirst 2013). The potential energy produced by the redox

reaction is coupled to the transfer of $4H^+$ across the mitochondrial inner membrane from the matrix to the intermembrane space. This contributes to the proton motive force that supports ATP synthesis and the mitochondrial import and export of metabolites and proteins (Hirst 2013).

The second complex in the mitochondrial respiratory chain, complex II (succinate: ubiquinone oxidoreductase) is composed of 4 subunits and is the only complex in the mitochondrial respiratory chain encoded solely by the nuclear genome (Pearl 2013). Complex II is responsible for the oxidation of succinate to fumarate as part of the citric acid cycle, resulting in the transfer of electrons to covalently bound flavin adenine dinucleotide (FAD) to generate $FADH_2$. $FADH_2$ then transfers electrons via iron-sulphur clusters and cytochrome b to reduce ubiquinone to ubiquinol (Cecchini 2003; Pearl 2013).

The penultimate subunit in the mitochondrial respiratory chain is complex III (ubiquinol: cytochrome c oxidoreductase). This complex is formed of 11 subunits of which 3, cytochrome b, cytochrome c_1 and the Rieske iron sulfur protein are encoded by mtDNA (Pearl 2013). Complex III functions to catalyse the oxidation of ubiquinol and the reduction of cytochrome c operating though a Q-cycle mechanism which couples electron transfer to the generation of the proton gradient (Schapira 2003). To achieve this first, two electrons are removed from reduced ubiquinol at the ubiquinone binding site (Q_O-site) of the complex and sequentially passed to two different chains. The first electron is transferred via the Rieske iron sulfur protein (ISP) and cytochrome c_1 to reduce cytochrome c, enabling the small heme-containing protein to diffuse away from complex III. The second electron from ubiquinol is transferred via low- and high-potential hemes of cytochrome *b* (cytochrome b_L and cytochrome b_H, respectively) to oxidised ubiquinone bound at a second quinone processing site,

the Q_i-site, producing a ubisemiquinone. The process is then repeated, a second molecule of reduced ubiquinol binds at Q_O, transferring one electron to a cytochrome c molecule and a second electron to ubisemiquinone at Q_i to give ubiquinol. Each reduction of a ubiquinol molecule results in the release of $2H^+$ into the intermembrane space. In addition, $2H^+$ from the mitochondrial matrix are utilised by the reduction of ubiquinone at Q_i (De Vries *et al.*, 1982; Crofts 2004).

Complex IV (cytochrome c oxidase) is the terminal enzyme in the mitochondrial respiratory chain and is made up of 13 subunits. The three subunits composed of copper redox centres, cytochrome and heme are endoed by mtDNA with 10 smaller subunits which are nuclear encoded (Pearl 2013). The role of complex IV is to transfer four electrons, from four molecules of cytochrome c, in order to catalyse the reduction of oxygen to two water molecules (Brzezinski and Gennis 2008). Cytochrome c oxidase has four redox centres two of which are copper centres, Cu_A and Cu_B, and two of which are heme centres, heme *a* and heme a_3. An electron from the first molecule of oxidised cytochrome c is transferred via Cu_A, heme *a* and heme a_3, to Cu_B reducing Cu^{2+} to Cu^+. An electron from a second molecule of cytochrome c is transferred via Cu_A, heme *a* and heme a_3 reducing Fe^{3+} to Fe^{2+}. Subsequently oxygen binds to heme a_3 followed by Cu_B resulting in a peroxide bridge forming between these two centres. Third and fourth electrons from two further oxidised cytochrome c molecules and $2H^+$ from the mitochondrial matrix sequentially break this bond, producing hydroxyl groups bound to the copper and iron in Cu_B and heme a_3, respectively. Finally, the addition of $2H^+$ from the mitochondrial matrix produces $2H_2O$ from the hydroxyl groups. Concurrently $4H^+$ are removed from the mitochondrial matrix

and translocated across the membrane to the intermembrane space, contributing to the proton gradient (Wikström 1977; Wikström 2004).

Of the mitochondrial respiratory chain enzymes complexes I, III and IV all contribute during electron transport to the H^+ gradient across the mitochondrial inner membrane. This H^+ gradient is used to generate the proton motive force that supports ATP synthesis via ATP synthase (complex V or F_0F_1-ATP synthase). ATP synthase is a large protein complex composed of a membrane-embedded domain (F_0), central and side stalks and a large headpiece (F_1). ATP synthase can be thought of as a complex of two motors, an ATP driven F_1 motor and a proton driven F_0 motor which are connected by a common rotary shaft (von Ballmoos, Cook, and Dimroth 2008). In functional mitochondria the proton flow through F_0 causes rotation of the F_0 rotor which in turn changes the conformational state of subunits within the F_1 domain resulting ultimately in the synthesis of ATP. However, the reaction is reversible and when the H^+ gradient across the mitochondrial inner membrane decreases ATP synthase can utilise ATP hydrolysis in the F_1 domain to induce the rotation of the F_0 rotor in the reverse direction thereby driving proton pumping (Orriss *et al.*, 1998; Stock, Leslie and Walker 1999).

The mitochondrial respiratory chain has been recognised as a potential source of reactive oxygen species (ROS) which include superoxide (O_2-), hydrogen peroxide (H_2O_2) and the hydroxyl free radical (·OH). Within the respiratory chain, complex I and complex III are considered as the main producers of superoxide anions that are released into the mitochondrial matrix and the intermembrane space, respectively. Damage to the mitochondrial respiratory chain could alter ATP synthesis resulting in a perturbation of energy to the cell and mitochondrial ROS production has been associated with the aging process

and in the pathogenesis of neurodegenerative diseases such as Parkinson's disease (Liu, Fiskum and Schubert 2002; Dröse and Brandt 2012).

In the study described in the previous chapter an increase in ATP synthase activity was demonstrated when the enzyme was exposed to both Gb_3 and lyso-Gb_3 at levels representative of those observed in Fabry disease. Therefore, in the present study the activities of the enzymes that precede ATP synthase, the mitochondrial respiratory chain enzymes, were investigated in the tissues of a Fabry mouse model.

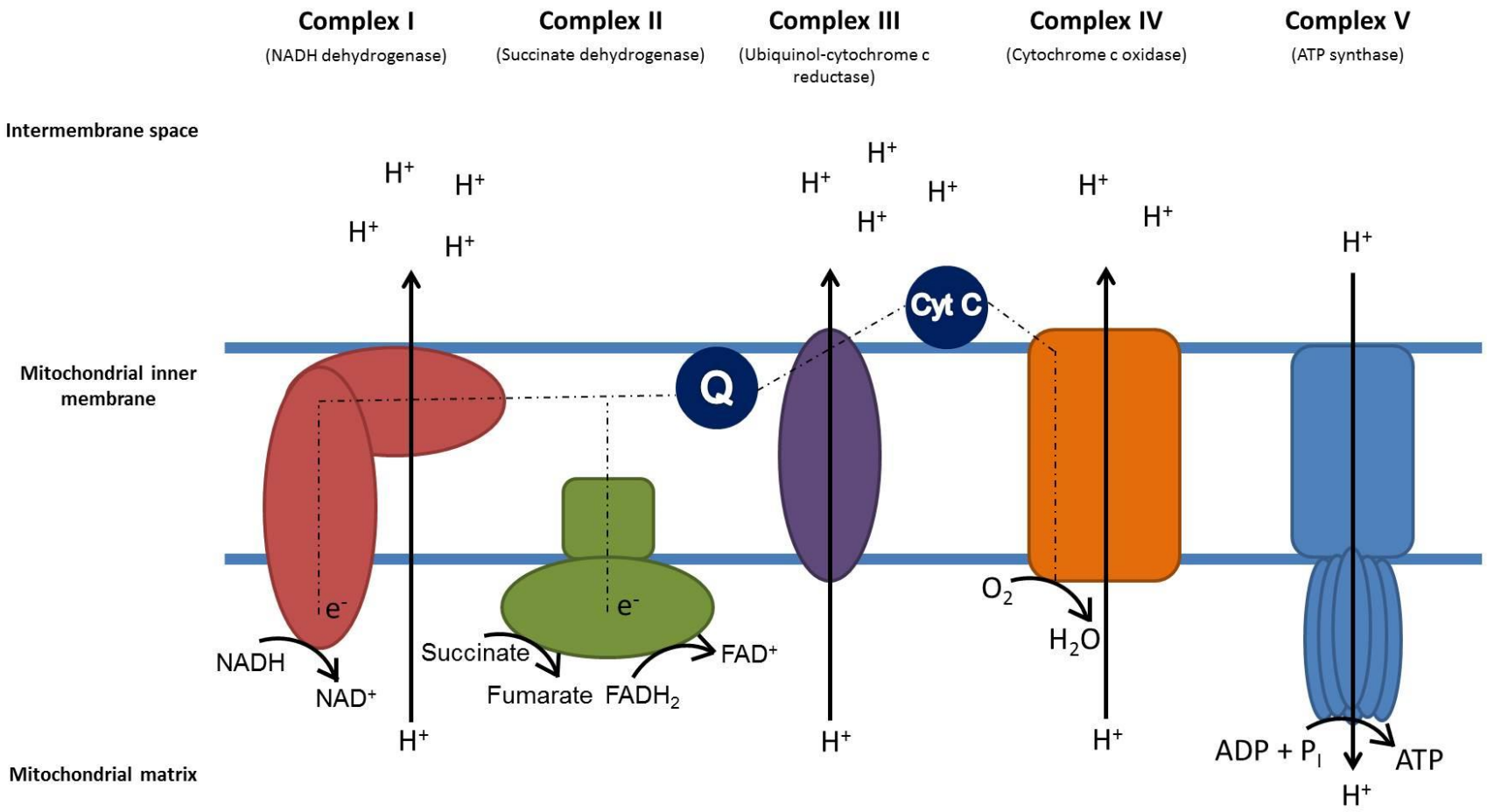

Figure 6.1 Schematic representation of the mitochondrial respiratory chain. Electron (e^-) flow, depicted by the dotted line, drives the translocation of 10 protons from the mitochondrial matrix to the intermembrane space. Q; ubiquinone; Cyt C; cytochrome c;

6.2 Results

All investigations outlined in the following section were performed on tissues from a Fabry mouse model (see section 2.1.2.4) provided by Dr Raphael Schiffmann, Baylor University Medical Centre as part of a collaborative project. All tissues were homogenised prior to analysis as described in section 2.2.8.1.

6.2.1 Gb_3 and lyso-Gb_3 analyses of Fabry mouse tissues

Gb_3 and lyso-Gb_3 analyses (as described in section 2.2.1) were performed on liver, kidney, heart and brain tissue from Fabry mice (n = 8) and wild-type control mice (n = 8). Both Gb_3 (Figure 6.2) and lyso-Gb_3 (Figure 6.3) levels were found to be statistically and significantly elevated by Students t-test ($p < 0.05$) in each tissue type compared to the respective control tissue group.

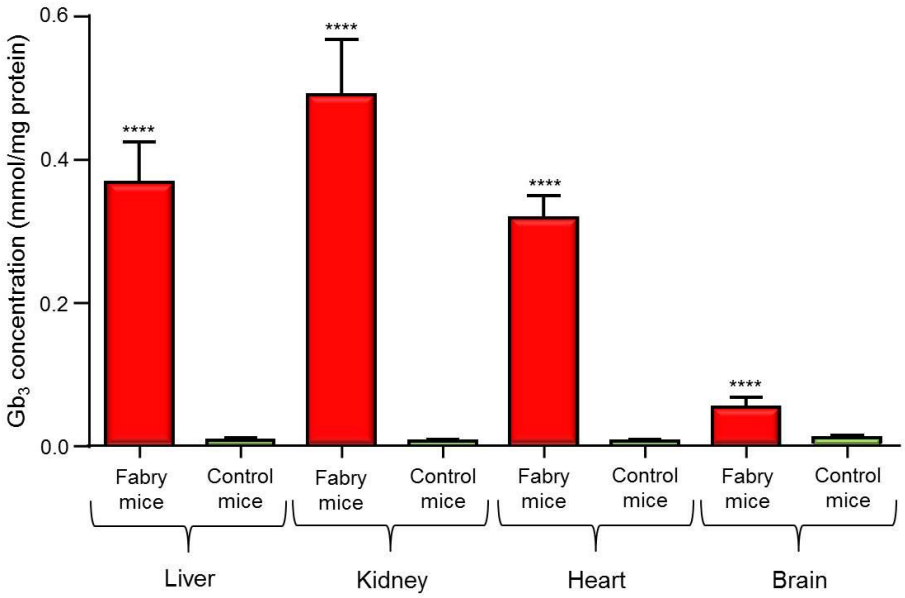

Figure 6.2 Globotriaosylceramide (Gb_3) levels in liver, kidney, heart and brain tissues from a Fabry mouse model (n = 8 per group). Data expresses as mean ± standard deviation. **** $p < 0.0001$

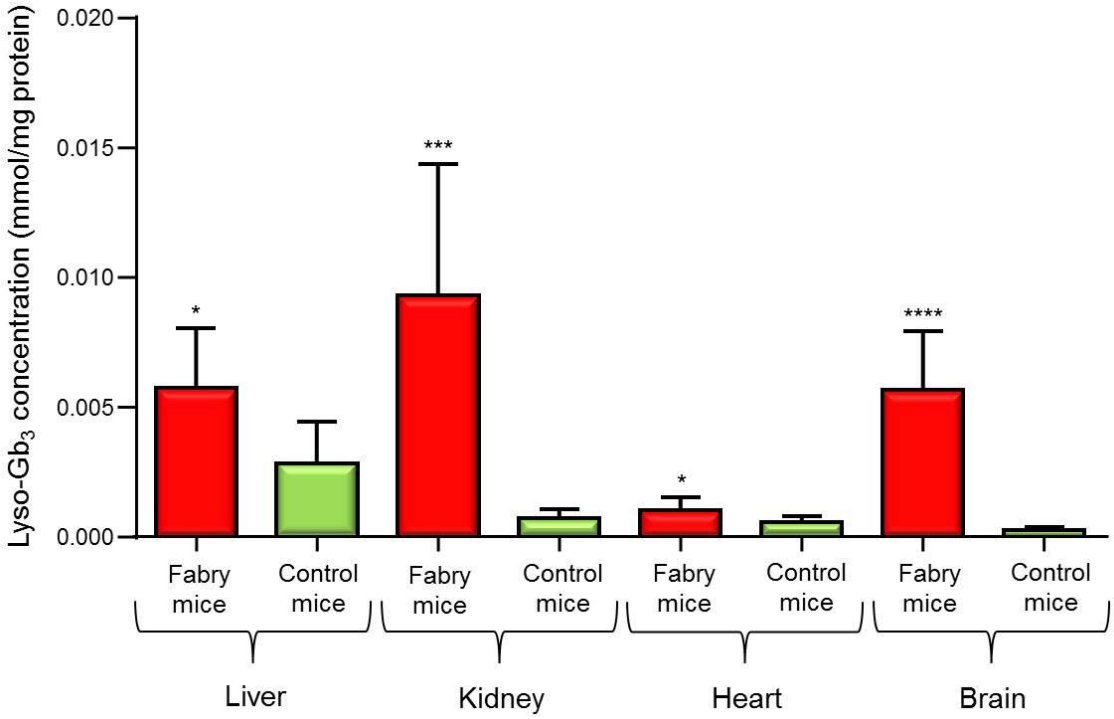

Figure 6.3 Globotriaosylsphingosine levels in liver, kidney, heart and brain tissues from a Fabry mouse model (*n* = 8 per group). Data expressed as mean ± standard deviation. * $p < 0.05$, **** $p < 0.0001$

6.2.2 Assessment of mitochondrial respiratory chain enzymes in the tissues of a Fabry mouse model

Citrate synthase activity is frequently used as a mitochondrial marker and also as a measure of mitochondrial enrichment (Winder and Holloszy 1977; Fatania and Dalziel 1980; Hargreaves, Heales and Land 1999). Following homogenisation of Fabry mouse tissues citrate synthase assays were performed on all samples as described in section 2.2.8.5. All mitochondrial respiratory chain enzyme activities are subsequently shown expressed as a ratio to citrate synthase with transformation of data prior to statistical analyses as described in section 2.2.8.6.

6.2.3 Assessment of complex I activity in the tissues of a Fabry mouse model

Assessment of complex I activity as described in section 2.2.8.2 was determined in tissues from Fabry mice (*n* = 8) and wild-type control mice (*n* = 8). No statistically significant differences in complex I activity were observed by Students *t*-test in liver (*p* = 0.18), kidney (*p* = 0.18), heart (*p* = 0.56) or brain (*p* = 0.97) tissue from Fabry mice compared to the respective wild-type control group (Figure 6.4). A summary of the data is shown in Table 6.1.

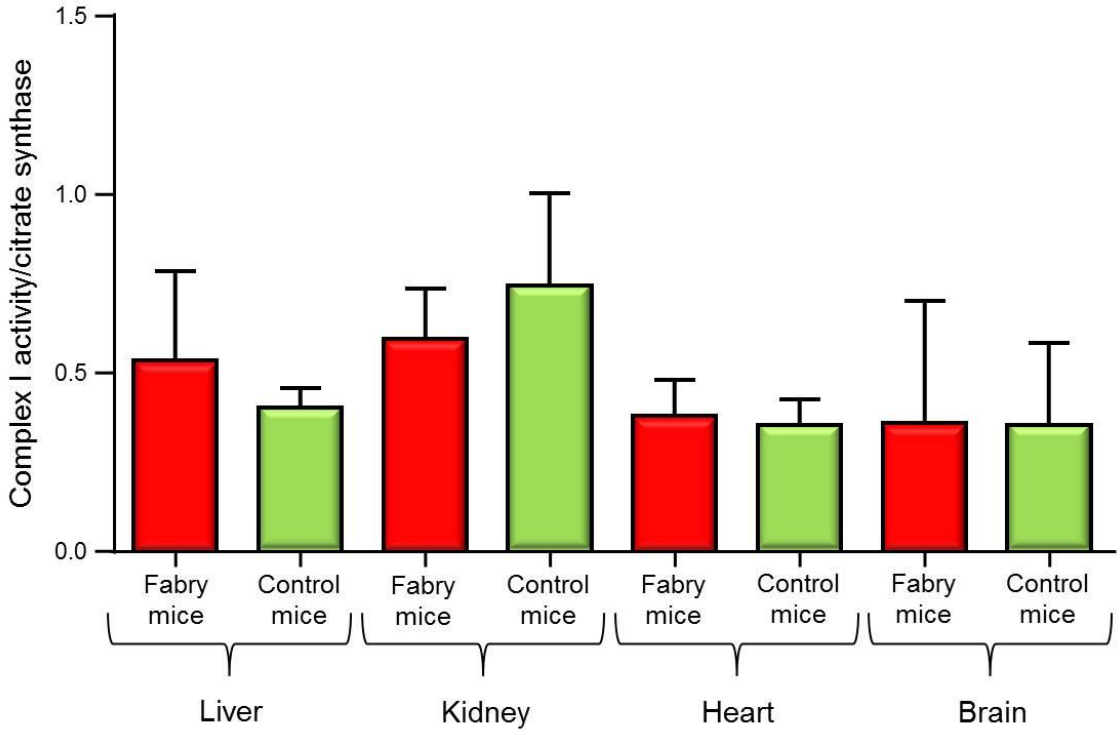

Figure 6.4 Complex I activity in liver, kidney, heart and brain tissues from Fabry and wild-type control mice. Data shown as a ratio to citrate synthase with transformation (*n* = 8 per group). Data expressed as mean ± standard deviation.

6.2.3 Assessment of complex II/III activity in the tissues of a Fabry mouse model

A combined complex II/III assay was used to assess enzyme activity in Fabry mouse tissues as described in section 2.2.8.3. A statistically significant decrease ($p < 0.02$) in complex II/III activity was observed by Students *t*-test in kidney tissues from Fabry mice ($n = 8$) compared to kidney tissues from wild-type control mice ($n = 8$) (Figure 6.5). However, no statistically significant alterations were observed in liver ($p = 0.57$), heart ($p = 0.06$) or brain ($p = 0.34$) tissues from Fabry mice ($n = 8$) compared to the respective control group ($n = 8$). The operation of the complex II/III assay is dependent on ubiquinone availability and therefore it should be noted that a low activity of complex II/III may also be related to ubiquinone status. A summary of the data is shown in Table 6.1.

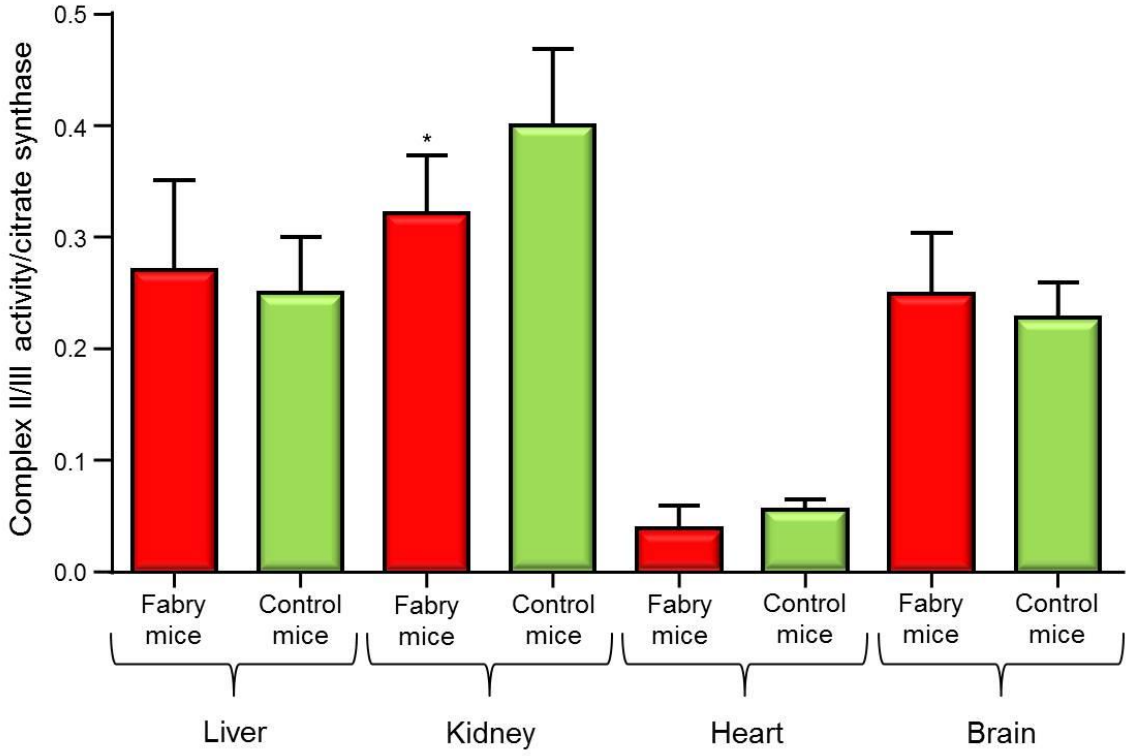

Figure 6.5 Complex II/III activity in liver, kidney, heart and brain tissues from Fabry and wild-type control mice. Data shown as a ratio to citrate synthase with transformation (*n* = 8 per group). Data expressed as mean ± standard deviation. * $p < 0.05$

6.2.4 Assessment of complex IV activity in the tissues of a Fabry mouse model

Assessment of complex IV activity as described in section 2.2.8.4 was determined in tissues from Fabry mice ($n = 8$) and wild-type control mice ($n = 8$) (Figure 6.6). No statistically significant differences in complex IV activity were observed by Students *t*-test in liver ($p = 0.12$), kidney ($p = 0.36$), heart ($p = 0.14$) or brain ($p = 0.25$) tissues from Fabry mice compared to the respective wild-type control mouse tissue. A summary of the data is shown in Table 6.1.

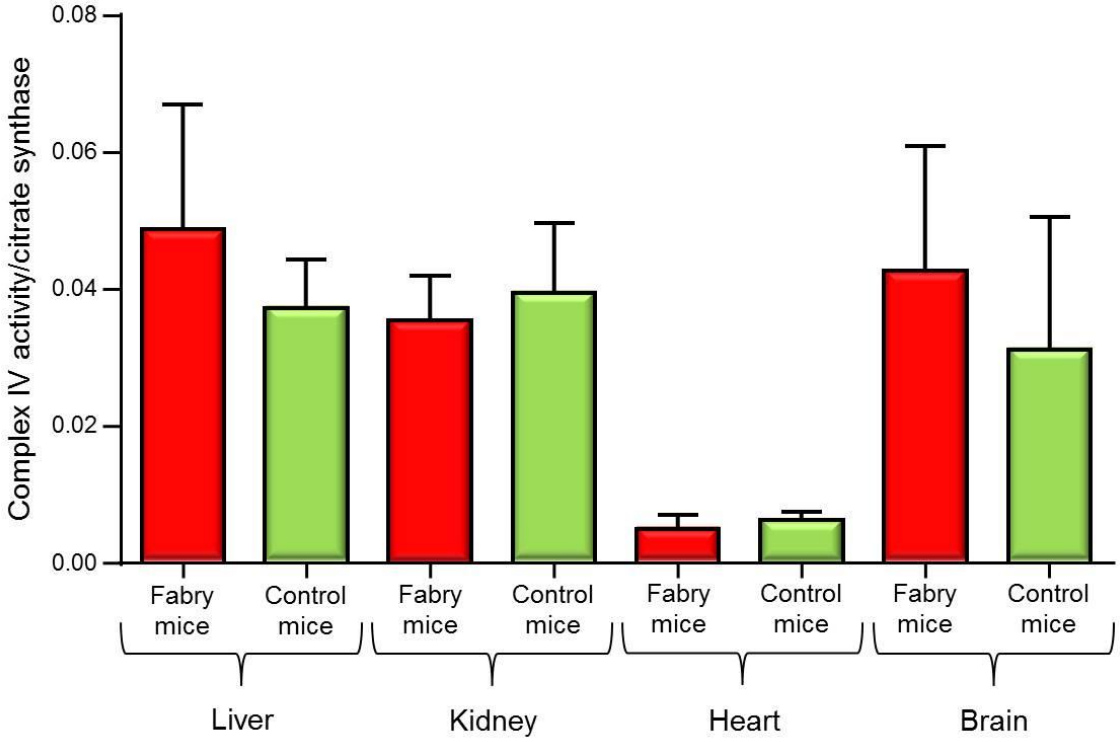

Figure 6.6 Complex IV activity in liver, kidney, heart and brain tissues of Fabry and wild-type control mice. Data shown as a ratio to citrate synthase with transformation (*n* = 8 per group). Data expressed as mean ± standard deviation.

Table 6.1 Mitochondrial respiratory chain enzyme activities in liver, kidney, heart and brain tissues from Fabry mice (*n* = 8) and wild-type control mice (*n* = 8). CS = citrate synthase; SD = standard deviation

Tissue type	Complex I (corrected for CS and transformed)			Complex II/III (corrected for CS and transformed)			Complex IV (corrected for CS and transformed)		
	Fabry	**Control**	***p* value**	**Fabry**	**Control**	***p* value**	**Fabry**	**Control**	***p* value**
Liver Mean ± SD	0.53 ± 0.25	0.40 ± 0.05	0.18	0.27 ± 0.08	0.25 ± 0.05	0.57	0.05 ± 0.02	0.04 ± 0.01	0.12
Kidney Mean ± SD	0.60 ± 0.14	0.74 ± 0.26	0.18	0.32 ± 0.05	0.40 ± 0.07	**0.02**	0.04 ± 0.01	0.04 ± 0.01	0.34
Heart Mean ± SD	0.38 ± 0.10	0.35 ± 0.07	0.56	0.04 ± 0.02	0.06 ± 0.01	0.06	0.005 ± 0.002	0.006 ± 0.001	0.14
Brain Mean ± SD	0.36 ± 0.34	0.35 ± 0.23	0.97	0.25 ± 0.05	0.23 ± 0.03	0.34	0.04 ± 0.02	0.03 ± 0.02	0.25

6.2.5 Relationship of Gb_3 and lyso-Gb_3 levels to mitochondrial respiratory chain activity in a Fabry mouse model

Following the observation that complex II/III activity was reduced statistically and significantly in kidney tissues from a Fabry mouse model, the relationship between these mitchondrial respiratory chain complexes with Gb_3 (Figure 6.7a) and lyso-Gb_3 (Figure 6.7b) levels were assessed. However, no correlation between complex II/III and Gb_3 level (r = 0.4) or lyso-Gb_3 level (r = -0.1) in Fabry mouse kidney tissues was demonstrated.

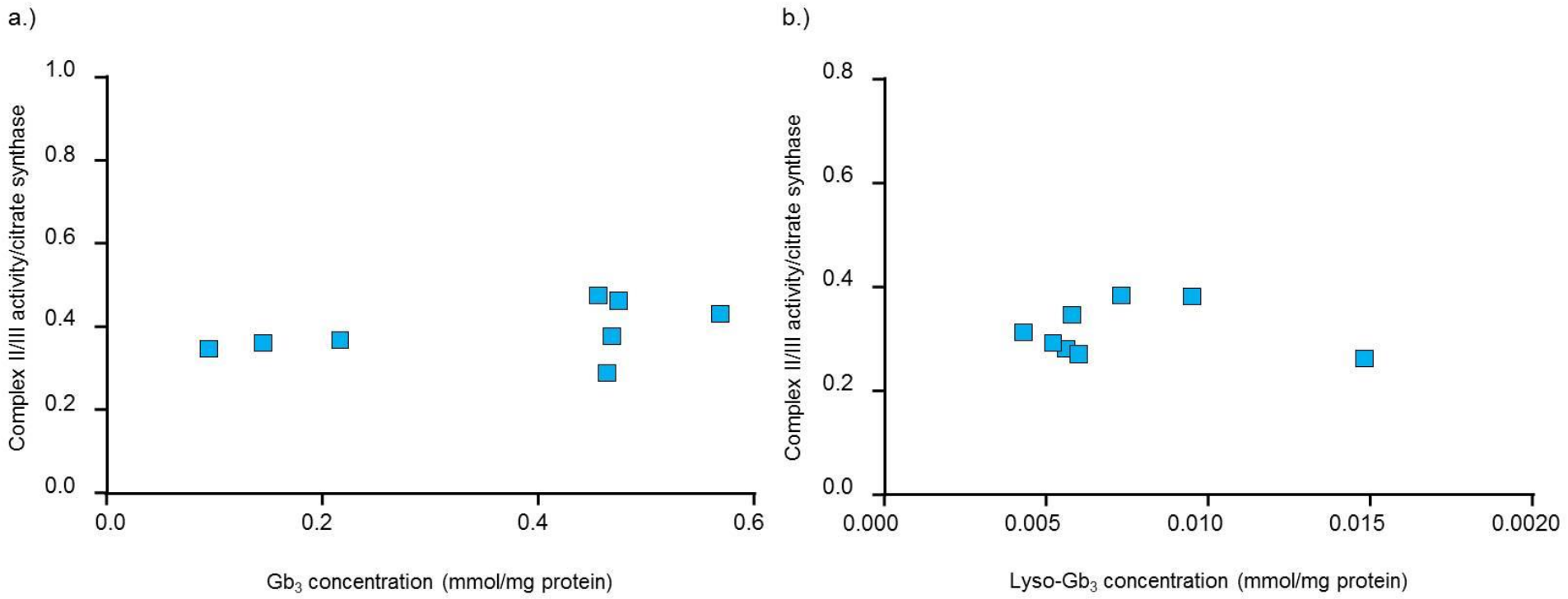

Figure 6.7 Lack of correlation observed between complex II/III activity with a.) Gb_3 levels and; b.) lyso-Gb_3 levels in kidney tissues from Fabry mice (*n* = 3).

6.3 Discussion

Mitochondria are the so-called “powerhouses” of the cell. They are referred to as such due to the energy they produce in the form of ATP which provides more than 90 % of the cellular energy required to maintain its physiological activities (Szewczyk and Wojtczak 2002; Bertram *et al.*, 2006). However, mitochondria provide much more than just the provision of ATP and exert multiple roles within the cell. Mitochondria are an important source of reactive oxygen species (Murphy 2009), function to maintain Ca^{2+} homeostasis (Patergnani *et al.* 2011) and play a key role in activating cellular proliferation and apoptosis (Wang and Youle 2009). Therefore, it is not surprising that mitochondrial dysfunction has been described in a number of diseases including neurodegenerative diseases such as Alzheimer’s disease and Parkinson’s disease (Mandemakers, Morais and Strooper 2007), diabetes (Blake and Trounce 2013) and epilepsy (Folbergrová and Kunz 2012).

In the present study, mitochondrial respiratory chain enzyme activity has been assessed in the tissues of a Fabry disease mouse model. However, due to the discreet phenotype displayed by the Fabry disease mouse model, initial investigations to determine Gb_3 and lyso-Gb_3 levels in the tissues of Fabry and control mice were performed. This showed that statistically significant increases of both of these toxic metabolites were present in the liver, kidney, heart and brain tissues of the Fabry mice confirming that the tissues were suitable for subsequent analyses of the mitochondrial respiratory chain enzymes.

Following analysis of the mitochondrial respiratory chain enzymes using established spectrophotometric methodologies a statistically significant reduction in complex II/III activity was observed in kidney tissues from Fabry mice compared to that of control mice. The kidneys are known to possess a

high density of mitochondria which are required in the production of ATP (Hall *et al.*, 2008). ATP is essential to drive the sodium-potassium ATPase pump which in turn generates the electrical gradient across the proximal tubular epithelium responsible for maintaining low intracellular sodium levels (Niaudet 1998). The gradient drives all the activities of the renal proximal tubular cell including transport activity responsible for the reabsorption of > 99 % of the daily glomerular filtrate, most of which occurs along the proximal tubule (Hall *et al.*, 2008). Renal disease due to mitochondrial dysfunction or cytopathy has been described with common clinical manifestations including tubular disorders, chronic tubulointerstitial nephritis and glomerular diseases (Niaudet and Rotig 1997; Doleris *et al.*, 2000). The most common biochemical findings in these disorders are defects in complex III and/or complex IV (Emma *et al.*, 2011). In this study the spectrophotometric methodology used determines combined complex II and complex III activity and therefore further analyses would be required to conclude if the significant reduction observed in this study was attributable solely to a reduction in the activity of complex III. In addition, the complex II/III assay is dependent on ubiquinone availability and therefore the reduced activities observed during this study may be attributable to an alteration in ubiquinone status however, subsequent analyses would be required to investigate this hypothesis.

Renal impairment is reported in approximately half of all patients with Fabry disease with the developing proteinuric kidney complications similar to those experienced by diabetic patients (Schiffmann *et al.*, 2009; Branton *et al.*, 2002; Mehta *et al.*, 2004). Previous studies have suggested that diabetes induces alterations in mitochondrial respiratory chain complex activity as well as mitochondrial respiration in the kidney (Rosca *et al.*, 2005; Katyare and Satav

2005) and renal complex III has been shown to be a target for glycation and inhibition during chronic diabetes (Rosca *et al.*, 2005). More recently, complex III activity has also been shown to be reduced significantly in rats induced with diabetes (Munusamy *et al.*, 2009).

The collective term ROS is used to describe a number of reactive molecules, such as H_2O_2, and free radicals, such as O_2^{-}, derived from molecular oxygen. Most molecular oxygen is reduced to water by complex IV of the mitochondrial respiratory chain. However, 1 – 4 % of oxygen is incompletely reduced to O_2^{-} which primarily occurs at complex I and complex III making these complexes susceptible to oxidative damage (Bolaños *et al.*, 1994; Bolaños *et al.*,1996). The production of O_2^{-} at complex III is due to autoxidation of ubisemiquinone formed during the Q cycle process. The Q_O site of the complex is located close to the intermembrane space and is thought to be the major site of O_2^{-} production (Zhang and Gutterman 2007). Interestingly, excess intracellular Gb_3 levels have been shown to induce oxidative stress in vascular endothelial cells from Fabry disease patients (Shen *et al.*, 2008). In addition, a study performed in a Fabry mouse model demonstrated uncoupling of endothelial nitric oxide synthase (eNOS) within the endothelium resulting in the subsequent generation of ROS (Shayman 2010). Furthermore, uncoupling of NOS has been shown to result in the formation of peroxynitrite which in addition to directly inhibiting the mitochondrial respiratory chain enzymes (Szabó 2003) has also been shown to inhibit various ion pumps including calcium pumps (Klebl, Ayoub, and Pette 1998), calcium-activated potassium channels and membrane Na^+/K^+ ATPase activity (Muriel and Sandoval 2000). The effect of the inhibition of an ion pump would invariably lead to the dysregulation of ion balance in peroxynitrite-challenged cells (Szabó 2003) and unsurprisingly, imbalance of ion

homeostasis has previously been described in lysosomal storage disorders (Miedel *et al.*, 2008).

Although a statistically significant reduction in complex II/III activity was observed in the kidney of the Fabry mouse model, this result was not replicated in the other organs analysed. The activity of complex II/III in Fabry mouse heart tissue was shown to be reduced compared to that of control tissue however, this reduction did not quite reach statistical significance (p = 0.057). A large proportion of patients with Fabry disease experience cardiac involvement (see section 1.3.6.1) with the predominant cardiac manifestation reported to be left ventricular hypertrophy (Weidemann *et al.*, 2005; Linhart *et al.*, 2000; Kampmann *et al.*, 2002; Senechal and Germain 2003). A number of patients with mitochondrial cytopathies are also reported to develop left ventricular hypertrophy and this condition is often attributable to inherited mutations in genes encoding metabolic pathways and mitochondrial proteins (Bos, Towbin and Ackerman 2009). The similarities in cardiac symptoms experienced by those patients with Fabry disease and mitochondrial cytopathies suggests that a common mechanism perhaps even reduction of complex II/III activity, which has previously been reported in heart failure (Jarreta *et al.*, 2000), may be a contributing factor in the development of hypertrophic cardiomyopathy in these patients.

No statistically significant alterations were observed in the activity of complex I or complex IV of the mitochondrial respiratory chain in any tissue type analysed in this study (see Table 6.1). Contrastingly however, Lücke *et al.,* (2004) have previously reported statistically significant reductions in complex I and complex IV in fibroblasts from three patients with Fabry disease. An explanation for the difference in mitochondrial respiratory chain enzyme activity observed in this

study with that of Lücke *et al.*, (2004) first and foremost may be attributable to the differences in biological material used for the analyses. In this study liver, kidney, heart and brain tissues from Fabry mice was analysed and therefore a comparison to activities in human Fabry fibroblasts may not be appropriate. In addition, the methodology used for the measurement of mitochondrial respiratory chain activity by Lücke *et al.*, (2004) used a combined complex I + III and complex II + III assay. This differs to the methodology used in this study where a specific complex I activity protocol was used. Therefore, a direct comparison of these methods may not be suitable and may go some way to explain the differences observed.

6.4 Conclusion

In conclusion, in this study a clear statistical reduction in the activities of the mitochondrial respiratory chain complex, complex II/III, in the kidney tissues of a Fabry mouse model has been demonstrated. When considering the high density of mitochondria in the kidneys combined with the amount of renal impairment observed in Fabry disease this finding is somewhat unsuprising. Futhermore, the fact that complex III is a primary site of ROS production and that uncoupling of eNOS within the endothelium resulting in the subsequent generation of ROS has been demonstrated in Fabry disease, further supports a reduction in complex II/III activity and suggests that this finding is most likely due to a reduction in complex III activity. However, due to the combined complex II/III assay used during this study further investigations are required to establish if the reduction in complex II/III observed in this study is attributable solely to a reduction of complex III. In addition, the nature of the complex II/III assay relies on the availability of ubiquinone and investigations to establish ubiquinone status would be required to fully establish the origin of the reduction of complex II/III activity. Additional investigations would enable a full and complete understanding of complex II/III in the Fabry mouse model to be achieved.

Chapter 7

General discussion

7.0 General discussion

The aim of this study was to identify potential diagnostic biomarkers and disease mechanisms in the lysosomal storage disorder Fabry disease. To achieve this goal both proteomic and metabolomic mass spectrometry based methodologies, as well as a number of complementary techniques, have been used.

The initial aspect of this study used a label-free quantitative proteomic methodology to analyse urine samples obtained from paediatric Fabry disease patients prior to the initiation of ERT and again following 12 months of treatment. This enabled a typical urinary proteomic profile from paediatric Fabry disease patients to be created and also identified alterations in protein levels pre- and 12 months post-treatment. One protein, the lysosomal protein prosaposin, was shown to have a statistically significant reduction in the urine of these patients. Prosaposin is the precursor protein for the mature saposins A, B, C and D which are necessary for the hydrolysis of glycolipids with short glycan chains by lysosomal luminal hydrolases (Sandhoff, Kolter and Harzer 2001). Therefore it was unsurprising that prosaposin would be elevated in the urine of these patients prior to treatment and previous studies have indeed demonstrated accumulations of the mature saposins in plasma and tissue of various lysosomal storage disorders (Chang *et al.*, 2000; Morimoto *et al.*, 1990). However, the MRM-based UPLC MS/MS assay that was developed in this study has enabled the rapid and reliable quantitation of prosaposin, verifying the findings of the label-free study, and providing confirmation that prosaposin was reduced significantly following one-year of treatment in paediatric Fabry disease patients. In addition to the Fabry disease patient group, an age- and sex-matched healthy control group and a paediatric type I diabetic patient group

were also analysed. The type I diabetic patient group were selected for inclusion, for use as a positive control group, due to the fact that the developing proteinuric kidney complications are similar to those that develop in Fabry disease. Following analysis of prosaposin in these additional patient groups this protein was found to be elevated in only the pre-treatment Fabry disease group suggesting that a reduction in this protein biomarker, as observed following one-year of ERT, may be indicative of an improvement in lysosomal function. However, to fully investigate this hypothesis in order to draw conclusions regarding the validity of prosaposin as a biomarker of improved lysosomal function and therefore of lysosomal storage orders in general, requires additional analyses. Furthermore, whilst the mature saposins A-D were able to be detected using the MRM UPLC-MS/MS assay developed in this study only saposin A was detectable in all patients. Saposins B, C and D were detectable in approximately 50 % of patients and whilst there could be a number of reasons for this, further development of the assay is required to optimise the detection of these mature saposins. A complete saposin assay would provide further information on a patient's lysosomal status and could be a diagnostic tool in those sphingolipidoses requiring mature saposins as cofactors.

In addition to the mature saposins A-D, the known saposins include the genetically distinct GM_2AP. A small reduction in this protein was detected during the proteomic profiling study and due to the relationship with the saposins this protein was selected for inclusion into the initial MRM UPLC-MS/MS assay. The increased sensitivity and specificity of the MRM UPLC-MS/MS assay enabled a statistically significant reduction in this protein to be observed following 12 months of treatment in paediatric Fabry disease patients. However, in contrast to prosaposin which was only found to be increased in the pre-treatment Fabry

disease patient group, GM_2AP was also found to be increased in the paediatric type I diabetic group. Renal involvement is a major contributor to morbidity in Fabry disease patients with the developing proteinuric kidney complications, the same as those experienced by diabetic patients. Therefore it was postulated that the elevation in GM_2AP levels in both the paediatric Fabry disease and type I diabetic patients could be an indicator of pre-symptomatic kidney disease. To investigate this hypothesis further a second MRM UPLC-MS/MS assay was developed. This assay encompassed a number of known and potential biomarkers of established renal disease. However, to assess the ability of these biomarkers to detect pre-symptomatic kidney disease a number of 'at-risk' paediatric patient groups, with no signs of microalbuminuria using conventional methods, were investigated. In addition, samples obtained from an adult Fabry disease and an adult type II diabetic group with a degree of renal involvement, as well as an adult control group were also analysed.

Albumin, which at present is the principle biomarker used to monitor kidney function, was included in the assay. However, whilst none of the paediatric patients displayed detectable levels of microalbuminuria using conventional methods, this assay was able to detect alterations in this protein in these paediatric patient groups. This demonstrated the sensitivity of the assay and the ability of the method to detect pre-symptomatic kidney disease in 'at-risk' patient groups. Eleven potential biomarkers, in addition to albumin, were analysed in the multiplex pre-symptomatic kidney disease assay. A number of alterations in these proteins were identified in both the paediatric and adult patient groups. Many of the differences observed between the adult Fabry disease, type II diabetic and control groups reached statistical significance. This was expected as these patients have a degree of impaired kidney function however, by

analysing these potential biomarkers in the adult patient groups and relating them with levels observed in paediatric cohorts provides essential information as to the biomarkers most likely to become increased in the respective paediatric groups as kidney impairment progresses.

As expected few of the changes detected in the paediatric patient groups reached statistical significance. This is most likely due to the age of these patients and that there is not, as yet, any significant kidney damage. This assay has demonstrated the ability to detect changes in a number of known renal biomarkers as well as a number of potential new renal biomarkers at extremely low levels demonstrating its potential to detect pre-symptomatic kidney disease in these patients. With the continued analysis of those patients most ‘at risk’ this assay may not only have the ability to detect pre-symptomatic kidney disease but also to establish the most appropriate time for therapeutic intervention. In addition, differences in the levels of these biomarkers between each of the patient groups suggests that this assay is sensitive enough to detect the rate of progression of renal disease and may highlight different aspects of renal disease to which different patient groups may be susceptible. Using the renal assay the assessment of renal biomarkers in pre-treatment Fabry disease patients and their levels following one- two and three-years of ERT was also assessed. Alterations in these potential biomarkers were revealed and importantly this assay further highlighted differences between those patients with the most disease and least disease burden. However, in order to draw conclusions about the effectiveness of ERT on renal disease assessment of progression of renal disease in those patients not receiving treatment would be required. With the growth of diabetes and obesity in society those ‘at-risk’ of developing renal disease is also increasing. Therefore a panel of biomarkers

with the ability to detect renal disease, before conventional methods, and the onset of severe and irreversible complications is vital. However, further investigation and longitudinal observational studies are required in order to fully validate these biomarkers prior to their routine use.

Following the proteomic study a metabolomic study to identify potential metabolite biomarkers in Fabry disease was carried out in Professor Christiane Auray-Blais laboratory at the Centre for Research, University of Sherbrooke, Quebec, Canada. The targeted metabolomic approach to biomarker discovery was used to identify potential Gb_3-related biomarkers in the circulation of treatment naive adult male Fabry disease patients. This study revealed the presence of seven novel biomarkers which required subsequent structural elucidation and characterisation. Of the seven potential biomarkers five were shown to be Gb_3-related analogs/isoforms three corresponded to Gb_3 having an extra double bond on the sphingosine chain (d18:2) with C16:0, C18:0 and C22:1 fatty acids. The fourth biomarker was shown to correspond to a mixture of two structural isomers, the first with a d16:1 sphingosine and a C16:0 fatty acid and the second with a d18:1 sphingosine and a C14:0 fatty acid. This finding was of particular importance as it is the first time that a Gb_3 analogue with a d16:1 sphingosine moiety has been reported. Furthermore, this Gb_3 analogue was also present in its methylated form. Two of the seven potential biomarkers did not show fragmentation profiles similar to Gb_3 and were therefore not considered to be Gb_3-related analogs/isoforms. Unfortunately the concentration of these two potential biomarkers was too low to permit the structural elucidation of these metabolites.

In addition to the five novel Gb_3-related analogs/isoforms detected in this aspect of the study a number of Gb_3-related analogs/isoforms identified previously in

the urine of Fabry patients were also detected. All known and novel Gb_3-related analogs/isoforms were analysed subsequently in the plasma of treatment naïve female Fabry disease patients. This analysis showed that as with conventional Gb_3 and lyso-Gb_3 measurements, these biomarkers, where present, were detectable at reduced levels in female patients. This finding further demonstrates that women are often less severely affected than their male counterparts.

The final aspect of the metabolomic study compared the relative concentrations of all Gb_3-related analogs/isoforms between plasma and urine. This exposed significant differences in the levels of excretion of the Gb_3-related analogs/isoforms and suggests that specific analyses comprising certain analogs/isoforms may be beneficial depending on the biological matrix used for analysis. Unfortunately due to the low abundance of many of the Gb_3-related analogs/isoforms detected in this study it is unlikely that all of the metabolites will be able to be incorporated into routine analyses. However, variations in the relative quantitation of Gb_3-related analogs/isoforms between urine and plasma have been exposed. Furthermore, it has been demonstrated that the metabolic profile in these patients is much more complex than thought previously and cannot be elucidated fully by the analysis of Gb_3 and lyso-Gb_3 levels alone. In addition, this study has provided a metabolic profile of Gb_3-related analogs/isoforms in Fabry patients however further studies are needed in order to better understand the underlying metabolic process occurring in Fabry disease.

In addition to identifying potential biomarkers this study has aimed to elucidate the underlying molecular mechanisms associated with Fabry disease. In order to achieve this Gb_3 and lyso-Gb_3 toxicity in the Fabry mouse model, with

particular focus on protein: glycosphingolipid interactions, has been investigated. This aspect of the study first used label-free quantitative proteomics to create a proteomic profile of Fabry mouse tissues enabling differences between protein levels in Fabry disease and control mouse tissues to be identified. Data from the proteomic study were analysed using two software platforms, ProteinLynx and Progenesis LC-MS. Results obtained from each software were cross-referenced and those proteins found to be altered using both software platforms, were selected for further investigation. Using this workflow the proteins ATP synthase subunit beta (mitochondrial), ATP synthase subunit alpha (mitochondrial), ribonuclease UK114, agmatinase (mitochondrial), alpha synuclein and ATP binding cassette sub-family B member 8 (mitochondrial) were all determined to be proteins of interest. These proteins were subsequently interrogated with the GO annotation system using the PANTHER website. By analysing the data in this way a large number of common molecular functions, biological processes and/or biological pathways were identified which link the proteins. Alterations in proteins contributing to any or all of the functions, processes or pathways identified would most likely result in their sub-optimal operation and costly downstream effects. However, the extent to which they contribute to disease pathology requires further investigation.

Following the proteomic profiling aspect of this study, two complementary novel protein: glycosphingolipid interaction methodologies were used to identify proteins that interact solely with Gb_3 as well as proteins that interact with both Gb_3 and other glycosphingolipids in the glycosphingolipid biosynthetic pathway. The use of other glycosphingolipids as positive controls enabled the detection of potential common but also any unique molecular mechanisms associated with

the lysosomal storage disorders to be detected. Both methodologies used the same underlying principles to bind deacylated or 'lyso' versions of the glycosphingolipids through the primary amine group to either a RS100 ProteinChip or Dynabeads® M-270 Epoxy and a C12 or C5 linker-arm, respectively. Both methodologies effectively restore the deacylated glycosphingolipids to their acylated forms and although binding the molecules in this way renders the fatty acid group unavailable for interactions importantly the sugar portion, unique to each of the molecules, is available for binding.

Using the RS100 ProteinChip 157 proteins were detected interacting with Gb_3 and/or GM_1 ganglioside in control mouse brain tissue. Although PBS was used to control for non-specific binding this could indicate that a more stringent wash procedure is required. Unfortunately, due to time constraints optimisation of binding conditions in order to minimise non-specific binding was not possible for the purpose of this thesis. However, before further experimentation using this methodology is performed optimum binding conditions should be established. Of the 157 proteins detected in this study 32 proteins were found to interact with both Gb_3 and GM_1 ganglioside. Interestingly three proteins, ATP synthase subunit alpha, ATP synthase subunit beta and alpha-synuclein were also detected in Fabry mouse tissues during the proteomic profiling study. All proteins that interact with Gb_3 and/or GM_1 ganglioside were classified subsequently according to the GO annotation system. This analysis revealed many molecular functions, biological processes and biological pathways linking the proteins but most importantly a large proportion of the proteins detected were found to be located in the mitochondria or to possess catalytic activity involving ATP. This suggests that those proteins that interact with Gb_3 and/or

GM_1 ganglioside may have a role in energy production which may be affected by binding to a glycosphingolipid.

The second, complimentary protein: glycosphingolipid interaction study used Dynabeads® M-270 epoxy to identify proteins that interacted with Gb_3, GM_1 ganglioside, galactosylceramide and ceramide in control mouse kidney tissues. When results for those proteins found to interact with Gb_3 and/or GM_1 ganglioside using both protein: glycosphingolipid interaction methodologies were cross-referenced three common interactions were revealed. The proteins beta-actin-like protein 2 and tubulin alpha-1B chain were detected to bind only to GM_1 ganglioside and aspartate aminotransferase (mitochondrial) was detected to bind to both Gb_3 and GM_1 ganglioside.

As with the RS100 ProteinChip methodology a number of common connections with proteins that interact with glycosphingolipids and ATP and/or that have an association with the mitochondrial respiratory chain enzymes were also revealed using the Dynabead® methodology. Although no protein was found to bind to all four glycosphingolipids in the Dynabeads® study, voltage dependent anion selective channel protein 1 (VDAC1), was found to interact with Gb_3, galactosylceramide and ceramide. Interestingly this protein binds a number of ATP-dependent enzymes and is also an important regulator of Ca^{2+} transport in and out of the mitochondria (Báthori *et al.*, 2006). This is of particular importance as aberrant Ca^{2+} handling has been described in the lysosomal storage disorders (Kiselyov et al., 2010). Another ion channel, potassium-voltage gated channel subfamily H member 1, was found to bind explicitly to Gb_3. A role for voltage-gated potassium channels (K_V) in neuropathic and nociceptive pain has been demonstrated (Klein *et al.*, 2012). As neuropathic pain is one of the most frequent, early and debilitating clinical manifestations

experienced in patients with Fabry disease, the effect of Gb_3 and also lyso-Gb_3, on pain thresholds in mice was assessed using a von Frey assay. The results obtained from the von Frey assay demonstrated that, following exposure to high levels of either Gb_3 or lyso-$Gb_{3,}$ a significant increase in sensitivity to mechanical stimuli was produced. No difference in the effect on sensitivity between injection with Gb_3 or lyso-Gb_3 was observed when each metabolite was injected at a high concentration level. The level of Gb_3 used in this assay was based on the plasma Gb_3 level of Fabry patients with a severe disease phenotype. The lyso-Gb_3 concentration although significantly less concentrated, than the Gb_3 levels used, remains much greater than lyso-Gb_3 levels observed *in vivo*. This suggests that it is probably Gb_3 that is causing the pain response in Fabry disease. However, this hypothesis requires further investigation with a wider array of glycosphingolipids and their deacylated counterparts at high, medium and low concentration levels.

Of particular interest during this study was the observation that ATP synthase subunits alpha and beta (mitochondrial) were shown to be increased in Fabry mice during the proteomic profiling study. As a result the effect of high, medium and low level glycosphingolipids and their corresponding deacylated or ‘lyso’ counterparts, as well as the phospholipid cardiolipin were assessed regarding their effect on ATP synthase activity. As expected cardiolipin, which is essential for the catalytic and structural operation of ATP synthase demonstrated the greatest effect on the enzyme demonstrating significant increase in ATP synthase activity at the high, medium and low concentrations. In addition, the high concentration level of GM_1 ganglioside, Gb_3, sulfatide and lactosylceramide and their deacylated counterparts, as well as lyso-glucocerebroside were all shown to increase significantly ATP synthase activity. At the medium

concentration level GM_1 ganglioside, lactosylceramide, lyso-GM_1, lyso-Gb_3 and lyso-glycosylceramide were shown to increase significantly ATP synthase activity. However, no significant increases in ATP synthase activity were demonstrated using any glycosphingolipid or lyso-glycosphingolipid at the lowest concentration level assessed. When high, medium and low level glycosphingolipids were compared with their deacylated counterparts the effect on ATP synthase activity was shown to be very similar.

As with the von Frey assay the high level of glycosphingolipids used was based on the plasma Gb_3 level of Fabry patients with a severe disease phenotype. With the medium level the equivalent to that of a mild disease phenotype and the low level equivalent to those levels observed in controls. In comparison the levels of lyso-glycosphingolipids, although considerably less concentrated, are still higher than those levels observed in a diseased state. The low concentration level of lyso-Gb_3 used in this study is comparable to physiological levels observed in Fabry disease. However, at this level no lyso-glycosphingolipids produced any effect on ATP synthase activity. Therefore as with those results observed in the von Frey assay it is most likely that it is the glycosphingolipids and not their deacylated counterparts that are affecting ATP synthase activity *in vivo*.

A hypothesis to explain how glycosphingolipids alter ATP synthase activity could be that in cases where there are increased concentrations of certain glycosphingolipids, such as in lysosomal storage disorders, the glycosphingolipids are able to displace cardiolipin and bind to ATP synthase in its place. Further evidence to support this, is the finding demonstrated in this study, that ATP synthase subunits alpha and beta were shown to bind to the glycosphingolipids Gb_3 and GM_1 ganglioside when immobilised on an RS100

ProteinChip. However, it should be noted that the demonstration that glycosphingolipids affect ATP synthase activity does not necessarily mean that an increase in ATP production or indeed any noticeable disruption to this pathway will result *in vivo*. Therefore, further analyses are required to assess not only ATP synthase activity but also ATP production *in vivo*. Only once these investigations have been completed will the full relevance of the findings in this study become apparent.

During the investigation of Gb_3 and lyso-Gb_3 toxicity in the Fabry mouse model a number of common connections with proteins that are located in the mitochondria or have an association with the mitochondrial respiratory chain enzymes were revealed. In addition, the finding that increased concentrations of glycosphingolipids and their deacylated counterparts increase ATP synthase activity (complex V) prompted the investigation of the enzymes preceding complex V in the OPHOS system. In this aspect of the study the mitochondrial respiratory chain enzymes, complex I, complex II/III and complex IV were assessed in the tissues (liver, kidney, heart and brain) of a Fabry mouse model. Following this analysis a significant reduction in complex II/III activity was observed in kidney tissues from Fabry mice compared to that of control mice. However, no other significant reductions were observed in complex II/III activity in heart, liver, or brain Fabry mouse tissues. In addition, no statistically significant alterations were observed in the activity of complex I or complex IV of the mitochondrial respiratory chain in any tissue type analysed in this study.

The significant reduction observed in complex II/III activity in the kidney is of particular interest as complex III is susceptible to oxidative damage (Bolaños *et al.*, 1994; Bolaños *et al.*,1996). The production of O_2^- at complex III is due to autoxidation of ubisemiquinone formed during the Q cycle process. The Q_O site

of the complex is located close to the intermembrane space and is thought to be the major site of O_2^- production (Zhang and Gutterman 2007). Interestingly, excess intracellular Gb_3 levels have been shown to induce oxidative stress in vascular endothelial cells from Fabry disease patients (Shen *et al.*, 2008). In addition, a study performed in a Fabry mouse model demonstrated uncoupling of endothelial nitric oxide synthase (eNOS) within the endothelium resulting in the subsequent generation of ROS (Shayman 2010). In this study a combined complex II/III assay was used and therefore further investigations are required to establish if the reduction in complex II/III observed in this study is attributable solely to a reduction of complex III. In addition, the nature of the complex II/III assay relies on the availability of ubiquinone and investigations to establish ubiquinone status would be required to fully establish the origin of the reduction in complex II/III activity.

Furthermore, In contrast to the results obtained in this study, a study by Lücke *et al.,* (2004) has reported statistically significant reductions in complex I and complex IV in fibroblasts from three patients with Fabry disease. Differences in the results obtained between these studies could be attributable to both differences in the biological starting materials and the methodologies used. However, further investigations are required to confirm these findings. Only once these studies have been completed will a full and complete understanding of complex II/III in the Fabry mouse model be achieved.

7.1 Conclusions

In conclusion, this study has used both proteomic and metabolomic mass spectrometry based methodologies to identify and validate a number of potential biomarkers that can be used in conjunction with Gb_3 and lyso-Gb_3 to provide a more detailed understanding of Fabry disease progression and response to treatment. A novel and rapid multiplex assay for the detection of prosaposin and GM_2AP, as well as a second multiplex assay with the potential to detect pre-symptomatic kidney disease in those patients most 'at risk' have been developed. Both assays have the potential to be translated for use in chemical pathology departments. Importantly proteomic and metabolomic aspects of the study have highlighted the fact that a panel of biomarkers is required in order to gain a greater understanding of this multisystemic disease.

In addition to proteomic and metabolomic methodologies, a number of complementary techniques have been used in order to elucidate the underlying pathological disease mechanisms in Fabry disease. This has revealed a number of interesting avenues requiring further investigation but has demonstrated that there is much still to be learned about this complex disease.

7.2 Further work

The work completed in this thesis has revealed a number of biomarkers that when used in conjunction with Gb_3 and lyso-Gb_3 may provide further information and understanding in not only Fabry disease but other lysosomal disorders. However, in order to complete this work to enable the most information to be gathered requires the further development of the prosaposin and GM_2AP UPLC-MS/MS assay to optimise the detection of the mature saposins in order to analyse a larger cohort of Fabry patients as well as other lysosomal storage disorders which require saposins as cofactors. In addition, the continued analysis of renal biomarkers in those 'at-risk' patient groups is required in order to fully validate these biomarkers prior to their routine use.

The metabolomic aspect of this study revealed a large number of analogs/ isoforms in the plasma of Fabry patients. In order for these biomarkers to provide valuable information requires incorporation of the most abundant of the analogs/isoforms into routine Gb_3 analyses. In addition, the low abundance of two of the metabolite biomarkers revealed during the study prevented the elucidation of their structures. Only by establishing the structure of these potential biomarkers can we gain the fullest possible picture of the metabolic profile in Fabry disease.

The study in chapter 5 to investigate the toxicity of Gb_3 and lyso-Gb_3 in a Fabry mouse model has revealed a number of avenues for exploration which have as yet have received little attention. Particularly, the use of immunohistochemistry to validate the proteins detected as altered in mouse tissues during the label-free proteomic profiling study should be performed. In addition, further investigations into the finding that ATP synthase is increased by increasing levels of glycosphingolipids and their deacylated counterparts, using blue native

gel, should be performed in Fabry mice to confirm the increases observed in this study. In addition, an assessment of the levels of ATP production is required to ascertain to what, if any, the effect an increase in ATP synthase activity will have.

8.0 References

Abe A, Gregory S, Lee L *et al.* (2000) Reduction of globotriaosylceramide in Fabry disease mice by substrate deprivation. *J Clin Invest* **105**: 1563–71.

Ackermann BL, Hale JE, Duffin KL (2006) The role of mass spectrometry in biomarker discovery and measurement. *Curr Drug Metab* **7**: 525–39.

Aebersold R, Mann M (2003) Mass spectrometry-based proteomics. *Nature* **422**:198–207.

Aerts JM, Kallemeijn WW, Wegdam W *et al.* (2011) Biomarkers in the diagnosis of lysosomal storage disorders: proteins, lipids and inhibodies. *J Inherit Metab Dis* **34**: 605–19.

Aerts JM, Groener JE, Kuiper S *et al.* (2008) Elevated globotriaosylceramide is a hallmark of Fabry disease. *Proc Natl Acad Sci U S A* **105**: 2812–7.

Aerts JM, Hollak CE, van Breemen M *et al.* (2005) Identification and use of biomarkers in Gaucher disease and other lysosomal storage diseases. *Acta Paediatr Suppl* **94**: 43–6.

Allikmets R, gerrard B, Hutchinson A, Dean M (1996) Characterization of the human ABc superfamily: isolation and mapping of 21 new genes using the expressed sequence tags database. *Hum Mol Genet* **5**: 1649–55.

Altarescu GM (2010) Clinically relevant examples of genotype-phenotype correlation. In *Fabry disease*. New York, USA: Springer. pp. 105–109.

Altarescu GM, Goldfarb LG, Park KY *et al.* (2001) Identification of fifteen novel mutations and genotype-phenotype relationship in Fabry disease. *Clin Genet* **60**: 46–51.

Álvarez-Sánchez B, Priego-Capote F, Luque de Castro MD (2010) Metabolomics analysis II. Preparation of biological samples prior to detection. *Trends Analyt Chem* **29**: 120–7.

Anderson W (1898) A case of angiokeratoma. *Br J Dermatol* **10**: 113–17.

Andrade J, Waters PJ, Singh RS *et al.* (2008) Screening for Fabry disease in patients with chronic kidney disease: limitations of plasma alpha-galactosidase assay as a screening test. *Clin Am Soc Nephrol* **3**: 139–45.

Ashley GA, Shabbeer J, Yasuda M, Eng CM, Desnick RJ (2001) Fabry disease: twenty novel alpha-galactosidase A mutations causing the classical phenotype. *J Hum Genet* **46**: 192–6.

Ashton-Prolla P, Tong B, Shabbeer J *et al*. (2000) Fabry disease: twenty-two novel mutations in the alpha-galactosidase A gene and genotype/phenotype correlations in severely and mildly affected hemizygotes and heterozygotes. *J Investig Med* **48**: 227–35.

Auray-Blais C, Cyr D, Mills K, Giguère R, Drouin R (2007) Development of a filter paper method potentially applicable to mass ans high-risk urinary screenings for Fabry disease. *J Inherit Metab Dis* **30**: 106.

Auray-Blais C, Boutin M (2012) Novel Gb_3 isoforms detected in urine of Fabry disease patients: a metabolomic study. *Curr Med Chem* **19**: 3241–52.

Auray-Blais C, Boutin M, Gagnon R *et al.* (2012) Urinary globotriaosylsphingosine-related biomarkers for Fabry disease target by metabolomics. *Anal Chem* **84**: 2745–53.

Auray-Blais C, Cyr D, Ntwari A *et al*. (2008) Urinary globotriaosylceramide excretion correlates with the genotype in children and adults with Fabry disease. *Mol Genet Metab* **93**: 331–40.

Auray-Blais C, Ntwari A, Clarke JT *et al.* (2010) How well does urinary lyso-Gb_3 function as a biomarker in Fabry disease? *Clin Chim Acta* **411**: 1906–14.

Backenroth R, Landau EH, Goren M, Raas-Rothschild A (2010) Fabry disease and G6PD in three family members with priaprism: is the nitric oxide pathway to blame? *J Sex Med* **7**: 1588–91.

Banerjee S, Mazumdar S (2012) Electrospray ionization mass spectrometry: a technique to access the information beyond the molecular weight of the analyte. *Int J Anal Chem* doi: 10.1155/2012/282574.

Banikazemi M, Bultas J, Waldek S *et al.* (2007) Agalsidase-beta therapy for advanced Fabry disease: a randomised trial. *Ann Intern Med* **146**: 77–86.

Baptista MV, Ferreira S, Pinho-E-Melo T *et al.* (2010) Mutations of the GLA gene in young patients with stroke: the PORTYSTROKE study – screening genetic conditions in Portuguese young stroke patients. *Stroke* **41**: 431–6.

Baradaran R, Berrisford JM, Minhas GS, Sazanov LA (2013) Crystal structure of the entire respiratory complex I. *Nature* **494**: 443–8.

Barbey F, Brakch N, Linhart A *et al.* (2006) Increased carotid intima-media thickness in the absence of atherosclerotic plaques in an adult population with Fabry disease. *Acta Paediatr Suppl* **95**: 63–8.

Bard J, Wall MD, Lazari O, Arjomand J, Munoz-Sanjuan I (2014) Advances in Huntington disease drug discovery: novel approaches to model disease phenotypes. *J Biomol Screen* **19**: 191–204.

Barton NW, Brady RO, Dambrosia JM *et al.* (1991) Replacement therapy for inherited enzyme deficiency – macrophage-targeted glucocerebrosidase for Gaucher's disease. *N Engl J Med* **324**: 1464–70.

Báthori G, Csordas G, Garcia-Perez C *et al.* (2006) Ca2+ dependent control of the permeability properties of the mitochondrial outer membrane and voltage-dependent anion-selective channel (VDAC). *J Biol Chem* **281**: 17347–58.

Beck M (2001) Variable clinical presentation in lysosomal storage disorders. *J Inherit Metab Dis* **24**: 45–51.

Beck M (2010) Therapy for lysosomal storage disorders. *IUBMB Life* **62**: 33–40.

Beck M, Ricci R, Widmer U *et al.* (2004) Fabry disease: overall effects of agalsidase alfa treatment. *Eur J Clin Invest* **34**: 838–44.

Beer G, Reinecke P, Gabbert HE, Hort W, Kuhn H (2002) Fabry disease in patients with hypertrophic cardiomyopathy (HCM). *Z Kardiol* **91**: 992–1002.

Bekri S (2006) Laboratory diagnosis of lysosomal storage diseases. In *Fabry Disease: Perspectives from 5 years of FOS.* Oxford, UK: Oxford PharmaGenesis Ltd. pp. 45–50.

Bekri S, Lidove O, Jaussaud R, Knebelmann B, Barbey F (2006) The role of ceramide trihexoside (globotriaosylceramide) in the diagnosis and follow-up of the efficacy of treatment of Fabry disease: a review of the literature. *Cardiovasc Hematol Agents Med Chem* **4**: 289–97.

Benjamin ER, Khanna R, Schilling A *et al.* (2012) Co-administration with the pharmacological chaperone AT1001 increases recombinant human α-galactosidase A tissue uptake and improves substrate reduction in Fabry mice. *Mol Ther* **20**: 717–26.

Bennett K, Callard R, Heywood W *et al.* (2010) New role for LEKTI in skin barrier formation: label-free quantitative proteomic identification of caspase 14 as a novel target for the protease inhibitor LEKTI. *J Proteome Res* **9**: 4289–94.

Bertram R, Gram Pederson M, Luciani DS, Sherman A (2006) A simplified model for mitochondrial ATP production. *J Theor Biol* **243**: 575–86.

Bierer G, Kamangar N, Balfe D, Wilcox WR, Mosenifar Z (2005) Cardiopulmonary exercise testing in Fabry disease. *Respiration* **72**: 504–11.

Bishop DF, Calhoun DH, Bernstein HS *et al.* (1986) Human alpha-galactosidase A: nucleotide sequence of a cDNA clone encoding the mature enzyme. *Proc Natl Acad Sci U S A* **83**: 4859–63.

Bishop DF, Kornreich R, Desnick RJ (1988) Structural organization of the human alpha-galactosidase A gene: further evidence for the absence of a 3' untranslated region. *Proc Natl Acad U S A* **85**: 3903–7.

Blake R, Trounce IA (2013) Mitochondrial dysfunction and complications associated with diabetes. *Biochim Biophys Acta* pii: S0304 – 4165(13)00490-X.

Blaydon D, Hill J, Winchester B (2001) Fabry disease: 20 novel GLA mutations in 35 families. *Hum Mutat* **18**: 459.

Bolaños JP, Heales SJ, Peuchen S *et al.* (1996) Nitric oxide-mediated mitochondrial damage: a potential neuroprotective role for glutathione. *Free Radic Biol Med* **21**: 995–1001.

Bolaños JP, Peuchen S, Heales SJ, Land JM, Clark JB (1994) Nitric oxide-mediated inhibition of the mitochondrial respiratory chain iun cultured astrocytes. *J Neurochem* **63**: 910–6.

Bolignano D, Lacquaniti A, Coppolino G *et al.* (2009) Neutrophil gelatinase-associated lipocalin as an early biomarker of nephropathy in diabetic patients. *Kidney Blood Press Res* **32**: 91–8.

Bos JM, Towbin JA, Ackerman MJ (2009) Diagnostic, prognostic, and therapeutic implications of genetic testing for hypertrophic cardiomyopathy. *J Am Coll Cardiol* **54**: 201–11.

Bostanci N, Heywood W, Mills K *et al.* (2010) Application of label-free absolute quantitative proteomics in human gingival crevicular fluid by LC/MS E (gingival exudatome). *J Proteome Res* **9**: 2191–9.

Boutin M, Gagnon R, Lavoie P, Auray-Blais C (2012) LC-MS/MS analysis of plasma lyso-Gb_3 in Fabry disease. *Clin Chem Acta* **414**: 273–80.

Boutouyrie P, Laurent S, Laloux B *et al.* (2001) Non-invasive evaluation of arterial involvement in patients affected with Fabry disease. *J Med Genet* **38**: 629–31.

Boutouyrie P, Laurent S, Laloux B *et al.* (2002) Arterial remodelling in Fabry disease. *Acta Paediatr Suppl* **91**: 62–6.

Bouwman MG, Hollak CE, van den Bergh Weerman MA, Wijburg FA, Linthorst GE (2010) Analysis of placental tissue in Fabry disease with and without enzyme replacement therapy. *Placenta* **31**: 344–6.

Bradová V, Smid F, Ulrich-Bott B *et al.* (1993) Prosaposin deficiency: further characterization of the sphingolipid activator protein-deficient sibs. Multiple glycolipid elevations (including lactosylceramidosis), partial enzyme deficiencies and ultrastructure of the skin in this generalized sphingolipid storage disease. *Hum Genet* **92**: 143–52.

Brady RO, Gal AE, Bradley RM *et al.* (1967) Enzymatic defect in Fabry's disease. Ceramidetrihexosidase deficiency. *N Engl J Med* **276**: 1163–7.

Brakch N, Dormond O, Bekri S *et al.* (2010) Evidence for a role of sphingosine-1 phosphate in cardiovascular remodelling in Fabry disease. *Eur Heart J* **31**: 67–76.

Branton MH, Schiffmann R, Kopp JB (2002) Natural history and treatment of renal involvement in Fabry disease. *J Am Soc Nephrol* **13**: S139–43.

Branton MH, Schiffmann R, Sabnis SG *et al.* (2002) Natural history of Fabry renal disease: influence of alpha-galactosidase A activity and genetic mutations on clinical course. *Medicine (Baltimore)* **81**:122–38.

Brouns R, Sheorajpanday R, Braxel E *et al.* (2007) Middelheim Fabry Study (MiFaS): a retrospective Belgain study on the prevalence of Fabry disease in young patients with cryptogenic stroke. *Clin Neurol Neurosurg* **109**: 479–84.

Brouns R, Thijs V, Eyskens F *et al.* (2010) Belgian Fabry study: prevalence of Fabry disease in a cohort of 1000 young patients with cerebrovascular disease. *Stroke* **41**: 863–8.

Brown LK, Miller A, Bhuptani A *et al.* (1997) Pulmonary involvement in Fabry disease. *Am J Respir Crit Care Med* **155**: 1004–10.

Brzezinski P, Gennis RB (2008) Cytochrome c oxidase: exciting progress and remaining mysteries. *J Bioenerg Biomembr* **40**: 521–31.

Buechner S, Moretti M, Burlina AP *et al.* (2008) Central nervous system involvement in Anderson-Fabry disease: a clinical and MRI retrospective study. *J Neurol Neurosurg Psychiatry* **79**: 1249–54.

Burlina AP, Manara R, Caillaud C *et al.* (2008) The pulvinar sign: frequency and clinical correlations in Fabry disease. *J Neurol* **255**: 738–44.

Burlina AP, Politei J, Cinque S *et al.* (2012) The pulvinar sign in Fabry patients: the first report in female patients. *J Neurol* **259**: 1227–8.

Callahan BL, Gil AS, Levesque A, Mogil JS (2008) Modulation of mechanical and thermal nociceptive sensitivity in the laboratory mouse be behavioural state. *J Pain* **9**: 174–84.

Callea L, Arese M, Orlandini A *et al.* (1999) Platelet activating factor is elevated in cerebral spinal fluid and plasma of patients with relapsing-remitting multiple sclerosis. *J Neuroimmunol* **94**: 212–21.

Calles-Escandon J, Cipolla M (2001) Diabetes and endothelial dysfunction: a clinical perspective. *Endocr Rev* **22**: 36–52.

Campdelacreu J, Muñoz E, Gómez B *et al.* (2002) Gernealised dystonia with an abnormal magnetic resonance imaging signal in the basal ganglia: a case of adult-onset GM1 gangliosidosis. *Mov Disord* **17**: 1095–7.

Canuel M, Korkidakis A, Konnyu K, Morales CR (2008) Sortilin mediates the lysosomal targeting of cathepsins D and H. *Biochem Biophys Res Commun* **373**: 292–7.

Carroll J, Fearnley IM, Skehel JM *et al.* (2006) Bovine complex I is a complex of 45 different subunits. *J Biol Chem* **281**: 32724–7.

Caudron E, Molière D, Zhou JY, Prognon P, Germain DP (2005) [Recent advances of Fabry disease screening for at risk population.]. *Med Sci (Paris)* **21**: 48–50.

Cecchini G (2003) Function and structure of complex II of the respiratory chain. *Annu Rev Biochem* **72**: 77–109.

Chamoles NA, Blanco M, Gaggioli D (2001) Fabry disease: enzymatic diagnosis in dried blood spots on filter paper. *Clin Chim Acta* **308**: 195 – 6.

Chang MH, Bindloss CA, Grabowski GA *et al.* (2000) Saposins A, B, C and D in plasma of patients with lysosomal storage disorders. *Clin Chem* **46**: 167–74.

Chapman JR (2000) *Mass spectrometry of proteins and peptides*. Totowa, New Jersey: Humana Press.

Chaudhuri TK, Paul S (2006) Protein-misfolding diseases and chaperone-based therapeutic approaches. *FEBS J* **273**: 1331–49.

Chegary M, Brinke Ht, Ruiter JP *et al.* (2009) Mitochondrial long chain fatty acid beta-oxidation in man and mouse. *Biochim Biophys Acta* **1791**: 806–15.

Choi H, Cho YM, Suh KS *et al.* (2008) Short-term efficacy of enzyme replacement therapy in Korean patients with Fabry disease. *J Korean Med Sci* **23**: 243–50.

Choi JO, Lee MH, Park HY, Jung SC (2010) Characterization of Fabry mice treated with recombinant adeno-associated virus 2/8-mediated gene transfer. *J Biomed Sci* **17**:26.

Choi JS, Kim CS, Park JW *et al.* (2012) A novel small insertion mutation, C.1030_1031ins (T) in α-galactosidase A leads to renal variant Fabry disease. *Ren Fail* **34**: 390–3.

Chong CL, Huang SF, Hu CP *et al.* (2008) Decreased expression of UK114 is related to the differentiation status of human hepatocellular carcinoma. *Cancer Epidemiol Biomarkers Prev* **17**: 535–42.

Christensen EL, Birn H (2001) Megalin and cubilin: synergistic endocytic receptors in renal proximal tubule. *Am J Physiol Renal Physiol* **280**: F562–73.

Clavelou P, Besson G (2007) [Neurological aspects of Fabry disease]. *Presse Med* **36**: 1S65–8.

Cleland WW, Kennedy EP (1960) The enzymatic synthesis of psychosine. *J Biol Chem* **235**: 45–51.

Cole AL, Lee PJ, Hughes DA *et al.* (2007) Depression in adults with Fabry disease: a common and under-diagnosed problem. *J Inherit Metab Dis* **30**: 943–51.

Conti G, Sergi B (2003) Auditory and vestibular findings in Fabry disease: a study of hemizygous males and heterozygous females. *Acta Paediatr Suppl* **92**: 33–7.

Cook C, Stetler C, Petrucelli L (2012) Disruption of protein quality control in Parkinson's disease. *Cold Spring Harb Perspec Med* **2**: a009423.

Coutinho MF, Prata MJ, Alves S (2012) A shortcut to the lysosome: the mannose-6-phosphate-independent pathway. *Mol Genet Metab* **107**: 257–66.

Cox-Brinkman J, Vedder A, Hollak C *et al.* (2007) Three-dimensional face shape in Fabry disease. *Eur J Hum Genet* **15**: 535–42.

Cravatt BF, Simon GM, Yates JR 3rd (2007) The biological impact of mass-spectrometry based proteomics. *Nature* **450**: 991–1000.

Crofts AR (2004) The cytochrome bc1 complex: function in the context of structure. *Annu Rev Physiol* **66**: 689–733.

Crosbie TW, Packman W, Packman S (2009) Psychological aspects of patients with Fabry disease. *J Inherit Metab Dis* **32**: 745–53.

Cummings J, Raynaud F, Jones L, Sugar R and Dive C (2010) Fit-for-purpose biomarker method validation for application in clinical trials of anticancer drugs. *Br J Cancer* **103**: 1313–7.

Dajak M, Ignjatović S, Stojimirović B, Galić S, Majkić-Singh N (2011) Evaluation of renal damage by urinary beta-trace protein in patients with chronic kidney disease. *Clin Lab* **57**: 29–36.

Davies P, Eng CM, Hill JA *et al.* (1996) Fabry disease: fourteen alpha-galactosidase A mutations in unrelated families from the United Kingdom and other European countries. *Eur J Hum Genet* **4**: 219–24.

Decramer S, Gonzalez de Peredo A, Breuil B *et al.* (2008) Urine in clinical proteomics. *Mol Cell Proteomics* **7**: 1850–62.

Deegan PB, Baehner AF, Barba Romero MA *et al.* (2006) Natural history of Fabry disease in females in the Fabry Outcome Survey. *J Med Genet* **43**: 347–52.

de Hoffmann E, Stroobant V (2013) *Mass spectrometry: principles and applications.* Chichester, UK: ohn Wiley & Sons.

Dehout F, Schwarting A, Beck M *et al.* (2003) Effects of enzyme replacement therapy with agalsidase alfa on glomerular filtration rate in patients with Fabry disease: preliminary data. *Acta Paediatr Suppl* **92**: 14–5.

Desnick RJ, Ioannou YA, Eng CM (2001) alpha-galactosidase A deficiency: Fabry disease. In *The Metabolic and Molecular Bases of Inherited Disease*. Mcgraw-Hill, New York, USA. pp. 3733 – 3774.

Desnick RJ, Brady R, Barranger J *et al.* (2003) Fabry disease, an under-recognised multisystemic disorder: expert recommendations for diagnosis, managememnt, and enzyme replacement therapy. *Ann Intern Med* **138**: 338 – 46.

De Vries S, Albrachy SP, Berden JA, Slater EC (1982) The pathway of electrons through OH2: cytochrome c oxidoreductase studied by pre-steady – state kinetics. *Biochim Biophys Acta* **681**: 41–53.

Doleris LM, Hill GS, Chedin P *et al.* (2000) Focal segmental glomerulosclerosis associated with mitochondrial cytopathy. *Kidney Int* **58**: 1851–8.

Dröse S, Brandt U (2012) Molecular mechanisms of superoxide production by the mitochondrial respiratory chain. *Adv Exp Med Biol* **748**: 145–69.

Duman RS, Aghajanian GK (2012) Synaptic dysfunction in depression: potential therapeutic targets. *Science* **338**: 68–72.

Dupont FO, Gagnon R, Boutin M, Auray-Blais C (2013) A metabolomic study reveals novel plasma lyso-Gb3 analogs as Fabry disease biomarkers. *Curr Med Chem* **20**: 280–8.

Durant B, Forni S, Sweetman L *et al.* (2011) Sex differences of urinary and kidney globotriaosylceramide and lyso-globotriaosylceramide in Fabry mice. *J Lipid Res* **52**: 1742–6.

Eckardt KU, Coresh J, Devuyst O *et al.* (2013) Evolving importance of kidney disease: from sub-speciality to global health burden. *Lancet* **382**: 158–69.

Edelstein C (2010) *Biomarkers of Kidney Disease*. New York, USA: Elsevier.

eHealthMe (2004) Review: could Fabryzyme cause aspartate aminotransferase increase? http://www.ehealthme.com/ds/fabrazyme/aspartate+aminotransferase+increased Accessed 21/01/14.

Ejerblad E, Fored CM, Lindblad P *et al.* (2006) Obesity and risk factor for chronic renal failure. *J Am Soc Nephrol* **17**: 1695–702.

Elliott PM, Kindler H, Shah JS *et al.* (2006) Coronary microvascular dysfunction in male patients with Anderson-Fabry disease ad the effect of treatment with alpha galactosidase A. *Heart* **92**: 357–60.

Ellis JM, Mentock SM, Depetrillo MA *et al.* (2011) Mouse cardiac acyl coenzyme a synthetase 1 deficiency impairs fatty acid oxidation and induces cardiac hypertrophy. *Mol Cell Biol* **31**: 1252–62.

Emma F, Bertini E, Salviati L, Montini G (2012) Renal involvement in mitochondrial cytopathies. *Pediatr Nephrol* **27**: 539–50.

Eng CM, Ashley GA, Burgert TS *et al.* (1997) Fabry disease: thirty-five mutations in the alpha-galactosidase A gene in patients with classic and variant phenotypes. *Mol Med* **3**: 174–82.

Eng CM, Guffon N, Wilcox WR *et al.* (2001) Safety and efficacy of recombinant human alpha-galactosidase A—replacement therapy in Fabry's disease. *N Engl J Med* **345**: 9–16.

Eng CM, Germain DP, Banikazemi M *et al.* (2006) Fabry disease: guidelines for the evaluation and management of multi-organ system involvement. *Genet Med* **8**: 539–48.

Fabry J (1898) Ein Beitrag Zur Kenntnis Der Purpura Haemorrhagica Nodularis (Purpura Papulosa Haemorrhagica Hebrae). *Arch Dermatol Syph* **43**: 187–200.

Fabry J (1916) Zur Klinik Und Aetiologie Des Angiokeratoma. *Arch Dermatol Syph* **123**: 294–307.

Fabry J (1930) Beitrag Zur Klinik Des Angiokeratoma Naeviforme. *Dermatol Wochenschr* **90**: 339.

Fassett RG, Venuthurupalli SK, Gobe GC *et al.* (2011) Biomarkers in chronic kidney disease: a review. *Kidney Int* **80**: 806–21.

Fatania HR, Dalziel K (1980) Intracellular distribution of NADP-linked isocitrate dehydrogenase, fumarase and citrate synthase in bovine heart muscle. *Biochim Biophys Acta* **631**: 11–9.

Fellgiebel A, Keller I, Marin D *et al.* (2009) Diagnostic utility of different MRI and MR angiography measures in Fabry disease. *Neurology* **72**: 63–8.

Fellgiebel A, Albrecht J, Dellani PR *et al.* (2007) Quantification of brain tissue alterations in Fabry disease using diffusion-tensor imaging. *Acta Paediatr Suppl* **96**: 33–6.

Fenn JB, Mann M, Meng CK, Wong SF, Whitehouse CM (1989) Electrospray ionization for mass spectrometry of large biomolecules. *Science* **246**: 64–71.

Fernández-Vizarra E, Tiranti V, Zeviani M (2009) Assembly of the oxidative phosphorylation system in humans: what we have learned by studying its defects. *Biochim Biophys Acta* **1793**: 200 – 11.

Fervenza FC, Torra R, Larger DJ (2008) Fabry disease: an under-recognised cause of proteinuria. *Kidney Int* **73**: 1193–9.

Filatov V, Muhariamova K, Klimenko A *et al.* (2012) Poster B-234: Retinol-binding protein 4. *HyTest Ltd*. http://wwww.hytest.fi/poster-b-234-retinol-binding-protein-4.

Fletcher JM (2006) Screening for lysosomal storage disorders – a clinical perspective. *J inherit Metab Dis* **29**: 405–8.

Foda MM, Mahmood K, Rasuli P *et al.* (1996) High flow priapism associated with Fabry's disease in a child: a case report and review of the literature. *Urology* **48**: 949–52.

Folbergrová J, Kunz WS (2012) Mitochondrial dysfunction in epilepsy. *Mitochondrion* **12**: 35 – 40.

Frangogiannis Ng, Smith CW, Entman ML (2002) The inflammatory response in myocardial infarction. *Cardiovasc Res* **53**: 31 – 47.

Frey SK, Nagl B, Henze A *et al.* (2008) Isoforms of retinol binding protein 4 (RBP4) are increased in chronic diseases of the kidney but not of the liver. *Lipids Health Dis* **7**: 29.

Froissart R, Piraud M, Maire I (2010) [Contribution of genotyping in Fabry's disease]. *Rev Med Interne* **31**: S275–8.

Frustaci A, Chimenti C, Ricci R *et al.* (2001) Improvement in cardiac function in the cardiac variant of Fabry's disease with galactose-infusion therapy. *N Engl J Med* **345**: 25–32.

Fukuda T, Ewan L, Bauer M *et al.* (2006) Dysfunction of endocytic and autophagic pathways in a lysosomal storage disease. *Ann Neurol* **59**: 700–8.

Fuller M, Meikle PJ, Hopwood JJ (2006) Epidemiology of lysosomal storage diseases: an overview. In *Fabry Disease: Perspectives from 5 Years of FOS*. Oxford, UK: Oxford PharmaGenesis Ltd. pp. 9–20.

Garcia SF, Virág L, Jagtap P *et al.* (2001) Diabetic endothelial dysfunction: the role of poly(ADP – ribose) polymerase activation. *Nat Med* **7**: 108–13.

Garman SC (2007) Structure-function relationships in alpha-galactosidase A. *Acta Paediatr Suppl* **96**: 6–16.

Garman SC, Garboczi DN (2004) The molecular defect leading to Fabry disease: structure of human alpha-galactosidase. *J Mol Biol* **337**: 319–35.

Gegg ME, Beltran B, Salas-Pino S *et al.* (2003) Differential effect of nitric oxide on glutathione metabolism and mitochondrial function in astrocytes and neurones: implications for neuroprotection/neurodegeneration? *J Neurochem* **86**: 228–237.

Gekle M (1998) Renal proximal tubular albumin reabsorption: daily prevention of albuminuria. *News Physiol Sci* **13**: 5–11.

Gelb MH, Turecek F, Scott CR, Chamoles NA (2006) Direct multiplex assay of enzymes in dried blood spots by tandem mass spectrometry for the newborn screening of lysosomal storage disorders. *J Inherit Metab Dis* **29**:397–404.

Germain DP (2006) General aspects of X-linked disease. In *Fabry Disease: Perspectives from 5 Years of FOS*. Oxford, UK: Oxford PharmaGenesis Ltd. pp. 63–68.

Germain DP, Avan P, Chassaing A, Bonfils P (2002a) Patients affected with Fabry disease have an increased incidence of progressive hearing loss and sudden deafness: an investigation of twenty-two hemizygous male patients. *BMC Med Genet* **3**: 10.

Germain DP, Benistan K, Boutouyrie P, Mutschler C (2005a) Osteopenia ans osteoporosis: previously unrecognised manifestations of Fabry disease. *Clin Genet* **68**: 93–5.

Germain DP, Benistan K, Khatchikian L, Mutschler C (2005b) [Bone involvement in Fabry disease]. *Med Sci (Paris)* **21**: 43–4.

Germain DP, Shabbeer J, Cotigny S, Desnick RJ (2002b) Fabry disease: twenty novel alpha-galactosidase A mutations and genotype-phenotype correlations in classical and variant phenotypes. *Mol Med* **8**: 306–12.

Germain DP (2010) Fabry disease. *Orphanet J Rare Dis* **5**: 30.

Germain DP, Waldek S, Banikazemi M *et al.* (2007) Sustained, long-term renal stabilization after 54 months of agalsidase beta therapy in patients with Fabry disease. *J Am Soc Nephrol* **18**: 1547-57.

Giacomello M, Hudec R, Lopreiato R (2011) Huntington's disease, calcium, and mitochondria. *Biofactors* **37**: 206–18.

Giuseppe P, Daniele R, Rita BM (2013) Cutaneous complications of Anderson-Fabry disease. *Curr Pharm Des* **19**: 6031–6.

Gold KF, Pastores GM, Botteman MF *et al.* (2002) Quality of life of patients with Fabry disease. *Qual Life Res* **11**: 317–327.

Griffiths WJ, Wang Y (2009) Mass spectrometry: from proteomics to metabolomics and lipidomics. *Chem Soc Rev* **38**:

Gross JH (2011) *Mass spectrometry: A textbook*. Dordrecht, Netherlands: Springer.

Gunta SS, Mark RH (2013) Is obesity a risk factor for chronic kidney disease in children? *Pediatr Nephrol* **28**: 1949–56.

Hagège AA, Caudron E, Damy T *et al.* (2011) Screening patients with hypertrophic cardiomyopathy for Fabry disease using a filter-paper test: the FOCUS study. *Heart* **97**: 131–6.

Hall AM, Unwin RJ, Hanna MG, Duchen MR (2008) Renal function and mitochondrial cytopathy (MC): more questions than answers? *QJM* **101**: 755–66.

Happle R (1985) Lyonization and the lines of Blaschko. *Hum Genet* **70**: 200–206.

Hargreaves IP, Heales SJ, Land JM (1999) Mitochondrial respiratory chain defects are not accompanied by an increase in the activities of lactate dehydrogenase or manganese superoxide dismutase in paediatric skeletal muscle biopsies. *J Inherit Metab Dis* **22**: 925–31.

Haskins ME, Giger U, Patterson DF (2006) Animal models of lysosomal storage disease: their development and clinical relevance. In *Fabry Disease: Perspectives from 5 years of FOS.* Oxford UK: Oxford PharmaGenesis Ltd. pp. 51–61.

Hauser AC, Gessl A, Lorenz *et al.* (2005) High prevalence of subclinical hypothyroidism in patients with Anderson-Fabry disease. *J Inherit Metab Dis* **28**: 715–22.

Heare T, Alp N, Priestman DA *et al.* (2007) Severe endothelial dysfunction in the aorta of a mouse model of Fabry disease; partial prevention by N-butyldeoxynojirimycin treatment. *J Inherit Metab Dis* **30**: 79–87.

Heywood W, Wang D, Madgett TE *et al.* (2012a) The development of a peptide SRM-based tandem mass spectrometry assay for prenatal screening of Down syndrome. *J Proteomics* **75**: 3248–57.

Heywood WE, Mills K, Wang D *et al.* (2012b) Identification of new biomarkers for Down's syndrome in maternal plasma. *J Proteomics* **75**: 2621–8.

Higashi K, Kubo H, Watanabe H *et al.* (2011) Adipokine ganglioside GM_2 activator protein stimulates insulin secretion. *FEBS Lett* **585**: 2587–91.

Hilz MJ, Marthol H, Schwab S *et al.* (2010) Enzyme replacement therapy improves cardiovascular responses to orthostatic challenge in Fabry patients. *J Hypertens* **28**: 1438–48.

Hilz MJ, Kolodny EH, Brys M *et al.* (2004) Reduced cerebral blood flow velocity and impaired cerebral autoregulation in patients with Fabry disease. *J Neurol* **251**: 564–70.

Hiraiwa M, Martin BM, Kishimtot Y *et al.* (1997) Lysosomal proteolysis of prosaposin, the precursor of saposins (sphingolipid activator proteins): its mechanism and inhibition by ganglioside. *Arch Biochem Biophys* **341**: 17–24.

Hirawa N, Uehara Y, Ikeda T *et al.* (2001) Urinary prostaglandin D synthase (beta-trace) excretion increases in the early stage of diabetes mellitus. *Nephron* **87**: 321–7.

Hirst J (2009) Towards the molecular mechanism of respiratory complex I. *Biochem J* **425**: 327–39.

Hirst J (2013) Mitochondrial complex I. *Annu Rev Biochem* **82**: 551–75.

Ho CS, Lam CW, Chan MH *et al.* (2003) Electrospray ionisation mass spectrometry: principles and clinical applications. *Clin Biochem Rev* **24**: 3–12.

Hoffman B, Beck M, Sunder-Plassmann G *et al.* (2007a) Nature and prevalence of pain in Fabry disease and its response to enzyme replacement therapy – a retrospective analysis from the Fabry Outcome Survey. *Clin J Pain* **23**: 535 – 42.

Hoffmann B, Georg Koch H, Schweitzer-Krantz S, Wendel U, Mayatepek E (2005) Deficient alpha-galactosidase A activity in plasma but no Fabry disease – a pitfall in diagnosis. *Clin Chem Lab Med* **43**: 1276 – 7.

Hoffmann B, Schwarz M, Mehta A, Keshav S, Fabry Outcome Survey European Investigators (2007b) Gastrointestinal symptoms in 342 patients with Fabry disease: prevalence and response to enzyme replacement therapy. *Clin Gastroenterol Hepatol* **5**:1447–53.

Hoffmann E, Stroobant V (2013) *Mass Spectrometry: Principles and Applications*. Chichester, UK: John Wiley & Sons.

Hollak CE, Hughes D, van Schaik IN, Schwierin B, Bembi B (2009) Miglustat (Zavesca) in type I Gaucher disease: 5-year results of a post-authorisation safety surveillance programme. *Pharmacoepidemiol Drug Saf* **18**: 770–7.

Hopkin RJ, Bissler J, Banikazemi M *et al.* (2008) Characterization of Fabry disease in 352 pediatric patients in the Fabry registry. *Pediatr Res* **64**: 550–5.

Hughes DA, Elliott PM, Shah J *et al.* (2008) Effects of enzyme replacement therapy on the cardiomyopathy of Anderson-Fabry disease: a randomised, double-blind, placebo-controlled clinical trial of agalsidase alfa. *Heart* **94**: 153–8.

Hughes DA, Barba Romero MÁ, Hollak CE, Giugliani R, Deegan PB (2011) Response of women with Fabry disease to enzyme replacement therapy: comparison with men, using data from FOS – the Fabry Outcome Survey. *Mol Genet Metab* **103**: 207–14.

Hulka BS (1990). Overview of biological markers. In: Biological markers in epidemiology, pp 3 – 15. New York: Oxford University Press.

Hůlková H, Ledvinová J, Poupětová H *et al.* (1999) [Postmortem diagnosis of Fabry disease in a female heterozygote leading to the detection of undiagnosed manifest disease in the family]. *Cas Lek Cesk* **138**:660–4.

Hung YH, Chen LM Yang JY, Yang WY (2013) Spatiotemporally controlled induction of autophagy-mediated lysosome turnover. *Nat Commun* **4**:2111.

Hwu WL, Chien YH, Lee NC *et al.* Newborn screening for Fabry disease in Taiwan reveals a high incidence of the later-onset GLA mutation c.936+919>A (IVS4+919G>A). *Hum Mutat.* **30**:1397–405.

Ichinose M, Nakayama M, Ohashi T *et al.* (2005) Significance of screening for Fabry disase among male dialysis patients. *Clin Exp Nephrol* **9**: 228–32.

Ingwall JS (2009) Energy metabolism in heart failure and remodelling. *Cardiovasc Res* **81**: 412–9.

Ioannou YA, Zeidner KM, Gordon RE, Desnick RJ (2001) Fabry disease: preclinical studies demonstrate the effectiveness of alpha-galactosidase A replacement in enzyme-deficient mice. *Am J Hum Genet* **68**: 14–25.

Iribarne JV, Thomson BA (1976) On the evaporation of small ions from charged droplets. *J Chem Phys* **64**: 2287–2294.

Ishii S (2012) Pharmacological chaperone therapy for Fabry disease. *Proc Jpn Acad Ser B Phys Biol Sci* **88**: 18–30.

Ishii S, Chang HH, Yoshioka *et al.* (2009) Preclinical efficacy and safety of 1-deoxygalactonojirimycin in mice for Fabry disease. *J Pharmacol Exp Ther* **328**: 723–31.

Issaq HJ, Veenstra TD (2013) *Proteomic and metabolomic approaches to biomarker discovery.* London, UK: Academic Press.

Ivleva VB, Yu YQ, Gilar M (2010) Ultra-performance liquid chromatography/tandem mass spectrometry (UPLC/MS/MS) and UPLC/MS(E) analysis of RNA oligonucleotides. *Rapid Commun Mass Spectrom* **24**: 2631–40.

Jardim L, Vedolin L, Schwartz IV *et al.* (2004) CNS involvement in Fabry disease: clinical and imaging studies before and after 12 months of enzyme replacement therapy. *J Inherit Metab Dis* **27**: 229–40.

Jarreta D, Orús J, Barrientos A *et al.* (2000) Mitochondrial function in heart muscle from patients with idiopathic dilated cardiomyopathy. *Cardiovasc Res* **45**: 860–5.

Jeyakumar M, Dwek RA, Butters TD, Platt FM (2005) Storage solutions: treating lysosomal disorders of the brain. *Nat Rev Neurosci* **6**: 713–25.

Kalliokoski RJ, Kantola I, Kalliokoski KK *et al.* (2006) The effect of 12-month enzyme replacement therapy on myocardial perfusion in patients with Fabry disease. *J Inherit Metab Dis* **29**: 112–8.

Kampmann C, Baehner F, Whybra C *et al.* (2002) Cardiac manifestations of Anderson-Fabry disease in heterozygous females. *J Am Coll Cardiol* **40**: 1668–74.

Katyare SS, Satav JG (2005) Effect of streptozotocin-induced diabetes on oxidative energy metabolism in rat kidney mitochondria. A comparative study of early and late effects. *Diabetes Obes Metab* **7**: 555–62.

Kaushik S and Cuervo AM (2012) Chaperone-mediated autophagy: a unique way to enter the lysosome world. *Trends Cell Biol* **22**: 407–17.

Kawli T, He F, Tan MW (2010) It takes nerves to fight infections: insights on neuro-imune interactions form C. elegans. *Dis Model Mech* **3**: 721–31.

Khan M, Haq E, Giri S, Singh I, Singh AK (2005) Peroxisomal participation in psychosine-mediated toxicity: implications for Krabbe's disease. *J Neurosci Res* **80**: 845 – 54.

King TE (1967) Preparation of succinate cytochrome c reductase and cytochrome b-cl particle and reconstitution of succinate cytochrome c reductase. *Meth Enzymol* **10**: 217–235.

Kirsztajn GM, Nishida SK, Silva MS *et al.* (2002) Urinary retinol-binding protein as a prognostic marker in glomerulopathies. *Nephron* **90**: 424–31.

Kiselyov K, Yamaguchi S, Lyons CW, Muallem S (2010) Aberrant Ca_2^+ handling in lysosomal storage disroders. *Cell Calcium* **47**: 103–11.

Kishimoto Y, Hiraiwa M, O'Brien JS (1992) Saposins: structure, function, distribution, and molecular genetics. *J Lipid Res* **33**: 1255–67.

Kitagawa T, Ishige N, Suzuki K *et al.* (2005) Non-invasive screening method for Fabry disease by measuring globotriaosylceramide in whole urine samples using tandem mass spectrometry. *Mol Genet Metab* **85**: 196–202.

Klebl BM, Ayoub AT, Pette D (1998) Protein oxidation, tyrosine nitration, and inactivation of sarcoplasmic reticulum Ca2+-ATPase in low-frequency stimulated rabbit muscle. *FEBS Lett* **422**: 381–4.

Klein CJ, Lennon VA, Aston PA, McKeon A, Pittock SJ (2012) Chronic pain as a manifestation of potassium channel-complex autoimmunity. *Neurology* **79**: 1136–44.

Kleinert J, Dehout F, Schwarting A *et al.* (2005) Anemia is a new complication in Fabry disease: data from the Fabry Outcome Survey. *Kidney Int* **67**: 1955–60.

Klionsky DJ and Schulman BA (2014) Dynamic regulation of macroautophagy by distinctive ubiquitin-like proteins. *Nat Struct Mol Biol* **21**: 336–45.

Kobayshi T, Goto I, Okada S *et al.* (1992) Accumulation of lysosphingolipids in tissues from patients with Gm1 and GM2 gangliosidoses. *J Neurochem* **59**: 1452–8.

Kornreich R, Desnick RJ, Bishop DF (1989) Nuclotide sequence of the human alpha-galactosidase A gene. *Nucleic Acids Res* **17**: 3301–2.

Kurtz DM, Rinaldo P Rhead WJ *et al.*, (1998) Targeted disruption of mouse long-chain acyl-CoA dehydrogenase gene reveals crucial roles for fatty acid oxidation. *Proc Natl Acad Sci U S A* **95**: 15592–7.

Labarthe F, de Bodman C, Maruani A *et al.* (2010) [Priaprism: a severe paediatric complication of Fabry disease]. *Rev Med Interne* **31**: S217–9.

Larralde M, Boggio P, Amartino H, Chamoles N (2004) Fabry disease: a study of 6 hemizygous men and 5 heterozygous women with emphasis on dermatological manifestations. *Arch Dermatol* **140**: 1440–6.

Lattenist L, Kers J, Claessen N *et al.* (2013) Renal and urinary levels of endothelial protein C receptor correlate with acute renal allograft rejection. *PLoS One* **8**: e64994.

Lee AG (1995) *Biomembranes: general principles*. Hamption Hill, Middlesex: Jai Press LTD.

Lefrancois S, Zeng J, Hassan AJ, Canuel M, Morales CR (2003) The lysosomal trafficking of sphingolipid activator proteins (SAPs) is mediated by sortilin. *EMBO J* **22**: 6430–7.

Lehman TJA (2009) *A clinicians guide to rheumatic disease in children*. Oxford, UK: Oxford University Press.

Lemasters JJ, Qian T, He L *et al.* (2002) Role of mitochondrial inner membrane permeabilization in necrotic cell death, apoptosis, and autophagy. *Antioxid Redox Signal* **4**: 769–81.

Levin Y, Schwarz E, Wang L, Leweke FM, Bahn S (2007) Label-free LC-MS/MS quantitative proteomics for large-scale biomarker discovery in complex samples. *J Sep Sci* **30**: 2198–203.

Li Y, Scott CR, Chamoles NA *et al.* (2004) Direct multiplex assay of lysosomal enzymes in dried blood spots for newborn screening. *Clin Chem* **50**: 1785–96.

Lidove O, Ramaswami U, Jaussaud R *et al.* (2006) Hyperhidrosis: a new and often early symptom in Fabry disease. International experience and data from the Fabry Outcome Survey. *Int J Clin Pract* **60**: 1053–9.

Lidove O, Jaussaud R, aractingi S (2006) Dermatological and soft-tissue manifestations of Fabry disease: characteristics and response to enzyme replacement therapy. In *Fabry disease: Perspectives from 5 years of FOS.* Oxford, UK: Oxford PharmaGenesis Ltd. pp. 233–239.

Lindsberg P, Hallenbeck JM, Feuerstein G (1991) Platelet-activating factor in stroke and brain injury. *Ann Neurol* **30**: 117–29.

Linhart A, Palecek T, Bultas J *et al.* (2000) New insights in cardiac structural changes in patients with Fabry's disease. *Am Heart J* **139**: 1101–8.

Linhart A (2006) the heart in Fabry disease. In *Fabry disease: Perspectives from 5 years of FOS.* Oxford, UK: Oxford PharmaGenesis Ltd. pp. 189 – 201.

Linhart A, Elliott PM (2007) The heart in Anderson-Fabry disease and other lysosomal storage disorders. *Heart* **93**: 528–35.

Linthorst GE, Vedder AC, Aerts JM, Hollak CE (2005) Screening for Fabry disease using whole blood spots fails to identify one-third of female carriers. *Clin Chim Acta* **353**: 201–3.

Liu Y, Fiskum G, Schubert D (2002) Generation of reactive oxygen species by the mitochondrial electron transport chain. *J Neurochem* **80**: 780–7.

Lobo T, Morgan J, Bjorksten A *et al.* (2008) Cardiovascular testing in Fabry disease: exercise capacity reduction, chronotropic incompetence and improved anaerobic threshold after enzyme replacement. *Intern Med J* **38**: 407–14.

Louis ED, Lee P, Quinn L, Marder K (1999) Dystonia in Huntington's disease: prevalence and clinical characteristics. *Mov Disord* **14**: 95–101.

Lücke T, Höppner W, Schmidt E, Illsinger S, Das AM (2004) Fabry disease: reduced activities of respiratory chain enzymes with decreased levels of energy-rich phosphates in fibroblasts. *Mol Genet Metab* **82**: 93–7.

Lukacs Z, Keil A, Kohlschütter A, Beck M, Mengel E (2005) The ratio of alpha-galactosidase to beta-glucuronidase activities in dried blood for the identification of female Fabry disease patients. *J Inherit Metab Dis* **28**: 903–5.

Kunz JB, Schwarz H and Mayer A (2004) Detemination of four sequential stages during microautophagy in vitro. *J Biol Chem* **279**: 9987–96.

Lyon MF (1961) Gene activation in the X-chromosome of the mouse (Mus musculus L.). *Nature* **190**: 372–3.

MacDermot KD, Holmes A, Miners AH (2001) Anderson-Fabry disease: clinical manifestations and impact of disease in a cohort of 98 hemizygous males. *J Med Genet* **38**: 750–60.

Magage S, Lubanda JC, Susa Z *et al.* (2007) Natural history of the respiratory involvement in Anderson-Fabry disease. *J Inherit Metab Dis* **30**: 790–9.

Magage S, Lubanda JC, Germain DP *et al.* (2005) [Respiratory involvement in patients with Fabry disease.]. *Med Sci (Paris)* **21**: 37–9.

Mak SK, McCormack AL, Langston JW, Kordower JH, Di Monte DA (2009) Decreased alpha-synuclein expression in the aging mouse substantia nigra. *Exp Neurol* **220**: 359–65.

Malyszko J, Malyszko JS, Bachorzewska-Gajewska H *et al.* (2009) Neutrophil gelatinase-associated lipocalin is a new and sensitive marker of kidney function in chronic kidney disease patients and renal allograft recipients. *Transplant Proc* **41**: 158–61.

Mandemakers W, Morais VA, De Strooper B (2007) A cell biological perspective on mitochondrial dysfunction in Parkinson disease and other neurodegenerative diseases. *J Cell Sci* **120**: 1707–16.

Manwaring V, Prunty H, Bainbridge K *et al.* (2012) Urine analysis of glucose tetrasaccharide by HPLC; a useful marker for the investigation of patients with Pompe and other glycogen storage diseases. *J Inherit Metab Dis* **35**: 311–6.

Marques O, Outeiro TF (2012) Alpha-synuclein: from secretion to dysfunction and death. *Cell Death Dis* **3**: e350.

Marshall AG, Hendrickson CL, Jackson GS (1998) Fourier transform ion cyclotron resonance mass spectrometry: a primer. *Mass Spectrom Rev* **17**: 1–35.

Marshall J, Ashe KM, Bangari D *et al.* (2010) Substrate reduction augments the efficacy of enzyme therapy in a mouse model of Fabry disease. *PLoS One* **5**: e15033.

Marzella L, Ahlbergg J, Glaumann H (1981) Autophagy, heterophagy, microautophagy and crinophagy as the means for intracellular degradation. *Virchows Arch B Cell Pathol Incl Mol Pathol* **36**: 219–34.

Mayes JS, Scheerer JB, Sifers RN, Donaldson ML (1981) Differential assay for lysosomal alpha-galactosidase in human tissues and its application to Fabry's disease. *Clin Chim Acta* **112**: 247–51.

Mayor S, Pagano RE (2007) Pathways of clathrin-independent endocytosis. *Nat Rev Mol Cell Biol* **8**: 603 – 612.

Mechtler TP, Stary S, Metz TF *et al.* (2012) Neonatal screening for lysosomal storage disorders: feasibility and incidence form a nationwide study in Austria. *Lancet* **379**: 335–41.

Mehta A, Beck M, Elliott P *et al.* (2009a) Enzyme replacement therapy with agalsidase alfa in patients with Fabry's disease: an analysis of registry data. *Lancet* **374**: 1986–96.

Mehta A, Clarke JT, Giugliani R *et al.* (2009b) Natural course of Fabry disease: changing pattern of causes of death in FOS – Fabry Outcome Survey. *J Med Genet* **46**: 548–52.

Mehta A, Ginsberg L, FOS Investigators (2005) Natural history of the cerebrovascular complications of Fabry disease. *Acta Paediatr Suppl* **94**: 24–7.

Mehta A, Ricci R, Widmer U *et al.* (2004) Fabry disease defined: baseline clinical manifestation of 366 patients in the Fabry Outcome Survey. *Eur Clin Invest* **34**: 236–42.

Mehta AB, Winchester B (2013) *Lysosomal storage disorders a practical guide*. Chichester, West Sussex: Wiley-Blackwell.

Meikle PJ, Hopwood JJ, Clague AE, Carey WF (1999) Prevalence of lysosomal storage disorders. *JAMA* **281**: 249 – 254.

Mersebach H, Johansson JO, Rasmussen AK *et al.* (2007) Osteopenia: a common aspect of Fabry disease. Predictors of bone mineral density. *Genet Med* **9**: 812–8.

Miedel MT, Rbaibi Y, Guerriero CJ *et al.* (2008) Membrane traffic and turnover in TRP-ML1-deficient cells: a revised model for mucolipidosis type IV pathogenesis. *J Exp Med* **205**: 1477–90.

Millington DS (2008) Rapid and effective screening for lysosomal storage disease: how close are we? *Clin Chem* **54**: 1592–4.

Mills K, Johnson A, Winchester B (2002) Synthesis of novel internal standards for the quantitative determination of plasma ceramide trihexoside in Fabry disease by tandem mass spectrometry. *FEBS Lett* **515**: 171–6.

Mills K, Mills P, Jackson M *et al.* (2006) Diagnosis of congenital disorders of glycosylation type-I using protein chip technology. *Proteomics* **6**: 2295–304.

Mills K, Morris P, Lee P *et al.* (2005) Measurement of urinary CDH and CTH by tandem mass spectrometry in patients hemizygous and heterozygous for Fabry disease. *J Inherit Metab Dis* **28**: 35–48.

Mills K, Vellodi A, Morris P *et al.* (2004) Monitoring the clinical and biochemical response to enzyme replacement therapy in three children with Fabry disease. *Eur J Pediar* **163**: 595–603.

Milne SB, Mathews TP, Myers DS, Ivanova PT, Brown HA (2013) Sum of the parts: mass spectrometry-based metabolomics. *Biochemistry* **52**: 3829–40.

Miners AH, Holmes A, Sherr L, Jenkinson C, MacDermot KD (2002) Assessment of health-related quality-of-life in males with Anderson Fabry disease before therapeutic intervention. *Qual Life Res* **11**: 127–33.

Mirković K, Doorenbos CR, Dam WA *et al.* (2013) Urinary vitamin D binding protein: a potential novel marker of renal interstitial inflammation and fibrosis. *PLoS One* **8**: e55887.

Mitsias P, Levine SR (1996) Cerebrovascular complications of Fabry's disease. *Ann Neurol* **40**: 8 – 17.

Moheimani F, Kim CH, Rahmanto AS, van Reyk DM, Davies MJ (2012) Inhibition of lysosomal function in macrophages incubated with evaluated glucose concentrations: a potential contributory factor in diabetes-associated atherosclerosis. *Atherosclerosis* **223**: 144–51.

Moore DF, Ye F, Schiffmann R, Butman JA (2003) Increased signal intensity in the pulvinar on T1-weighted images: a pathognomonic MR imaging sign of Fabry disease. *AJNR Am J Neuroradiol* **24**: 1096–101.

Morimoto S, Yamamoto Y O'Brien JS, Kishimoto Y (1990) Distribution of saposin proteins (sphingolipid activator proteins) in lysosomal storage and other diseases. *Proc Natl Acad Sci U S A* **87**: 3493–7.

Motwani M, Banypersad S, Woolfson P, Waldek S (2012) Enzyme replacement therapy improves cardiac features and severity of Fabry disease. *Mol Genet Metab* **107**: 197–202.

Müller KB, Galdieri LC, Pereira VG, Martins AM, D'Almeida V (2012) Evaluation of oxidative stress markers and cardiovascular risk factors in Fabry disease patients. *Genet Mol Biol* **35**: 418–23.

Müller MJ, Fellgiebel A, Scheurich A *et al.* (2006) Recurrent brief depression in a female patient with Fabry disease. *Bipolar Disor* **8**: 418–9.

Munusamy S, Saba H, Mitchell T *et al.* (2009) Alteration of renal respiratory Complex-III during experimental type-1 diabetes. *BMC Endocr Disord* **9**:2.

Muriel P, Sandoval G (2000) Nitric oxide and peroxynitrite anion modulate liver plasma membrane fluidity and Na()/K(+)-ATPase activity. *Nitric Oxide* **4**:333–42.

Murphy MP (2009) How mitochondria produce reactive oxygen species. *Biochem J* **417**: 1–13.

Nakao S, Takenaka T, Maeda M *et al.* (1995) An atypical variant of Fabry's disease in men with left ventricular hypertrophy. *N Engl J Med* **333**: 288–93.

Nakao S, Kodama C, Takenaka T *et al.* (2003) Fabry disease: detection of undiagnosed hemodialysis patients and identification of a "renal variant" phenotype. *Kidney Int* **64**: 801–7.

Nayak Shivananda B (2007) *Manipal manual of clinical biochemistry (for medical laboratory and MSc students).* New Delhi, India: Jaypee Brothers Publishers Ltd.

Naylor S (2003) Biomarkers: current perspectives and future prospects. *Expert Rev Mol Diagn* **3**: 525–9.

Nelson MP, Tse TE, O'Quinn DB *et al.*, (2014) Autophagy-lysosome pathway associated neuropathology and axonal degeneration in the brains of alpha-galactosidase A-deficient mice. *Acta Neuropathol Commun* **2**: 20.

Nguyen TT, Gin T, Nicholls K *et al.* (2005) Ophthalmological manifestations of Fabry disease: a survey of patients at the Royal Melbourne Fabry Disease Treatment Centre. *Clin Experiment Ophthalmol* **33**: 164–8.

Niaudet P (1998) Mitochondrial disorders and the kidney. *Arch Dis Child* **78**: 387–90.

Niaudet P, Rotig A (1997) The kidney in mitochondrial cytopathies. *Kidney Int* **51**: 1000–7.

Niemann M, Breunig F, Beer M *et al.* (2010) The right ventricle in Fabry disease: natural history and impact of enzyme replacement therapy. *Heart* **96**: 1915–9.

Nissim I, Daikhin Y, Nissim I *et al.* (2006) Agmatine stimulates hepatic fatty acid oxidation<: a possible mechanism for up-regulation of ureagenesis. *J Biol Chem* **281**: 8486–96.

Ni X, Canuel M, Morales CR (2006) The sorting and trafficking of lysosomal proteins. *Histol Histopathol* **21**: 899–913.

Nozza S, Pogliaghi M, Chiappetta S *et al.* (2012) Levels of soluble endothelial protein C receptor are associated with CD4+ changes in Maraviroc-treated HIV-infected patients. *PLoS One* **7**: e37032.

Nys A, Aubert X, de Duve C (1949) The distribution of glycogen in the liver of rabbits. *Biochem J* **43**: 245.

Ogawa K, Hirai Y, Ishizaki M *et al.* (2009) Long-term inhibition of glycosphingolipid accumulation in Fabry model mice by a single systemic injection of AAV1 vector in the neonatal period. *Mol Genet Metab* **96**: 91–6.

Ohshima T, Murray GJ, Swaim WD *et al.* (1997) Alpha-galactosidase A deficient mice: a model of Fabry disease. *Proc Natl Acad Sci U S A* **94**: 2540–4.

Oshima T, Schiffmann R, Murray GJ *et al.* (1999) Aging accentuates and bone marrow transplantation ameliorates metabolic defects in Fabry disease mice. *Proc Natl Acad Sci U S A* **96**: 6423–7.

Olanow CW, Brundin P (2013) Parkinson's disease nad alpha synuclein: is Parkinson's disease a prion-like disorder? *Mov Disord* **28**: 31–40.

Oliveira JP, Valbuena C, Baldaia Moreira A *et al.* (2008) Splenomegaly, hypersplenism and peripheral blood cytopaenias in patients with classical Anderson-Fabry disease. *Virchows Arch* **453**: 291–300.

O'Mahoney C, Elliott P (2010) Anderson-Fabry disease and the heart. *Prog Cardiovasc Dis* **52**: 326–335.

O'Mahony C, Coats C, Cardona M *et al.* (2011) Incidence and predictors of anti-bradycardia pacing in patients with Anderson-Fabry disease. *Europace* **13**: 1781–8.

Orriss GL, Leslie AG, Braig K, Walker JE (1998) Bovine F1-ATPase covalently inhibited with 4-chloro-7-nitrobenzofurazan: the structure provides further support for a rotary catalytic mechanism. *Structure* **6**: 831–7.

Orssaud C, Dufier J, Germain D (2003) Ocular manifestations in Fabry disease: a survey of 32 hemizygous male patients. *Ophthalmic Genet* **24**: 129–39.

Ortiz A, Oliveira JP, Waldek *et al.* (2008) Nephropathy in males and females with fabry disease: cross-sectional description of patients before treatment with enzyme replacement therapy. *Nephrol Dial Transplant* **23**: 1600–7.

Palecek T, Dostalova G, Kuchynka P *et al.* (2008) Right ventricular involvement in Fabry disease. *J Am Soc Echocardiogr* **21**: 1265–8.

Palla A, Hegemann S, Widmer U, Straumann D (2007) Vestibular and auditory deficits in Fabry disease and their response to enzyme replacement therapy. *J Neurol* **254**: 1433–42.

Parkinson-Lawrence EJ, Shandala T, Prodoehl M *et al.* (2010) Lysosomal storage disease: revealing lysosomal function and physiology. *Physiology (Bethesda)* **25**: 102–15.

Pastores GM (2009) *Lysosomal Storage Disorders: Principles and Practice*. Singapore: World Scientific Publishing.

Patergnani S, Suski JM, Agnoletto C *et al.* (2011) Calcium signalling around Mitochondria Associated Membranes (MAMs). *Cell Commun Signal* **9**: 19.

Pearl P (2013) Inherited metabolic epilepsies. New York, USA: Demos Medical Publishing.

Pieroni M, Chimenti C, Ricci R *et al.* (2003) Early detection of Fabry cardiomyopathy by tissue Doppler imaging. *Circulation* **107**: 1978–84.

Pieroni M, Chimenti C, Russo A *et al.* (2004) Tissue Doppler imaging in Fabry disease. *Curr Opin Cardiol* **19**: 452–7.

Pinto R, Caseiro C, Lemos M *et al.* (2004) Prevalence of lysosomal storage disease in Portugal. *Eur J Hum Genet* **12**: 87–92.

Platt FM, Walkley S (2004) *Lysosomal Disorders of the Brain*. Oxford UK: Oxford University Press.

Poorthuis BJ, Wevers RA, Kleijer WJ *et al.* (1999) The frequency of lysosomal storage disease in The Netherlands. *Hum Genet* **105**: 151–6.

Popli S, Leehey DJ, Molnar ZV, Nawab ZM, Ing TS (1990) Demonstration of Fabry's disease deposits in placenta. *Am J Obstet Gynecol* **162**: 464–5.

Poupetová H, Ledvinová J, Berná L *et al.* (2010) The birth prevalence of lysosomal storage disorders in the Czech Republic: comparison with data in different populations. *J Inherit Metab Dis* **33**: 387–96.

Prichard ER (2003) *High Performance Liquid Chromatography*. Cambridge, UK: Royal Society of Chemistry.

Prabakaran T, Nielsen R, Satchell SC *et al.* (2012) Mannose 6-phosphate receptor and sortilin mediated endocytosis of α-galactosidase A in kidney endothelial cells. *PLoS One* **7**: e39975.

Ragan CI, Wilson MT, Darley-Usmar VM, Lowe PN (1987) Subfractionation of mitochondria and isolation of proteins of oxidative phosphorylation. In *Mitochondria: a practical approach*. Oxford, UK: IRL Press. pp 79–112.

Ramaswami U, Parini R, Pinto-Morell G *et al.* (2012) Fabry disease in children and response to enzyme replacement therapy: results for the Fabry Outcome Survey. *Clin Genet* **81**: 485–90.

Ramaswami U, Wendt S, Pintos-Morell G *et al.* (2007) Enzyme replacement therapy with agalsidase alfa in children with Fabry disease. *Acta Paediatr* **96**: 122–7.

Ramaswami U, Whybra C, Pairini R *et al.* (2006) Clinical manifestation of Fabry disease in children: data from the Fabry outcome Survey. *Acta Paediatr* **95**: 86–92.

Ries M, Clarke JT, Whybra C *et al.* (2006a) Enzyme-replacement therapy with agalsidase alfa in children with Fabry disease. *Pediatrics* **118**: 924–32.

Ries M, Moore DF, Robinson CJ *et al.* (2006b) Quantitative dysmorphology assessment in Fabry disease. *Genet Med* **8**: 96–101.

Ries M, Ramaswami U, Parini R *et al.* (2003) The early clinical phenotype of Fabry disease: a study on 35 European children and adolescents. *Eur J Pediatr* **162**: 767–72.

Rigat B, Yeger H, Shehnaz D, Mahuran D (2009) GM_2 activator protein inhibits platelet activating factor signalling in rats. *Biochem Biophys Res Commun* **385**: 576–80.

Rolfs A, Böttcher T, Zschiesche M *et al.* (2005) Prevalence of Fabry disease in patients with cryptogenic stroke: a prospective study. *Lancet* **366**: 1794–6.

Rombach SM, Dekker N, Bouwman MG *et al.* (2010) Plasma globotriaosylsphingosine: diagnostic value and relation to clinical manifestations of Fabry disease. *Biochim Biophys Acta* **1802**: 741–8.

Rombach SM, Smid BE, Bouwman MG *et al.* (2013) Long term enzyme replacement therapy for Fabry disease: effectiveness on kidney, heart and brain. *Orphanet J Rare Dis* **8**: 47.

Rosca MG, Mustata TG, Kinter MT *et al.* (2005) Glycation of mitochondrial proteins from diabetic rat kidney is associated with excess superoxide formation. *Am J Physiol Renal Physiol* **289**: F420–30.

Rosenberg DM, Ferrans VJ, Fulmer JD *et al.* (1980) Chronic airflow obstruction in Fabry's disease. *Am J Med* **68**: 898–905.

Roze E, Paschke E, Lopex N *et al.*, (2005) Dystonia and parkinsonism in GM1 type 3 gangliosidosis. *Mov Disord* **20**: 1366–9.

Ruivo R, Anne C, Sagné C, Gasnier B (2009) Molecular and cellular basis of lysosomal transmembrane protein dysfunction. *Biochim Biophys Acta* **1793**: 636–49.

Sacre K, Lidove O, Giroux Leprieur B *et al.* (2010) Bone and joint involvement in Fabry disease. *Scand J Rheumatol* **39**: 171–4.

Sadek, Shellhaas R, Camfield CS, Camfield PR, Burley J (2004) Psychiatric findings in four female carriers of Fabry disease. *Psychiatr Genet* **14**: 199–201.

Sado DM, White SK, Piechnik SK *et al.* (2013) Identification and assessment of Anderson-Fabry disease bby cardiovascular magnetic resonance noncontrast myocardial T1 mapping. *Circ Cardiovasc Imaging* **6**: 392–8.

Saftig P (2005) *Lysosomes*. New York, USA: Springer.

Saftig P, Klumperman J (2009) Lysosome biogenesis and lysosomal membrane protein: trafficking meets function. *Nat Rev Mol Cell Biol* **10**: 623–35.

Sakuraba H, Oshima A, Fukuhara Y *et al.* (1990) Identification of point mutations in the alpha-galactosidase A gene in classical and atypical hemizygotes with Fabry disease. *Am J Hum Genet* **47**: 784–9.

Sakurai Y, Kojima H, Shiwa M *et al.* (2009) The hearing status in 12 female and 15 male Japanese Fabry patients. *Auris Nasus Larynx* **36**: 627–32.

Salehi A, Henningsson R, Mosén H *et al.* (1999) Dysfunction of the islet lysosomal system conveys impairment of glucose-induced insulin release in the diabetic GK rat. *Endocrinology* **140**: 3045–53.

Satoh H, Yamato O, Asano T *et al.* (2007) Cerebrospinal fluid biomarkers showing neurodegeneration in dogs with GM1 gangliosidosis: possible use for assessment of a therapeutic regimen. *Brain Res* **1133**: 200–8.

Schapira A (2003) *Mitochondrial Function and Dysfunction*. California, USA: Academic Press.

Schiffmann R, Kopp JB, Austin HA 3rd *et al.* (2001) Enzyme replacement therapy in Fabry disease: a randomized controlled trial. *JAMA* **285**: 2743–9.

Schiffmann R (2009) Fabry disease. *Pharmacol Ther* **122**: 65–77.

Schiffmann R, Martin RA, Reimschisel T *et al.* (2010) Four-year prospective clinical trial of agalsidase alfa in children with Fabry disease. *J Pediatr* **156**: 832–7.

Schiffmann R, Moore D (2006) Neurological manifestations of Fabry disease. In *Fabry Disease: Perspectives from 5 years of FOS.* Oxford, UK: Oxford PharmaGenesis Ltd. pp. 215–225.

Schiffmann R, Ries M, Timmons M, Flaherty JT, Brady RO (2006) Long-term therapy with agalsidase alfa for Fabry disease: safety and effects on renal function in a home infusion setting. *Nephrol Dial Transplant* **21**: 345–54.

Schiffmann R, Warnock DG, Banikazemi M *et al.* (2009) Fabry disease: progression of nephropathy, and prevalence of cardiac and cerebrovascular events before enzyme replacement therapy. *Nephrol Dial Transplant* **24**: 2102–11.

Schuette CG, Pierstorff B, Huettler S, Sandhoff K (2001) Sphingolipid activator proteins: proteins with complex functions in lipid degradation and skin biogenesis. *Glycobiology* **11**: 81R–90R.

Schultz ML, Tecedor L, Chang M, Davidson BL (2011) Clarifying Lysosmal Storage Diseases. *Trends Neurosci* **34**: 401–410.

Schwarting A, Debout F, Feriozzi S *et al.* (2006) Enzyme replacement therapy and renal function in 201 patients with Fabry disease. *Clin Nephrol* **66**: 77–84.

Scigelova M, Makarov A (2006) Orbitrap mass analyser – overview and applications in proteomics. *Proteomics* **6**: 16–21.

Senechal M, Germain DP (2003) Fabry disease: a functional and anatomical study of cardiac manifestations in 20 hemizygous male patients. *Clin Genet* **63**: 46–52.

Sergi B, Conti G, Paludetti G, Interdisiplinary Study Group On Fabry Disease (2010) Inner ear involvement in Anderson-Fabry disease: long-term follow-up during enzyme replacement therapy. *Acta Otorhinolaryngol Ital* **30**: 87–93.

Settembre C, Fraldi A, Jahreiss L *et al.* (2008) A block of autophagy in lysosomal storage disorders. *Hum Mol Genet* **17**: 119–29.

Shabbeer J, Yasuda M, Benson SD, Desnick RJ (2006) Fabry disease: identification of 50 novel alpha-galactosidase A mutations causing the classic phenotype and three-dimensional structural analysis of 29 missense mutations. *Hum Genomics* **2**: 297–309.

Shah JS, Hughes DA, Sachdev B *et al.* (2005) Prevalence and clinical significance of cardiac arrhythmia in Anderson-Fabry disease. *Am J Cardiol* **96**: 842–6.

Shayman J (2010) Experimental studies in mice on the vasculopathy of Fabry disease. In *Fabry Disease*. Springer: New York, USA. pp. 365–377.

Shen JS, Meng XL, Moore DF *et al.* (2008) Globotriaosylceramide induces oxidative stress and up-regulates cell adhesion molecule expression in Fabry disease endothelial cells. *Mol Genet Metab* **95**: 163–8.

Shepherd D and Garland PB (1969) The kinetic properties of citrate synthase from rat liver mitochondria. *Biochem J* **114**: 597–610.

Shiozuka C, Taguchi A, Matsuda J *et al.* (2011) Increased globotriaosylceramide levels in a transgenic mouse expressing human alpha 1, 4-galactosyltransferase and a mouse model for treating Fabry disease. *J Biochem* **149**: 161–70.

Sims K, Politei J, Banikazemi, Lee P (2009) Stroke in Fabry disease frequently occurs before diagnosis and in the absence of other clinical events: natural history data from the Fabry Registry. *Stroke* **40**: 788–94.

Sodi A, Ioannidis AS, Mehta A *et al.* (2007) Ocular manifestations of Fabry's disease: data from the Fabry Outcome Survey. *Br J Ophthalmol* **91**: 210–4.

Sodi A, Ioannidis AS, Pitz S (2006) Opthalmological manifestations of Fabry disease. In *Fabry Disease: Perspectives from 5 years of FOS.* Oxford, UK: Oxford PharmaGenesis Ltd. pp. 249–261.

Spada M, Pagliardini S, Yasuda M *et al.* (2006) High incidence of later-onset Fabry disease revealed by newborn screening. *Am J Hum Genet* **79**: 31–40.

Spinelli L, Pisani A, Sabbatini M *et al.* (2004) Enzyme replacement therapy with agalisidase beta improves cardiac involvement in Fabry's disease. *Clin Genet* **66**: 158–65.

Steen H, Mann M (2004) The ABC's (and XYZ's) of peptide sequencing. *Nat Rev Mol Cell Biol* **5**: 699–711.

Stock D, Leslie AG, Walker JE (1999) Molecular architecture of the rotary motor in ATP synthase. *Science* **286**: 1700–5.

Street NJ, Yi MS, Bailey LA, Hopkin RJ (2006) Comparison of health-related quality of life between heterozygous women with Fabry disease, a healthy control population, and patients with other chronic disease. *Genet Med* **8**: 346–53.

Sullards MC, Liu Y, Chen Y, Merrill AH Jr (2011) Analysis of mammalian sphingolipids by liquid chromatography tandem mass spectrometry (LC-MS/MS) and tissue imaging mass spectrometry (TIMS). *Biochim Biophys Acta* **1811**: 838–53.

Susuki K (2010) Myelin: a specialized membrane for cell communication. *Nature education* **3**: 59.

Swaney DL, Wenger CD, Coon JJ (2010) Value of using multiple proteases for large-scale mass spectrometry-based proteomics. *J Proteome Res* **9**: 1323 – 9.

Swartz M (2013) UPLC: an introduction. *J Liq Chromatogr Relat Technol* **28**: 8–14.

Szabó C (2003) Multiple pathwyas of peroxynitrite cytotoxicity. *Toxicol Lett* **140 – 141**: 105–12.

Szewczyk A, Wojtczak L (2002) Mitochondria as a pharmacological target. *Pharmacol Rev* **54**: 101–27.

Takeda M, Tsuboi Y, Kitagawa J *et al.* (2011) Potassium channels as a potential therapeutic target for trigeminal neuropathic pain and inflammatory pain. *Mol Pain* **7**: 5.

Tapasi S, Padma P, Setty OH (1998) Effect of psychosine on mitochondrial function. *Indian J Biochem Biophys* **35**: 161 – 5.

Thomson BA, Iribarne JV (1979) Field induced ion evaporation from liquid surfaces at atmospheric pressure. *J Chem Phys* **71**: 4451 – 63.

Thrailkill KM, Jo CH, Cockrell GE, Moreau CS, Fowlkes JL (2011) Enhanced excretion of vitamin D binding protein in type 1 diabetes: a role in vitamin D deficiency? *J Clin Endocrinol Metab* **96**: 142–9.

Togawa T, Kawashima I, Kodama T *et al.* (2010) Tissue and plasma globotriaosylsphingosine could be a marker for assessing enzyme replacement therapy for Fabry disease. *Biochem Biophys Res Commun* **399**: 716–20.

Tøndel C, Bostad L, Hirth A, Svarstad E (2008) Renal biopsy findings in children and adolescents with Fabry disease and minimal albuminuria. *Am J Kidney Dis* **51**: 767–76.

Topaloglu AK, Ashley GA, Tong B *et al.* (1999) Twenty novel mutations in the alpha-galactosidase A gene causing Fabry disease. *Mol Med* **5**: 806–11.

Törnroth-Horsefield S, Neutze R (2008) Opening and closing the metabolite gate. *Proc Natl Acad Sci U S A* **105**: 19565–6.

Uribe A, Giugliani R (2013) Selective screening for lysosomal storage disease with dried blood spots collected on filter paper in 4,700 high-risk Columbian subjects. *JIMD Rep* **11**: 107–16.

Usenovic M, Krainc D (2012) Lysosomal dysfunction in neurodegeneration: the role of ATP13A2/PARK9. *Autophagy* **8**: 987–8.

Valenzano K, Khanna R, Powe AC *et al.* (2011) Identification and characterization of pharmacological chaperones to correct enzyme deficiencies in lysosomal storage disorders. *Assay Drug Dev Technol* **9**: 213–35.

van Breemen MJ, Rombach SM, Dekker N *et al.* (2011) Reduction of elevated plasma globotriaosylsphingosine in patients with classic Fabry disease following enzyme replacement therapy. *Biochim Biophys Acta* **1812**: 70–6.

van Gelder CM, Vollebregt AA, Plug I, van der Ploeg AT, Reuser AJ (2012) Treatment options for lysosomal storage disorders: developing insights. *Expert Opin Pharmacother* **13**: 2281–99.

Vanier M, Svennerholm L (1976) Chemical pathology of Krabbe disease: the occurrence of psychosine and other neutral sphingolipids. *Adv Exp Med Biol* **68**: 115–26.

Vedder AC, Strijland A, vd Bergh Weerman MA *et al.* (2006) Manifestations of Fabry disease in placental tissue. *J Inherit Metab Dis* **29**: 106–11.

Viana-Baptista M (2012) Stroke and Fabry Disease. *J Neurol* 259: 1019–1028.

von Ballmoos C, Cook GM, Dimroth P (2008) Unique rotary ATP synthase and its biological diversity. *Annu Rev Biophys* **67**: 43–64.

von Scheidt W, Eng CM, Fitzmaurice TF *et al.* (1991) An atypical variant of Fabry's disease with manifestations confined to the myocardium. *N Engl J Med* **324**: 395–9.

Waldek S, Patel MR, Banikazemi M, Lemay R, Lee P (2009) Life expectancy and cause of death in males and female with Fabry disease: findings from the Fabry Registry. *Genet Med* **11**: 790–6.

Walker JE, Dickson VK (2006) The peripheral stalk of the mitochondrial ATP synthase. *Biochim Biophys Acta* **1757**: 286–96.

Walkley SU, (2009) Pathogenic cascades in lysosomal disease – why so complex? *J Inherit Metab Dis* **32**: 181–9.

Wang C, Youle RJ (2009) The role of mitochondria in apoptosis. *Annu Rev Genet* **43**: 95–118.

Wang RY, Abe, JT, Cohen AH, Wilcox WR (2008) Enzyme replacement therapy stabilizes obstructive pulmonary Fabry disease associated with respiratory globotriaosylceramide storage. *J Inherit Metab Dis* **31**: S369–74.

Wang RY, Bodamer OA, Watson MS *et al.* (2011) Lysosomal storage disease: diagnostic confirmation and management of pre-symptomatic individuals. *Genet Med* **13**: 457–84.

Warnock DG, Ortiz A, Mauer M *et al.* (2012) Renal outcomes of agalsidase beta treatment for Fabry disease: role of proteinuria and timing of treatment initiation. *Nephrol Dial Transplant* **27**: 1042–9.

Weidemann F, Breunig F, Beer M *et al.* (2005) The variation of morphological and functional cardiac manifestation in Fabry disease: potential implications for the time course of the disease. *Eur Heart J* **26**: 1221–7.

Weidemann F, Breunig F, Beer M *et al.* (2003) Improvement of cardiac function during enzyme replacement therapy in patients with Fabry disease: a prospective strain rate imaging study. *Circulation* **108**: 1299–301.

Weidemann F, Niemann M, Breunig F *et al.* (2009) Long-term effects of enzyme replacement therapy on Fabry cardiomyopathy: evidence for a better outcome with early treatment. *Circulation* **119**: 524–9.

Westermeier R, Naven T, Höpker HR (2008) *Proteomics in Practice: A guide to successful experimental design.* Chichester, UK: John Wiley & Sons.

West M, Nicholls K, Mehta A *et al.* (2009) Agalsidase alfa and kidney dysfunction in Fabry disease. *J Am Soc Nephrol* **20**: 1132–9.

Wharton DC, Tzagoloff A (1967) Cytochrome oxidase from beef heart mitochondria. *Meth Enzymol* **10**: 245–253.

Whybra C, Kampmann C, Willers I *et al.* (2001) Anderson-Fabry disease: clinical manifestations of disease in female heterozygotes. *J Inherit Metab Dis* **24**: 715–24.

Whybra C, Miebach E, Mengel W *et al.* (2009) A 4-year study of the efficacy and tolerability of enzyme replacement therapy with agalsidase alfa in 36 women with Fabry disease. *Genet Med* **11**: 441–9

Wikström MK (1977) Proton pump coupled to cytochrome c oxidase in mitochondria. *Nature* **266**: 271–3.

Wikström M (2004) Cytochrome c oxidase: 25 years of the elusive proton pump. *Biochim Biophys Acta* **1655**: 241–7.

Wilcken B (2003) Ethical issues in newborn screening and the impact of new technologies. *Eur J Pediatr* **162**: S62–6.

Wilcox WR, Banikazemi M, Guffon N *et al.* (2004) Long-term safety and efficacy of enzyme replacement therapy for Fabry disease. *Am J Hum Genet* **75**: 65–74.

Wilcox WR, Oliveira JP, Hopkin RJ *et al.* (2008) Females with Fabry disease frequently have major organ involvement: lessons from the Fabry Registry. *Mol Genet Metab* **93**: 112–28.

Winder WW, Holloszy JO (1977) Response of mitochondria of different types of skeletal muscle to thyrotoxicosis. *Am J Physiol* **232**: C180–4.

Wittmann J, Karg E, Turi S *et al.* (2012) Newborn screening for lysosomal storage disorders in Hungary. *JIMD Rep* **6**: 117–25.

Wood JN, Abrahamsen B Baker MD *et al.* (2004) Ion channel activities implicated in pathological pain. *Novartis Found Symp* **261**: 32–40.

Wraith JE, Tylki-Szymanska A, Guffon N *et al.* (2008) Safety and efficacy of enzyme replacement therapy with agalsidase beta: an international, open-label study in pediatric patients with Fabry patients. *J Pediatr* **152**: 563–70.

Wu X, Katz E, Della Valle MC *et al.* (2011) A pharmacogenetic approach to identify mutant forms of a α-galactosidase A that respond to a pharmacological chaperone for Fabry disease. *Hum Mutat* **32**: 965–77.

Wu Z, Fellenburg K, Lemeer S, Kuster B (2010) Comparison of label-free protein quantification approaches for chemical proteomics. *Poster – 58th Conference on Mass Spectrometry and Allied Topics.* Utah, USA.

Xie C, Turley SD, Pentchev PG, Dietschy JM (1999) Cholesterol balance and metabolism in mice with loss of function of Niemann-Pick C protein. *Am J Physiol* **276**: E336–44.

Xie Y, Sakatsume M, Nishi S *et al.* (2001) Expression, roles, receptors, and regulation of osteopontin in the kidney. *Kidney Int* **60**: 1645–57.

Yamadera M, Yokoe M, Beck G *et al.* (2009) Amelioration of white-matter lesions in a patient with Fabry disease. *J Neurol Sci* **279**: 118–20.

Young E, Mills K, Morris P *et al.* (2005) Is globotriaosylceramide a useful biomarker in Fabry disease? *Acta Paediatr Suppl* **94**: 51–4.

Young-Ggamana B, Brignol N, Chang HH *et al.* (2013) Migalastat HCl reduces globotriaosylsphingosine (lyso-Gb_3) in Fabry transgenic mice and in the plasma of Fabry patients. *PLoS One* **8**: e57631.

Zampetti A, Orteu CH, Antuzzi D *et al.* (2012) Angiokeratoma: decision-making aid for the diagnosis of Fabry disease. *Br J Dermatol* **166**: 712–20.

Zarate YA, Hopkin RJ (2008) Fabry's disease. *Lancet* **372**: 1427–35.

Zhang DX, Gutterman DD (2007) Mitochondrial reactive species-mediated signalling in endothelial cells. *Am J Physiol Heart Circ Physiol* **292**: H2023–31.

Zhang ZX, Shek K, Wang S *et al.* (2010) Osteopontin expressed in tubular epithelial cells regulates NK cell-mediated kidney ischemia reperfusion injury. *J Immunol* **185**: 967–73.

Zhou SL, Gordon RE, Bradbury M *et al.* (1998) Ethanol up-regulated fatty acid uptake and plasma membrane expression and export of mitochondrial aspartate aminotransferase in HepG2 cells. *Hepatology* **27**: 1064–74.

9.0 Appendices

9.1 Appendix A

9.1.1 Supplementary data

The calibration curves shown in Figure 9.1 were generated during the analysis of prosaposin (Figure 9.1a) and GM_2AP (Figure 9.1b) as described in section 2.2.5.7.

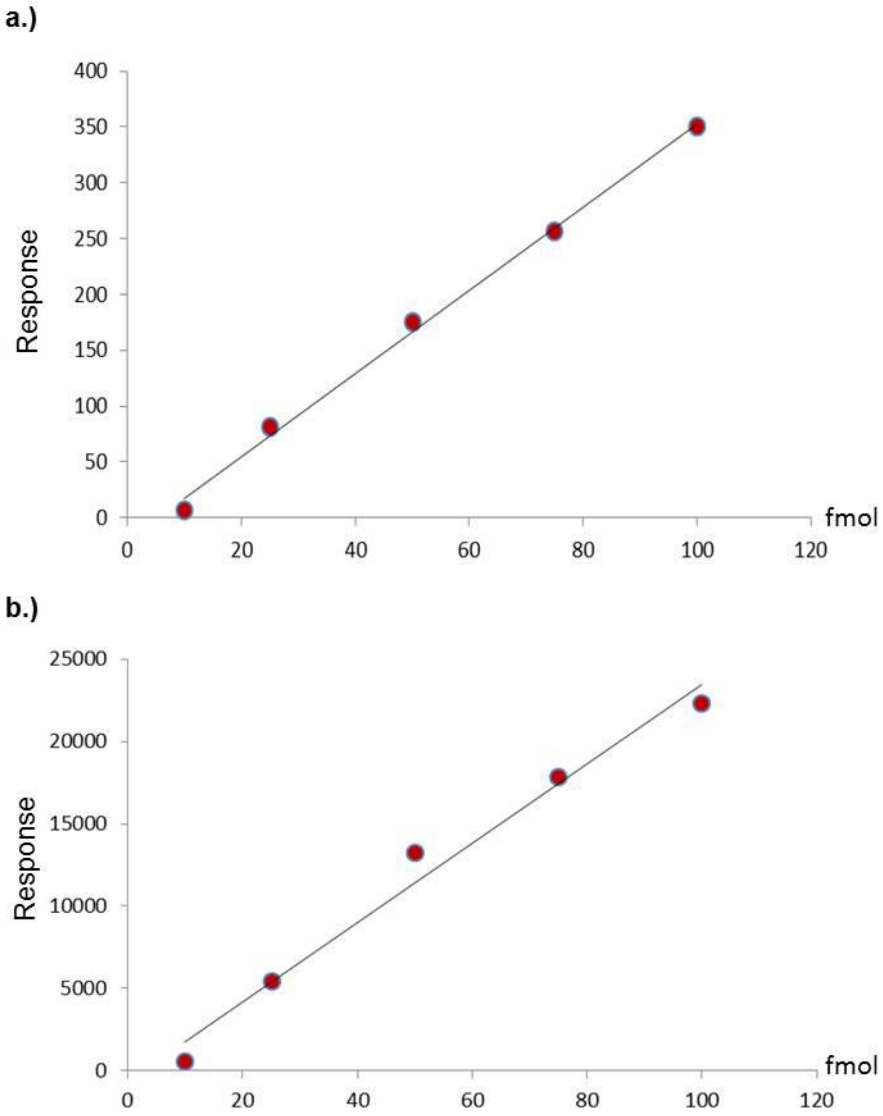

Figure 9.1 Calibration curve generated during the analysis a.) Prosaposin using a marker peptide from the saposin A region of the molecule (R^2 = 0.99); and b.) GM_2 activator protein (R^2 = 0.98).

The calibration curves shown in Figures 9.2.1 and 9.2.2 were generated during the analysis of the pre-symptomatic kidney disease biomarkers as described in section 2.2.5.8. It should be noted that the concentrations of albumin, osteopontin and prostaglandin-H2 D-isomerase are displayed in nmol whilst all other peptides concentrations are displayed in pmol.

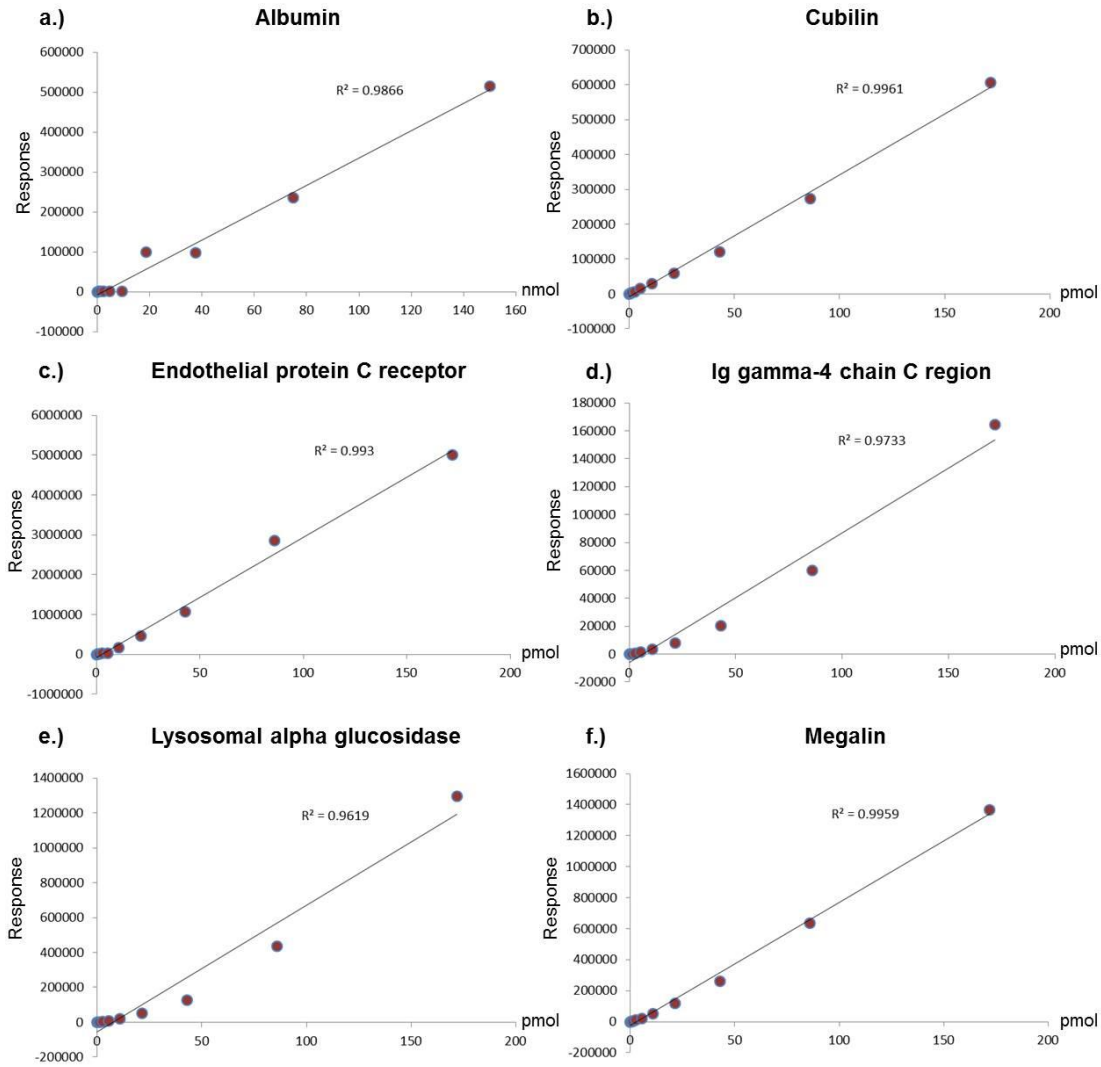

Figure 9.2.1 Calibration curves generated during the analysis of a.) albumin; b.) cubilin; c.) endothelial protein C receptor; d.) Ig gamma-4 chain C region; e.) lysosomal alpha glucosidase; and f.) megalin.

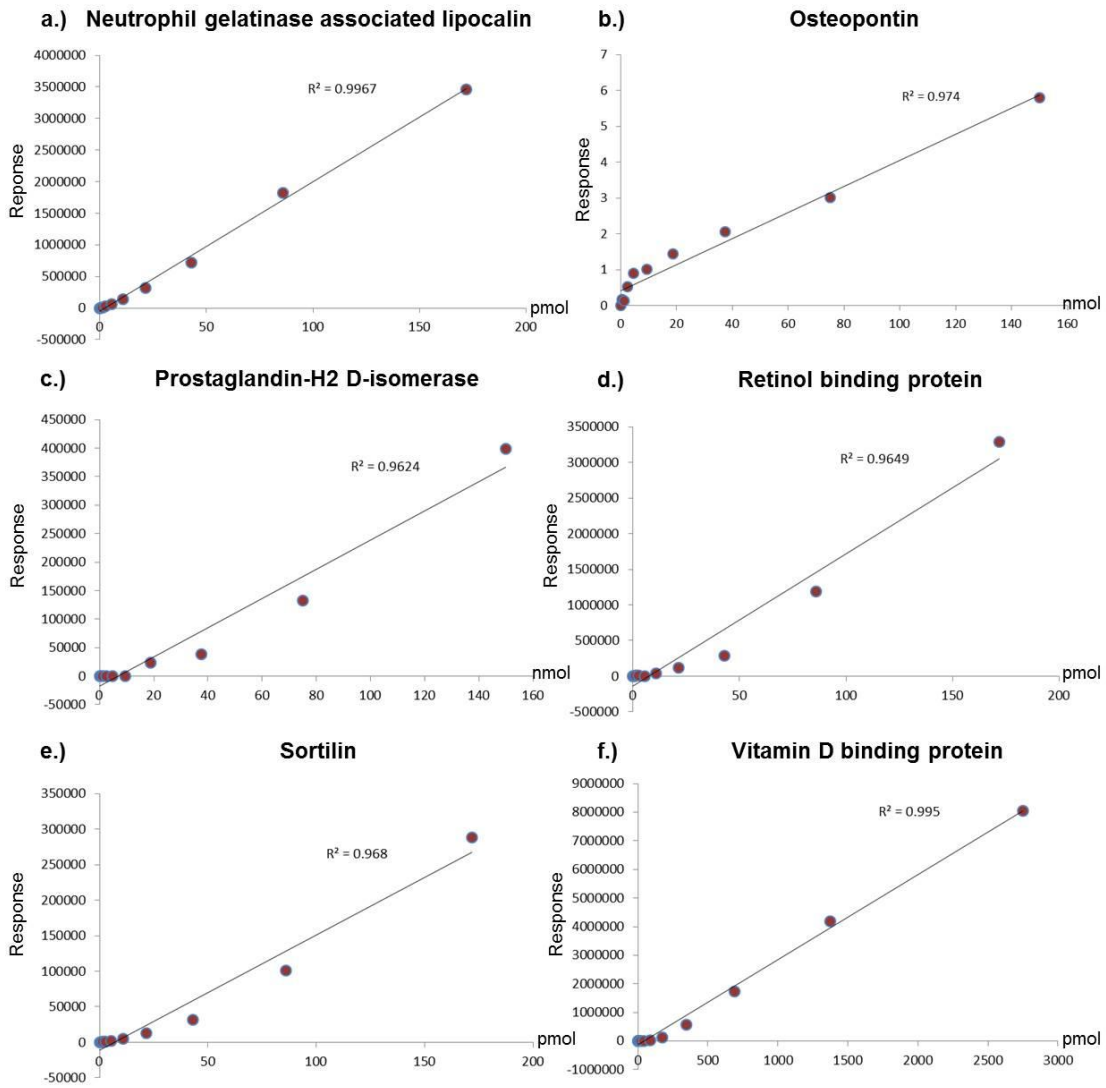

Figure 9.2.2 Calibration curve generated during the analysis of a.) neutrophil gelatinase associated lipocalin; b.) osteopontin c.) prostaglandin-H2 D-isomerase; d.) retinol binding protein; e.) sortilin; and f.) vitamin D binding protein.

9.2 Appendix B

9.2.1 List of published journal articles related to this thesis:

Manwaring V, Boutin M, and Auray-Blais C (2013) A metabolomic study to identify new globotriaosylceramide-related biomarkers in the plasma of Fabry disease patients. *Anal Chem* **85**: 9039–48.

Manwaring V, Heywood W, Clayton R *et al.* (2012) The identification of new biomarkers for identifying and monitoring kidney disease and their translation into a rapid mass spectrometry-based test: Evidence of presymptomatic kidney disease in paediatric Fabry and Type-I diabetic patients. *J Proteome Res* **12**: 2013–21.

9.2.2 List of conference abstracts related to this thesis:

Manwaring V, Sirka E, Heywood W *et al.* (2013) Increased urinary megalin and cubilin excretion in children with type I diabetes mellitus – an association with low molecular weight protein loss. BSPED, Brighton, UK. – Oral presentation

Manwaring V, Sirka E, Heywood W, Mills K (2013) The development of a MS based assay for the identification of pre-symptomatic kidney disease. Focus on Fabry Nephropathy, Hong Kong – Poster Prize

Manwaring V, Boutin M, Auray-Blais C (2013) A metabolomic study to identify new globotriaosylceramide-related biomarkers in the plasma of Fabry disease patients. Focus on Fabry Nephropathy, Hong Kong.

Manwaring V, Heywood W, Heales S and Mills K (2012) Identification of the Potential Urinary Biomarker Proactivator Polypeptide in Fabry Disease, SSIEM, Birmingham, UK.

Manwaring V, Heywood W and Mills K (2011) New biomarkers for lysosomal storage disease and their development into triple quadrupole tests'. Waters Meeting, London, UK. – oral presentation

Manwaring V, Heywood W, Heales S and Mills K (2011) Trying to elucidate the mechanism of kidney damage in Fabry disease – the use of glycolipid arrays to study protein:lipid interactions in the kidney. SSIEM, Geneva, Switzerland. – oral presentation

Manwaring V, Heywood W, Heales S, Mills K (2011) Identification of potential urinary biomarkers for the diagnosis of lysosomal storage disease. Focus on Fabry Nephropathy: Biomarkers, Progression and Treatment Opportunities, Vancouver, Canada – Poster Prize.